THE UNIVERSITY OF MICHIGAN

COLLEGE OF ENGINEERING
Department of Meteorology and Oceanography

Final Report

ATMOSPHERIC POLLUTION BY AEROALLERGENS: METEOROLOGICAL PHASE

(1 March 1962 to 28 February 1965)

Vol. II

Atmospheric Diffusion of Ragweed Pollen in Urban Areas: Text

J. B. Harrington, Jr.

Project Director: E. W. Hewson

ORA Project 06342

supported by:

DIVISION OF AIR POLLUTION
BUREAU OF STATE SERVICES
U. S. PUBLIC HEALTH SERVICE
RESEARCH GRANT NO. AP-00006
WASHINGTON, D.C.

administered through:

OFFICE OF RESEARCH ADMINISTRATION ANN ARBOR

November 1965

Volumes II and III of this report were also a dissertation submitted in partial fulfillment of the requirements for the degree of Doctor of Philosophy in The University of Michigan, 1965.

TABLE OF CONTENTS

TABLE OF CONTENTS (Continued)

TABLE OF CONTENTS (Continued)

TABLE OF CONTENTS (Continued)

TABLE OF CONTENTS (Concluded)

LIST OF TABLES

LIST OF TABLES (Concluded)

A complete set of tables is in Volume III.

LIST OF FIGURES

LIST OF FIGURES (Continued)

LIST OF FIGURES (Concluded)

ABSTRACT

The purpose of this study is to develop a method for predicting the concentration of ragweed pollen advected into a ragweed free urban area from an infinite surrounding source region and to compare the concentration so produced with that from a small local source.

From among the many diffusion equations reviewed the parabolic equations are selected as most applicable to this problem. A detailed technique for the solution of each equation is given.

The vertical and temporal variations of the three parameters needed to solve the diffusion equations, namely wind speed, the vertical component of diffusivity and the lateral component of diffusivity, are discussed at length and methods for their measurement or estimation given.

A surface deposition model is proposed and used as a lower boundary condition in the solution of the diffusion equations. Comparison of theoretical and experimental results suggests that deposition of ragweed pollen occurs at about the gravitational rate.

Theoretically computed pollen profiles are compared with observations reported in the literature and with the results of three diffusion experiments. The values of source strength, diffusivity and the rate of deposition computed from experimental observations are used in the diffusion calculations. Satisfactory agreement between theory and observation is obtained.

In conclusion it is shown that except in the immediate vicinity of small ragweed sources within an urban area the pollen from such sources is of negligible importance compared to that advected from the surrounding countryside.

1. INTRODUCTION

1.1 PURPOSE OF THE STUDY

One of the major problems of the 20th century is and will continue to be the poisoning of man's environment by the by-products of his own activities. These by-products are not limited to sewage, industrial wastes, and combustion products, but include biological materials such as pollens and spores which often occur in toxic quantities as a consequence of intensive land cultivation.

To those millions of persons sensitive to aeroallergens the poisoning of the atmosphere by biological materials constitutes a serious health hazard. For example, it is estimated that 18 to 27 million Americans suffer from asthma and hayfever caused by ragweed pollen alone.

Ragweed pollen, one of the most noxious of the aeroallergens, lends itself to control since, unlike grass and trees, the ragweed plant can be eradicated. In the cities, where an increasing percentage of the population lives, one remedy has been to destroy systematically the ragweed plants within the cities boundaries. The success of such a program depends upon whether the pollen in the city originates locally or in the surrounding countryside. Because control programs are costly, the answer to this question is of considerable economic importance.

The purpose of this study is to develop a technique for predicting the concentration of ragweed pollen within an urban area and to compare the relative contributions to that concentration from internal and ex-

ternal sources.

1.2 AN APPROACH TO A SOLUTION

Computation of the concentration of ragweed pollen over an urban area requires a satisfactory mathematical model, a knowledge of the appropriate parameter values and boundary conditions and a method of solution which does not require overly restrictive assumptions.

1.2.1 Selection of a Diffusion Model

At present the three following types of diffusion models are in use

1. Equations based on statistical theory;
2. Hyperbolic diffusion equations; and
3. Parabolic diffusion equations.

The best known of all the practical equations based on statistical theory is that of Sutton (1934) which in the form applicable to an instantaneous point source is expressed as

$$\chi(x,y,z,t) = \frac{Q}{\pi^{3/2} C_x C_y C_z (\bar{u}t)^{3/2(2-n)}} \exp\left[-(\bar{u}t)^{n-2}\left(\frac{x^2}{C_x^2} + \frac{y^2}{C_y^2} + \frac{z^2}{C_z^2}\right)\right] \quad (1.1)$$

where the C's are diffusion parameters and n is a stability parameter. By equating n to unity and letting

$$C_i^2 = \frac{4K_i}{\bar{u}} \quad (1.2)$$

Equation (1.1) reduces to Roberts' (1932) solution of the unsteady three dimensional parabolic diffusion equation with constant diffusivity

$$\chi(x,y,z,t) = \frac{Q}{(4\pi t)^{3/2}(K_x K_y K_z)^{1/2}} \exp\left[-\frac{1}{4t}\left(\frac{x^2}{K_x} + \frac{y^2}{K_y} + \frac{z^2}{K_z}\right)\right] \quad (1.3)$$

No means have yet been found to incorporate the height variability of the diffusivity and wind speed into these equations. Near the ground, where the meteorological parameters vary most rapidly with height, this represents a serious limitation to their successful use. This is particularly true in the problem under consideration since here the ground serves as both a source and a sink for pollen.

Other statistical theories have been equally unsuccessful in dealing with the effects of the variability of wind speed and diffusivity with height. The most widely used equation, that of Hay and Pasquill (1959), may be written

$$\sigma_p^2 = \overline{\theta'^2}_{\tau,s} \quad (1.4)$$

and relates the variance of the aerosol distribution σ_p^2 to the variance of the wind direction distribution $\overline{\theta'^2}$, where the latter is measured over the period of emission τ and averaged over periods of duration S equal to the travel time divided by a scale factor called β. Equation (1.4) can only be successfully used where the variance of the wind direction fluctuations are spatially constant in the vertical and is therefore inapplicable to the problem at hand.

The hyperbolic equation was introduced by Goldstein (1951) who considered the problem of diffusion by discontinuous movements. The limiting form of his solution is the well-known "telegraph" equation

$$\frac{\partial^2 \chi}{\partial t^2} + \frac{1}{A}\frac{\partial \chi}{\partial t} = \overline{w^2}\frac{\partial^2 \chi}{\partial z^2} \qquad (1.5)$$

where $\overline{w^2}$ is the variance of the vertical component of wind speed and A is a constant. The hyperbolic form of Eq. (1.5) ensures that at all times short of infinity the spread of particles from a finite source is limited.

Further refinement of the hyperbolic equation has been undertaken by Monin (1955, 1956, 1959) who has written it in a form suitable for describing the vertical spread of smoke downwind of a point source. In his equation Monin permits the vertical wind speed to be a function of height. His equations,

$$\left.\begin{aligned} \frac{\partial \chi}{\partial t} + \frac{\partial S}{\partial z} &= 0 \\ \frac{\partial S}{\partial t} + 2aS + w^*\partial\frac{(w^*\chi)}{\partial z} &= 0 \end{aligned}\right\} \qquad (1.6)$$

where S is the particle flux and w* is the maximum velocity of vertical propagation of the diffusion smoke, reduce to Eq. (1.5) for constant w^*.

The hyperbolic equations appear entirely reasonable, but have not been widely used due at least in part to a reluctance to abandon the parabolic equations the solutions of which exhibit the familiar Gaussian form.

Of the four diffusion models outlined above the parabolic equations have been selected as most appropriate for this study because

they are most familiar to the author and because with the numerical techniques now available they may be solved under completely realistic boundary conditions and with virtually any distribution of meteorological parameter values.

1.2.2 Historical Development of the Parabolic Diffusion Equations

The earliest diffusion model was introduced by Fick in 1855 (see Crank, 1956, p. 2) and was based on the theory of heat conduction (Fourier, 1822). The Fickian equations correspond to the parabolic diffusion equation with constant diffusivity

$$\frac{d\chi}{dt} = K\nabla^2\chi \qquad (1.7)$$

where χ represents the concentration of some conservative entity and K the diffusivity.

The earliest solutions to Eq. (1.7) applicable to the atmosphere were carried out by G. I. Taylor (1915) who measured the eddy diffusivity from observations of temperature profiles measured on the Eiffel Tower in Paris and from kite ascents aboard the "Scotia" of the Grand Banks of Newfoundland. Only the simplest forms of Eq. (1.7) were considered, namely

$$\frac{\partial\theta}{\partial t} = K_z \frac{\partial^2\theta}{\partial z^2} \qquad (1.8)$$

and

$$u \frac{\partial\theta}{\partial x} = K_z \frac{\partial^2\theta}{\partial z^2} \qquad (1.9)$$

where θ is the potential temperature.

An extension of the theory to the diffusion of matter from instantaneous point, continuous point and continuous line sources was made by Roberts (1923) who considered a non-isotropic but homogeneous atmosphere. In these cases Eq. (1.7) takes the forms, respectively,

$$\frac{\partial \chi}{\partial t} = K_x \frac{\partial^2 \chi}{\partial x^2} + K_y \frac{\partial^2 \chi}{\partial y^2} + K_z \frac{\partial^2 \chi}{\partial z^2} \tag{1.10}$$

$$u \frac{\partial \chi}{\partial x} = K_y \frac{\partial^2 \chi}{\partial y^2} + K_z \frac{\partial^2 \chi}{\partial z^2} \tag{1.11}$$

and

$$u \frac{\partial \chi}{\partial x} = K_z \frac{\partial^2 \chi}{\partial z^2} \tag{1.12}$$

Recognizing that the solutions to Eqs. (1.10), (1.11), and (1.12) are not applicable near the ground where the diffusivity varies rapidly with height, Roberts in an unpublished paper explored solutions to the steady two-dimensional non-Fickian diffusion equation (Sutton, 1953, p. 280)

$$u(z) \frac{\partial \chi}{\partial x} = \frac{\partial}{\partial y}\left(K_z \frac{\partial \chi}{\partial z}\right) \tag{1.13}$$

in which both wind speed and diffusivity were allowed to vary as a power of the height and were related by the Schmidt conjugate-power law (Sutton, 1953 p. 85).

The first to introduce the concept of a finite particle fall speed were Bosanquet and Pearson (1936) who treated the fall speed of a

particle as though it were a downward wind. They solved the equation

$$u(z)\,\frac{\partial \chi}{\partial x} = \frac{\partial}{\partial z}\left(K_z\,\frac{\partial \chi}{\partial z} + q\chi\right) \qquad (1.14)$$

with the assumption that wind speed u was constant and diffusivity K_z a linear function of height. Here q is the settling speed of the particle in still air.

Early solutions to Eq. (1.14) required simple conditions on the lower boundary such as a constant concentration or flux and simple distributions of wind and diffusivity in the vertical. W.G.L. Sutton (1943) found solutions for a variable flux condition at the lower boundary; Frost (1946) permitted the wind and diffusivity profiles to vary independently; Calder (1949) replaced the diffusivity with measurable physical variables and later (Calder, 1952) was able to solve the equation in a form containing no empirical parameters; Yih (1952) and Philip (1959) repeated the work done earlier by Frost using more elegant methods; Rounds (1955) using the Deacon wind profile (Deacon, 1949) found solutions which could be made to fit an arbitrary initial distribution; Smith (1957, (a),(b),(c)) solved for various distributions of diffusivity and later (Smith, 1962) solved the equations using a variable ground absorption term suggested by Calder (1961)

$$\left[K\,\frac{\partial \chi}{\partial z} + q\chi\right]_{z=o} = \alpha\chi \qquad (1.15)$$

where α is a constant.

The three dimensional diffusion equation

$$u(z)\,\frac{\partial \chi}{\partial x} = \frac{\partial}{\partial z}\left(K_z\,\frac{\partial \chi}{\partial z}\right) + \frac{\partial}{\partial y}\left(K_y(z)\,\frac{\partial \chi}{\partial y}\right) \qquad (1.16)$$

has been solved analytically by Davis (1950) for the case in which the wind speed and vertical component of diffusivity are related by the Schmidt conjugate-power law (Sutton, 1953) and the lateral component of diffusivity is a constant. Solutions have also been obtained by Smith (1957, (a),(b),(c)) which incorporate various vertical distributions of diffusivity including one which increases linearly to the midpoint of the turbulent boundary layer and decreases linearly to the top.

Despite the increasing accuracy of analytic solutions they are inadequate for two reasons: First, the profiles of wind and diffusivity are still not sufficiently realistic and second, even when the models approach reality the solutions become so complex that one of the main purposes of an analytic solution, namely the insight it provides, is lost.

More recently, numerical techniques have been applied to the solution of the parabolic diffusion equations. One of the first meteorological applications was by Brock (1961 (a),(b)) who solved the two- and three-dimensional equations using an electronic analog computer. His solutions for continuous point and line sources permitted the use of any distributions of eddy diffusivity and wind speed, of virtually any initial distribution and of realistic boundary conditions.

The analog computer is a particularly attractive tool for solving differential equations since it integrates continuously in one variable and therefore has considerable computational stability. Its main disadvantage lies in its limited capacity. A moderate to large computer having 200 integrators can, for example, handle no more than a 14 by 14 grid space which, although adequate for many problems, is too small for the task under consideration here.

The first meteorological application of the digital computer to the solution of the parabolic diffusion equations was carried out by Yamamoto and Shimanuki (1960, 1964). Their solutions for the steady three-dimensional Eq. (1.16) were undertaken using ordinary finite differencing, a technique which requires a small downwind step size to ensure stability. As with the analog solutions realistic initial conditions and profiles of wind speed and diffusivity were used; however, the effect of emission or absorption at the lower boundary and of gravitational settling were not considered.

In the present study the work of Yamamoto and Shimanuki is extended to include gravitational settling and realistic conditions at the lower boundary. The numerical method used to solve the parabolic diffusion equation is stable and extremely fast compared to older techniques.

1.2.3 Particulate Flux at the Ground

Previous solutions to the parabolic diffusion equations have used one of the three following conditions at the lower boundary:

$$\left.\begin{aligned} &1.\quad \chi(\ell) = \text{const} \\ &2.\quad K(\ell)\left(\frac{\partial \chi}{\partial z}\right)_{\ell} = \text{const} \\ &3.\quad \left(K\frac{\partial \chi}{\partial z} + q\chi\right)_{\ell} = \alpha\chi(\ell) \end{aligned}\right\} \qquad (1.17)$$

where ℓ is the level of the lower boundary. It will be seen that none of these is applicable to the problem being considered here.

During the ragweed season pollen is emitted at the level of the plant inflorescence at a rate which is entirely independent of its concentration in the air. This can be expressed in terms of a combination of Conditions 1 and 2 above, i.e.:

$$\left(K\frac{\partial \chi}{\partial z} + q\chi\right)_{\ell} = -P \qquad (1.18)$$

where P is a constant equal to the rate of upward flux of pollen through the emission layer at height ℓ.

Pollen also flows downward through the level ℓ and is eventually deposited on the ground or on vegetation either by impaction or gravitational setting. The downward flux is directly proportional to the concentration and can be represented by Condition 3 of Eq. (1.17). The combined effect of emission and deposition may then be written

$$\left(K\frac{\partial \chi}{\partial z} + q\chi\right)_{\ell} = -P + F\chi(\ell) \qquad (1.19)$$

where F is a complicated function depending on the distributions of wind speed and diffusivity within the vegetative layer, on the distribution of the vegetation itself and on other factors such as the shape

and collection efficiency of the leaf surfaces. Chapter 5 is devoted to the development of a realistic deposition model.

1.2.4 The Selection of Appropriate Models for the Distributions of Meteorological Parameters

Despite the intensive study of the lower atmosphere conducted over the past half century surprisingly little is known regarding the vertical distributions of the atmospheric variables within the turbulent boundary layer. For example, no one has been able to specify completely the wind distribution near the ground even in the relatively simple case of a locally uniform surface and a neutral lapse rate. When more complicated surfaces or non-neutral lapse rates are considered the problem is compounded.

Near the ground, models which describe the diffusivity and wind speed profiles are available, and, despite the pessimistic tone of the preceeding paragraph, are adequate for most purposes. They are particularly satisfactory for the problem considered here, since only the grossest average effects can be considered.

Further aloft above the height of meteorological masts and towers, and particularly during periods of natural convection, so little is known about the distribution of wind and eddy diffusivity that no model provides more than a crude estimate of these parameters.

In Chapt. 6 of this study the vertical and temporal variations of the three parameters needed to solve the diffusion equations, namely wind speed, the vertical component of diffusivity and the lateral com-

ponent of diffusivity are discussed at length and methods for their measurement or estimation given.

1.2.5 The Specification of an Initial Pollen Distribution

The vertical profile of pollen concentration over an infinite homogeneous source region can be computed using the unsteady one-dimensional diffusion equation

$$\frac{\partial \chi}{\partial t} = \frac{\partial}{\partial z}\left(K(z)\ \frac{\partial \chi}{\partial z} + q\chi\right) \qquad (1.20)$$

with an appropriate boundary condition, Eq. (1.19). The resulting profile may then be used as an initial condition along the upwind boundary of the ragweed free urban area under consideration in this study.

Equation (1.20) is solved using estimates of the various parameters obtained from the results of three experiments reported in Appendices A, B, and C. The resulting solutions and comparisons with observed profiles are given in Chapt. 7.

1.3 AEROSOL PROFILES IN THE ATMOSPHERE

Observations of the distributions of aerosols in the atmosphere provide the only means of testing the validity of diffusion models. The disappointingly few observations are reported and discussed in Chapt. 3.

Additional observations of ragweed pollen distributions obtained in this study from both natural and artificial sources are reported in the three appendices.

1.4 THE MECHANICS OF DIFFUSION

Atmospheric diffusion is essentially a problem in statistical mechanics and, therefore, true insight into the problem can only be achieved through the statistical theory. The following chapter contains a brief résumé of this theory and develops equations needed later for the computation of diffusivity from experimental data.

2. THE DIFFUSION MECHANISM

2.1 INTRODUCTION

This chapter is a brief review of certain aspects of statistical mechanics which apply directly to the problem of atmospheric diffusion, and more particularly to the problems encountered during the course of this study.

The approach has been to bring together the work of several authors in order to present a self contained development of the practical statistical atmospheric diffusion theory. The steps in this development are:

1. The relationship between atmospheric diffusion and the Lagrangian velocity autocorrelation coefficient is derived.

2. The power spectrum function is defined and related to the autocorrelation coefficient.

3. The relationship between atmospheric diffusion and the power spectrum is explored.

4. A practical diffusion model is developed from the concepts of 1 to 3 above.

5. The major region of application of statistical theory to this study is outlined.

2.2 DIFFUSION BY CONTINUOUS MOVEMENTS

As one reviews the historical development of diffusion theory, a surprising fact emerges; namely, that practically every major advance stems from the work of one man, G. I. Taylor. This section is a partial résumé of one of his early papers (Taylor, 1921).

Consider a one dimensional homogeneous fluid in turbulent motion such that the statistical properties of that motion are everywhere the same. Assume that each particle of the fluid has an instantaneous velocity u and that the correlation coefficient between its velocity at two times separated by an interval ξ is $R(\xi)$.

Next consider the equality

$$\int_0^t \overline{u_t u_\xi}\, d\xi = \int_0^t \overline{u_t u_{t+\xi}}\, d\xi = \overline{u^2} \int_0^t R(\xi)\, d\xi \qquad (2.1)$$

where

$$\overline{u_t^2} = \overline{u_{t+\xi}^2} = \overline{u^2} \qquad (2.2)$$

because the statistical properties of the turbulence are unchanging in time, and

$$\int_0^t R(\xi - t)\, d\xi = \int_0^t R(\xi)\, d\xi \qquad (2.3)$$

because $R(\xi)$ is an even function of ξ.

Integration after reversing the order of averaging and integration in Eq. (2.1) yields the following equalities

$$\int_0^t \overline{u_t u_\xi}\, d\xi = \overline{u_t \int_0^t u_\xi\, d\xi} = \overline{u_t x} = \frac{1}{2} \frac{d}{dt} \overline{x^2} \qquad (2.4)$$

Therefore

$$\frac{1}{2}\frac{d}{dt}\overline{x^2} = \overline{u^2}\int_0^t R(\xi)\,d\xi \qquad (2.5)$$

and

$$\overline{x^2} = 2\overline{u^2}\int_0^T\int_0^t R(\xi)\,d\xi\,dt \qquad (2.6)$$

From Eq. (2.6) we see that the variance of a group of particles originating at a point can be found if the particles move with the air and if the autocorrelation coefficient of the turbulent velocities of the particles is known. A system such as this, in which measurements are made relative to the moving particle, is called Langrangian.

To achieve a better understanding of the significance of Eq. (2.5) consider the definition of eddy diffusivity in one dimension, i.e.,

$$K_x = \frac{\overline{\chi u}}{\partial\chi/\partial x} \qquad (2.7)$$

where $\overline{\chi u}$ represents the particle flux across a point, say x = 0. The value of χ at x = 0 is

$$\chi(0) = \frac{\partial\chi}{\partial x} \cdot x \qquad (2.8)$$

where x is the point of origin of the air parcel. Substituting Eq. (2.8) into Eq. (2.7) yields the equation

$$K_x = \overline{xu} \qquad (2.9)$$

and this is seen from Eq. (2.4) to be equal to Eq. (2.5).

Taylor's theory (1921) therefore provides us with a certain insight into the meaning of eddy diffusivity; namely, it is equal to one

half the rate of change of the particle distribution variance.

To make practical use of Eq. (2.6) requires a knowledge of the functional form of the Lagrangian autocorrelation coefficient. If, for example, $R(\xi)$ remains unity over the period of observation then

$$\begin{aligned} K_x &= \overline{u^2}T \\ \overline{x^2} &= \overline{u^2}T^2 \end{aligned} \tag{2.10}$$

and the diffusion proceeds as a linear function of time, i.e., the particles diverge at a constant rate. If, on the other hand, $R(\xi)$ reduces to zero for some value of ξ, say T,

$$\int_0^T R(\xi)d\xi = I \tag{2.11}$$

a constant, and for time greater than T

$$K_x = \overline{u^2}I \tag{2.12}$$

a constant, and

$$\overline{x^2} = 2\overline{u^2}IT \tag{2.13}$$

In this example the diffusivity is a constant and therefore the diffusion is Fickian. A typical example of the latter is given by molecular diffusion since in this case the time required for $R(\xi)$ to decrease to zero is negligibly small.

The constant I, termed the time scale of the turbulence, is really a measure of the period of the largest energy containing eddy. In atmospheric motions, where there is virtually no limit to the eddy size (at least for the zonal component of wind) the time scale ceases to have a clear cut meaning.

Numerous attempts have been made to describe the functional form of the autocorrelation coefficient. The earliest was patterned after atmospheric observations of $R(\xi)$ (Taylor, 1921) in the form

$$R(\xi) = e^{-\alpha\xi} \tag{2.14}$$

where α is a constant. Another form, suggested by Sutton (1934), and used in the development of his diffusion model (see 1.2.1 Eq. (1.1)) is

$$R(\xi) = \left(\frac{u_* z_o}{u_* z_o + \overline{w^2}\xi}\right)^n \tag{2.15}$$

where n is a constant calculated from the shape of the wind profile, $u_* z_o$ is the macroviscosity (see Sutton, 1953, p. 82) and $\overline{w^2}\xi$ is an eddy diffusivity applicable to eddies of period ξ.

A complete discussion of the relative merits of various forms for $R(\xi)$ is given in a doctoral thesis by Munn (1961) who proposes another empirically derived expression. He shows that none of the models is really satisfactory and that even his own is too complex for routine practical use.

In summary, it has been demonstrated how in a field of homogeneous turbulence the specification of the velocity autocorrelation coefficient can determine two useful quantities, the variance of the particle distribution and the diffusivity. It has also been noted that the ideal conditions under which the theory is derived are generally not attained in the atmosphere.

2.3 THE POWER SPECTRUM OF EDDY ENERGY

The rate of dispersion of an aerosol in the atmosphere is determined not only by the total turbulent energy present, but also by the distribution of that energy among the eddies. Thus, for example, a puff of smoke 10 m in diameter will be virtually unaffected by eddies smaller than 10 cm or larger than 1 km if the dispersion is measured relative to the center of the puff, but will be literally torn apart by eddies having the same order of size as the puff itself.

Power spectrum analysis is a tool which permits us to compute the distribution function of the eddy energy according to the frequency or wave number from autocorrelation measurements of the wind speed. It was introduced into the meteorological literature by G. I. Taylor (1938) giving a new impetus to the use of statistical theory.

The wind speed recorded at a point in space is a continuous random variable which can be represented by the Fourier integral

$$u(y) = \int_0^\infty \Phi(\omega)\, e^{i\omega y} d\omega \qquad (2.16)$$

(Simmons and Salter, 1938), where ω is the angular frequency $2\pi n$, ξ is a fixed time and $y = t + \xi$. Then from the Fourier transform a relation can be found for $\Phi(\omega)$ in the form

$$\Phi(\omega) = \frac{1}{\pi}\int_{-\infty}^{\infty} u(y)\, e^{-i\omega y} dy \tag{2.17}$$

Now multiply both sides of Eq. (2.16) by $u(t)$, take the integral over $-\infty \leq t \leq \infty$ and reverse the order of integration on the right hand side to obtain

$$\int_{-\infty}^{\infty} u(t)u(y)\,dt = \pi\int_{0}^{\infty} \Phi^2(\omega)\cos(\omega\xi)\,d\omega \tag{2.18}$$

Setting $\xi = 0$ and integrating $u(t)$ and $\Phi(\omega)$ over a time T rather than infinity and averaging yields the equation

$$\lim_{T\to\infty} \frac{1}{2T}\int_{-T}^{T} u^2(t)\,dt = \pi\int_{0}^{\infty} \lim_{T\to\infty} \frac{\Phi^2(\omega)}{2T}\, d\omega$$

or

$$\overline{u^2} = 2\pi^2\int_{0}^{\infty} \lim_{T\to\infty} \frac{\Phi^2(n)}{2T}\, dn \tag{2.19}$$

and therefore

$$\overline{u^2}F(n) = \lim_{T\to\infty} 2\pi^2\left(\frac{\Phi^2(n)}{2T}\right) \tag{2.20}$$

where $F(n)$ is the fractional contribution to the total variance by frequencies between n and n + dn.

If the same averaging process is applied to Eq. (2.18)

$$\frac{\overline{u(t)u(t+\xi)}}{\overline{u^2}} = R(\xi) = \int_0^\infty F(n)\cos 2\pi n\xi \, dn \qquad (2.21)$$

and from the Fourier transform of Eq. (2.21)

$$F(n) = 4\int_0^\infty R(\xi)\cos 2\pi n\xi \, d\xi \qquad (2.22)$$

Thus it is seen that the power spectrum function and the autocorrelation coefficient of turbulent motion are related by the Fourier transform. The value of the power spectrum will be demonstrated in succeeding sections.

2.4 THE EFFECT OF SAMPLING DURATION AND AVERAGING TIME

Part of the observed particle dispersion in any atmospheric diffusion experiment will be caused by eddies having periods greater than the duration of the experiment because, as noted in Section 2.1, there is virtually no upper limit to the spectrum of the zonal component of atmospheric turbulence.

The contribution to the variance of the wind by eddies of greater duration than the sampling period can be computed as follows: Let the frequency of the eddy in question be n. Then

$$y(n) = A \sin(2\pi nt) \qquad (2.23)$$

and the short term mean of y(n) will be $\overline{y(n)}$, where

$$\overline{y(n)} = \frac{1}{\Delta t}\int_{t-\Delta t/2}^{t+\Delta t/2} A \sin(2\pi mt)\,dt = A\,\frac{\sin(\pi m\Delta t)}{\pi m\Delta t}\sin(2\pi mt) \tag{2.24}$$

The short term variance will be $\sigma^2_{\Delta t}$, where

$$\sigma^2_{\Delta t} = \frac{A^2}{\Delta t}\int_{t-\Delta t/2}^{t+\Delta t/2} \sin^2(2\pi m\xi)\left(1 - \frac{\sin(\pi m\Delta t)}{\pi m\Delta t}\right)^2 d\xi \tag{2.25}$$

or

$$\sigma^2_{\Delta t} = \frac{A^2}{2}\left[1 - \cos(4\pi mt)\,\frac{\sin(2\pi m\Delta t)}{2\pi m\Delta t}\right]\left[1 - \frac{\sin(\pi m\Delta t)}{\pi m\Delta t}\right]^2 \tag{2.26}$$

Averaged over the entire period of the eddy,

$$\overline{\sigma^2_{\Delta t}} = \frac{A^2}{2}\left[1 - \frac{\sin(\pi m\Delta t)}{\pi m\Delta t}\right]^2 \tag{2.27}$$

The large eddy under consideration contributes very little of its variance to the total when the sampling period, Δt, is very small compared to n^{-1}, about 0.12 of its variance when the sampling period is one half of n^{-1} and all of its variance when the sampling period is equal to n^{-1}.

Instead of considering the contribution of long period eddies to the short period variance let us now consider the effect of averaging time on the total measured variance.

Equation (2.24) gives the average value of y(n). Integrating over the entire period of the wave results in a variance

$$\sigma^2_{\infty,\Delta t} = \frac{A^2}{2}\frac{\sin^2(\pi n\Delta t)}{(\pi n\Delta t)^2} \tag{2.28}$$

where $\sigma^2_{\infty,\Delta t}$ is the variance measured over an infinite time and averaged over a period Δt. It is seen that the total variance is reduced by an amount equal to $\sin^2(\pi n\Delta t)/(\pi n\Delta t)^2$.

Integrated over the entire eddy spectrum this can be expressed as (Pasquill, 1962, p. 13)

$$\sigma^2_{\infty,s} = \sigma^2_{\infty,o}\int_o^\infty F(n)\,\frac{\sin^2(\pi ns)}{(\pi ns)^2}\,dn \tag{2.29}$$

where s has been substituted for Δt and $\sigma^2_{\infty,o}$ for $A^2/2$, the total variance.

The effect of a finite sampling time may be seen by considering the equality

$$\sigma^2_{\infty,o} = \sigma^2_{\infty,\tau} + [\sigma^2_{\tau,o}]_\infty \tag{2.30}$$

where the square bracket indicates averaging over the subscripted interval. Substituting from Eq. (2.29) gives

$$[\sigma^2_{\tau,o}]_\infty = \sigma^2_{\infty,o}\int_o^\infty F(n)\left(1 - \frac{\sin^2(\pi n\tau)}{(\pi n\tau)^2}\right)dn \tag{2.31}$$

which shows that the average value of the variance measured over a period τ is equal to the total variance reduced by the term in brackets.

A measure of the total reduction in variance effected both by sampling over a period τ and averaging over a period s may be obtained by combining Eqs. (2.29) and (2.31) assuming that

$$\sigma^2_{\infty,s} = \sigma^2_{\infty,\tau} + [\sigma^2_{\tau,s}]_\infty \tag{2.32}$$

In the resulting equation

$$[\sigma^2_{\tau,s}]_\infty = \sigma^2_{\infty,o} \int_0^\infty F(n)\left(\frac{\sin^2(\pi ns)}{(\pi ns)^2} - \frac{\sin^2(\pi n\tau)}{(\pi n\tau)^2}\right) dn \tag{2.33}$$

the high frequency components are damped due to the averaging time and the low frequency components are damped due to the sampling time. A spectral window which passes only intermediate frequencies results, as indicated in Fig. 2.1 (Pasquill, 1962, p. 14).

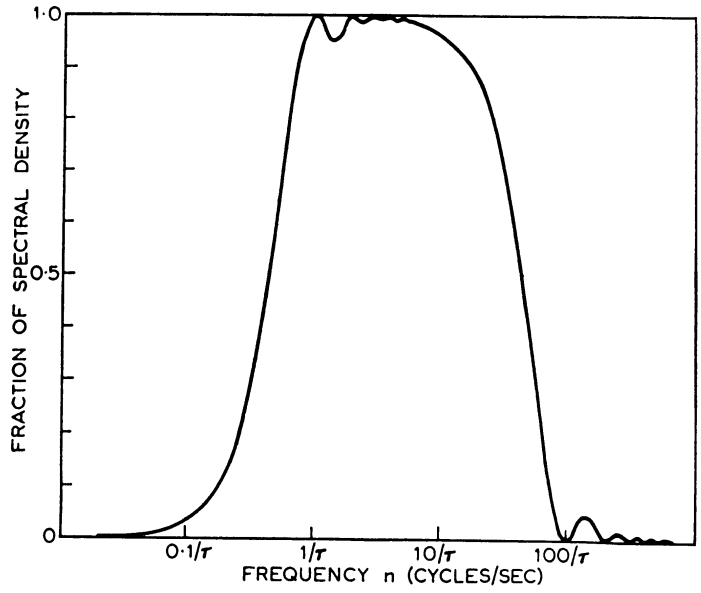

Fig. 2.1. The spectral window equivalent to a sampling-duration τ and an averaging-time $\tau/100$ (Pasquill, 1962).

An equivalent form of Eq. (2.31) applicable to the autocorrelation coefficient has been derived (Ogura, 1957) in the form

$$[R(\xi)_{\tau}]_{\infty} = \int_{o}^{\infty} F(n)\left(1 - \frac{\sin^2(\pi n\tau)}{(\pi n\tau)^2}\right)\cos 2\pi n\xi \, dn \qquad (2.34)$$

and according to Pasquill (1962) a form similar to Eq. (2.33) may be derived which includes the effects of both sampling and averaging time.

2.5 DEVELOPMENT OF A PRACTICAL STATISTICAL DIFFUSION MODEL

Equation (2.6) for the variance of the particle distribution in the direction of the wind may under certain conditions be applied to the cross wind particle distribution

$$\overline{Y^2} = 2\overline{v^2}\int_{o}^{T}\int_{o}^{t} R(\xi)\, d\xi \, dt \qquad (2.35)$$

where $R(\xi)$ applies here to the autocorrelation coefficient of velocities in the cross wind direction.

Referring to the figure below it may be seen that the order of integration may be changed without affecting the area over which the integration is performed (Kempé de Fériet, 1939)

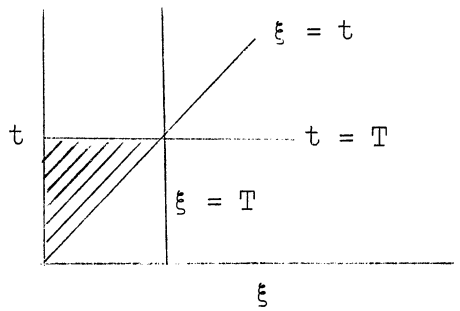

giving

$$\overline{Y^2} = 2\overline{v^2}\int_0^T \int_\xi^t R(\xi)\,d\xi\,dt$$

or

$$\overline{Y^2} = 2\overline{v^2}\int_0^T (T-\xi)R(\xi)\,d\xi \qquad (2.36)$$

an expression which could also have been written directly using the Dirichlet formula

$$\int_a^b \int_a^x F(x,y)\,dy\,dx = \int_a^b \int_y^b f(x,y)\,dx\,dy$$

An expression for $\overline{Y^2}$ in terms of the power spectrum function may be derived by substituting Eq. (2.21) for $R(\xi)$ in Eq. (2.36), reversing the order of integration and integrating (Batchelor, 1949):

$$\overline{Y^2} = \overline{v^2}\,T^2\int_0^\infty F(n)\left[\frac{\sin(\pi nT)}{(\pi nT)}\right]^2 dn \qquad (2.37)$$

Comparing Eq. (2.37) and Eq. (2.29) it is seen that the former may be written (see Orgura, 1952 (a),(b); 1959)

$$Y^2 = v^2_{\infty,s}\,T^2 \qquad (2.38)$$

In practice the emission time is not of infinite duration and a further reduction of the variance occurs, which may be expressed as (Pasquill,

1962, p. 91)

$$Y^2 = v^2_{\tau,s} T^2 \tag{2.39}$$

where the wind speed variations are now measured over a period τ and averaged over intervals s.

If the angular deviation of the wind, θ, is sufficiently small it may be written

$$\sin\theta \approx \theta = \frac{v}{\bar{u}} \tag{2.40}$$

and similarly if the angular particle displacement P is small

$$\sin P = \frac{Y}{X} \tag{2.41}$$

Substituting into Eq. (2.39) $x/\bar{u}$ for T and Eqs. (2.40) and (2.41) for $\overline{v^2_{\tau,s}}$ and $\overline{Y^2}$ respectively an expression is derived for the variance of the angular displacement of the particles in terms of the variance of the wind direction (Hay and Pasquill, 1959);

$$\sigma^2_p = \overline{\theta^2}_{\tau,s} \tag{2.42}$$

The derivation of the preceding equations follows from Taylor's theory (1921) and therefore is written in terms of Lagrangian measurements. In practice, however, the wind direction is usually measured in an Eulerian framework, i.e., at a fixed point, and therefore, because the Lagrangian and Eulerian measurements are certainly not the same (Mickelson, 1955), some means must be found for expressing $\overline{\theta^2}_{\tau,s}$ in Lagrangian terms.

Mickelson's (1955) wind tunnel study demonstrated that the Lagrangian autocorrelation coefficient as determined from the variance of the particle dispersion decayed much more slowly than the observed Eulerian autocorrelation coefficient, as illustrated by Fig. 2.2.

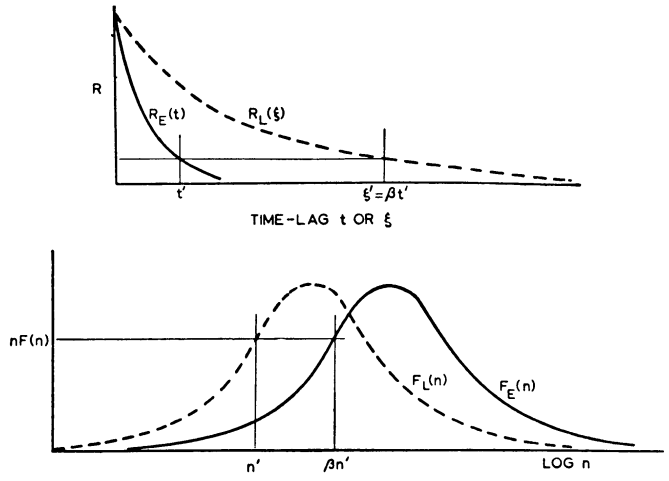

Fig. 2.2. Hypothetical scale relation between Lagrangian and Eulerian (fixed point) correlograms and spectra (Hay and Pasquill, 1959).

Hay and Pasquill (1959) present a simple hypothesis, namely, that the two autocorrelation coefficients can be equated by means of a change in scale;

$$R_L(\xi) = R_E(t) \quad \text{when} \quad \xi = \beta t \tag{2.43}$$

Thus from Eq. (2.22)

$$F_L(n) = 4\int_0^\infty R(\beta t)\cos(2\pi\beta n t)\, d\,\beta t$$

and introducing Eq. (2.43)

$$F_L(n) = \beta\left[4\int_0^\infty R_E(t)\cos(2\pi\beta n t)\, dt\right]$$

it follows that

$$F_L(n) = \beta F_E(\beta n) \tag{2.44}$$

Introducing Eq. (2.44) into (2.37)

$$\overline{Y^2} = \overline{v^2} T^2 \int_0^\infty \beta F_E(\beta n) \left[\frac{\sin(\pi nT)}{\pi nT}\right]^2 dn$$

and letting $\beta n = n$

$$\overline{Y^2} = \overline{v^2} T^2 \int_0^\infty F_E(n) \left[\frac{\sin(\pi mT/\beta)}{\pi nT/\beta}\right]^2 dn \tag{2.45}$$

From Eqs. (2.37), (2.38), and (2.45) it is seen that the transformation is accomplished by simply letting the averaging time s be

$$s = T/\beta \tag{2.46}$$

By conducting a series of diffusion experiments Hay and Pasquill (1959) were able to compare the equated terms of Eq. (2.42) for various values of s and to select the value which satisfied the equality. Substituting the s values so computed into Eq. (2.46) gave values of β ranging from 1.1 to 8.5 and averaging 4.0.

To gain some insight into the meaning of the term β consider a non-decaying eddy of radius r and constant vorticity (angular velocity ω) moving with the mean external wind speed $\bar{u}$ and consider the rate of decay of velocity correlation in the Lagrangian and Eulerian frameworks.

As the eddy passes an anemometer the correlation between the velocity measured at one time and at subsequent times will decay to

zero in a time not exceeding $r/\bar{u}$. Now define a Eulerian time scale for the eddy as

$$t_E \propto \frac{r}{\bar{u}} \tag{2.47}$$

Following the motion of an identifiable particle circulating in the eddy we find that the correlation between its velocity at one time and at subsequent times oscillates sinusoidally, initially decreasing to zero in a time $\pi/2\omega$. Define a Lagrangian time scale for the eddy as

$$t_L = \frac{\pi}{2\omega} \tag{2.48}$$

which is the time needed to execute one quarter revolution.

If one assumes that these time scales are related by a proportionality factor β^*, then

$$t_L = \beta^* t_E$$

and

$$\beta^* \propto \frac{\bar{u}}{r\omega}$$

averaged over a large number of eddies the average velocity relative to the moving eddies will be approximately equal to the root mean square value of the deviation from the mean velocity measured at a stationary point, i.e., $\overline{r\omega} \approx \sqrt{\overline{v^2}}$ and therefore

$$\beta^* \propto \frac{1}{i} \tag{2.49}$$

where i is the intensity of turbulence, $\sqrt{\overline{v^2}}/\bar{u}$.

The question then may be asked, does β^* have any relation to the β of Eq. (2.43)? Evidence that it does is offered by Wandel and

Kofoed-Hansen (1962) who, using the equilibrium theory of turbulence, show that for small i

$$\beta = \frac{\sqrt{4}}{\pi i} \tag{2.50}$$

Taking a typical value for i of 0.1 gives β the value 4.5, which is strikingly similar to the mean value 4.0 found by Hay and Pasquill (1959) from experimental data. It also explains at least some of the variability in the latter value since β must vary with the intensity of turbulence.

2.6 REMARKS ON THE APPLICATION OF STATISTICAL THEORY

Observations of the diffusion of particulates in a plume emitted from a stationary point source appear to indicate that close to the source the dispersion may be divided into two components, the spreading and the meandering (Gifford, 1959). The former is due to dispersion within the plume itself by eddies of a comparable size (the Lagrangian component) and the latter is due to the variation in wind direction at the source (the Eulerian component).

The Lagrangian component of diffusion may be predicted on the basis of statistical theory (Taylor, 1921) if the Lagrangian autocorrelation coefficient $R(\xi)$ is known and if the turbulence is homogeneous. Although the precise form of $R(\xi)$ is not known, it has been shown (Inoue, 1950) that the rate of dispersion is not sensitive to it, and therefore any reasonable distribution will be satisfactory. The second

condition above is not satisfied near the ground, and therefore the theory may only be applied at elevations well above that level.

The diffusivity, measured in the Lagrangian sense, is proportional to the time integral of $R(\xi)$ (see Eq. (2.5)) and since in atmospheric turbulence $R(\xi)$ does not decrease to zero with increasing time but remains finite, the Lagrangian component of diffusion must increase indefinitely with the downwind passage of the plume.

The Eulerian component of diffusion behaves quite differently because, as shown by Batchelor (1950), at and near the source all eddies contribute to the dispersion in proportion to their energies. With increasing distance from the source a slow reduction in the influence of the smaller eddies occurs but because most of the energy is contained in the larger eddies the rate of diffusion is virtually constant over a considerable distance downwind. This fact greatly simplifies the specification of the diffusivity in experiments which are conducted in an Eulerian framework, i.e., using a stationary array and relatively long sampling period.

In the present study one hour averages of the concentrations are computed for points located within an urban area. This means that the Eulerian framework of the preceding paragraph is applicable with the important consequence that the diffusivity can be assumed to be constant across the breadth of the city.

3. OBSERVED ATMOSPHERIC AEROSOL PROFILES

3.1 INTRODUCTION

This chapter contains examples of measured vertical aerosol profiles and discusses the significance of the profile shapes. Although it would be advantageous to confine the observations to ragweed pollen and other particles similar in size this is impractical because of the paucity of such data.

3.2 SOURCES AND SINKS FOR AEROSOLS

3.2.1 Definition of an Aerosol

Junge (1963) defines an aerosol as "dispersed solid or liquid matter suspended in air" and includes particles which range in size from $10^{-4}\mu$ to 20μ in radius.

At the lower end of the size spectrum are the small ions of radius about $6 \times 10^{-4}\mu$, composed of a loosely knit group of air molecules clustered about an ionized molecule.

Between the small ions and the true aerosols, which commence at $5 \times 10^{-3}\mu$, there is a distinct gap due to the extremely rapid rate at which very small particles coagulate.

The upper boundary of the aerosol range is subjectively established for particles of 20μ radius because larger particles settle so rapidly they cannot truly be regarded as being "suspended in air."

The radii of allergenic pollens and spores range from 1 to 50μ and thus border on the upper limit of the aerosols. To avoid semantic confusion no distinction is made between the main body of the aeroallergens and the few that exceed the 20μ limit.

3.2.2 Aerosol Sources

It is important in the interpretation of an aerosol profile to know the locations of sources and sinks because, as will be seen later the shape of the vertical profile is strongly dependent upon the rate of flux at the boundary.

Some of the more common aerosols and their sources are: sea salt particles which originate as spray in surf and from the bursting of tiny bubbles; compounds containing sulphur and other elements of volcanic origin; the decay products of radon which emanates from the land masses; wind blown clay and dusts from arid regions; smokes from combustion processes; micrometeorites from outer space; hydrocarbons from the burning and refining of fuels, from bursting bubbles over the sea and from emanations from vegetation; and pollen and spores from the flora of land regions.

Since a considerable portion of the discussion to follow concerns steady state profiles it is of interest to note that with the exception of micrometeorites the source regions above have marked areal variations in strength and for the most part are not of global scale.

3.2.3 Removal of Aerosols from the Atmosphere

An aerosol may be removed from the atmosphere by evaporation, by deposition in precipitation and by dry deposition as indicated in Fig. 3.1. The number of particles within certain size ranges may also be changed by coagulation.

Coagulation, effective only for particles of radius less than 0.1μ, does not remove particles but simply shifts the particle size spectrum toward larger radii. The rate of coagulation can be predicted using Smoluchowski's law (Green and Lane, 1957, p. 129).

Precipitation removes aerosols by two processes, rainout and washout. The former operates in two distinct ways: 1. Aerosols are utilized as condensation nucleii and 2. Aerosols are attached to cloud droplets by the action of molecular diffusion. The former is effective over a broad range of particle sizes as indicated in Fig. 3.1 while the latter is of consequence only in the 0.1 to 1.0μ range. Washout, in which aerosols are intercepted by falling precipitation, is effective only for particles exceeding 1μ in radius.

Dry deposition may occur through gravitational settling, inertial impaction, electrical attraction, thermal pressures, molecular diffusion, radiation pressure, etc. Even gases are found to have a sizable deposition rate if the sorption is sufficiently strong (Chamberlain, 1956). Only gravitational settling and inertial impacting are of significance for particles larger than 1μ such as the pollen and spores (Green and Lane, 1957, Chapt. 6; Owen, 1960, p. 8).

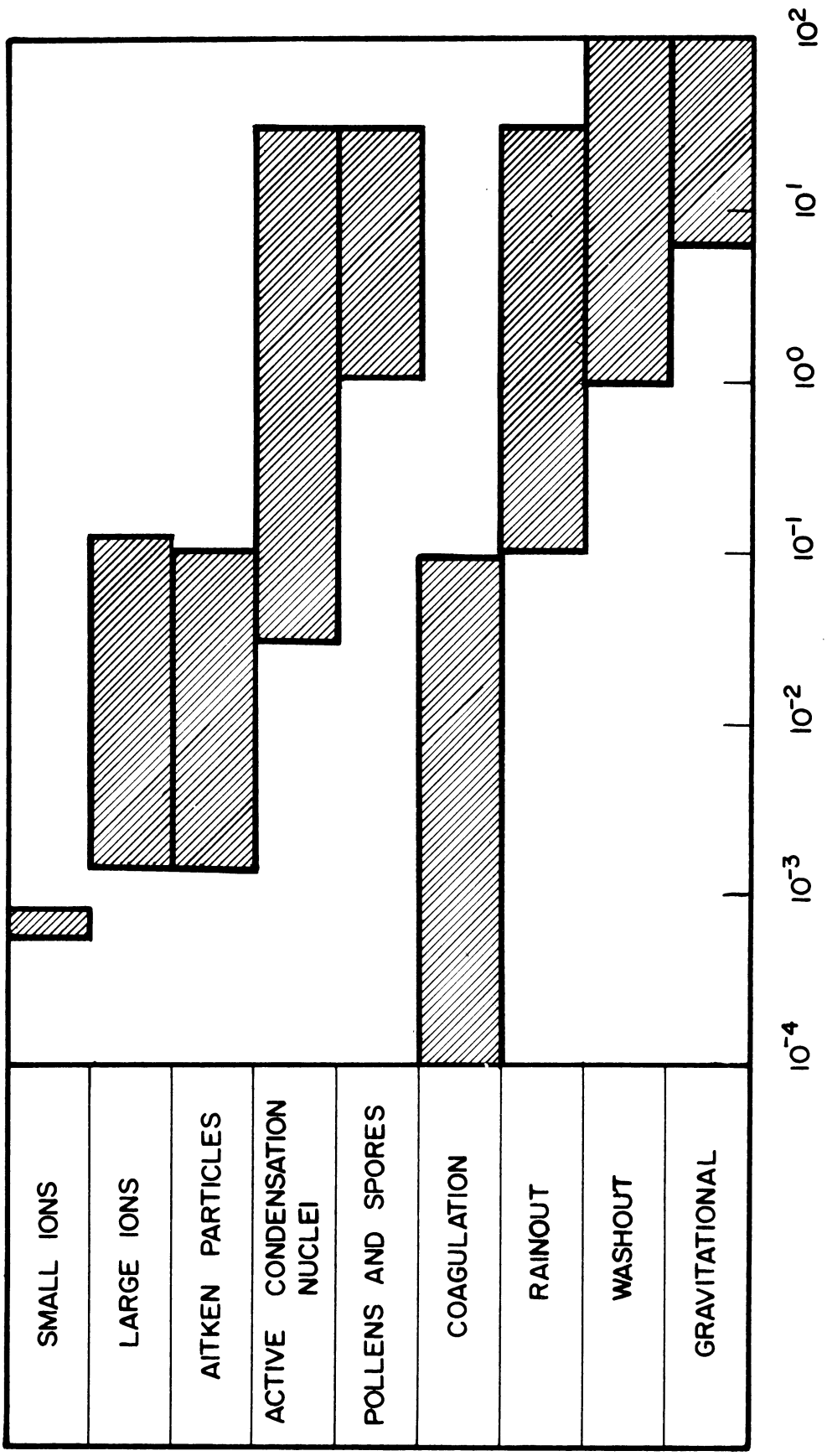

Fig. 3.1. Size range and effective removal mechanism for various aerosol types.

3.3 CONSERVATIVE PROPERTIES OF CONCENTRATION AND MIXING RATIO

Suppose a given quantity of an aerosol having zero settling velocity is released into the atmosphere and thoroughly mixed between two impervious reflecting surfaces exemplified by the ground and the tropopause. Suppose further that the atmospheric flow is non-divergent and the aerosol incompressible. Then, the mixing ratio (grams of aerosol per gram of dry air) will have to be constant within the layer. Under the same conditions what will the shape of the concentration profile be?

Given a steady state mixing ratio X, the concentration at levels Z_o and Z is

$$\chi_o = \frac{X}{V_o} \quad \text{and} \quad \chi = \frac{X}{V} \tag{3.1}$$

where V_o and V are the volumes of one gram of air at the two heights. Invoking the adiabatic law the ratio of the concentration becomes

$$\frac{\chi}{\chi_o} = \left(\frac{P}{P_o}\right)^{1/\gamma} \tag{3.2}$$

where γ is the ratio of the specific heats, 1.4.

Assuming a linear decrease of temperature with height

$$T = T_o - \alpha z$$

where subscript zero signifies measurement at ground level and α is the lapse rate, and introducing the hydrostatic assumption, Eq. (3.2) can be written

$$\chi = \chi_o\left(\frac{T_o-\alpha z}{T_o}\right)^{g/\alpha R\gamma} \tag{3.3}$$

showing that the concentration should decrease exponentially with height.

Substituting typical values into Eq. (3.3), say T_o = 293°K and α = 5°C/km, the exponent becomes about 5 and the ratio χ/χ_o becomes 0.92 at 1 km and 0.70 at 10 km. From this it is concluded that below 1 km the concentration and mixing ratio can be regarded as nearly proportional whereas above that level they cannot.

In future sections the concentration will be assumed to be a conservative property for vertical motions unless otherwise stated because the region under consideration will be limited to the lower one or two kilometers.

3.4 SEMI-STEADY PROFILES

3.4.1 Semi-Steady Profiles of Non-Settling Particles

Over an aerosol source region a steady state profile can only be achieved if some removal mechanism is present which can exactly compensate for the additions by the source. Since this balance seldom occurs in nature, true steady state profiles are rarely if ever observed. If, on the other hand the rate at which the concentration at any level changes with time is small compared to the flux through that level, the profile is termed semi-steady, a condition frequently achieved in the atmosphere.

The equation of continuity in the case of a semi-steady profile can be written

$$\frac{\partial}{\partial z}\left(K(Z)\,\frac{\partial \chi}{\partial z}\right) \approx 0 \qquad (3.4)$$

Integrating once with respect to height (from ℓ to z)

$$K(z)\,\frac{\partial \chi}{\partial z} \approx -P(\ell) \qquad (3.5)$$

where $-P(\ell)$ is the flux at the lower boundary, and integrating a second time for two assumed distributions of K,

1. for K constant

$$\chi(z) = \chi(\ell) - P(\ell)\,z/K \qquad (3.6)$$

2. for $K(z) = K(\ell)\,z/\ell$, a linear function of height

$$\chi(z) = \chi(\ell) - \frac{\ell P(\ell)}{K(\ell)}\,\ell n\, z/\ell \qquad (3.7)$$

An absorbing rather than an emitting surface at the lower boundary simply leads to a reversal in sign of the second term of Eqs. (3.6) and (3.7).

The following conclusions may be drawn from Eqs. (3.6) and (3.7); namely

1. Over an emitting surface the profile will have a negative slope and the reverse will be true over an absorbing surface.

2. In the absence of emission or absorption the steady profile will have a zero slope.

3. The semi-steady profile is determined by the diffusivity profile.

3.4.2 Semi-Steady Profiles of Settling Particles

Suppose the aerosol particles have a settling speed -q, where the negative sign indicates a downward velocity. It follows that the equation of continuity for a semi-steady profile can be written

$$\frac{\partial}{\partial z}\left(K(z)\ \frac{\partial \chi}{\partial z} + q\chi\right) \approx 0 \qquad (3.8)$$

A single integration of Eq. (3.8) between ℓ and z yields

$$K(z)\ \frac{\partial \chi}{\partial z} + q\chi = -P(\ell) \qquad (3.9)$$

and a second integration gives

1. for K constant

$$\chi(z) = \left[\chi(\ell) + \frac{P(\ell)}{q}\right]\exp\left(-\frac{q(z-\ell)}{K}\right) - \frac{P(\ell)}{q} \qquad (3.10)$$

2. for $K(z) = K(\ell)\,z/\ell$

$$\chi(z) = \left[\chi(\ell) + \frac{P(\ell)}{q}\right]\left(\frac{z}{\ell}\right)^{-q\ell/K(\ell)} - \frac{P(\ell)}{q} \qquad (3.11)$$

From the terms in square brackets in Eqs. (3.10) and (3.11) it can be seen that the slope of the profile depends upon whether the surface flux $P(\ell)$ is greater than, less than or equal to the gravitational settling rate $q\cdot\chi(\ell)$.

In an attempt to compute the eddy diffusivity from the aerosol profile many authors (see Section 3.7) have invoked the zero flux condition, but have made the error of not carrying the same reasoning to

the lower boundary. If $P(\ell)$ is zero then Eqs. (3.6) and (3.7) for which q is zero reduce to constant profiles from which the diffusivity cannot be computed. When q is not zero the assumption of zero surface flux is equivalent to saying that emission is exactly balanced by the loss, a condition not often attained due to the inhomogeneity of the sources.

If, however, the zero flux boundary condition can be satisfied then the diffusivity may be computed from equations of the types (3.10) and (3.11).

$$K = \frac{q(z_2-z_1)}{\ell n\left(\frac{\chi(z_1)}{\chi(z_2)}\right)} \tag{3.12}$$

and

$$K(z_2) = \frac{q\ell\ \ell n\left(\frac{z_2}{z_1}\right)}{\ell n\left(\frac{\chi(z_1)}{\chi(z_2)}\right)} \cdot \left(\frac{z_2}{z_1}\right) \tag{3.13}$$

respectively. The assumption usually made is that K in the region of interest is approximately constant and that Eq. (3.12) can be adopted. One unfortunate aspect of this method, as will be seen later, is that its very simplicity has led many workers to attempt to fit all data to the presumed exponential form (see Section 3.7).

3.5 THE EFFECT ON AEROSOL PROFILES OF SUBSIDENCE AND INVERSIONS

One assumption often made in micrometeorological studies is that the average vertical velocity is zero. For short term diffusion studies in the highly turbulent region near the ground this assumption is reasonable, but for large scale studies at higher elevations it is not.

Each high and low pressure area on a sea level synoptic weather map is a region of atmospheric descent and ascent respectively. The slow subsidence in anticyclones effectively limits the upward diffusion of aerosols, producing what is commonly observed as a "smoke horizon." In Michigan in August a typical smoke horizon level is 2 km.

Subsidence also inhibits the vertical transport of aerosols by creating stable layers or so-called subsidence inversions. Turbulence in these regions may be damped to such an extent that the diffusivity is virtually reduced to zero.

3.6 THE EFFECT ON AEROSOL PROFILES OF NON-STEADY SOURCES AND ADVECTION

The combination of strong wind shear at low levels in the atmosphere and inhomogeneities in surface source strength leads to profile abnormalities which would not occur with either effect alone. For example, observed profiles at great distances from a source rarely exhibit a constant concentration with height as one might expect, but rather exhibit layers of high and low concentration reflecting the different source regions of air at those levels.

One must be extremely cautious in drawing conclusions regarding flux conditions at the surface from profile data because shearing effects are most pronounced near the ground. For example, a profile observed to have a positive slope might suggest that the ground is receiving the aerosol at a rate faster than the gravitational settling rate, whereas in truth it might simply result from an unsteady condition in which the aerosol is being advected rapidly aloft in large concentrations.

3.7 OBSERVATIONS OF AEROSOL PROFILES

3.7.1 Introduction

Historically, the measurement of aerosol profiles followed closely the discoveries which made those observations possible. First to be studied were the fungal spores and bacteria since they could be cultured and observed without the aid of a microscope. Later, as microscopic and sampling techniques improved, finer particles were identified and their distributions measured. Full reviews of this topic have been given by Gregory (1961, Chapts. 1 and 10) and Junge (1963).

3.7.2 Spore Profiles

The first evidence that spore concentrations decreased with increasing elevation was presented by Louis Pasteur (1861) who opened sealed culture flasks at various elevations in the Alps and found a contamination rate of 40% on the first plateau of the Jura mountains,

25% at 850 m and 5% at 2000 m.

Other investigators using towers, kites and balloons observed a confusing variety of bacteria and spore profiles (Blackley, 1873) but in general found a decrease of concentration with elevation. At a greater height the air was found to be spore free (Hahn, 1909).

The use of aircraft permitted the extension of profile observations to greater heights (Stakman, 1923). These observations were of great value at the time in identifying viable pathogens aloft and roughly indicating the levels at which they could be found and their probable range of travel. Unfortunately they were basically qualitative in nature and unrelated to pertinent meteorological variables.

More quantitative investigations of spore profiles were undertaken for wheat stem rust by Peturson (1931), yellow leaf rust by Hubert (1932), and tree pollen by Rempe (1937) (see Gregory, 1961, p. 137).

Hubert's profile (Fig. 3.2) exhibits a linear decrease of concentration with height as does the upper portion of the averaged daytime observations of Rempe. These curves correspond to the semi-steady profile (Eq. (3.6)) if K is assumed constant and the fall speed q is negligible compared to K. Equation (3.10) may also be approximated by a linear function of height when $K \gg qz$.

A simple example will illustrate the method of computing the diffusivity from such profile measurements. Referring to Hubert's profile

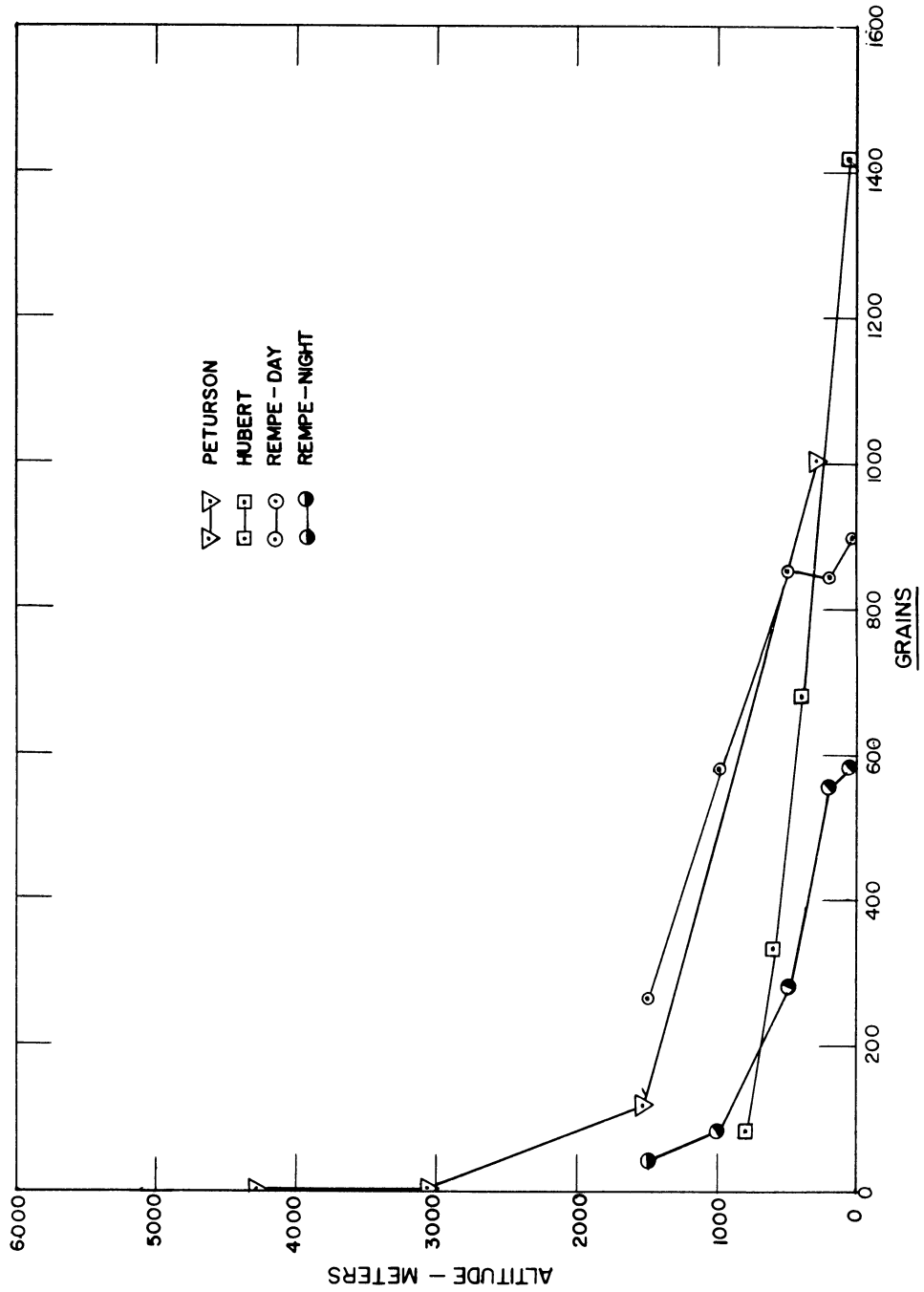

Fig. 3.2. Spore profiles sampled by aircraft as follows:

1. Wheat stem rust (Peturson, 1931)
2. Yellow leaf rust of wheat (Hubert, 1932)
3. Tree pollen (Rempe 1937).

(Fig. 3.2), first suppose that q is negligible, K is constant and that the spores have been emitted at a steady rate for 4 hours. The computations are as follows:

$$P(\ell) = \frac{\text{total spore load}}{\text{emission time}} \approx 40 \frac{\text{grains m sec}^{-1}}{\text{unspecified vol.}}$$

where the unit of concentration is unspecified. Then

$$K = \frac{P(\ell)\, z}{\chi(\ell) - \chi(z)} \approx 23 \text{ m}^2\text{sec}^{-1}$$

On the other hand if $P(\ell)$ is equated to zero and Eq. (3.10) used, assuming $K \gg qz$ and $q = 0.03$ m sec^{-1}

$$K = \frac{q(z-\ell)}{1 - \frac{\chi(z)}{\chi(\ell)}} \approx 24 \text{ m}^2\text{sec}^{-1}$$

Under the assumption that Hubert's curve of Fig. 3.2 is exponential rather than linear and that the surface flux is zero Gregory (1961, p. 137) computes K to be 1.5 m^{2}sec^{-1}, a rather low value for daytime observations in summer.

3.7.3 Condensation Nuclei Profiles

The distributions of larger particles measured by a number of investigators have been displayed graphically by Penndorf (1954) in an effort to substantiate Eq. (3.12). Penndorf's graph for the light scattering coefficient data of Krug (1949) is shown in Fig. 3.3. The same data together with measurements of condensation nuclei concentration (Wigand, 1919), when graphed as log χ versus log z in Fig. 3.4,

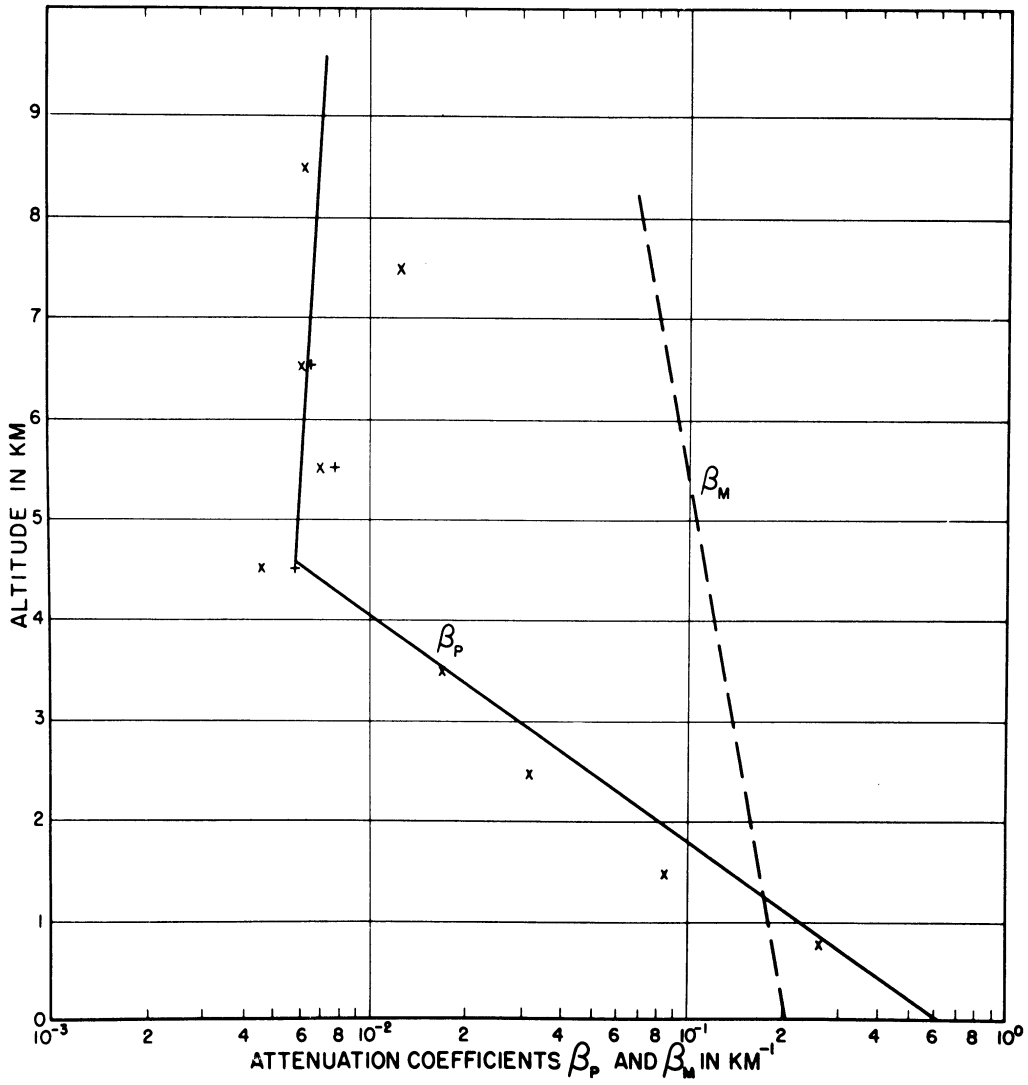

Fig. 3.3. Computed vertical distribution of the attenuation coefficients β_M and β_P from Krug's observations. β_M is the attenuation coefficient for molecules; β_P is the attenuation coefficient for Mie particles (Penndorf, 1954).

show that the data conform much more reasonably to a power law relationship of the type given by Eq. (3.13).

Profiles of large chloride particles observed by Lodge (1955) on the windward and leeward sides of Puerto Rico are presented in Fig. 3.5. The fall speeds of the particles under consideration (radius less than 6μ for the most part) are negligible compared to the rate of vertical eddy diffusion in the lower few thousand feet and therefore a semi-steady profile if such does exist must satisfy Eq. (3.4).

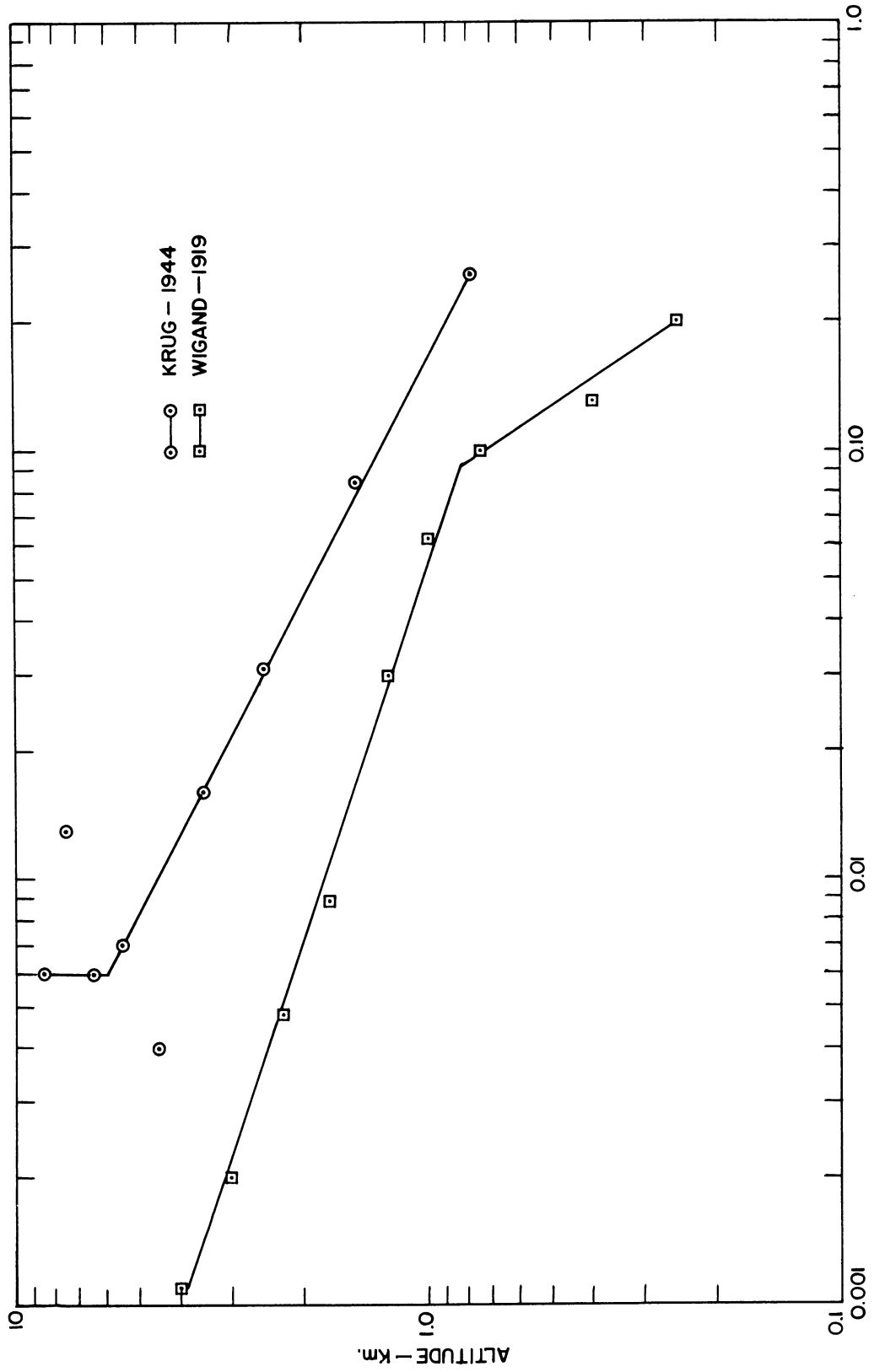

Fig. 3.4. Vertical profiles of the Mie light scattering coefficients (Krug, 1949) and condensation nuclei concentration (Wigand, 1919).

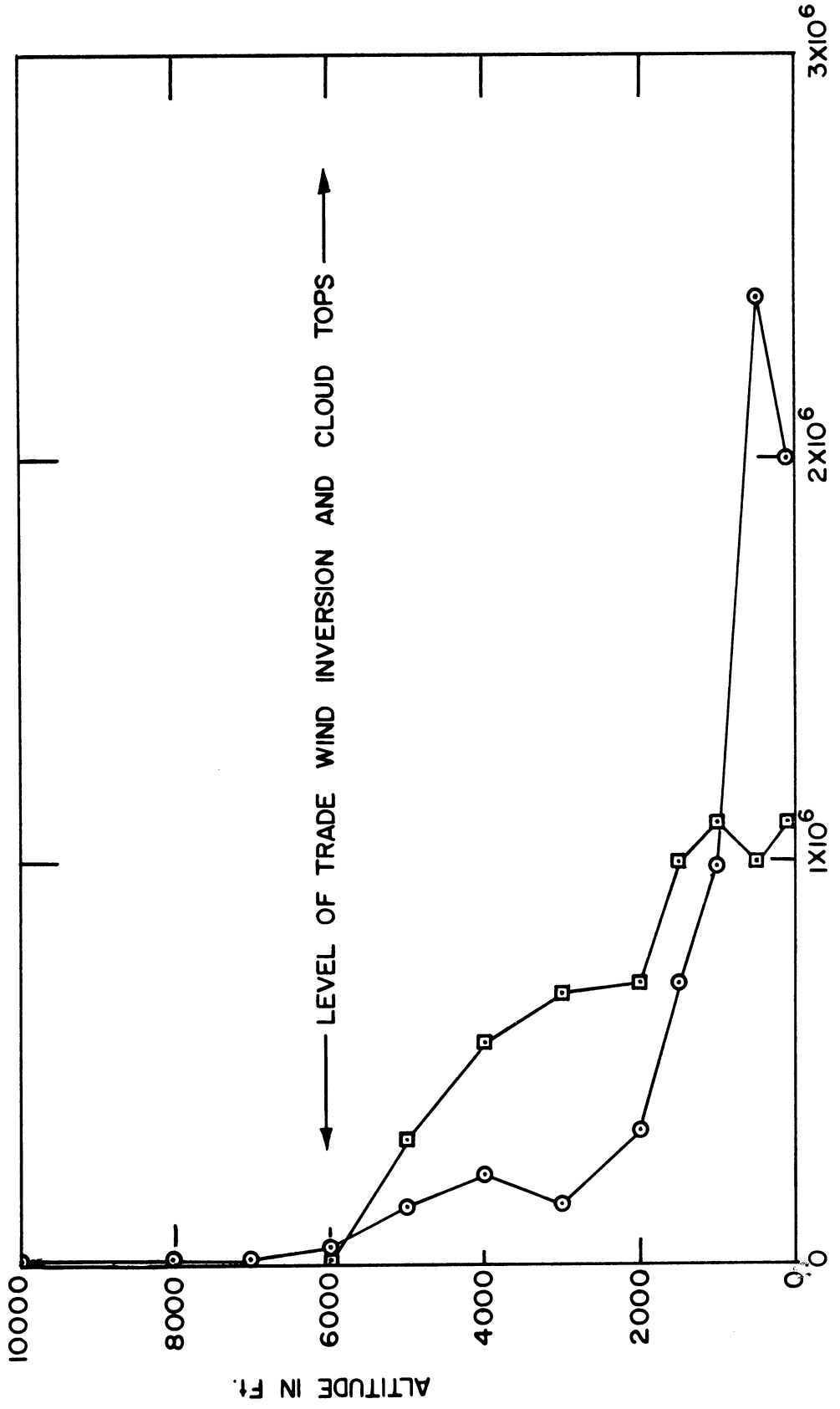

Fig. 3.5. Vertical profiles of chloride particle concentration over Puerto Rico; ⊙ windward side, ⊡ leeward side (Lodge, 1952).

Unfortunately, the exact distribution of K cannot be inferred from the profiles because the scatter in the data allows many interpretations.

Both profiles show evidence of discontinuities caused by variations in source strength or by advection from different source regions. The leeward curve is most interesting in this respect because after a traverse of 100 mi. or more across a land surface one would expect a more or less constant concentration of salt nuclei with height. The curve suggests that the air on the leeward side of Puerto Rico really did not originate on the windward side, but is of local origin, having experienced at least two short periods of residence over a source free area. Unfortunately, Lodge did not have the data necessary to make air trajectory studies.

Byers et al. (1955) have published three sets of chloride particle profiles observed over central Illinois (Fig. 3.6). Assuming that the particles are of oceanic origin one would expect that a steady profile would exhibit either a constant concentration with height or an increasing concentration with height depending on whether the ground is a neutral or an absorbing surface respectively. Since all the profiles indicate an increase of concentration with height it is tempting to assume as Byers has done, that the ground is absorbing the particles at a rate faster than could be accounted for by their gravitational settling speed.

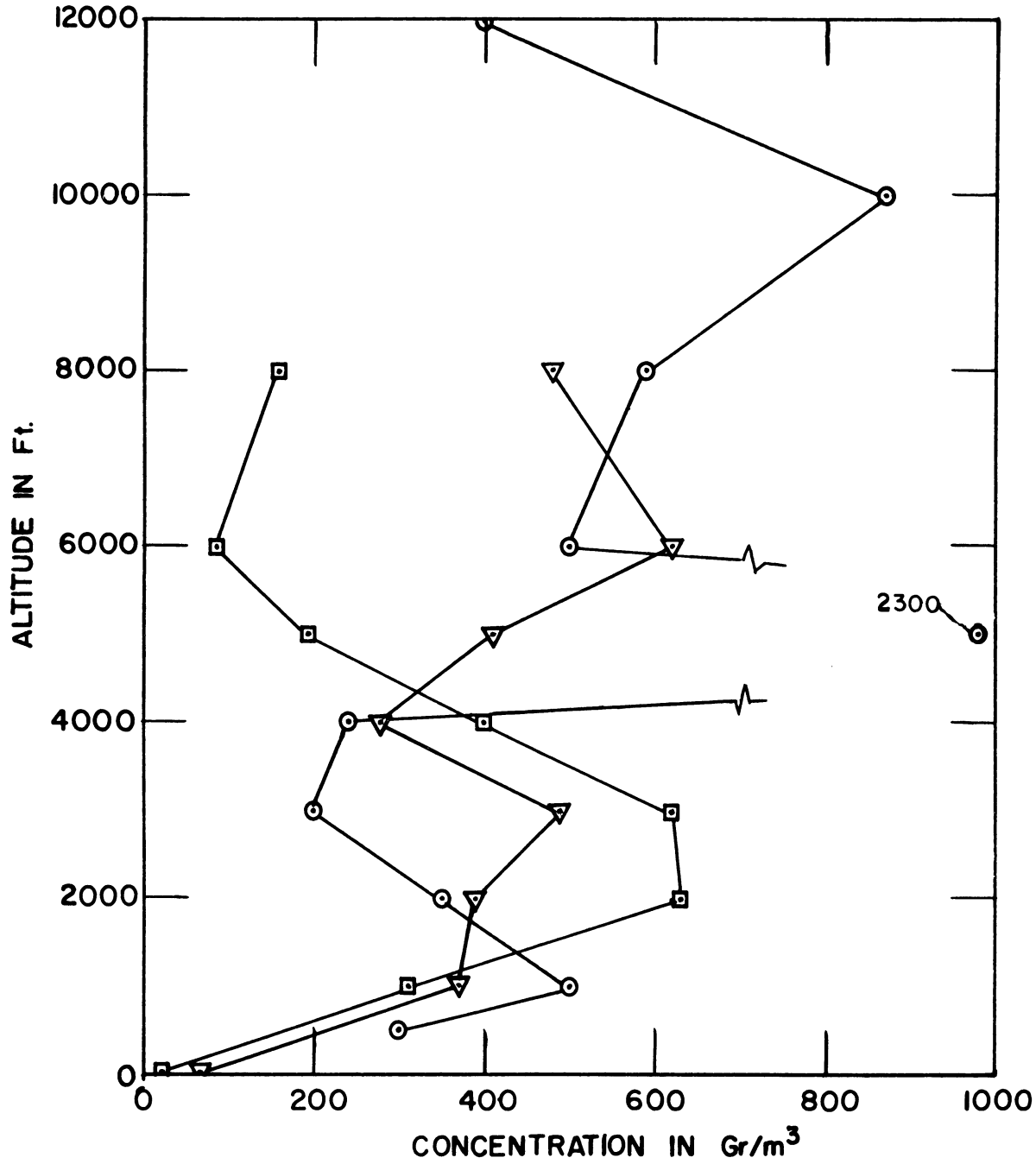

Fig. 3.6. Vertical profiles of chloride particle concentration over central Illinois; June 11, 1954, November 5, 1954, November 10, 1954 (Byers, et al., 1955).

Junge (1963 p. 321) has questioned Byers' conclusion on the basis of observations which, except in precipitation areas, show little reduction in the salt nuclei content of the air as it passes over the

continents. Ericksson (1959, 1960), however, shows from measurements of chlorine in rainfall and in runoff that only one third of the total chlorine deposition can be attributed to rainfall.

The overall complexity of the profiles certainly cannot be explained without a detailed knowledge of the physical processes which have affected the air at each level. Other factors which could have influenced the profile such as the possible lack of efficiency of the ground based samplers, the presence of chlorides in industrial pollution, the creation of giant chloride nuclei by coagulation of smaller particles in cloud droplets and differential advection may explain all the anomalies in the curves. Until such an explanation is successfully made, however, the possibility of surface absorption exceeding the gravitational rate must be borne in mind.

3.7.4 Profiles of Gaseous Constituents of the Atmosphere

The vertical distribution of water vapor in the atmosphere, although the most frequently measured, is also the most complex due to condensation and evaporation processes. Therefore, no water vapor profiles are discussed.

One would expect numerous profiles of carbon dioxide to be available because of its basic importance to plant growth and to the heat balance of the globe, but except for a few profiles close to the ground nothing appears in the literature.

Tropospheric profiles of ozone made by Regener (Junge, 1963, p. 49) under conditions of strong vertical mixing indicated a constant mixing ratio with height, suggesting that the downward flux from the stratosphere and loss to the ground were sufficiently small on these occasions to be neglected. A profile of this type is shown in Fig. 3.7 (Hering, 1964). Most other profiles such as the one illustrated in Fig. 3.8 indicate a slow increase in mixing ratio with height as would be expected (Junge, 1963).

Profile data for other gases are rare. Such observations as have been made were usually performed at ground level by the observation of light transmission through the atmosphere. The resulting profiles generally indicate a constant mixing ratio with height but are too crude to determine weak gradients (see Goldberg and Muelly, 1953).

Since many gases, CH_4, CO, N_2O, etc., are emitted at the earth's surface in relatively restricted areas, and absorbed by the surface or deposited in precipitation elsewhere, one would expect to find decreasing concentrations with height over the sources and the converse over the sinks. Such profiles might permit the use of Eq. (3.4) and the computation of the eddy diffusivity, but better observations will be required before this can be accomplished.

Radon gas is emitted continuously into the atmosphere from the land masses of the earth. Both radon and its daughter decay products make excellent atmospheric tracers, although modelling is complicated by their radioactive decay.

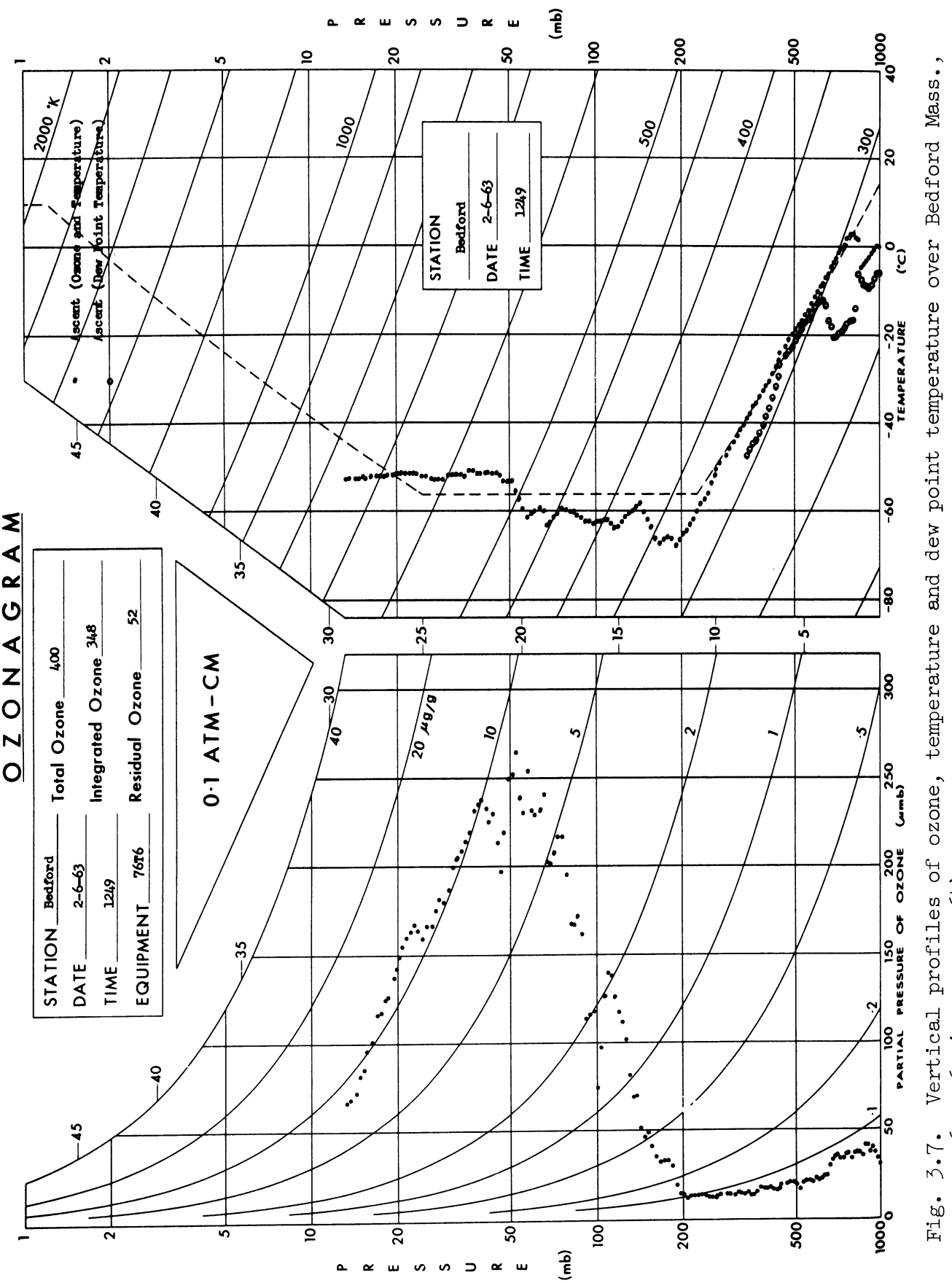

Fig. 3.7. Vertical profiles of ozone, temperature and dew point temperature over Bedford Mass., January 6, 1963 (Hering, 1964).

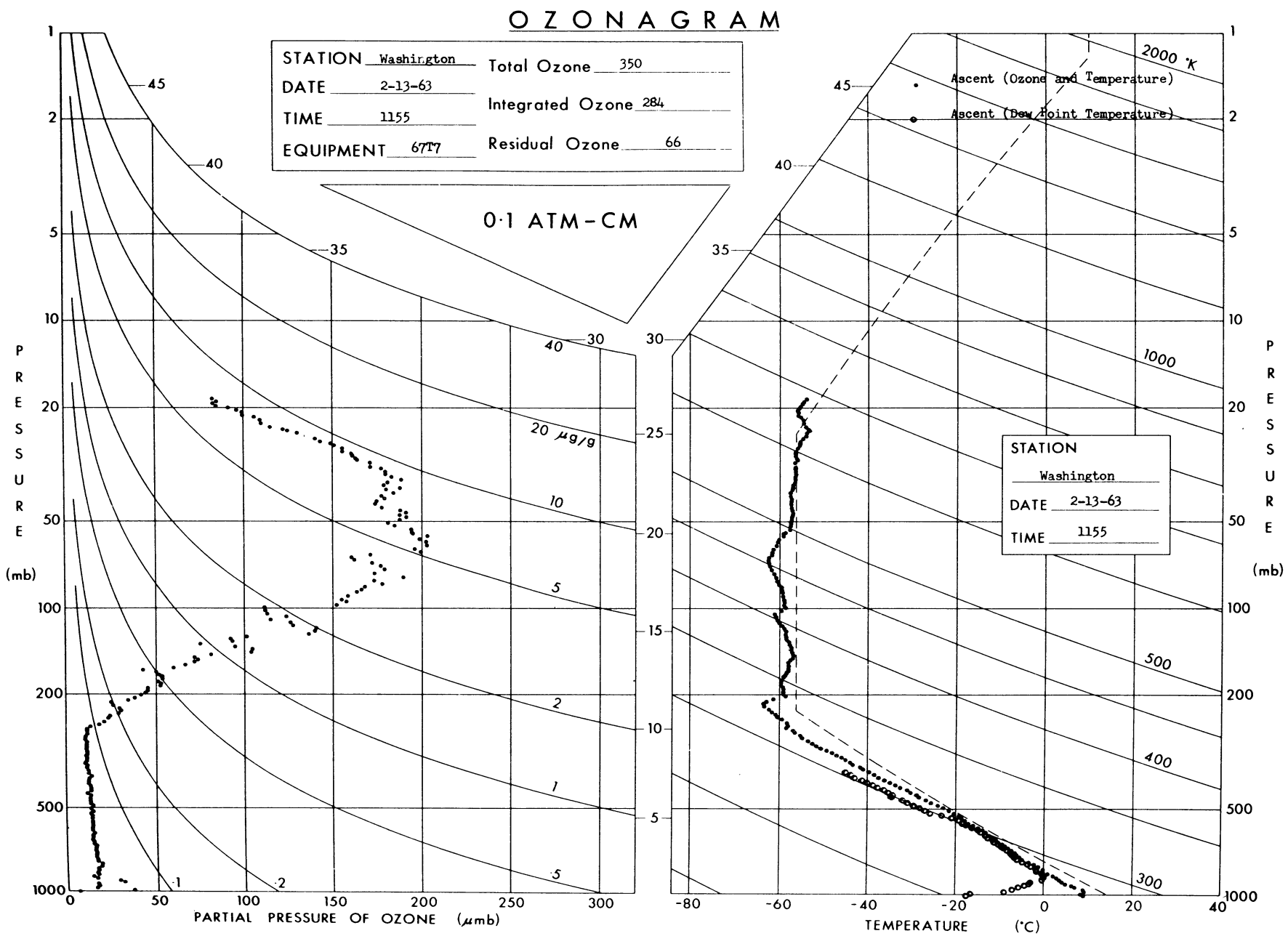

Fig. 3.8. Vertical profiles of ozone, temperature and dew point temperature over Washington D.C., January 13, 1963 (Hering, 1964).

Jacobi and Andre (1963) have attempted to measure the diffusivity using radon gas concentration profiles. Their method was to solve an assumed mathematical model using various diffusivity distributions and hence to select the distribution leading to the best fit to the radon profile. Unfortunately this technique does not lead to accurate distributions of diffusivity although certain gross features can be determined.

3.7.5 Summary

Detailed profile measurements in the atmosphere are extremely rare and those which are available may be used to infer the value of the diffusivity only with the greatest caution. Few aerosols have uniform source regions and therefore advective effects must always be considered.

4. SOLUTIONS TO THE PARABOLIC DIFFUSION EQUATIONS

4.1 INTRODUCTION

The prediction of ragweed pollen concentration in an unsteady atmosphere over a non-homogeneous surface of variable emission and absorption characteristics requires an unsteady three-dimensional model. Existing numerical techniques are sufficient to permit solution of the equations describing such a model but the computational time and storage capacity required would be prohibitive. It has been necessary therefore to simplify the model first, by assuming that conditions are steady in time and second, by assuming no wind direction shear.

In this chapter a steady three-dimensional model is proposed which is suitable for computing the ragweed pollen concentration over a source free area lying within a homogeneous source. The assumptions required in the development of the model are carefully examined and detailed methods of solution given. Solutions are also given for a slightly modified version of the same model which permits computations of pollen concentration downwind of a small pollen source to be more.

A method for solving the steady two-dimensional diffusion equation is given. This model may be used to compare computed and observed pollen profiles downwind of a source region of sufficient cross wind extent that the lateral component of diffusion is negligible.

A detailed method for solving the unsteady one-dimensional equation is also given. This model is of value in computing pollen pro-

file over source regions of unlimited extent. Such profiles are used as initial conditions on the upwind boundary of the ragweed free area mentioned above.

4.2 VALIDITY OF THE EXCHANGE COEFFICIENT HYPOTHESIS

4.2.1 The Estimation of the Flux

The flux of an entity of concentration χ across a point $x = h$ in a one-dimensional space is equal to

$$f(h) = \overline{u(h)\chi(h)} \tag{4.1}$$

where u is the wind speed, assumed equal to the particle speed. The terms on the right of Eq. (4.1) when expanded in a Maclaurin series yield the equations

$$\begin{aligned} \chi(h) &= \chi(o) - h\chi'(o) - \frac{h^2}{2!}\chi''(o) \ldots \\ u(h) &= u(o) - hu'(o) - \frac{h^2}{2!}u''(o) \ldots \end{aligned} \tag{4.2}$$

where the primes denote derivatives with regard to x. If it is assumed that the average wind speed is constant with respect to x and the gradient of concentration varies linearly with x then the flux of the quantity at the point $x = h$ is

$$f(h) = \overline{u(o)[\chi(o) - h\chi'(o)]} \tag{4.3}$$

The applicability under natural atmospheric conditions of the assumptions involved in the derivation of Eq. (4.3) are considered in the following paragraphs.

Over normal terrain the presence of small fields, of woods and of varied agricultural cover leads to rapid variations in both meteorological parameters and ragweed pollen source strength. Viewed on the small scale neither assumption of the paragraph above is tenable, but they are on the broad scale, however, because the higher order terms become unimportant.

To illustrate by means of a crude example, assume that the standard deviation of the angular spread of particles from a point source is 12° (Pasquill, 1962, p. 142). Then for two point sources separated by a distance r the linear standard deviation of the particle positions will become r/2 at a distance approximately 2.5r downwind and no resolution of the sources in terms of the particle distribution will be possible. If at this distance the distribution is defined as being uniform, then the pollen concentration from fields separated by four tenths of a mile will become uniform one mile downwind. Indeed, other sources upwind of the fields in question also contribute significantly to the pollen concentration and will enhance the uniformity defined above.

Support for the contention that ragweed pollen concentration gradients are reasonably smooth at points removed from the source is provided by the results of automobile sampling throughout Ann Arbor and the surrounding countryside in the summer of 1958. The standard deviation of pollen concentration in the city was found to be small (Sheldon and Hewson, 1962).

The assumption of linearity in the pollen concentration gradient is weakest in the vicinity of discontinuities in source strength and near the ground over a source region. To minimize errors, special procedures are adopted in these areas as discussed in a later section.

4.2.2 Flux Components in Three Dimensions

Equation (4.3) may be put into a more familiar form by removing the transport term (the first term inside the brackets) and substituting the diffusivity, K_x for U(o)h (see Eq. (2.9)) to obtain

$$- f_x = K_x \chi \tag{4.4}$$

In three dimensions the retention of only the linear terms in the Maclaurin series expansion of χ leads to the set of equations

$$\left.\begin{aligned} - f_x &= K_{xx} \frac{\partial \chi}{\partial x} + K_{xy} \frac{\partial \chi}{\partial y} + K_{xz} \frac{\partial \chi}{\partial z} \\ - f_y &= K_{yx} \frac{\partial \chi}{\partial x} + K_{yy} \frac{\partial \chi}{\partial y} + K_{yz} \frac{\partial \chi}{\partial z} \\ - f_z &= K_{zx} \frac{\partial \chi}{\partial x} + K_{zy} \frac{\partial \chi}{\partial y} + K_{zz} \frac{\partial \chi}{\partial z} \end{aligned}\right\} \tag{4.5}$$

where $K_{xy}\partial\chi/\partial y$ represents the transport in the x direction due to the component of concentration gradient in the y direction (Carslaw and Jaeger, 1959, p. 38).

Consider for the moment an orthorhombic crystal, one having three unequal axes at right angles to one another. If diffusivities in the crystal are aligned with these axes, called the principal axes of diffusion, then all the off diagonal elements of the matrix in Eq. (4.5)

vanish (Carslaw and Jaeger, 1959, p. 40).

Similarly, in the atmosphere, if the height dependence of the wind direction is neglected, axes oriented parallel to the wind, horizontally cross wind and vertically constitute the principal axes of diffusion and only the diagonal elements of Eq. (4.5) need be considered; i.e.,

$$\mathbb{F} = i K_x \frac{\partial \chi}{\partial x} + j K_y \frac{\partial \chi}{\partial y} + k K_z \frac{\partial \chi}{\partial z} \qquad (4.6)$$

where $\mathbb{F}$ is the vector flux.

4.3 THE FULL PARABOLIC DIFFUSION EQUATION

4.3.1 Derivation

In one dimension the equation of continuity for χ can be written (see Crank, 1956, p. 5)

$$\frac{d\chi}{dt} = \frac{\partial \chi}{\partial t} + u \frac{\partial \chi}{\partial x} = \frac{\partial}{\partial x}\left(K_x \frac{\partial \chi}{\partial x}\right) \qquad (4.7)$$

where linearity in the derivatives is obtained by taking only the first term in the Maclaurin series expansion. In three dimensions the total change of concentration within a parcel of air is equal to the divergence of the flux, i.e.,

$$\frac{d\chi}{dt} = \nabla \cdot \mathbb{F}$$

or

$$\underset{①}{\frac{\partial \chi}{\partial t}} + \underset{②}{u(z) \frac{\partial \chi}{\partial x}} + \underset{③}{v(z) \frac{\partial \chi}{\partial y}} + \underset{④}{w(z) \frac{\partial \chi}{\partial z}} = \underset{⑤}{\frac{\partial}{\partial x}\left(K_x \frac{\partial \chi}{\partial x}\right)} + \underset{⑥}{\frac{\partial}{\partial y}\left(K_y \frac{\partial \chi}{\partial y}\right)} + \underset{⑦}{\frac{\partial}{\partial z}\left(K_z \frac{\partial \chi}{\partial z}\right)} \qquad (4.8)$$

A number of assumptions, normally introduced to reduce Eq. (4.8) to a more tractable form, will be discussed in the following paragraphs. It should be noted that one assumption has already been made; namely, that the mean wind vector is not a function of the horizontal coordinates.

4.3.2 The Steady State Assumption

Term 1 of Eq. (4.8) may be equated to zero if at a point in space the pollen concentration is invariant in time implying that the wind, diffusivity and ground level pollen flux are independent of time. That they are not is obvious, and it remains to estimate the magnitude of the error involved in the assumption of a steady state.

G. I. Taylor (1935) has shown from wind tunnel observations that the dispersion occurring between a fixed aerosol emitter and a fixed sampling array is independent of the wind speed. This means the diffusivity produced by mechanical mixing is directly proportional to wind speed.

In the atmosphere this relationship between wind speed and diffusivity is not exact because the characteristic roughness of the surface may be a function of wind speed. On the basis of Taylors observations it is reasonable to expect, however, that temporal changes in wind speed do not introduce a serious error into the solution of the steady diffusion equations.

The diffusivity is sensitive not only to the wind speed, but also to the thermal stratification. The latter changes most rapidly during two short periods, in the early morning and late afternoon, particularly during clear weather in summer (see Fig. 4.1 taken from App. C where a more thorough discussion of the figure is given).

The rate of ragweed pollen emission on a clear day increases rapidly as soon as the dew dries from the upper portions of the ragweed plant, reaches a peak roughly an hour and a half later, then decreases more gradually during the latter half of the morning and the early afternoon as indicated in Fig. 4.2 taken from Progress Report No. 4, Atmospheric Pollution by Aeroallergens (Sheldon and Hewson, 1960).

If small distances and short periods are considered the error due to the steady state assumption will be small. For example, in a wind of 4 m sec^{-1} air will traverse an area 1 km in width in 4 min, a period sufficiently short that pollen emission and diffusivity may be regarded as constant. If, however, the area under consideration is a city the size of Ann Arbor, roughly 10 km in width, the steady state assumption is less tenable, and for areas larger than 10 km in width, can no longer be justified.

The presence in the lower atmosphere of strong vertical wind shear causes changes in the concentration profile over one area to be carried downwind over another area more rapidly at a high elevation than

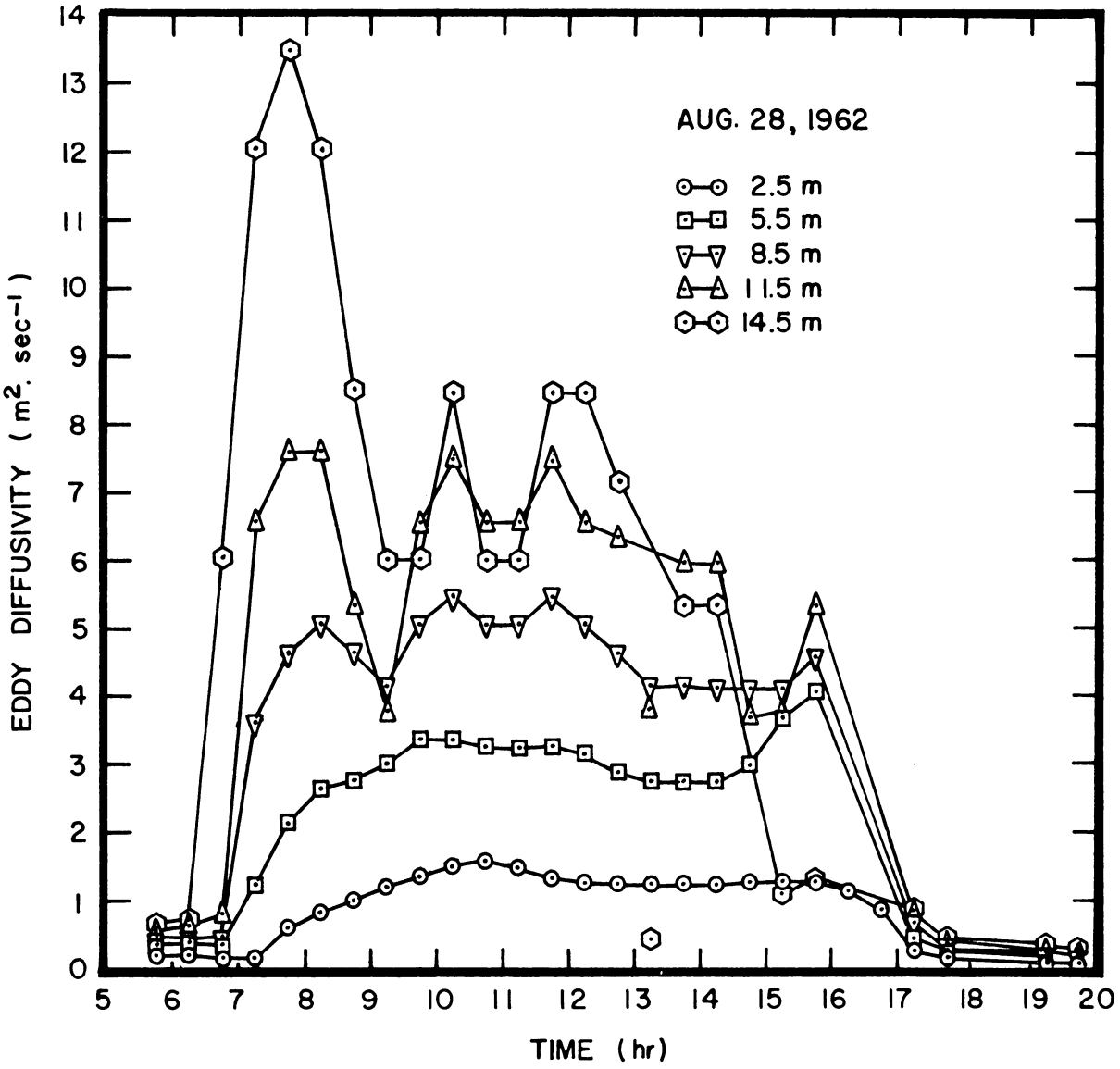

Fig. 4.1. Eddy diffusivity vs. time of day during clear August weather near Ann Arbor, Michigan. The abnormally high values between 0630 and 0800 are the result of using Prandtl's free convection equation during a period when R_j was less then -1.00 (see discussion in Chapt. 6).

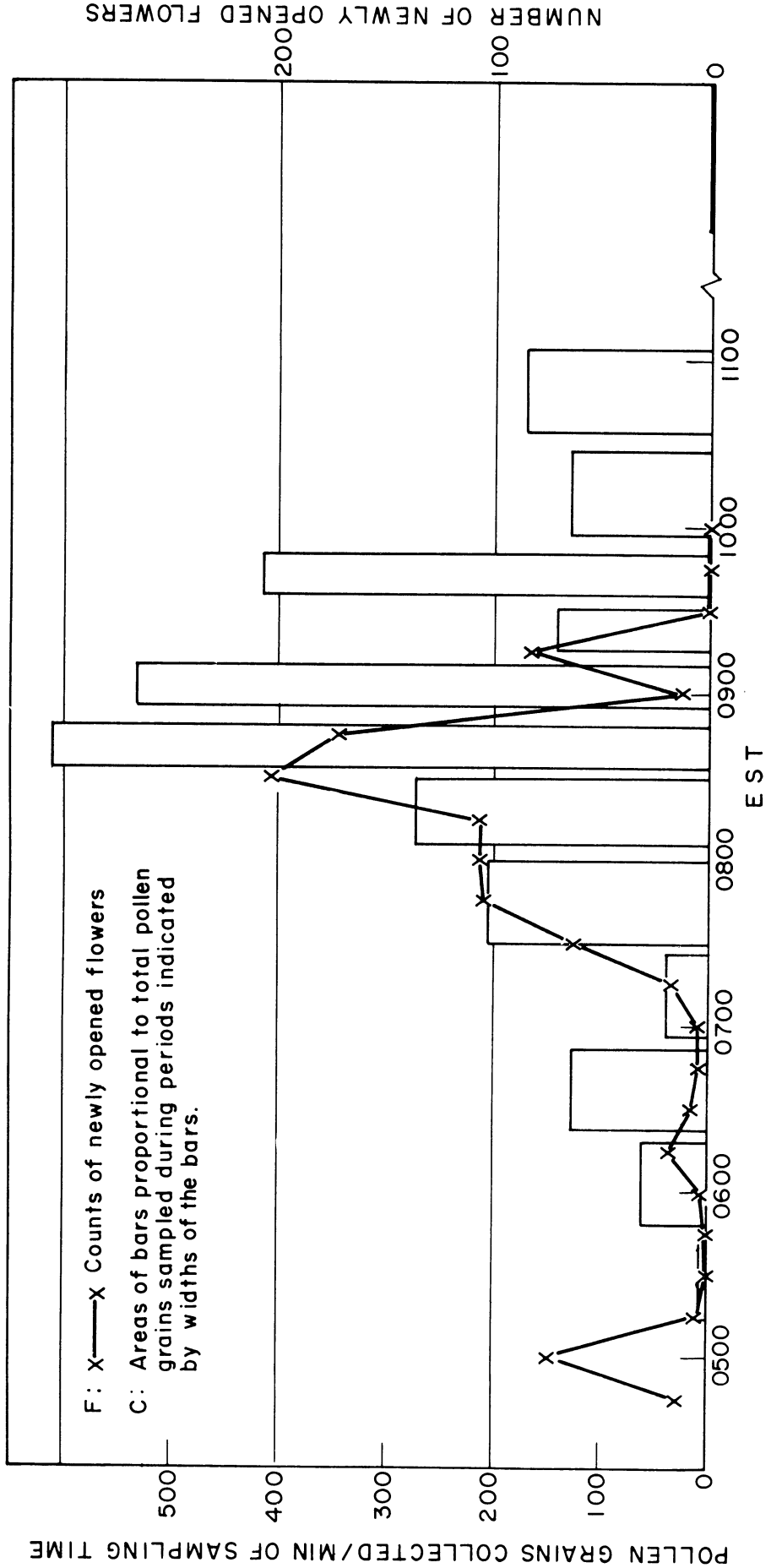

Fig. 4.2. Pollen grains sampled (bars) and flower opening counts (curves) as a function of time, June 26, 1959 (Sheldon and Hewson, 1960)

near the ground. Unsteadiness in source strength will therefore be felt more quickly at a high elevation over a downwind source free area than near the ground. Wind shear therefore compounds the problem caused by unsteadiness in source strength.

In the study under consideration the steady state equation is used despite the error involved because of the overwhelming computational advantage it affords. To minimize the error solutions are found for comparatively short downwind distances.

4.3.3 The Effect of Wind Direction Shear

Terms 2 and 3 of Eq. (4.8) contain horizontal wind components $u(z)$ and $v(z)$, which may be taken respectively as parallel and normal to the mean surface wind. In diffusion problems involving only a small height interval the wind direction may be considered constant and $v(z)$ vanishes. The present analysis, however, is concerned with a height of more than a kilometer and therefore the v component does not vanish.

The actual deviation of the ground level wind from the geostrophic value over a land surface is about 15-30° by day and 40-60° by night (Blackadar, 1962; Buajitti and Blackadar, 1957). Because most of the wind direction shear occurs in the lower 1 km the v component varies from zero at the ground to a value comparable to u at 1 km. It must be concluded therefore that, in diffusion problems of the scale considered here, Term 3 of Eq. (4.8) cannot be neglected without intro-

ducing a serious error.

4.3.4 The Effect of Large Scale Vertical Motion

The vertical component w of the mean wind speed in Term 4 of Eq. (4.8) is usually equated to zero because in the lower atmosphere broad scale ascent or descent is usually negligible compared to turbulent vertical motions. The average rate of descent in anticyclones, however, is estimated to be 1-2 cm sec^{-1} (Byers, 1937, P. 108; Brunt, 1939, p. 385), a sizeable fraction of the settling velocity of ragweed pollen which is 1.4 cm sec^{-1}. Of course this large scale subsiding motion must decrease to zero as the ground is approached, but even then the rate of subsidence near the top of the turbulent boundary layer must be of the order of 1/2 cm sec^{-1}.

The effect of large scale subsidence, although of negligible importance in the initial dispersion of pollen, has two measurable effects. First, the time required to bring all the pollen to the ground, and thus the maximum travel distance of the pollen, is reduced. Second, the shape of the steady profile is modified.

The principal effect of large scale descent is not in the direct transport of pollen, but rather in the creation of stable layers in which vertical eddy diffusion is inhibited. The presence of a sharp decline in salt nuclei concentration above the trade wind inversion (Woodcock, 1953) and of smoke horizons in industrial areas testifies to the importance of large scale subsidence in limiting the upward

diffusion of aerosols.

4.3.5 The Downwind Diffusion Term

The downwind diffusion Term 5 in Eq. (4.8) is usually neglected in comparison with the downwind transport Term 2. To assess the fractional error in this assumption let us examine the ratio of the two terms

$$E = \frac{K \frac{\partial^2 \chi}{\partial x^2}}{u \frac{\partial \chi}{\partial x}} \tag{4.9}$$

under two different conditions.

First, suppose that diffusion has progressed to the point where pollen is mixed uniformly between the ground and the level H at the top of the turbulent boundary layer. Let the pollen concentration within the layer be constant and let the loss at the lower boundary be at the gravitational rate. This is the "box model" which may be expressed mathematically as

$$\frac{\partial \chi}{\partial x} = - \frac{q\chi}{uH} \tag{4.10}$$

so that Eq. (4.9) becomes

$$E = - \frac{Kq}{u^2 H} \tag{4.11}$$

Assigning the following values: $K = 100\ m^2\ sec^{-1}$, $q = 0.014\ m\ sec^{-1}$, $u = 10\ m\ sec^{-1}$ and $H = 1000\ m$, E becomes 1.4×10^{-5}, a wholly negligi-

ble quantity. Even for light winds and a small value of H, E will continue to be negligible.

Second, consider the solution to the steady two dimensional diffusion equation in a neutral atmosphere (Calder, 1952).

$$\chi = \frac{Q}{ku_x x} \exp\left(-\frac{uz}{ku_* x}\right) \tag{4.12}$$

If values of the first and second derivatives are substituted in Eq. (4.9) and the log law for the wind speed profile invoked, then

$$E = -\frac{K_x}{xu_*}\left[\frac{z}{kx} - \frac{2k}{\ell n\left(\frac{z}{z_o}\right)}\right] \tag{4.13}$$

Taking $z = (x/10)$ m, u_* - 0.5 m sec^{-1}, $k = 0.4$, $z_o = 0.01$ m and $x = 100$ m the term in brackets becomes of order 0.1 and the error will be of order $K_x \cdot 10^{-3}$. For very small values of x or z the error may become significant.

The component of the diffusivity parallel to the wind can usually be neglected, as shown above. In three-dimensional problems, however, the wind turns with height so that the diffusivity normal to the plume at a given height may have a component parallel to the surface wind. For example, when the angle between the wind at the given level and the surface wind is more than 6° the component of diffusivity in the x direction will exceed 10% of the component normal to the plume axis.

It is apparent from the paragraph above that Term 5 of Eq. (4.8) can be important and should be retained; its retention, unfortunately,

will require a large increase in computer storage requirement.

4.3.6 Summary

The remarks of the preceding sections indicate the importance of several terms usually omitted from the complete three-dimensional diffusion equation. In the problem under consideration in this study all of the terms should be retained. To simplify the problem, reduce computer storage requirements and conserve time, terms 1, 3, 4 and 5 have been neglected. No further discussion of the error associated with the omission of these terms will be given.

4.4 SOLUTION OF THE UNSTEADY ONE-DIMENSIONAL DIFFUSION EQUATION

4.4.1 Introduction

The phrase one-dimensional diffusion refers here to vertical diffusion over a homogeneous infinite horizontal plane. To regard the earth as such a surface, particularly in terms of its pollen emission characteristics, is certainly a gross oversimplification. It is, however, instructive to carry out the theoretical computations for such a model and to compare the resulting profiles with those actually observed. If the model is correct and realistic parameter values are used, the difference between observation and computation leads to an assessment of the error involved in the assumption of homogeneity.

4.4.2 Derivation of the Equation and Statement of its Boundary Conditions

Under conditions of strict horizontal homogenity Eq. (4.8) reduces to

$$\frac{\partial \chi}{\partial t} = \frac{\partial}{\partial z}\left(K_z(z)\ \frac{\partial \chi}{\partial z} + q\chi\right) \tag{4.14}$$

where q is the settling speed of the pollen.

To solve Eq. (4.14) the distribution of the vertical component of diffusivity, the initial pollen profile and the upper and lower boundary conditions are required. Appropriate models for the diffusivity are discussed in Chapt. 6. The condition on the lower boundary given by Eq. (1.20) is discussed in Chapt. 5. The upper boundary is determined by selecting a level at which the pollen concentration never exceeds zero. Any initial pollen distribution may be selected, although most calculations begin with no pollen in the air.

In mathematical terms the conditions of the preceding paragraph are written

$$K_z(z) = K_z(\ell) f(z) \tag{4.15}$$

where ℓ is the level coincident with the top of the vegetation or roughness elements;

$$\chi = 0 \quad \text{for} \quad t = 0 \tag{4.16}$$

and

$$\left[K_z\ \frac{\partial \chi}{\partial z} + q\chi\right]_{\ell_+} = -P(t) + F\chi(\ell) \tag{4.17}$$

where ℓ_+ signifies the value at ℓ with gradients measured upward from ℓ, P(t) is the upward flux due to pollen emission and F is the deposition velocity or the rate of pollen flux into the vegetative layer per unit concentration; and,

$$\chi = 0 \quad \text{for} \quad z > H \tag{4.18}$$

4.4.3 Reduction to Dimensionless Form

To reduce Eq. (4.14) and its boundary condition to dimensionless form write

$$\left.\begin{aligned} \zeta &= \ell n\ z/\ell \qquad 0 \le \zeta \le \ell n\ H/\ell \\ K(z) &= K(\ell) f(\zeta) \\ Q &= \frac{\ell q}{K(\ell)} \\ T &= \frac{K(\ell) t}{\ell^2} \\ S &= \chi/\chi_{ARB} \end{aligned}\right\} \tag{4.19}$$

where χ_{ARB} is an arbitrarily chosen concentration.

Introducing Eq. (4.19) into Eq. (4.14)

$$\frac{\partial S}{\partial T} = \frac{1}{e^{\zeta}} \left(f'(\zeta) - f(\zeta) + Qe^{\zeta}\right) \frac{\partial S}{\partial \zeta} + f(\zeta) \frac{\partial^2 S}{\partial \zeta^2}\right)$$

$$\frac{\partial S}{\partial T} = G_1(\zeta) \frac{\partial S}{\partial \zeta} + G_2(\zeta) \frac{\partial^2 S}{\partial \zeta^2} \tag{4.20}$$

The nondimensionalized boundary conditions are

$$\left.\begin{aligned} S &= 0 && \zeta = \ell n\left(\frac{H}{\ell}\right) \\ \frac{\partial S}{\partial \zeta} + \left(Q - \frac{\ell F}{K(\ell)}\right) S &= -\frac{\ell P(t)}{K(\ell)\chi_{ARB}} && \zeta = 0 \end{aligned}\right\} \tag{4.21}$$

The parameter χ_{ARB} introduced into Eq. (4.19) is chosen in such a way that S is always fractional. This ensures that the solution of the equations to be developed in the next section will converge.

The maximum possible concentration at the level ℓ occurs when the loss exactly balances the maximum emission, i.e., when

$$\left(K(z)\ \frac{\partial \chi}{\partial z} + q\chi_{MAX}\right)_{\ell_-} = P_{MAX} \qquad (4.22)$$

If it can be assumed that pollen is deposited at approximately the gravitational rate (see App. A and B for confirmation) then, for $z < \ell$, the pollen gradient will be negligible and

$$\chi_{MAX}(\ell) = \frac{P_{MAX}}{q} \qquad (4.23)$$

Introducing Eq. (4.23) into Eq. (4.21) yields

$$\frac{\partial S}{\partial \zeta} + \left(Q - \frac{\ell F}{K(\ell)}\right)S = -\frac{P(T)\,Q}{P_{MAX}} \qquad (4.24)$$

4.4.4 Reduction to Finite Difference Form

Of the many finite difference expansions suitable for solving Eq. (4.20) (Richtmyer, 1957, p. 93) the Crank-Nicolson method has been selected because of its stability and accuracy—the error is $e = O(\Delta T^2) + O(\Delta \zeta^2)$—and because it requires no special starting procedure.

The basic Crank-Nicolson expansion (National Physical Laboratory, 1961, p. 116) is written

$$S_{T+\Delta T} - S_T = \frac{\Delta T}{2}\left\{\left(\frac{\partial S}{\partial T}\right)_{T+\Delta T} + \left(\frac{\partial S}{\partial T}\right)_T\right\} + (C_T S)_{T+\Delta T/2} \qquad (4.25)$$

where

$$C_T = -\frac{\delta^3 T}{12} + \frac{\delta^5 T}{120} - \cdots$$

is the correction containing higher order terms and δ is the central divided difference operation (Hildebrand, 1956, p. 136). It is normal practice to ignor C_T while retaining accuracy by keeping ΔT small.

The derivatives on the right of Eq. (4.20) are expanded in finite difference form

$$\frac{\partial S_\zeta}{\partial \zeta} = \frac{S_\zeta - S_\zeta}{2\Delta\zeta} + (C_{1\zeta} S)_\zeta \qquad (4.26)$$

where the correction term is

$$C_{1\zeta} = -\frac{\delta^3}{2 \cdot 3!} + \frac{2 \cdot \delta^5}{2^2 5!} - \frac{2^2 \cdot 3^2 \cdot \delta^7}{2^3 \cdot 7!} + \cdots$$

and

$$\frac{\partial^2 S_\zeta}{\partial \zeta^2} = \frac{S_{\zeta P\Delta} - 2S_\zeta + S_{\zeta - \Delta\zeta}}{(\Delta\zeta)^2} + (C_{2\zeta} S)_\zeta \qquad (4.27)$$

where the correction term is

$$C_{2\zeta} = -\frac{\delta^4}{12} + \frac{\delta^6}{90} - \frac{\delta^8}{560} + \cdots$$

The correction terms are omitted because, as shown by Hildebrand (1956, pp. 64, 82, 137), the use of high order finite difference techniques in estimating derivatives from experimental observations introduces

serious errors. Instead, whenever large gradients are present, such as near the ground or near horizontal discontinuities, logarithmic space increments are taken, reducing higher order terms to insignificance.

Introducing the finite difference expressions Eqs. (4.26) and (4.27) into Eq. (4.20) and using the Crank-Nicolson expansion, the equation becomes

$$S_j^{n+1} - S_j^n = \frac{\Delta T}{2(\Delta\zeta)^2}\left\{(G_2\delta^2 S)_j^{n+1} + (G_2\delta^2 S)_j^n + \frac{\Delta\zeta}{2}\left[(G_1\delta S)_j^{n+1} + (G_1\delta S)_j^n\right]\right\} \tag{4.28}$$

where j = 0,1,2.....M identifies the height increment,
and n = 0,1,2.....N identifies the time step.

The terms in Eq. (4.28) having superscript n are all known and therfore the equation may be written

$$C_1 S_{j+1}^{n+1} + C_2 S_j^{n+1} + C_3 S_{j-1}^{n+1} + C_4 = 0 \tag{4.29}$$

where

$$\left.\begin{aligned} C_1 &= -\phi_j(f_j^{n+1} + \psi_j^{n+1}) \\ C_2 &= 1 + 2\phi_j f_j^{n+1} \\ C_3 &= -\phi_j(f_j^{n+1} - \psi_j^{n+1}) \\ C_4 &= -S_{j+1}^n(\phi_j(f_j^n + \psi_j^n)) - S_j^n(1 - 2\phi f_j^n) - S_{j-1}^n(\phi_j(f_j^n - \psi_j^n)) \end{aligned}\right\} \tag{4.30}$$

and

$$\left.\begin{aligned} \phi_j &= \frac{\Delta T}{2(\Delta\zeta)^2 e^{2\zeta}} \\ \psi_j^n &= \frac{\Delta\zeta}{2}\left(\frac{f_{j+1}^n - f_{j-1}^n}{2\Delta\zeta} - f_j^n + Qe^{\zeta}\right) \end{aligned}\right\} \tag{4.31}$$

The condition at the lower boundary as given by Eq. (4.24) requires special care because it is here that all pollen passes into or out of the system. In particular it is important to minimize the error in approximating the derivative $\partial S/\partial \zeta$.

$S(\Delta\zeta)$ may be expanded in a Maclaurin series giving

$$S(\Delta\zeta) = S(o) + \Delta\zeta S'(o) + \frac{(\Delta\zeta)^2}{2!} S''(o) + \frac{(\Delta\zeta)^3}{3!} S'''(o) + \ldots$$

or

$$S'(o) = \frac{S(\Delta\zeta)-S(o)}{\Delta\zeta} - \frac{\Delta\zeta}{2!} S''(o) - \frac{(\Delta\zeta)^2}{3!} S'''(o) - \ldots \quad (4.32)$$

Thus the neglect of terms after the first one will result in an error of order $\Delta\zeta$, whereas the central difference formula

$$S'(o) = \frac{S(\Delta\zeta)-S(-\Delta\zeta)}{2\Delta\zeta} - \frac{(\Delta\zeta)^2}{2} \frac{S'''(o)}{3!} - \ldots \quad (4.33)$$

has an error of order $(\Delta\zeta)^2$. The central difference formula is clearly more accurate, but requires a value of S below the level ℓ.

To maintain accuracy and yet to remain within the layer in which S is known, two terms of the forward difference expansion Eq. (4.32) are retained. The second derivative $S''(o)$ is found by taking the derivative of Eq. (4.24) with respect to ζ, and substituting for $S''(o)$, giving

$$S'(o) = \frac{S(\Delta\zeta)-S(o)}{\Delta\zeta} \Big/ \left[1 + \frac{\Delta\zeta}{2!}\left(Q - \frac{\Delta F}{K(\ell)}\right)\right] \quad (4.34)$$

Substitution of $S'(o)$ in Eq. (4.24) yields

$$S(\Delta\zeta) - S(0)[1-\Delta\zeta AB] = \Delta\zeta \frac{BP(T)Q}{P_{MAX}} \qquad (4.35)$$

where $A = Q - \ell F/K(\ell)$, $B = 1 + \Delta\zeta A/2!$.

4.4.5 Solution of the Equations

Equation (4.29) constitutes a set of M-1 independent equations in the M+1 unknowns S(0).....S(M). The boundary conditions expressed by Eq. (4.35) and S(M) = 0 provide two additional equations and therefore the system has a unique solution.

Equation (4.29) can be expressed in the form

$$\begin{pmatrix} a_{12} & a_{13} & 0 & 0 & 0 & \cdots & & \\ a_{21} & a_{22} & a_{23} & 0 & 0 & \cdots & & \\ 0 & a_{31} & a_{32} & a_{33} & 0 & \cdots & & \\ \cdots & \cdots & \cdots & \cdots & \cdots & \cdots & & \\ \cdots & \cdots & \cdots & \cdots & \cdots & \cdots & & \\ \cdots & \cdots & \cdots & \cdots & \cdots & \cdots & & \\ 0 & 0 & 0 & 0 & \cdots & a_{M-1,2} & a_{M-1,2} & \end{pmatrix} \begin{pmatrix} S_1 \\ S_2 \\ \cdots \\ \cdots \\ \cdots \\ \cdots \\ S_{M-1} \end{pmatrix} = \begin{pmatrix} a_{1,4} \\ a_{2,4} \\ \cdots \\ \cdots \\ \cdots \\ \cdots \\ a_{M-1,4} \end{pmatrix} \qquad (4.36)$$

where the coefficient matrix is tridiagonal.

A very rapid and accurate method is available for the solution of a set of equations whose coefficient matrix is tridiagonal (Richtmyer, 1957, p. 103). First, find two sets of quantities α_j and β_j such that for any element of Eq. (4.36)

$$S_j = \alpha_j S_{j-1} + \beta_j \qquad (4.37)$$

Then at the upper boundary because $S_j = 0$ for all S_{j-1}

$$\alpha_M = \beta_M = 0 \qquad (4.38)$$

Substitute $\alpha_{j+1}S_j+\beta_{j+1}$ for S_{j+1} in Eq. (4.29) to obtain

$$S_j = - \frac{(C_3S_{j-1}+C_4+C_1\beta_{j+1})}{C_1\alpha_{j+1}+C_2} \tag{4.39}$$

Equate Eqs. (4.37) and (4.35), so that

$$\left.\begin{aligned} \alpha_j &= \frac{-C_3}{C_1\alpha_{j+1}+C_2} \\ \text{and} \\ \beta_j &= - \frac{C_4+C_1\beta_{j+1}}{C_1\alpha_{j+1}+C_2} \end{aligned}\right\} \tag{4.40}$$

Knowing the values of α and β at the upper boundary it is possible to solve for the remaining values by induction.

To find the values of S_j solve Eqs. (4.35) and (4.37) simultaneously at the lower boundary and use Eq. (4.37) to find the remaining values of S_j by induction.

4.5 SOLUTION OF THE STEADY TWO-DIMENSIONAL DIFFUSION EQUATION

4.5.1 Introduction

A two-dimensional diffusion problem is one in which all variables in one dimension are constant as typified by problems in which the sources are infinitely long in the cross wind dimension. Although such sources are not found in nature, reasonable approximations do exist.

During the summer of 1959 a large rectangular field adjoining Willow Run Airport, Ypsilanti, Michigan was used as a source of ragweed pollen and sampling was conducted a short distance downwind (see App. A). The limited distance over which diffusion was measured and the great

length of the pollen source permitted the steady two-dimensional assumption to be made. A solution to such an equation is given in this section to aid in interpreting the observations of the 1959 experiment.

4.5.2 Expression of the Two-Dimensional Equation in Finite Difference Form

Under steady two-dimensional diffusion, and with the assumption that

$$K_x \frac{\partial^2 \chi}{\partial x^2} \ll u \frac{\partial \chi}{\partial x}$$

Eq. (4.3) reduces to

$$u(z) \frac{\partial \chi}{\partial x} = \frac{\partial}{\partial z}\left(K(z) \frac{\partial \chi}{\partial z} + q\chi\right) \qquad (4.41)$$

where u is the component of wind speed normal to the boundary of the source.

Equation (4.41) is reduced to nondimensional form by means of the following transformations:

$$\left.\begin{aligned} \zeta &= \ell n\, z/\ell & K(z) &= K(\ell) f(\zeta) \\ u(z) &= u(\ell) g(\zeta) & Q &= \ell q / K(\ell) \\ X &= \frac{xK(\ell)}{u(\ell)\ell^2} & S &= \frac{\chi}{\chi_{MAX}} \end{aligned}\right\} \qquad (4.42)$$

The reduced equation is

$$g(\zeta) \frac{\partial S}{\partial X} = \frac{1}{e^{-\zeta}}\left[\left(f'(\zeta) - f(\zeta) + Qe^{\zeta}\right) \frac{\partial S}{\partial \zeta} + f(\zeta) \frac{\partial^2 S}{\partial \zeta^2}\right] \qquad (4.43)$$

which can be simplified further to

$$\frac{\partial S}{\partial X} = G_3(\zeta)\,\frac{\partial S}{\partial \zeta} + G_4(\zeta)\,\frac{\partial^2 S}{\partial \zeta^2} \qquad (4.44)$$

which is identical in form and can be solved in the same fashion as Eq. (4.20).

4.6 SOLUTION OF THE UNSTEADY TWO-DIMENSIONAL DIFFUSION EQUATION

The unsteady two-dimensional parabolic diffusion equation is written

$$\frac{\partial \chi}{\partial t} = -u(z)\,\frac{\partial \chi}{\partial x} + \frac{\partial}{\partial z}\left(K(z)\,\frac{\partial \chi}{\partial z} + q\chi\right) \qquad (4.45)$$

and can be nondimensionalized and expressed in finite difference form in a manner similar to that used in Sect. 4.4 and 4.5.

The finite difference expansion of Eq. (4.45) may be written

$$\underset{\textcircled{1}}{C_1 S_{j+1,k}^{(n+1)}} + \underset{\textcircled{2}}{C_2 S_{j,k}^{(n+1)}} + \underset{\textcircled{3}}{C_3 S_{j-1,k}^{(n+1)}} + \underset{\textcircled{4}}{C_4 S_{j,k-1}^{(n+1)}} + \underset{\textcircled{5}}{C_5 S_{j,k+1}^{(n+1)}} + \underset{\textcircled{6}}{C_6} = 0 \qquad (4.46)$$

where j is the increment in the vertical, k is the increment in the x direction and centered differences are taken in x. When backward differences in x are used Term 5 no longer appears.

There is no generalization of the inductive technique of Sect. 4.4 for solving vector equations containing nontridiagonal matrices and therefore an attempt was made to solve Eq. (4.46) by the Gauss-Siedel point successive overrelaxation iterative method (Varga, 1962, p. 59). A discussion of the technique will be given in Sect. 4.7.

A solution to Eq. (4.46) was not achieved because the equations were unstable. The instability can be traced directly to Terms 4 and

5 of Eq. (4.46) which stem from the transport term in Eq. (4.45). It is known that $\partial\chi/\partial x$ is usually small and that $u(z)$ is comparatively large. In the solution of Eq. (4.46) by relaxation, term $S^{(n+1)}_{j,k-1}$ is solved before term $S_{j,k+1}$ making the difference $S_{j,k-1}-S_{j,k+1}$ comparatively large, and tending to exaggerate the contribution of the transport term to S_j,k. On each successive step the difference is increased, causing the entire solution to be unstable.

It was hoped that stability could be attained by incorporating a backward difference in the transport term. Although this procedure did reduce the instability it did not eliminate it. No further consideration has been given to the solution of this problem.

4.7 SOLUTION OF THE STEADY THREE-DIMENSIONAL DIFFUSION EQUATION

4.7.1 A statement of the Problem

As shown in Sect. 4.3 none of the terms of the three-dimensional diffusion equation Eq. (4.8) may be dropped without introducing error. If, however, the downwind distance over which integration is to be performed is not too large (see Sect. 4.3.2) the steady assumption may be made. The resulting equation is

$$\underset{①}{u(z)\frac{\partial\chi}{\partial x}} + \underset{②}{v(z)\frac{\partial\chi}{\partial y}} + \underset{③}{w(z)\frac{\partial\chi}{\partial z}} = \underset{④}{\frac{\partial}{\partial x}\left(K_x(z)\frac{\partial\chi}{\partial x}\right)} + \underset{⑤}{\frac{\partial}{\partial y}\left(K_y(z)\frac{\partial\chi}{\partial y}\right)} + \underset{⑥}{\frac{\partial}{\partial z}\left(K_z\frac{\partial\chi}{\partial z}+q\chi\right)} \qquad (4.47)$$

In the present solution the wind is assumed to be horizontal and of constant direction, eliminating Terms 2 and 3. With these assumptions it is also reasonable to drop Term 4 in comparison with Term 1. The final equation becomes

$$u(z)\,\frac{\partial \chi}{\partial x} = K_y(z)\,\frac{\partial^2 \chi}{\partial y^2} + \frac{\partial}{\partial z}\left(K_z(z)\,\frac{\partial \chi}{\partial z} + q\chi\right) \qquad (4.48)$$

4.7.2 Reduction to Dimensionless Form

The following transformations reduce Eq. (4.48) to dimensionless form:

$$\left.\begin{aligned} \delta &= \ell n\,\frac{z}{\ell}\ ; \qquad X = \frac{K_z(\ell)\,x}{u(\ell)\,\ell^2}\ ; \qquad Y = \frac{y}{\ell}\sqrt{\frac{K_z(\ell)}{K_y(\ell)}}\ ; \\ Q &= \frac{\ell q}{K_z(\ell)}\ ;\ K_z(z) = K_z(\ell) f_1(\zeta)\ ;\ K_y(z) = K_y(\ell) f_2(\zeta)\ ; \\ u(z) &= u(\ell) f_3(\zeta)\ ;\ S = \chi(z)/\chi_{ARB} \end{aligned}\right\} \qquad (4.49)$$

where the f's are functions to be specified. The transformed equation can be written

$$\frac{\partial S}{\partial X} = F_1(\zeta)\,\frac{\partial^2 S}{\partial \zeta^2} + F_2(\zeta)\,\frac{\partial S}{\partial \zeta} + F_3(\zeta)\,\frac{\partial^2 S}{\partial Y^2} \qquad (4.50)$$

where

$$\left.\begin{aligned} F_1(\zeta) &= \frac{f_2(\zeta) f_1(\zeta)}{e^{2\zeta}} \\ F_2(\zeta) &= \frac{f_3(\zeta)}{e^{2\zeta}}\left(f_1'(\zeta) - f_1(\zeta) + e^{\zeta} Q\right) \\ F_3(\zeta) &= f_3(\zeta) f_2(\zeta) \end{aligned}\right\} \qquad (4.51)$$

4.7.3 Reduction to Finite Difference Form

The Crank-Nicolson expansion of Eq. (4.50) is

$$S_{i,j}^{(n+1)} - S_{i,j}^{(n)} = \frac{\Delta X}{2}\left[\left(\frac{\partial S}{\partial X}\right)_{i,j}^{(n+1)} + \left(\frac{\partial S}{\partial X}\right)_{i,j}^{(n)}\right] \tag{4.52}$$

Substituting for the derivatives on the right from Eq. (4.50) and arranging terms, Eq. (4.52) becomes

$$S_{i,j}^{(n+1)} + C_1 S_{i+1,j}^{(n+1)} + C_2 S_{i-1,j}^{(n+1)} + C_3\left[S_{i,j+1}^{(n+1)} + S_{i,j-1}^{(n+1)}\right] + C_4 = 0 \tag{4.53}$$

where

$$\left.\begin{aligned}
C_1 &= -\left(\frac{F_1(\zeta)}{(\Delta\zeta)^2} + \frac{F_2(\zeta)}{2\Delta\zeta}\right)\Big/\phi \\
C_2 &= -\left(\frac{F_1(\zeta)}{(\Delta\zeta)^2} - \frac{F_2(\zeta)}{2\Delta\zeta}\right)\Big/\phi \\
C_3 &= -\left(\frac{F_1(\zeta)}{(\Delta Y)^2}\right)\Big/\phi \\
C_4 &= S_{ij}^{(n)}\left[\phi - \frac{4}{\Delta X}\right]\Big/\phi + C_1 S_{i+1,j}^{(n)} + C_2 S_{i-1,j}^{(n)} + C_3\left[S_{i,j+1}^{(n)} + S_{i,j-1}^{(n)}\right]
\end{aligned}\right\} \tag{4.54}$$

and

$$\phi = \frac{2}{\Delta X} + \frac{2F_1(\zeta)}{(\Delta\zeta)^2} + \frac{2F_3(\zeta)}{(\Delta Y)^2}$$

4.7.4 Specification of the Initial and Boundary Conditions

To solve Eq. (4.53) initial and boundary conditions must be specified, calling for a more exact definition of the problem.

Assume that the ragweed free urban area is rectangular in shape of half width y_o and indeterminate length, as illustrated in Fig. 4.3.

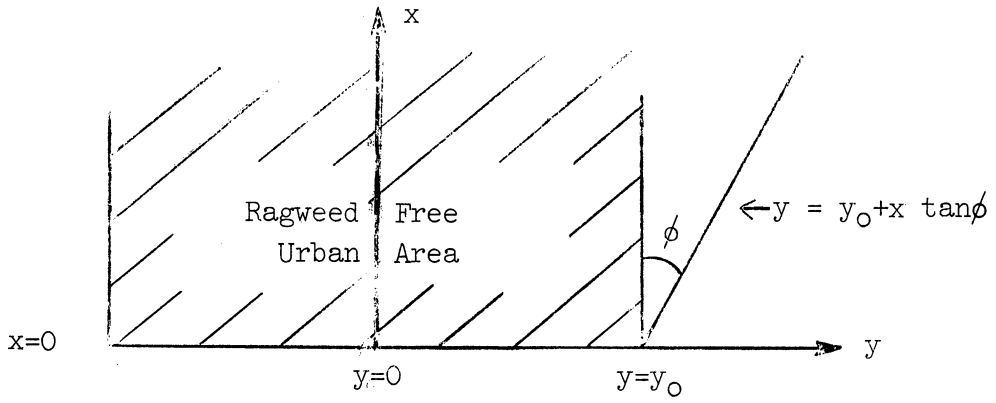

Fig. 4.3. A horizontal view showing a ragweed free urban area located within an infinite ragweed pollen source. The angle ϕ represents the maximum deviation of the wind from the x direction during the time interval under consideration.

The solution space can be reduced in size first by limiting the solution to the region $y \geq 0$, and second by carrying the integration only as far in the y direction as the influence of the urban area extends, i.e., $y \leq y_o + x \tan\phi$ (see Fig. 4.3), where ϕ represents the maximum angular deviation of the wind from the x direction during the time interval under consideration. This means that the solution is found over a y-z plane which expands with each increment in the downwind direction, and beyond which the concentration is invariant with increasing y.

Before starting with the solution of Eq. (4.53) an initial distribution over the plane x = 0 must be specified. Because any distribution is satisfactory as long as the lower boundary condition is satisfied, it has been possible to use both observed and computed profiles as initial conditions (see App. C and Chapt. 7 for examples of observed and computed profiles respectively).

Once the initial and boundary conditions are known the solution can proceed one step in the downwind direction at a time as shown in the following section. The solution at each step is found over the appropriate y-z plane for the M x P points illustrated in Fig. 4.4, where M and P are the numbers of solution points in the vertical and lateral directions respectively. The location of the border of the ragweed free area is indicated in Figs. 4.3 and 4.4 at $y = y_o$.

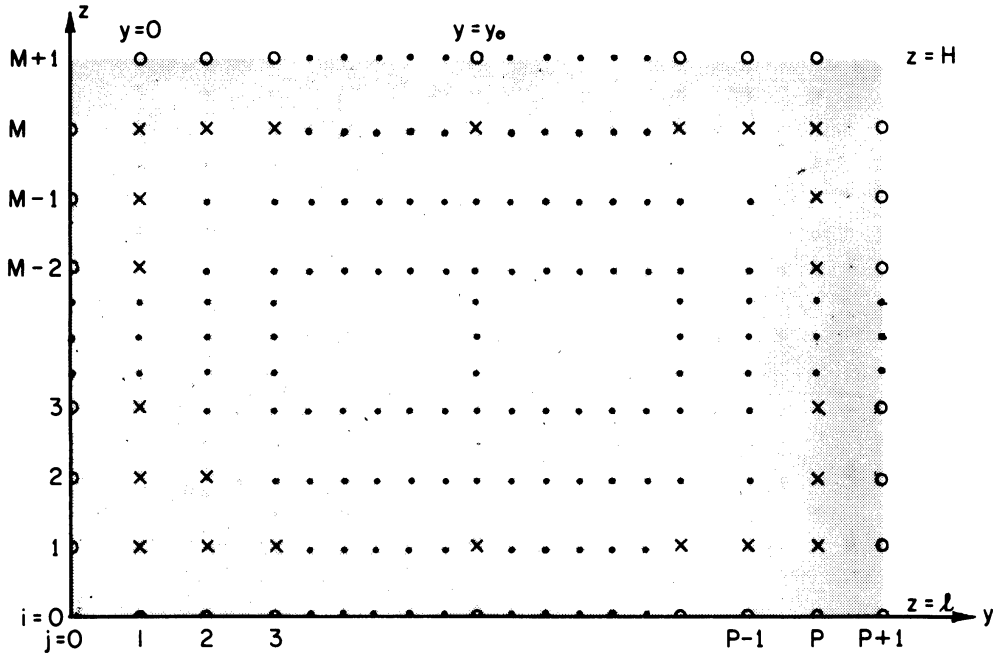

Fig. 4.4. A vertical section through the y-z plane showing a typical solution space; X- solution points; O - boundary value points.

The boundary values are given as follows:

$$
\begin{aligned}
&1.\ \text{On } j = o \qquad S_{i,o} = S_{i,2} \qquad \text{by symmetry}\\
&2.\ \text{On } j = P+1 \qquad S_{i,P+1} = S_{i,P}\\
&3.\ \text{On } i = M+1 \qquad S_{M+1,j} = 0\\
&4.\ \text{On } i = 0 \qquad \left(K(\ell)\frac{\partial S}{\partial z} + qS\right)_{\ell+} = \frac{-P}{\chi_{ARB}} + FS
\end{aligned}
\tag{4.55}
$$

and the boundary condition 4 is nondimensionalized and written in finite difference form exactly as in Eq. (4.35).

4.7.5 Solution by Relaxation

The Gauss-Seidel procedure is used to solve Eq. (4.53). The method is convergent if the spectral radius of the coefficient matrix (the absolute value of the largest eigenvalue) is less than unity (Fox, 1962, p. 31); the smaller the spectral radius the faster the rate of convergence. Solving for the spectral radius can itself be a tedious procedure but, fortunately, it is not always necessary to do so. If the matrix is irreducibly diagonally dominant it can be shown to converge (Varga, 1962, p. 73).

Equation (4.53) may be represented in matrix form by the equation

$$AS = D \tag{4.56}$$

where A is the matrix of coefficients and D is the vector composed of the constant terms. As can be seen from Eq. (4.53) the diagonal entries of A will all be unity.

Equation (4.56) can be decomposed into the form

$$(I-L-U)S = D \tag{4.57}$$

where I is the unit matrix and L and U are lower and upper triangular matrices having null diagonals.

The Gauss-Seidel iterative relaxation method can then be expressed in matrix notation as

$$S^{(n+1)} = LS^{(n+1)} + US^{(n)} + D \tag{4.58}$$

where the superscript denotes the n+1 th approximation of the solution vector S.

Introduction of typical coefficient values into A reveals a matrix whose spectral radius is very nearly unity. The rate of convergence for the Gauss-Seidel relaxation method of Eq. (4.58) is therefore slow and some acceleration of the solution is desirable.

Convergence of the solution can be accelerated by use of overrelaxation. The method, called point successive overrelaxation b Varga (1962, p. 59), is defined by the equation

$$S^{(n+1)} = S^{(n)} + \omega[D+LS^{(n+1)}-(I-U)S^{(n)}] \tag{4.59}$$

where the relaxation factor, ω is a number lying between 1 and 2.

The optimum value for ω is not known, but can be found by trial and error. It has been shown, however, that for a large class of matrices possessing property A or A^{π} (see Varga, 1962, Chapt. 4; Fox, 1962, p. 291) an optimum relaxation factor, ω_b exists and can be determined from the relation

$$\omega_b = \frac{2}{1+(1-\mu_1^2)^{1/2}} \tag{4.60}$$

where μ_1 is the spectral radius of the matrix L+U.

Simple iterative processes may be used to find the spectral radius (National Physics Laboratory, 1961, p. 24; Varga, 1962, p. 284). The rate of convergence of these processes depends on the rate at which

$$\left(\frac{\lambda_2}{\lambda_1}\right)^k \to 0 \quad \text{as} \quad k \to \infty$$

where λ_1 and λ_2 are the largest and second largest eigenvalues of the matrix A and k is the iteration. For small matrices the convergence is likely to be rapid, but for large matrices, such as the one under consideration in this section, the ratio λ_2/λ_1 is frequently close to unity and convergence is likely to be slow.

When the coefficient matrix is invariant, ω_b once computed may be used repeatedly, and therefore a considerable expenditure of time in its computation is rewarding. The computation of ω_b by the method of Eq. (4.60) is inefficient in the problem under consideration here, however, because the expanding grid technique changes ω_b at each downwind step. In this case a method by Carré (1961) may be used to estimate ω_b without a great expenditure of time.

Before outlining Carré's method of few necessary relations will be given without development. The reader who wishes to examine them further will find appropriate references in Carré's paper.

When the coefficient matrix M of Eq. (4.59) is positive definite, possesses Young's "Property A" or "A^{π}" and is consistently ordered

there is a simple relationship between the eigenvalues λ_i of M. the eigenvalues μ_i of (M-I) and the acceleration factor ω as set forth below:

$$(\lambda+\omega-1)^2 = \lambda\omega^2\mu^2 \tag{4.61}$$

Substituting Eq. (4.61) into Eq. (4.60)

$$\omega_b = \frac{2}{1+\left[1 - \frac{(\lambda_1+\omega-1)^2}{\lambda_1\omega^2}\right]^{1/2}} \tag{4.62}$$

Carre's method is as follows:

1. Perform one iteration of the overrelaxation procedure with $\omega = 1$.

2. Perform twelve iterations using a value of ω in the range $1 < \omega < \omega_b$, using $\omega = 1.375$ to start.

3. Obtain λ_1 by Aitken extrapolation.*

---

*Carre also suggests a method for obtaining an estimate λ_e of λ_1 as follows:

Let $\delta^{(n)}$ represent $S^{(n)}-S^{(n-1)}$. Let $\sigma^{(n)}$ be the arithmetic sum of the elements $\delta^{(n)}$ over all the nodal points.

1. Find $\sigma^{(n)}$ for the last 4 of the 12 iterations of step 2 above

2. Find three successive values of $P^{(n)}$ where

$$P^{(n)} = \frac{\sigma^{(n)}}{\sigma^{(n-1)}}$$

3. Following the first 12 iterations use the Aitken extrapolation formula to find λ_e if the differences between the P's decrease consistently;

$$\lambda_e = P^{(n-2)} - \frac{\left(P^{(n-1)}-P^{(n-2)}\right)^2}{\left(P^{(n-2)}+P^{(n)}-2P^{(n-1)}\right)}$$

Otherwise, let λ_e be equal to the latest $P^{(n)}$.

4. Subsequently, let λ_e be equal to the latest $P^{(n)}$.

4. Estimate ω_b from Eq. (4.62) after substituting approximate values for λ_1 and ω. Refer to the estimated value of ω_b as ω_e.

5. Reduce ω_e slightly to avoid the instability which results when ω values exceed the true value, ω_b.

$$\omega_m = \omega_e - \frac{(2-\omega_e)}{4} \tag{4.63}$$

6. Return to step 2 and continue until either

   i Two successive estimates of ω_b are sufficiently close, or

   ii The problem is solved to the desired accuracy.

It should be noted that Carré's method is extremely economical of time since ω_b is estimated during the regular iterative procedure used in solving the diffusion equation.

4.8 SOLUTION OF THE STEADY THREE-DIMENSIONAL EQUATIONS APPLICABLE TO A SMALL AREA SOURCE

The specific problem mentioned only briefly in this section concerns the prediction of the pollen concentration downwind from a small area source located in an otherwise source-free area. The problem is similar to that considered in the previous sections except that the scale is smaller and the regions of source and sink area are interchanged. With these minor changes the algorithm of Sect. 4.7 can be used to solve this problem.

4.9 THE UNSTEADY THREE-DIMENSIONAL PROBLEM

To be solved accurately the unsteady three-dimensional problem requires that every term in Eq. (4.8) be retained. Time and storage

requirements are therefore immense. Because the unsteady two-dimensional problem has not been solved there is little point in carrying the discussion of the unsteady three-dimensional problem any further. It should be remembered, however, that most real meteorological problems are unsteady and therefore, if accuracy is desired, it will be necessary to solve the unsteady equations.

4.10 CONCLUDING REMARKS

The methods for solving the parabolic diffusion equations which have been described in this chapter, may be performed with considerable accuracy once initial and boundary conditions and wind speed and diffusivity profiles are specified. For the solutions to be realistic, however, these specifications must conform to nature. Chapter 5, which follows, is devoted to a detailed investigation of the condition on the lower boundary. Chapter 6 contains a discussion of the meteorological variables.

5. PARTICLE FLUX AT THE GROUND

5.1 THE POLLEN FLUX EQUATION

The purpose of this chapter is to describe the factors contributing to the loss term F in the surface flux equation (Eq. (1.8))

$$\left(K_z \frac{\partial \chi}{\partial z} + q\chi\right)_{\ell_+} = - P + F\chi(\ell) \qquad (5.1)$$

and to derive a model for its description and computation.

The flux of pollen downward from the level ℓ may be represented by the equation

$$F\chi(\ell) = K_z(\ell)\left(\frac{\partial \chi}{\partial z}\right)_{\ell_-} + q\chi(\ell) \qquad (5.2)$$

where the terms on the right are the fluxes by turbulent diffusion and gravitational settling respectively. Omitted from Eq. (5.2) are terms corresponding to transport of particles by intertial forces, Magnus forces, molecular collisions, thermal forces, shear forces and fluctuating pressure gradients, all of which, excepting the inertial forces, are at least two orders of magnitude smaller than the particle weight (Owen, 1960).

For particles such as ragweed pollen one is fully justified in neglecting the inertial terms, as the following discussion shows. Table 5.1, taken from Owen's paper, illustrates the contribution to dust deposition on the walls, floors and ceiling of a wind tunnel by inertial forces. For large particles, i.e., for large q, deposition is mostly

TABLE 5.1

THE RATIO OF DEPOSITION TO SETTLING VELOCITIES FOR VARIOUS VALUES OF THE RATIO OF SETTLING TO FRICTION VELOCITIES

$\frac{q \times 10^4}{u_*}$	1.74	6.95	27.8	111.0	222.0
v_c/q	22.8	5.50	1.00	0.049	0.00046
v_f/q	25.0	6.45	2.44	1.07	1.00
v_w/q	23.8	5.94	1.48	0.37	0.19

Note: v_c, v_f and v_w are deposition velocities on ceiling, floor and walls respectively. The friction velocity u_* is the square root of the momentum transport per unit mass and therefore represents transport by mechanical turbulence.

on the floor and about equal to that due to the settling velocity alone. As the particle settling velocity decreases, inertial forces become increasingly important; for example, when $q \times 10^4/u_*$ is 1.74 the deposition velocity is 25 times the settling velocity and deposition occurs on walls, floor and ceiling with almost equal ease.

For ragweed pollen, with a fall velocity 0.014 m sec^{-1}, in a wind of 10 m sec^{-1} and for a friction velocity of 1 m sec^{-1} the ratio $q \times 10^4/u_*$ is 140 and, from Table 5.1, inertial factors can be seen to be of minor importance. Normally, of course, the friction velocity is much smaller.

In summary, because the inertial and other smaller forces may be neglected, Eq. (5.2) accurately represents the vertical flux of ragweed pollen in the atmosphere and may be assumed to hold within the air spaces

of the plant canopy. Very near vegetation elements, particularly those of a small size, however, inertial forces cannot be ignored as will be indicated in the following sections.

5.2 THE CONTINUITY EQUATION WITHIN THE PLANT CANOPY

Within the plant canopy the continuity equation for aerosols is

$$\frac{\partial}{\partial z}\left(K_z(z)\,\frac{\partial \chi}{\partial z} + q\chi\right) = \gamma(z)\,\chi \qquad (5.3)$$

where $\gamma(z)$ is the rate of loss per unit concentration within an elemental layer due to deposition on the foliage under steady conditions. The quantity γ will be called the particle scavenging rate by vegetation.

Writing $\gamma_1(z)$ for the fractional scavenging rate by inertial impaction on vegetation, and $\gamma_2(z)$ for the fractional scavenging rate by gravitational settling on vegetation,

$$\gamma_1(z) = u(z)\,A_v(z)\,E_i(z)\,E_a(z) \qquad (5.4)$$

where u is the wind speed, A_v is the vertically oriented area of vegetation exposed per unit depth, E_i is the impingement efficiency and E_a is the adhesive efficiency; and,

$$\gamma_2(z) = q\,A_h(z)\,E_h(z) \qquad (5.5)$$

where A_h is the horizontally exposed area of vegetation per unit depth and E_h is the horizontal sampling efficiency. Note that $E_i \cdot E_a$ is the vertical sampling efficiency.

It is possible to solve Eq. (5.3) if the parameter values of Eqs. (5.3) - (5.5) are known but, because only the grossest estimates of

their values can be made at present, any solution to Eq. (5.3) must be regarded as a rough approximation only. An important value of this first attempt to solve the problem of particulate flux into vegetation lies in outlining the areas requiring further investigation.

5.3 PARAMETER VALUES PERTAINING TO THE VEGETATION ITSELF

5.3.1 Nature of the Problem

To model mathematically the exact distribution of vegetation is patently impossible. Instead the vegetation must be represented by simplified geometric shapes which, by appropriate variation of their size, number and sampling efficiencies can be made to approximate the particle collecting characteristics of the real vegetation. Unfortunately, despite a diligent search, no measurements of the collecting efficiency of vegetation for particles of ragweed size have been found and therefore estimates will have to be used.

5.3.2 The Sampling Area

If the vegetation elements are replaced by cylinders of equivalent radius r, where r is chosen such that the original vegetation element and the cylinder present the same cross sectional area to the wind, then for vegetation consisting of n such elements per unit volume of length λ, the exposed sampling area per unit volume is

$$A = 2rn\lambda \qquad (5.6)$$

It is obvious that, except in the case of stems of cereal crops, twigs, needles or tree trunks, the estimate of r will at best be an order of magnitude approximation. This will be especially true of leaves because not only is their shape complex but their orientation varies with the wind speed. The estimation of r should, however, at least allow one to distinguish between the effects of such diverse objects as grass, wheat, corn, trees and buildings.

5.3.3 The Vertical Distribution of Vegetation

Within the plant canopy the distributions of wind speed, diffusivity and particle scavenging rate are all dependent upon the distribution of vegetation, of which quantitative measurements appear to be singularly lacking. Qualitatively, where vegetation is dense, the strong competition for light usually causes the leaves to be concentrated near the top of the canopy, leaving a relatively clear space beneath.

A suggested distribution for permanent forest vegetation (Benninghoff, 1964) may be fitted by a curve of the form

$$n(z) = n(0)A(z) \tag{5.7}$$

where $n(z)$ is the number of vegetation elements per unit volume at the level z and $n(0)$ is the corresponding number at ground level, and

$$A(z) = \left(1 - \frac{z}{\ell}\right)^{c_1} \exp\left(\frac{c_2 z}{\ell}\right) \tag{5.8}$$

It should be mentioned that Eq. (5.7) is a representation of a proposed vegetation distribution useful for inclusion in numerical computations but otherwise of no basic physical significance.

The constants c_1 and c_2 are determined by specifying the number of elements per unit volume and height at the level of maximum vegetation. If this level is h, then

$$\left.\begin{aligned} c_2 &= \frac{\ell n(n(h)/n(0))}{\left[\left(1 - \frac{h}{\ell}\right)\ell n\left(1 - \frac{h}{\ell}\right) + \frac{h}{\ell}\right]} \\ \text{and} \\ c_1 &= \left(1 - \frac{h}{\ell}\right) c_2 \end{aligned}\right\} \quad . \tag{5.9}$$

The distribution A(z) for $n(h)/n(0) = 50$ and $z/\ell = 0.8$, as shown in Fig. 5.1, appears to be a reasonable one for a mid-latitude deciduous forest (Benninghoff, 1964).

The grasses, contrary to the general distribution specified above, tend to maintain a density of vegetation which is roughly constant with height (Stoller and Lemon, 1963).

The ratio of the horizontally to vertically oriented areas will be assumed throughout the following sections to be unity although no confirmation of this assumption is available.

5.3.4 The Efficiency of Impingement

The collection efficiency E of a vegetation element is the product of the impingement efficiency E_i and the adhesive efficiency E_a.

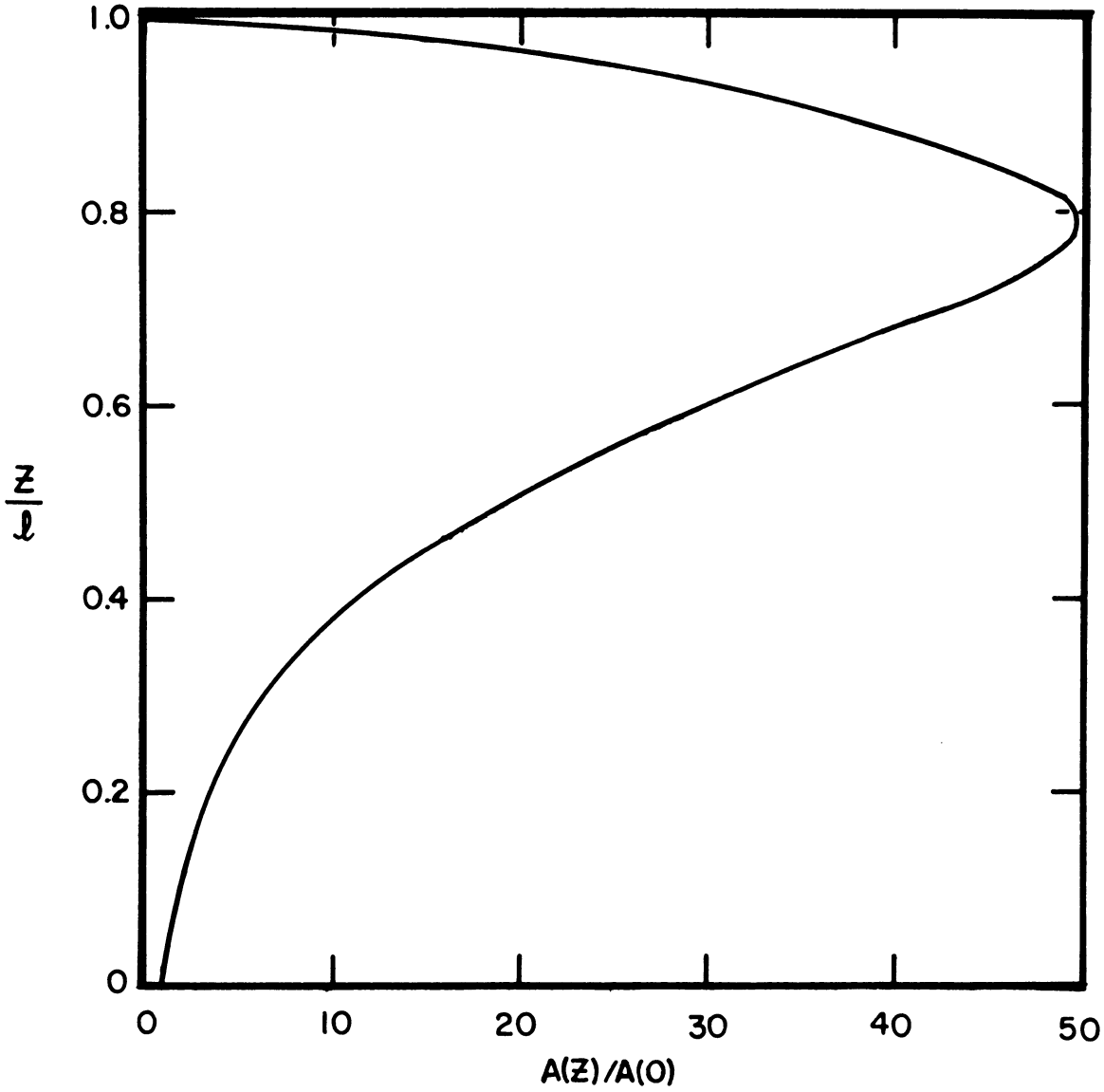

Fig. 5.1. A hypothetical distribution of vegetation density in a mid-latitude deciduous forest according to the equation

$$\frac{A(z)}{A(0)} = \left(1 - \frac{z}{\ell}\right)^{C_1} \exp \frac{(C_2 z)}{\ell}$$

where $C_1 = 1.64$, $C_2 = 8.18$.

As illustrated in Fig. 5.2, Brun and Mergler (1953) have computed the impingement efficiency of cylinders for spherical particles using an analog computer. Good correspondence between theory and observation has been obtained except for particles smaller than 1μ radius.

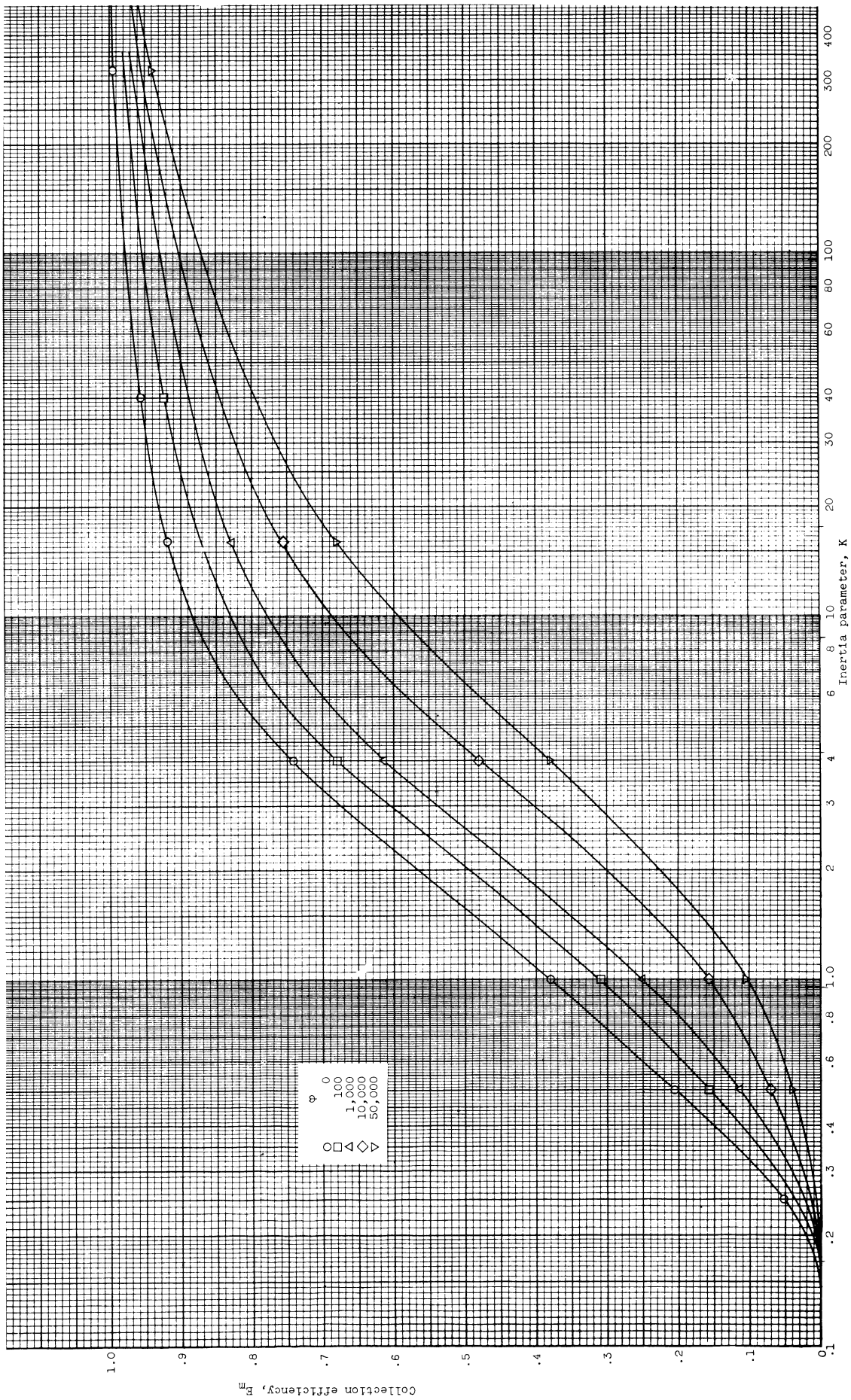

Fig. 5.2. Cylinder impingement efficiency (Brun and Mergler, 1953).

An empirical formula for E_i in terms of the inertia parameter* K for use in numerical computations is expressed by the relation

$$E_i = \frac{K-0.15}{K+1.35} \tag{5.10}$$

and

$$K = \frac{2}{9}\frac{\rho_p a^2 u}{\mu r} \tag{5.11}$$

where ρ_p and a are particle density and radius, u is wind speed, μ is the dynamic viscosity of the air and r is the cylinder radius.

As can be seen from Fig. 5.2 the impingement efficiency is also related to a second dimensionless parameter ϕ where

$$\phi = \frac{18\rho^2 ru}{\mu\rho_p} \tag{5.12}$$

and ρ is the air density. Within vegetation ϕ normally has a value close to zero.

Having computed the impingement efficiency, the capture may be computed if the adhesive efficiency can be estimated.

5.3.5 The Adhesive Efficiency

Virtually no information exists about the adhesive efficiency E_a of most common substances for pollen and other aerosols. Observations

*Some physical insight into the significance of the inertia parameter K may be gained by noting that rK is the stopping distance of a particle projected into still air with speed u, and is analogous to the mean free path of molecular physics.

from wind tunnel studies show that wood, metal and even the sticky surface of "Scotch" tape have very low adhesive efficiences compared to grease, rubber cement or gelatin. It is also known that the adhesive efficiency of "Scotch" tape decreases with increasing wind speed and there is some suggestion that the same is true of rubber cement (see App. B9.

Natural surfaces, unless they are moist or coated with an adhesive substance are assumed to have a low adhesive efficiency although the presence of many fine hairs on plants may increase it markedly.

5.3.6 The Optimum Cylinder Size

It can be seen from Fig. 5.2 and Eq. (5.11) that the impingement efficiency increases continuously with decreasing cylinder radius; however, for the purposes of this analysis, the efficiency of removal is of less importance than the total removal. To examine the latter quantity define the optimum cylinder size, for particles of a given radius, to be the size at which the cylinder collects the greatest number of particles.

The total capture N is proportional to the product of cylinder diameter and impingement efficiency, i.e ,

$$N \propto 2rE_i \tag{5.13}$$

and therefore it is possible to compute the optimum sampling radius by substituting Eqs. (5.10) and (5.11) into (5.13) and equating the derivative of N with respect to r to zero. The size for optimum capture is

found to occur at an impingement efficiency of 0.24 corresponding to an inertia parameter of 0.625 under all combinations of variables.

The optimum cylinder radius may be computed by substituting $K = 0.625$ into Eq. (5.11) and solving for r. As an example consider ragweed pollen in a wind of 5 m sec^{-1}; using appropriate values for the remaining parameters the optimum radius is found to be approximately 1 cm.

It is of interest to note that under the same conditions a cylinder having a radius of 4.2 cm or larger will, theoretically, collect no pollen at all as shown in Fig. 5.3. This suggests that large objects such as tree trunks or buildings are relatively ineffective in removing pollen from the air.

5.3.7 Gravitational Settling on Vegetation

It has been shown (Harrington et al. 1959) that the rate of ragweed pollen deposition on a horizontally placed 1 x 3 in. microscope slide is a function of the orientation of the slide relative to the wind direction, of the wind speed and of the amount of turbulence in the air. The same factors probably influence the rate of pollen deposition on the horizontally exposed surfaces of vegetation.

There are no observations which would permit making an estimate of the settling efficiency and therefore, in the deposition model to be proposed later in this chapter, it will be assumed to be unity, a reasonable value in view of the atmospheric and other factors involved.

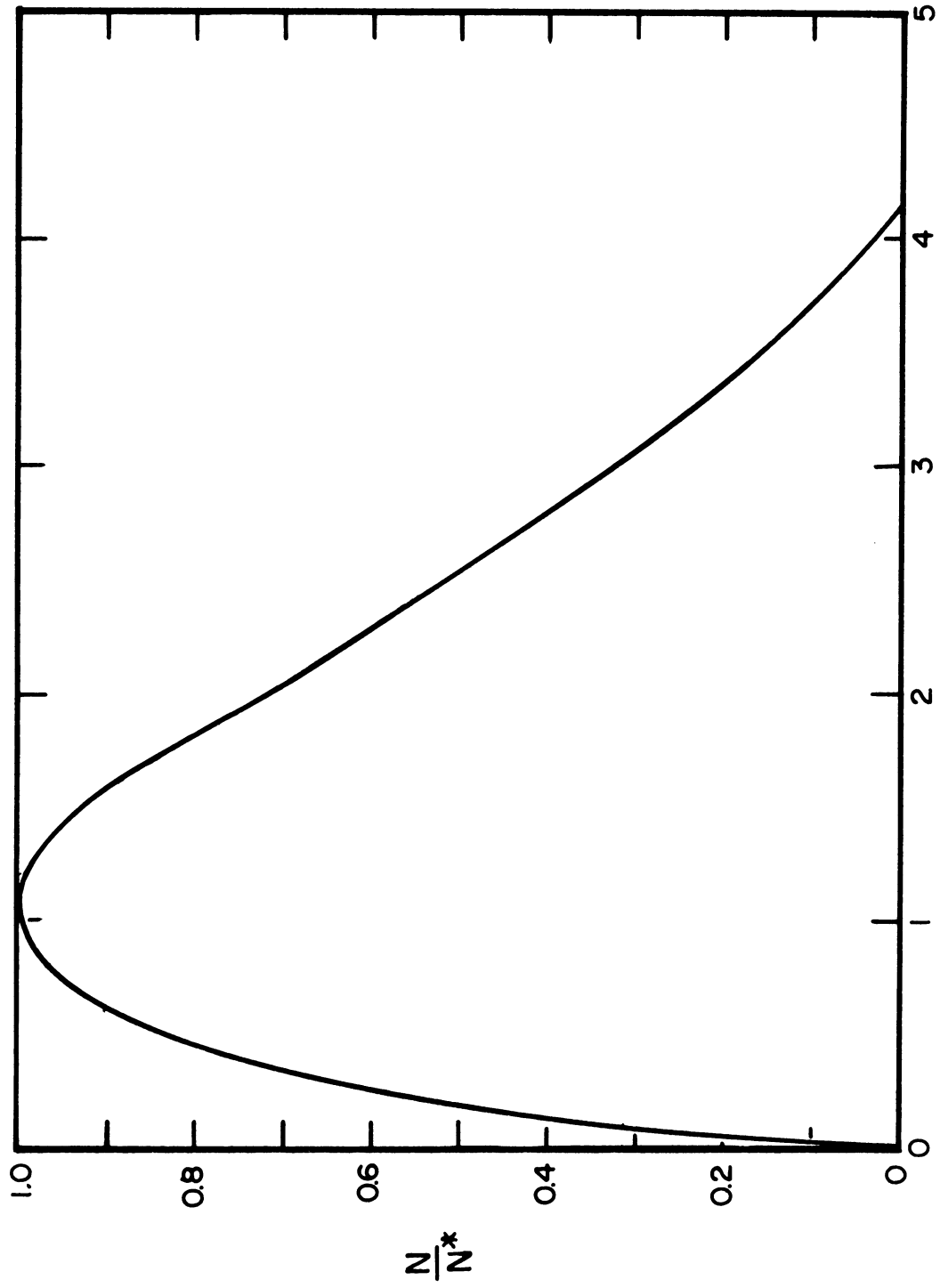

Fig. 5.3. The ratio of total to optimum capture as a function of the ratio of actual to optimum radius.

5.4 WIND PROFILES IN VEGETATION

5.4.1 Observed Wind Profiles in Vegetation

A substantial fund of knowledge exists concerning the distribution of wind within plant canopies. For present purposes the wind speed is required both directly in the computation of the particle scavenging rate $\gamma(z)$ and indirectly in the computation of the impingement efficiency E_i. Both observational and theoretical material are reviewed below.

Before 1940 most of the published work on wind profiles in vegetation was performed in Germany (Geiger, 1959). The papers by Paeschke (1912, 1937), Geiger (1925, 1926, 1931, 1932) and Woelfle (1939) refer to profiles measured in forests. Stocker (1923) in a largely descriptive treatment furnishes some wind measurements within Callunas branches in a heath.

More recently profile measurements have been reported by Fons (1940) in grass, brush and forest; by Ramdas (1946) in jowar, suran, sugar cane, cotton, wheat, tobacco and beans; by Poppendiek (1949) in trees and brush, by Baynton (1963) within a tropical rainforest and by Stoller and Lemon (1963) in wheat and corn.

Wind speed profiles measured by Fons (1940) in brush and forest and by Stoller and Lemon (1963) in corn are reproduced in Fig. 5.4 and 5.5. All profiles show a curvature which is opposite to that of the normal wind profile in the free air.

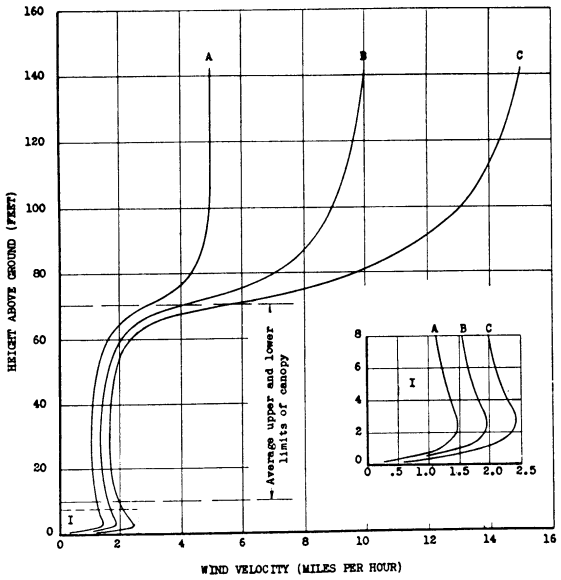

Fig. 5.4. Wind speed profiles in Ponderosa pine (Fons, 1940).

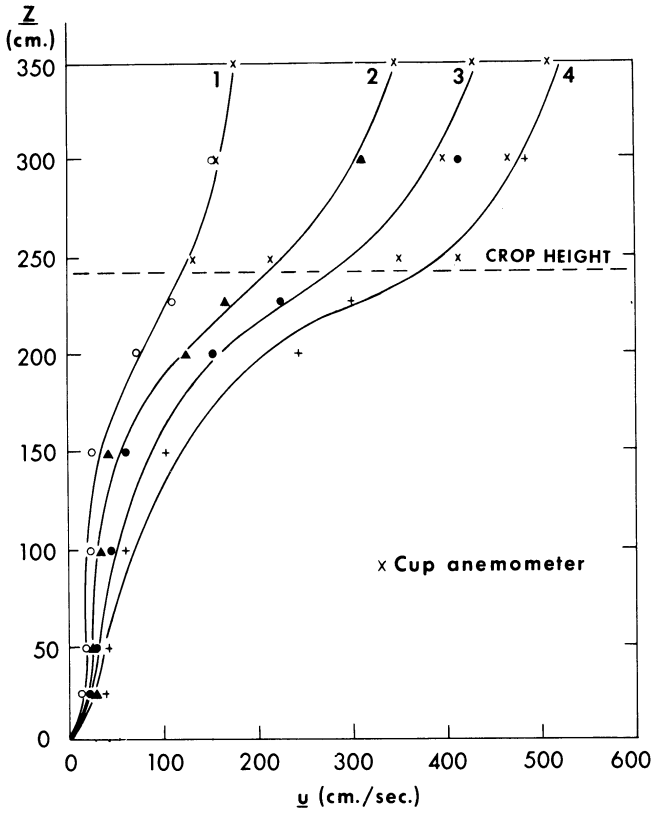

Fig. 5.5. Wind speed profiles in corn (Stoller and Lemon, 1963).

In broadleaf vegetation and trees the wind decreases rapidly with decreasing height through the upper foliage, becomes more or less constant in the region of trunks or strems and then decreases or is assumed to decrease, logarithmically near the ground.

In cereal crops the wind profile is less curved, the decrease in speed being distributed over a larger fraction of the plant depth.

5.4.2 Theoretical Wind Profiles in Vegetation

The only theoretical work on wind profiles inside plant canopies found by the author is that of Tan and Ling (1963). The canopy is represented by these authors as a distributed energy sink as shown in Eq. (5.14) where the energy equation is written

$$\frac{\partial \tau}{\partial z} = C_D A_V(z) \frac{\rho u^2(z)}{2} \qquad (5.14)$$

where τ is the shearing stress per unit area, C_D is the drag coefficient of the plants, A_V is the total vertical plane area per unit volume and the remaining terms have their usual significance.

The assumption of constant drag coefficient implicit in Eq. (5.14) holds quite accurately in the range of Reynolds numbers $10^2 \leq R_e \leq 10^5$ (Goldstein, 1952, p. 418) but not in the range $0 \leq R_e \leq 50$ wherein $C_D \propto R_e^{-1/n}$, for $1 \leq n \leq 2$. The following discussion will be limited to situations in which $R_e > 10^2$.

Substituting for the shearing stress

$$\frac{\tau(z)}{\rho} = K_V(z) \frac{\partial u}{\partial z} \qquad (5.15)$$

in Eq. (5.14) yields the equality

$$\frac{\partial}{\partial z}\left(K_v(z)\ \frac{\partial u}{\partial z}\right) = \frac{C_D A_v(z) u^2(z)}{2} \qquad (5.16)$$

which is used to compute the wind profile.

Equation (5.16) is nondimensionalized and written in the form

$$\frac{\partial^2 U}{\partial Z^2} + f(Z)\ \frac{\partial U}{\partial Z} + Sg(Z)U^2 = 0 \qquad (5.17)$$

where $Z = z/\ell$, $U = u(z)/u(\ell)$ and S is a parameter called the "shape factor of canopy flow."

Equation (5.17) is slightly nonlinear but yields readily to relaxation methods of solution. Tan and Ling (1963) introduce a linear increase of eddy viscosity with height and a constant leaf area and obtain wind distributions which correspond well to those observed in wheat and corn (Fig. 5.6). Figure 5.7 illustrates solutions computed by the author based on distributions of eddy diffusivity and leaf area believed to be more typical of forest canopies. These calculated profiles show good agreement with observed canopy wind profiles as set forth in Fig. 5.4.

5.5 THE EDDY VISCOSITY PROFILE IN VEGETATION

The eddy viscosity in the atmosphere may be found through the use of Eq. (5.15) by measuring the Reynolds stress per unit mass, i.e., $\overline{u'w'}$, and the wind shear. Within a plant canopy, however, the wind shear is frequently so small that it is unmeasurable and therefore this

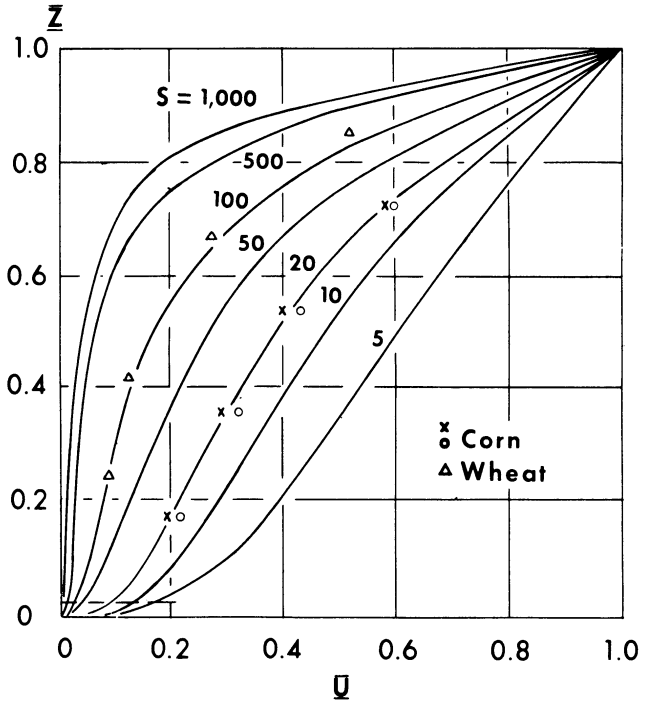

Fig. 5.6. Canopy wind profiles for various shape factors S, with vegetation density and diffusivity linear functions of height. (Tan and Ling, 1963).

method is inapplicable.

A second method, deriving from Taylor's (1921) theory, gives for the vertical component of the eddy diffusivity

$$K = \sqrt{\overline{w^2}}\, \ell_1 \tag{5.18}$$

where the scale length* ℓ_1 is defined to be

$$\ell_1 = \sqrt{\overline{w^2}} \int_0^\infty R_L(\xi)\, d\xi \tag{5.19}$$

*The spectrum of eddy sizes must be limited if ℓ_1 is to be finite. In the free atmosphere, where the horizontal eddies are virtually unlimited in size, ℓ_1, is undefined but in the plant canopy ℓ_1 is measurable and significant.

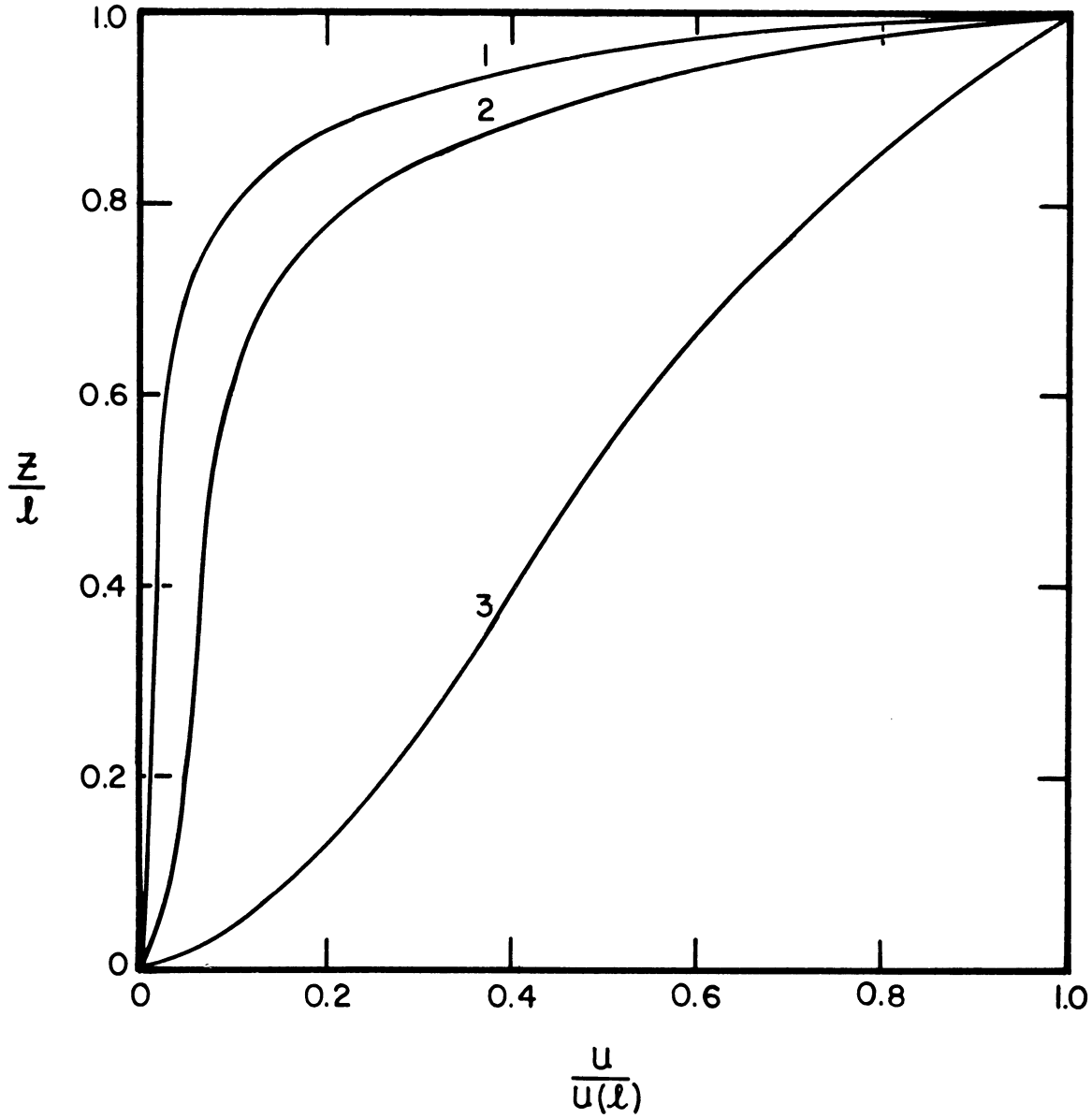

Fig. 5.7. Canopy wind profiles under the following conditions:

1. S = 1000; vegetation density constant; K increasing linearly with height.
2. S = 5; vegetation density distributed according to Eq. (5.8) with $h/\ell = 0.8$, $A(h)/A(0) = 50$; K increasing linearly with height.
3. S = 5; vegetation density constant; K increasing linearly with height.

and $R_L(\xi)$ is the Lagrangian auto-correlation coefficient. Wind measurements are made in an Eulerian frame of reference and it is therefore

necessary to substitute $R_E(t)$ for $R_L(\xi)$, where $\xi = \beta t$ (see Chapt. 2). The scale length ℓ_1 then becomes

$$\ell_1 = \beta \sqrt{\overline{w^2}} \int_0^\infty R_E(t)\,dt \qquad (5.20)$$

From measurements of the autocorrelation coefficient and variance of the downwind component of the wind within crops and under the assumption of isotropy Stoller and Lemon (1963) were able to compute both $R_E(t)$ and σ_w and hence to obtain an estimate for the eddy diffusivity from Eqs. (5.20) and (5.18) as shown in Fig. 5.8. In fact a simplified

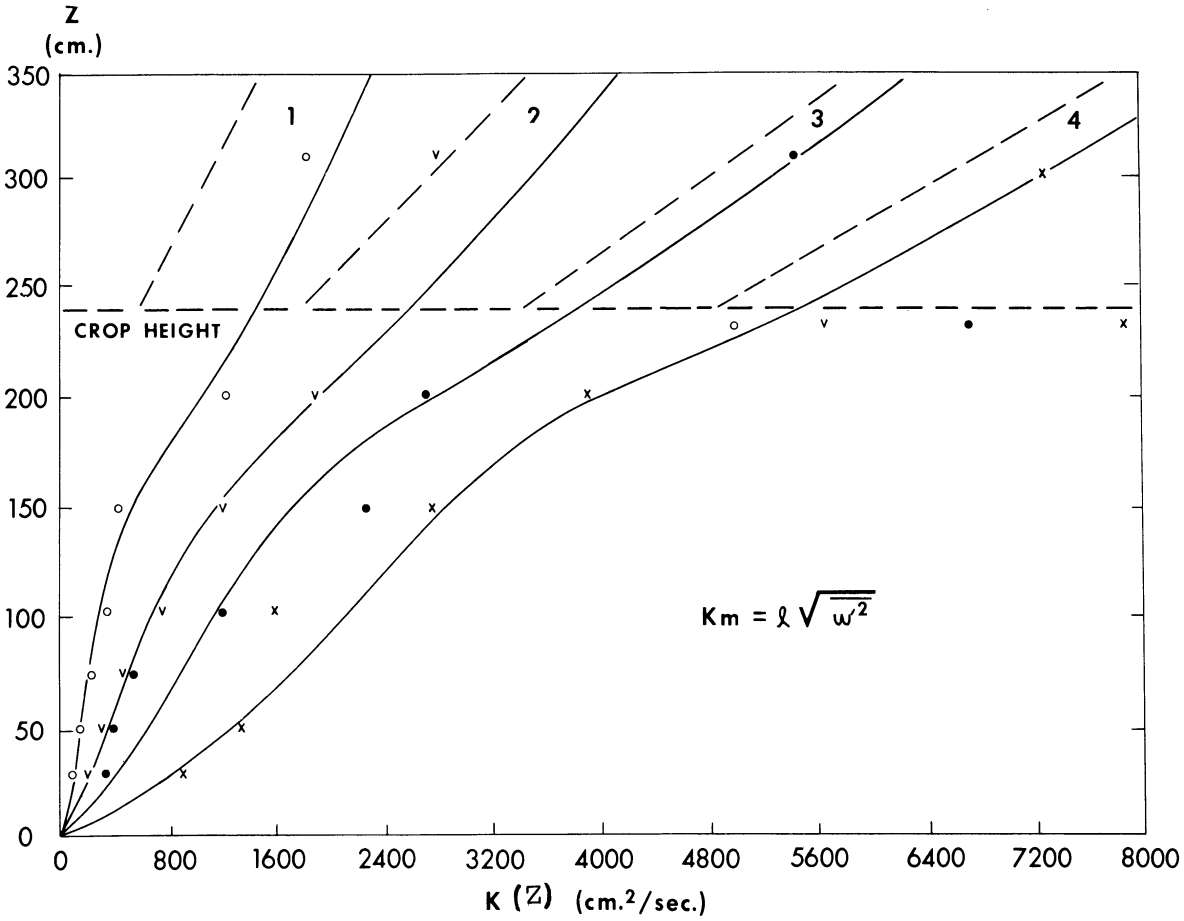

Fig. 5.8. The distribution of eddy viscosity in and above a cornfield, August 2, 1960 (Stoller and Lemon, 1963).

method of computing $R_E(t)$ was used, based on the assumption that observations were conducted within the inertial subrange.

5.6 POLLEN FLUX INTO VEGETATION

The assumption, estimation or measurement of all the parameters in Eq. (5.2) makes it possible to compute $F(\ell)$ as follows. First solve Eq. (5.3) for $\chi(z)$ by a simple relaxation process using as boundary conditions

$$\left.\begin{aligned} \chi(z) &= \chi(\ell) && z = \ell \\ \chi(z) &= \chi(\Delta z)\exp\left(\int_{\Delta z}^{0} A_h(z)\,E_h(z)\,dz\right) && \text{on } z = 0 \end{aligned}\right\} \qquad (5.21)$$

The last condition simply states that, in the elemental layer of depth Δz near the ground, the gravitational settling term predominates. The integration in Eq. (5.21) is performed using the five point Newton-Cotes formula (Hildebrand, 1956, p. 73).

Knowing the distribution of χ within the plant canopy, the function F, sometimes called the deposition velocity, may be computed from Eq. (5.2).

Theoretical profiles of ragweed pollen concentration within and fluxes of pollen into the plant canopy have been computed for a variety of vegetation types. The results for the parameter values listed in Table 5.2 are shown for six illustrative examples in Fig. 5.9. It should be noted that the deposition velocities greatly exceed the gravitational settling velocity, 0.012 m sec^{-1}.

TABLE 5.2

PARAMETER VALUES FOR THE COMPUTATION OF POLLEN PROFILES WITHIN THE PLANT CANOPY

		1	2	3	4	5	6
Gravitational Settling Velocity	q m sec^{-1}	0.012					
Computed Deposition Velocity	F m sec^{-1}	0.015	0.035	0.118	0.027	0.33	0.95
Height of the Vegetation	ℓ m	0.1	0.1	0.1	0.1	20	20
Equivalent Veg. Radius	r m	0.001	0.001	0.001	0.001	0.025	0.002
Number of Veg. Elements	N(0) m^{-2}	$1x10^3$	1.10^4	$1x10^5$	$1x10^4$	0.5	4.0
Height of Peak Veg. Density	h m					0.8	0.8
Veg. density at h	N(h) m^{-2}					50 N(0)	500 N(0)
Adhesive Efficiency	E_a	0.1	0.1	0.1	0.01	0.1	0.1
Horizontal Efficiency	E_h	1.0	1.0	1.0	1.0	1.0	1.0
Wind Speed at ℓ	U(ℓ) m sec	1.0	1.0	1.0	1.0	5.0	5.0
Diffusivity at ℓ	K(ℓ) m^2sec	0.01	0.01	0.01	0.01	2.0	2.0

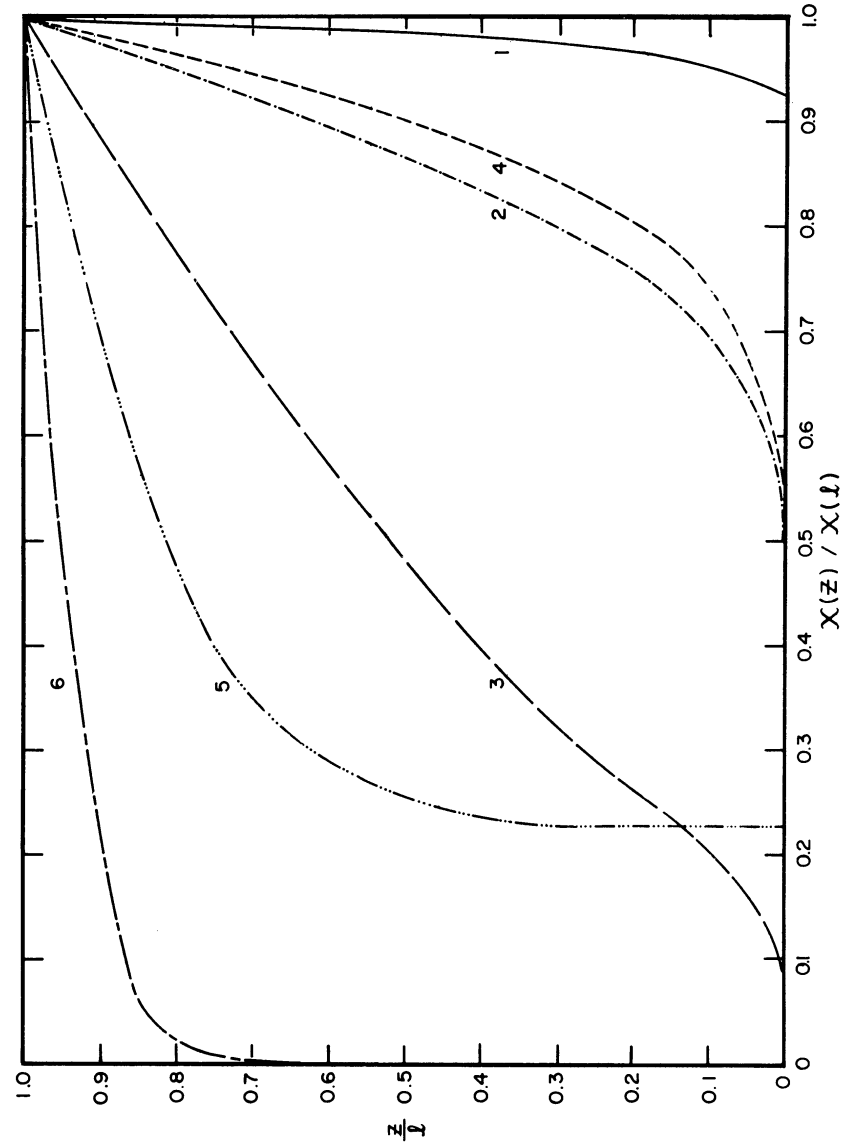

Fig. 5.9. Ragweed pollen profiles within a plant canopy:

1. Sparse grass, $E_a = 0.1$;
2. Moderate grass, $E_a = 0.1$;
3. Dense grass, $E_a = 0.1$;
4. Moderate grass, $E_a = 0.01$;
5. Deciduous forest with peak vegetation density of 500 leaves m^{-3} of dimension 5 x 10 cm;
6. Coniferous forest with peak vegetation density of 100,000 needles m^{-3} of dimension 0.02 x 2 cm.

From experimental observations, to be discussed in App. A, it is found that true deposition velocities depart very little from the gravitational settling velocity. To achieve theoretical results which conform more satisfactorily with these observations the adhesive efficiency must be decreased by one to two orders of magnitude from the value 0.1 used. When this is done the theoretical pollen profiles within vegetation become nearly constant with height. This interesting result could be very simply checked by measuring the vertical pollen profile in and above a woods.

In summary, a model for the process of pollen removal by vegetation has been proposed which permits the computation of the pollen scavenging efficiency. If the model is correct, the conclusion must be reached that most vegetation has a relatively low adhesive efficiency. To be most effective as a pollen filter vegetation should project high into strong winds, be composed of many small elements and have a relatively high adhesive efficiency. This description appears to be most applicable to the conifers.

6. EVALUATION OF THE ATMOSPHERIC VARIABLES

6.1 INTRODUCTION

This chapter is devoted to a discussion and evaluation of the atmospheric variables which appear in the three dimensional diffusion equations, namely, the components of wind velocity and eddy diffusivity. Where present understanding of the meteorological phenomenon under consideration is uncertain, several proposed theories are reviewed and the most reasonable selected for incorporation in the diffusion model.

6.2 THE WIND VELOCITY PROFILE

6.2.1 Low Level Wind Profiles

6.2.1.1 The Wind Vector

The layer near the ground is defined here to be that portion of the atmosphere between the ground and about 20 m, i.e. the layer in which most micrometeorological investigations have been conducted.

Within this layer, over level ground, for most conditions the mean vertical component of the wind vanishes and the mean wind direction is approximately constant with height. If U and V are the horizontal wind components parallel and normal to the mean wind direction and W is the component in the vertical, then the wind vector at any instant can be decomposed into $\overline{U(z)}$, the mean speed, and $u(z)$, $v(z)$ and

w(z), the deviations from the mean.

6.2.1.2 Low Level Wind Profiles in a Neutral Atmosphere

The form of the wind profile in a neutral atmosphere has been thoroughly reviewed (Sutton, 1953; Priestley, 1959, Chapt. 3; Lumley and Panofsky, 1954, Chapt. 3) so that only the briefest summary need be given here.

Near the ground in a neutral atmosphere the wind has been observed to increase logarithmically with height under conditions of steady fully developed turbulent flow if the surface is homogeneous and the roughness elements are small compared to the lowest observation point or, if large, are distant compared to the highest observation point. By large or small is meant a dimensional difference of about 1.7 orders of magnitude (Sutton, 1953, p. 233).

The profile under such circumstances can be written

$$u(z) = \frac{u_*}{k} \ell n \left(\frac{z-d}{z_o} \right) \qquad (6.1)$$

where u_* is the friction velocity, k is Karman's constant, z_o is the roughness length and d is the zero-plane displacement.

When the ground surface contains irregularities which are neither distant nor small according to the definition above, then the condition of homogeneity is not satisfied, the shearing stress is not necessarily constant with height and the logarithmic profile cannot be expected to hold exactly.

The roughness length z_o is the distance above the displacement height at which the wind speed, estimated by extrapolation of the log-law profile, becomes zero. The commonly held belief that z_o applies to the average roughness over a considerable area is only true when the wind field at the lowest observation level is horizontally homogeneous Within the region influenced by individual roughness elements, the field of turbulence is not homogeneous z_o is not constant with height and the wind speed profile cannot necessarily be accommodated to the logarithmic form.

The zero-plane displacement d is presumed to compensate first, for errors in the specification of the anemometer height and, second, for the depth of dead air within a vegetative canopy if such exists. The first is certainly valid if the anemometer heights are measured above some plane which does not correspond to the true ground height at the observing point. Usually, however, the anemometer heights are measured with reference to the ground and d is taken to be the difference in height between the ground at the observation point and the average height of the upwind terrain. Here again the concept is valid only if the wind speed at the lowest observation level is homogeneous over the entire upwind fetch affecting the profile at the observation point. If it is not, each anemometer may sense a different average ground level and therefore d may be a function of height.

The second explanation for the zero-plane displacement, i.e. that it represents the depth of dead air within vegetation, is compatible

with the proper use of the first explanation. Over vegetation composed of grasses or cereal crops, however, the stalks bend with the wind making d and z_o a function of wind speed.

Most profiles over high vegetation, unfortunately, have been observed within the layer of inhomogeneous flow where the log-law may well be invalid. An example of the error to be expected in this region is afforded by the work of Kung (1961) who has shown that the values of z_o and d computed from alternate sets of anemometers over high vegetation differ markedly.

In summary it has been suggested that in atmospheric motion near the ground under neutral buoyancy the log-law wind profile is only valid under carefully selected conditions. It can also be stated that no other theoretical profile exists which affords a better description of the wind. For the purposes of this study the log law affords a reasonable approximation to the true wind profile although it must be used with caution, particularly over rough surfaces.

6.2.1.3 Low Level Wind Profiles in a Diabatic Atmosphere

6.2.1.3.1 The Effect of Buoyancy

Turbulent energy in a diabatic atmosphere is damped or amplified by the action of buoyance forces thereby changing the rate of momentum transport and the shape of the wind profile. Of the many equations which purport to describe the wind profile under diabatic conditions three will be discussed here: the power-law profile, the log-plus-

linear-law profile and the exponential-law profile (see Sutton, 1953, p. 230; Priestley, 1959, p. 22; Lumley and Panofsky, 1964, p. 104 for a fuller discussion).

6.2.1.3.2 The Power-Law Wind Profile

To explain the obvious deviations of the wind from the log-law occurring during diabatic conditions Laikhtman (1944) proposed a power-law profile in the form

$$u(z) = \frac{u_*}{k(1-\beta)}\left[\left(\frac{z-d}{z_o}\right)^{1-\beta} - 1\right] \qquad (6.2)$$

where β is greater or less than unity as the atmosphere is unstable or stable respectively. Equation (6.2) reduces to the familiar log-law form when β equals unity.

Deacon (1949, 1957) presents evidence to show that Eq. (6.2) does indeed provide an adequate representation of the wind in diabatic conditions although the constancy of β with height has been questioned (Sutton, 1953, p. 230).

There is also doubt concerning the validity of Eq. (6.2) near the ground because in this region the shearing forces greatly exceed those due to buoyancy and all profiles are expected to approach the log-law form.

Frost (1947), DeMarrais (1959) and Johnson (1959) have tested the validity of another power-law expression

$$u(z) = u(z_1)\left(\frac{z-d}{z_1-d}\right)^{p} \qquad (6.3)$$

and found reasonable agreement with observation although p was observed to increase slightly with height. The parameter p ranges from one half for extreme stability to one sixteenth for extreme instability and takes the value one seventh for neutral conditions. Were the flow to become completely laminar the value of p would be unity, as in Couette flow, but no positive evidence for the existence of linear profiles appears in the micrometeorological literature.

It should be noted that Eq. (6.3) does not approach the log-law form as z approaches zero.

6.2.1.3.3 The Log-Plus-Linear-Law Wind Profile

Although the log-plus-linear-law wind profile

$$u(z) = \frac{u_*}{k}\left[\ell n\left(\frac{z-d}{z_o}\right) + \alpha\left(\frac{z-d}{L}\right)\right] \qquad (6.4)$$

was introduced by Halstead (1943), a sound theoretical basis was not introduced until a decade later when Monin and Obukhor (1954) developed the same equation on the basis of dimensional analysis (Sheppard, 1958). This work has been termed by Priestley (1959) "the most fundamental framework yet proposed for the analysis and unification of the wind profile."

The empirical parameter α in Eq. (6.4) is a constant equal to 0.6 although a considerable disagreement over this value has been expressed (Priestley, 1959, p. 27).

The parameter L is the scale height* defined as

$$L = \frac{-u_*^3}{kg\ H/\rho C_p T} \tag{6.5}$$

where H is the heat flux and the remaining symbols have their usual meanings.

The principal weakness of Eq. (6.4) stems from the assumption made in its derivation that z/L is small, a condition which rarely holds during clear weather (see App. C). Despite this weakness McVehil

---

*Because of the significance of L in later sections a brief discussion of its significance is in order. Introducing the following definitions

$$1.\quad H = \rho C_p K_H\, \partial\theta/\partial z \tag{6.6}$$

$$2.\quad u_*^2 = K_M\, \partial u/\partial z \tag{6.7}$$

$$3.\quad R_f = \frac{K_H}{K_M}\,\frac{g}{\theta}\,\frac{\frac{\partial\theta}{\partial z}}{(\partial u/\partial z)^2} = \frac{K_H}{K_M} R_i \tag{6.8}$$

and substituting into Eq. (6.5), we find that

$$L = -\frac{K_M}{u_* k R_f} \tag{6.9}$$

or in nearly neutral conditions where

$$K_M \approx u_* k (z-d) \tag{6.10}$$

$$R_f \approx -\frac{z-d}{L} \tag{6.11}$$

From Eq. (6.11) L is seen to be the height at which in an unstable or stable atmosphere R_f becomes -1 or +1, corresponding to the level at which natural convection begins or turbulence is damped out respectively.

(1964) finds reasonable agreement between theory and observation in stable conditions.

6.2.1.3.4 The Exponential-Law Profile

Swinbank (1964) proposes a wind profile law in the form

$$u(z) = \frac{u_*}{k} \ln \left\{ \frac{\exp\left[\frac{z-d}{L}\right] - 1}{\exp\left[\frac{z_o}{L}\right] - 1} \right\} \qquad (6.12)$$

an equation containing no empirical parameters.

It may be seen that for small z/L Eq. (6.12) reduces to the log-law profile. It is also of interest to note that the expanded form of the differential expression for Eq. (6.12), i.e.

$$\frac{\partial u}{\partial z} = \frac{u_*}{k(z-d)} \left[1 + 0.5 \left(\frac{z-d}{L}\right) + 0.083 \left(\frac{z-d}{L}\right)^2 + \ldots \right] \qquad (6.13)$$

is almost identical to the complete expression for the differential form of Eq. (6.4) which is

$$\frac{\partial u}{\partial z} = \frac{u_*}{k(z-d)} \left[1 + \alpha_1 \left(\frac{z-d}{L}\right) + \alpha_2 \left(\frac{z-d}{L}\right)^2 + \ldots \right] \qquad (6.14)$$

The value 0.5 of the coefficient of (z-d)/L in Eq. (6.13) agrees well with the value $\alpha_1 = 0.6$ given by Monin and Obukhov (1954).

The striking resemblance between the Swinbank and Monin-Obukhov equations is more than coincidental. Both are derived on the basis of temperature and wind speed profile similarity, but Swinbank's method by making use of the energy equation in which the gradient of wind speed and temperature are combined eliminates one arbitrary constant.

Because of its simplicity of form and excellent agreement with published data (Swinbank, 1964; MacKay, 1965) the exponential profile is adopted as the most appropriate expression for the wind profile near the ground.

6.2.1.3.5 An Extension of the Wind Profile to Higher Levels

Wind speed data observed at 12 levels on a tower near Dallas, Texas between 9 and 433 meters (Gerhardt et al., 1962) afford an opportunity to observe the extent to which the low level wind profile models are applicable at higher levels. In a recent analysis of the data Thuillier and Lappe (1964) present convincing evidence to demonstrate the applicability of the log-law of Eq. (6.1) to wind profiles in neutral and unstable conditions up to an elevation of 100 m. Above that level the wind speed tends to become constant with height. When the lapse rate is slightly stable the Laikhtman-Deacon model of Eq. (6.2) represents the wind profile reasonably well up to 150 m. When inversion conditions exist neither equation is satisfactory. The above authors do not attempt to use either the Monin-Obukhov or Swinbank models mentioned earlier.

The fact that log-law and power-law wind profiles provide reasonable agreement with the observations does not necessarily imply that all the assumptions leading to the derivations of those laws have been met; however, it can be stated that either the assumptions are not strongly violated or errors are compensating.

6.2.2 The Wind in the Convective Layer

6.2.2.1 The Balance of Forces in the Convective Layer

The convective layer of the atmosphere, also called the friction layer or planetary boundary layer is that portion of the atmosphere directly mixed by turbulence generated at the ground. The thickness of the convective layer varies with the wind speed, the coriolis force, the surface roughness and factors which affect the stability of the air. In southern Michigan during the ragweed hayfever season, extending from late August through early September, the convective layer is estimated to be about 2 km in height, but extends briefly to much greater heights with the development of heavy cumulus or cumulonimbus clouds in low pressure troughs.

To consider all the wind generating and dissipating forces acting within the convective layer would constitute a prodigious problem. The remarks here will therefore, be limited to the consideration of a steady, incompressible, barotropic flow, entirely dominated by the pressure gradient, the Coriolis force and the eddy viscosity. Under these simplified conditions the equations of motion are written

$$\left.\begin{aligned} \frac{\partial}{\partial z}\left(K_M(z)\,\frac{\partial u}{\partial z}\right) &= -f(v-v_g) \\ \frac{\partial}{\partial z}\left(K_M(z)\,\frac{\partial v}{\partial z}\right) &= f(u-u_g) \end{aligned}\right\} \qquad (6.15)$$

where u_g and v_g are the components of the geostrophic wind parallel

and normal to the surface wind respectively and f is the Coriolis parameter.

6.2.2.2 The Taylor Model

The earliest solution to Eq. (6.15) was found by Ekman (1902) for the velocity distribution in the upper layers of the ocean. The first application to the atmosphere was made by G. I. Taylor (1915) who, assuming constant K, found a solution which appeared to conform well to observed wind distributions (Fig. 6.1). From his solution Taylor

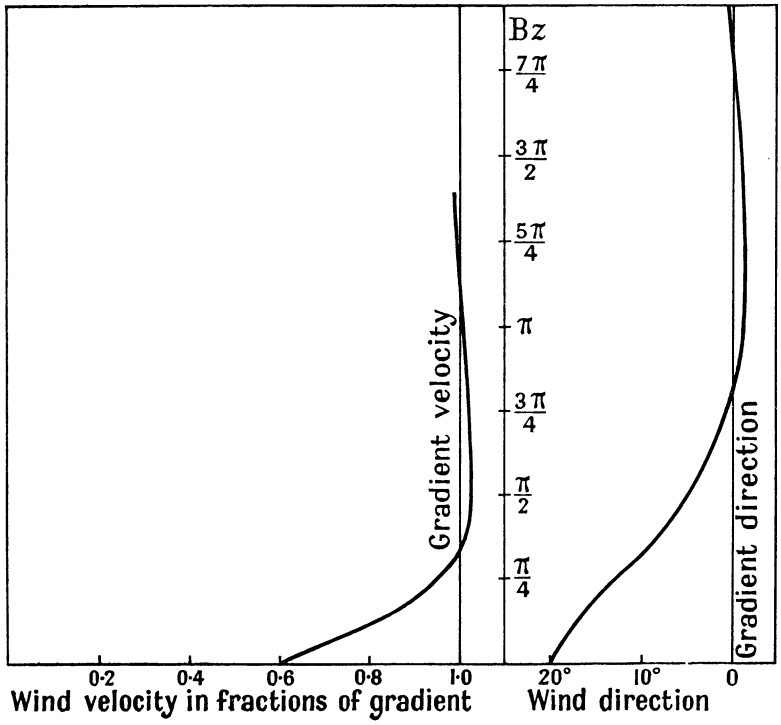

Fig. 6.1. The wind in the convective layer (Taylor, 1915).

was able to relate the angular deviation α of the geostrophic wind from the surface wind to the height H at which the geostrophic wind first obtains by the expression

$$\alpha = \sqrt{\frac{f}{2K}}\, H - \frac{3\pi}{4} \qquad (6.16)$$

An estimate of the height of the convective layer during neutral lapse conditions is found by substituting reasonable values for the parameters in Eq. (6.16). Taking $\alpha = 20°$ and $f = 10^{-4}$ sec^{-1}

$$H = 0.4 \times 10^{-3} \sqrt{K} \tag{6.17}$$

which gives, for K ranging from 0.1 to 36 m^2 sec^{-1} values of H ranging from 120 to 2400 meters.

Despite the reasonable appearance of Taylor's solutions they, in fact, do not adequately represent the wind in the convective layer, yielding values for H which are too large (Sheppard, et al., 1952). The error stems from the assumption of constant K whereas it actually increases with height in approximately the lower hundred meters above the ground. Efforts to solve Eq. (6.15) by other workers have revolved around the choice of a more realistic eddy viscosity profile.

6.2.2.3 The Rossby Model

Rossby and Montgomery (1935) propose a model in which the eddy viscosity increases linearly with height near the ground in the following manner

$$K_M = u_* k z \tag{6.18}$$

but decreases as the square of the height further aloft, i.e.

$$K_M = \frac{f}{3\sqrt{2}} (H-z)^2 \tag{6.19}$$

where H is the height of the geostrophic wind level. It should be noted that Eq. (6.19) is Rossby's (1932) solution for the distribution

of eddy viscosity in a neutral atmosphere free of the influence of the ground. One feels intuitively that the sharp peak in eddy viscosity, at the level h where the two regimes join, cannot exist; however, supporting observational evidence is given by Bunker (1952).

The restrictions imposed by continuity in mixing length, wind strength and frictional drag at the level h lead to a set of equations

$$\left.\begin{aligned} \frac{u_g}{fz_o} &= \frac{435}{\sin\alpha}\exp\left(3.9\cot(\alpha) - 2.76\right) \\ h &= 0.54\,\frac{k^2 u_g}{f}\sin\alpha \\ H &= 9.35h \end{aligned}\right\} \qquad (6.20)$$

which together with Eqs. (6.18) and (6.19) show that the entire distribution of eddy viscosity and thus the entire wind field are determined, in a neutral atmosphere, by the three parameters u_g, f and z_o.

According to the Rossby-Montgomery model the eddy viscosity decreases to zero at the level H whereas in the atmosphere a degree of residual turbulence is maintained throughout the troposphere. A model suggested by Rossby (1935) which incorporates the residual turbulence is illustrated in Fig. 6.2.

When stable stratification exists, the turbulent kinetic energy for the same shearing stress must increase or decrease in proportion to the available potential energy, i e.

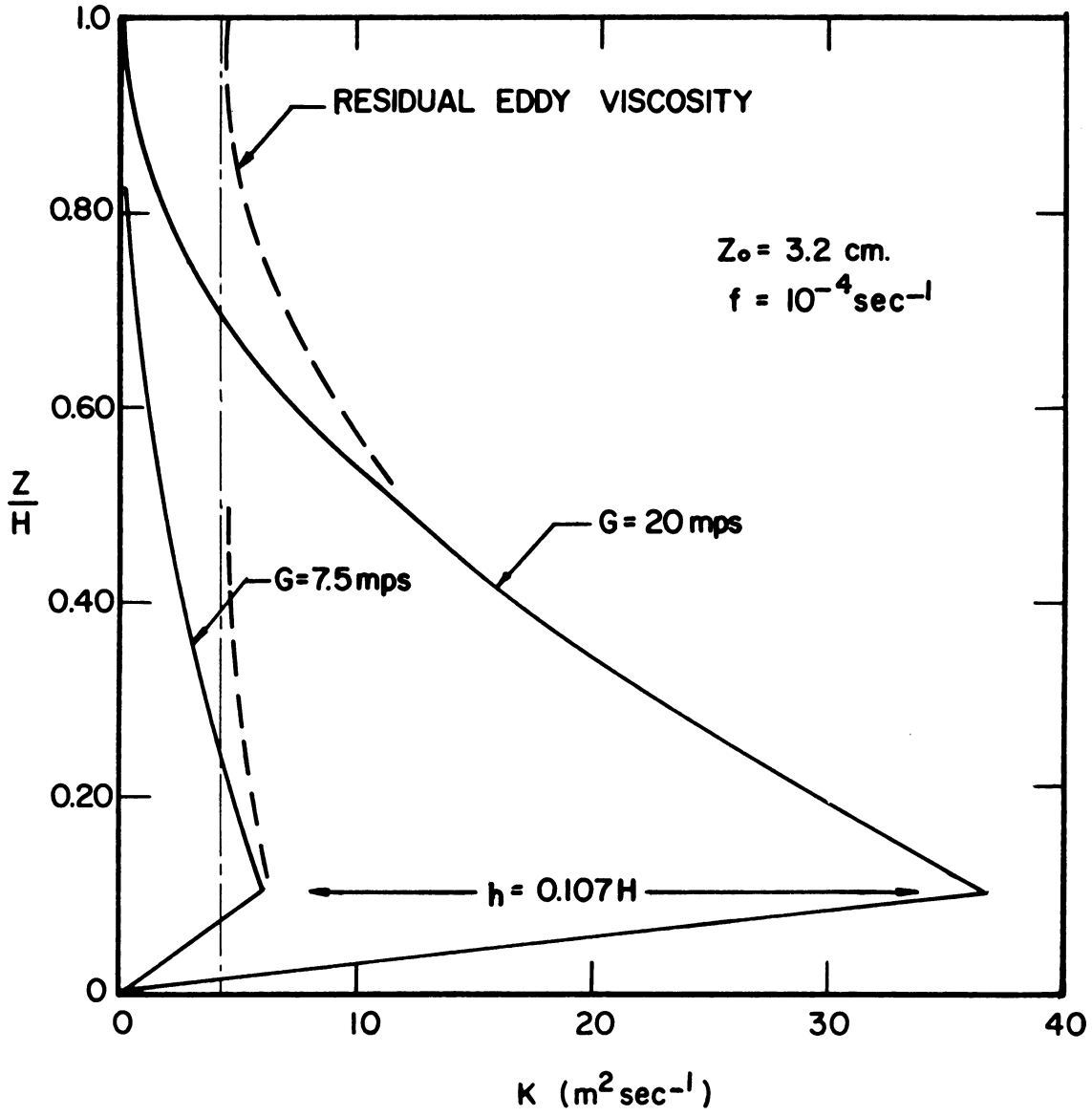

Fig. 6.2. The distribution of eddy viscosity with height (Rossby and Montgomery, 1935).

$$\ell^2\left(\frac{\partial u}{\partial z}\right)^2 = \ell_s^2\left[\left(\frac{\partial u}{\partial z}\right)^2 - \frac{\sigma g}{\theta}\frac{\partial \theta}{\partial z}\right] \qquad (6.21)$$

where σ is a constant and ℓ and ℓ_s are the mixing lengths under neutral and stable stratification. The similarity of this procedure to that used by Swinbank (see Sect. 6.1.3.2.4) should be noted. Equation (6.21) can be written in the form

$$K_M = \frac{u_* kz}{(1+\sigma R_i)^{1/2}} \qquad (6.22)$$

where R_i is the Richardson number and σ is a constant. For extreme stabilities Eq. (6.22) has an asymptotic value

$$K \propto z^{1/2} \qquad 0 \leq z \leq h \qquad (6.23)$$

The asymptotic value of the wind speed profile is also given by

$$u \propto z^{1/2} \qquad 0 \leq z \leq h \qquad (6.24)$$

In a critical discussion of the validity of Eq. (6.22) (Sutton, 1953, p. 265) it is pointed out that

1. σ is a function of stability and not a constant as implied by the equation.

2. The equality of the K's for momentum and heat has been assumed.

3. The eddy viscosity is implied to remain finite for all values of R_i.

If, as suggested by comment 2 above, the ratio K_H/K_M is a function of stability (see the discussion on this topic later in the chapter) then the error in Eq. (6.22) caused by equating the K's may be just the error observed in σ. Support for this statement is given by MacKay (1965) who observes a tenfold increase in the ratio K_H/K_M with increasing stability over a range of stabilities in which there is an equivalent increase in the value of σ (Deacon, 1949). The variation of K_H/K_M with stability is, however, a controversial question at the present time, as also is the existence of a critical value for R_i implied by comment 3 above.

6.2.2.4 The Lettau and Blackadar Models

Given a distribution for the eddy viscosity, Eq. (6.15) may be solved by numerical methods to find the wind profile in the convective layer. Such computations have been carried out successfully by Lettau (1961) and by Blackadar (1962).

The eddy viscosity may be determined indirectly through the mixing length ℓ by means of the relation

$$K_M = \ell^2 \frac{\partial u}{\partial z} \tag{6.25}$$

although it seems incongruous to compute the eddy viscosity by means of an uncertain relation (Eq. (6.25)) containing a hypothetical parameter, the mixing length, rather than simply by assuming a distribution for the eddy viscosity itself.

Lettau (1961) proposes what he calls a linear-hyperbolic-law which he derives from pipe flow and expects to apply universally to flows in a neutral atmosphere. His equation is written

$$\ell = \frac{kz}{1+4\left(\frac{z}{H}\right)^{5/4}} \tag{6.26}$$

Blackadar (1962) proposes a simple model similar in form to that of Lettau and written

$$\ell = \frac{kz}{1+\frac{kz}{\lambda}} \tag{6.27}$$

λ being the mixing length in the free atmosphere.

The mixing length models proposed by Lettau and Blackadar differ considerably from the model proposed by Rossby, as may be seen in Fig. 6.3. The Rossby model has been selected as most appropriate, for

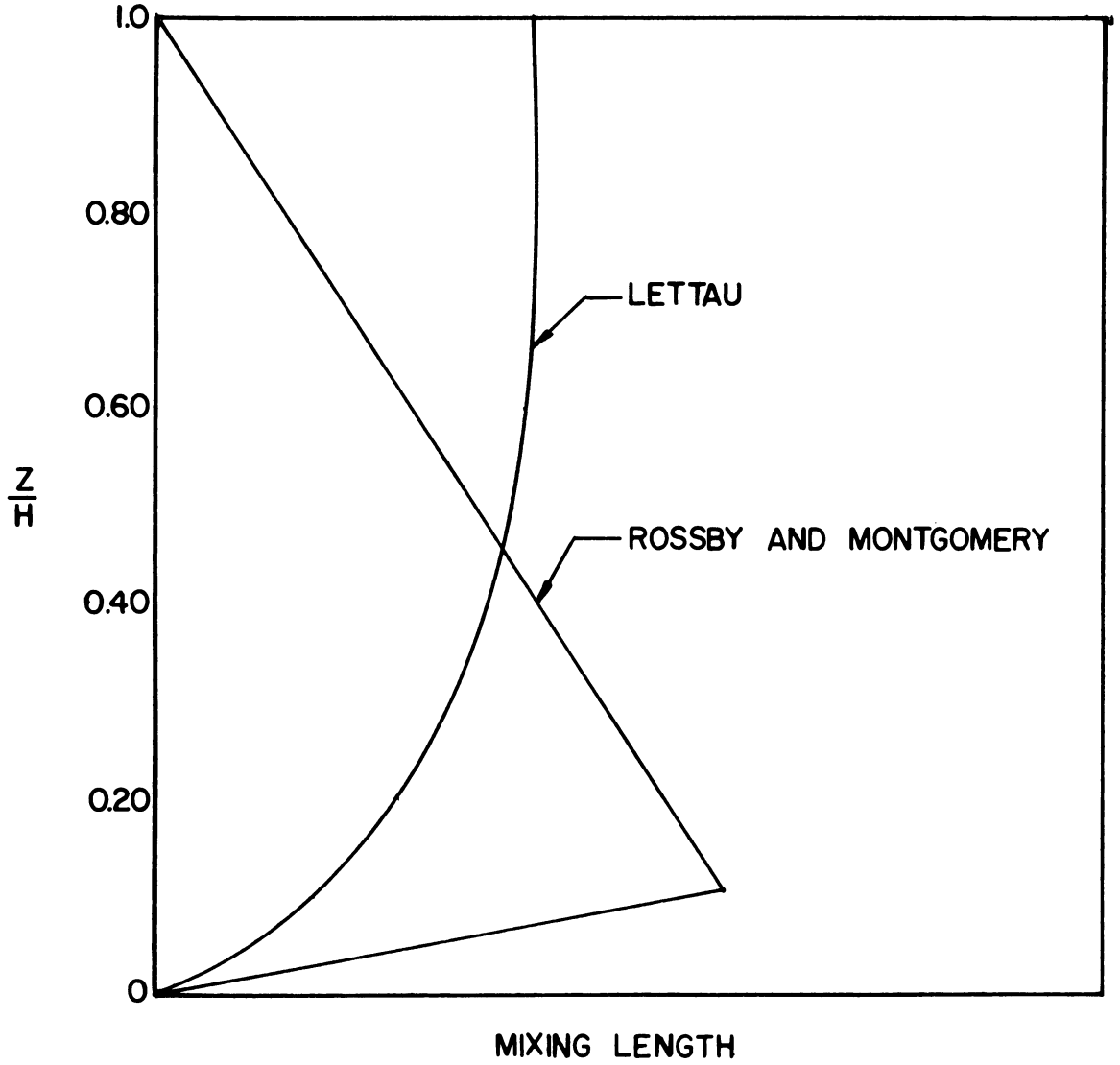

Fig. 6.3. The distribution of mixing length with height.

the following reasons:

1. The top of the convective layer is normally stable and therefore will damp turbulence in much the same way as it is damped at the ground.

2. Residual turbulence, i.e., that caused by the breakdown of synoptic systems, is normally much smaller than ground in-

duced turbulence and can therefore be neglected.

3. If there is a level above which ground generated eddies do not form and if eddy decay and eddy diffusion are accompanied by a reduction in eddy size, then there must be a level of maximum mixing length.

Once a distribution of mixing length or of eddy viscosity has been determined Eq. (6.15) can be solved by numerical methods. Typical solutions by Blackadar (1962) are shown in Fig. 6.4.

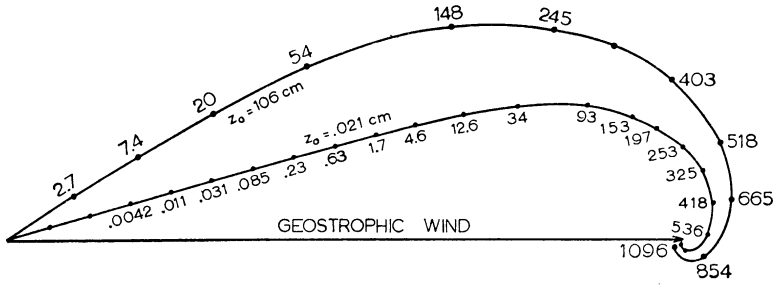

Fig. 6.4. The wind spiral in the convective layer (Blackadar, 1962).

6.3 THE VERTICAL COMPONENT OF EDDY DIFFUSIVITY

6.3.1 Statement of Purpose

The exchange coefficient hypothesis is based upon the premise that the flux of an entity is equal to the product of its gradient and a variable called the eddy diffusivity. It is the purpose of this section to review practical methods for computing the eddy diffusivity and to select the most appropriate models for inclusion in the diffusion equations.

6.3.2 The Equivalence of Eddy Viscosity, Eddy Diffusivity for Heat and Eddy Diffusivity for Mass

6.3.2.1 Equivalence of the Diffusion Coefficients-Inertial Effects

One might suppose that because all entities in the atmosphere are transported by the same eddies their diffusion coefficients would be equal; but, this is not necessarily so. Not only is it possible that the diffusion coefficients for heat, momentum and mass are different from one another, but the diffusion coefficient for mass may vary among particles of different sizes. The question which must be answered is, to what degree do they differ and of what magnitude is the error introduced by the assumption of their equality?

The eddy diffusivity K for gases or particles of negligible inertia is considered by Ellison (1957) to be identical to the eddy diffusivity for heat K_H because, as he states, both heat and mass are transported by the same eddies and there is no means within the scope of present theory by which they may be separated. K for particles of appreciable inertia however must be smaller than K_H because the motion of such particles will lag behind the eddy motion. This statement does not include the effect of the gravitational fall speed of large particles, which also serves to reduce the diffusivity (Yudine, 1959).

To achieve an estimate of the magnitude of the reduction of the eddy diffusivity due to inertial effects consider the equation of motion of a particle in a resistant medium of small Reynolds number (Fuks, 1964, p. 70), which is

$$m\frac{dv}{dt} = \underset{(1)}{F(t)} - \underset{(2)}{\frac{2}{3}\pi a^3\rho\frac{dv}{dt}} - \underset{(3)}{6\pi\eta av} - \underset{(4)}{6r^2\sqrt{\pi\eta\rho}}\int_0^t \frac{dv}{dx}\frac{dx}{\sqrt{t-x}} \quad (6.28)$$

where a is the particle radius, η is the dynamic fluid viscosity, ρ is the air density and the other symbols have their usual meanings.

The forces on the right of Eq. (6.28) are

1. the external body forces on the particle, e.g. gravity or electrical forces.

2. the force needed to accelerate the displaced mass of fluid,

3. the force needed to overcome the viscous drag of the fluid and

4. a force caused by the difference between the particle acceleration and that of the fluid.

For particles moving in air, Terms 2 and 4 are negligible because of the very low density of the air relative to that of the particle and therefore an accurate approximation to Eq. (6.28) may be written (Fuks, 1964, p. 71)

$$\frac{dv}{dt} + \frac{v}{\tau^*} - g = 0 \quad (6.29)$$

where the body force per unit mass is represented by the acceleration of gravity g and τ^* is the particle relaxation time mentioned in Chapt. 5 and given by the expression

$$\tau^* = \frac{2a^2\rho_p}{9\eta} \quad (6.30)$$

ρ_p being the particle density.

When the relaxation time is much smaller than the period of the energy containing eddies, the particle will follow the air motion closely (Liu, 1956); but, as the relaxation time increases the inertial lag increases until a state is reached in which the particle maintains a steady motion while the turbulent flow oscillates about it.

To assess the magnitude of the inertial lag for ragweed pollen let us compare its relaxation time with the period of the energy containing eddies. Appropriate values for the variables in Eq. (6.30) are, $a = 10^{-5}$ m, $\eta = 1\ 845 \times 10^{-2}$ gm m^{-1} sec^{-1} and $\rho_p = 0.83 \times 10^{6}$ gm m^{-3} and therefore from Eq. (6.30) $\tau^* = 0.1$ sec. The period of the smallest energy containing eddies of consequence at a height of 1 m in the diffusion of heat and presumably of matter is 0.1 sec (Perepelkina, 1957), but this is measured in an Eulerian system. A crude conversion to the Lagrangian system experienced by the particle can be accomplished by multiplying by $\sqrt{\pi}/4i$ where i is the intensity of turbulence (see Eq. (2.50)). If i is assumed to be equal to 0.1 then the period of the smallest energy containing eddy at 1 m above ground is approximately 0.4 sec or four times the relaxation time of ragweed pollen. It is concluded that ragweed pollen follows the air motion with considerable precision, a result confirmed by Csanady (1963).

The reduction in dispersion caused by the settling velocity of the particle, mentioned above, is negligible for particles the gravitational settling speed of which is less than 1 m sec^{-1} (Smith, 1959); consequently, this effect may be neglected in the case of ragweed

pollen whose fall speed is 0.012 m sec^{-1}.

From the foregoing discussion and on the basis of admittedly inadequate theory it is concluded that the eddy diffusivity for ragweed pollen is virtually identical to the eddy diffusivity for heat. The next question is, how are these related to the eddy vixcosity?

6.3.2.2 Equivalence of K_H and K_M - Ellison's Model

Although actual mass exchange is necessary for the transport of most entities in the atmosphere, momentum can be transferred by pressure forces alone, making it reasonable to suppose that the exchange coefficient for momentum may differ from those for heat or mass. Whether they do differ and, if so in what way, are questions which have not been satisfactorily answered.

It has been suggested (Ellison, 1957) that the ratio K_H/K_M is zero in extremely stable lapse conditions, increases with decreasing stability and finally approaches an asymptotic limit of about 1.6 under free convection. The argument is rather lengthy and involved, but will be sketched here because of its importance in assessing the value of various diffusivity models.

If the quality of K_H and K_M cannot be assumed, then the atmospheric stability criterion given by Richardson (1925) must be written in terms of the flux Richardson number R_f rather than the gradient Richardson number R_i, as follows

$$R_f = \frac{K_H R_i}{K_M} = \frac{K_H}{K_M} \frac{g\, \partial \bar{\rho}_a / \partial z}{\bar{\rho}_a (\partial u / \partial z)^2} = \frac{g\, \overline{\rho' w}\, K_M}{\bar{\rho} u_*^4} \qquad (6.31)$$

where the terms have their usual meanings. Richardson (1920) argued that R_f cannot exceed unity over any substantial depth of the atmosphere. Present observational evidence suggests that the limiting value of the flux Richardson number, $R_{f_{crit}}$, is considerably less than this (see Sutton 1953, p. 264). No such limit exists for R_i as noted by Ellison (1957) and therefore he concludes that with increasing R_i, i.e. with increasing stability, the ratio K_H/K_M must decrease, becoming zero in the limit. Confirming evidence for values of R_i much greater than unity in the atmosphere is given by Portman et al. (1962) who reports values of R_i exceeding 100.

To examine the behavior of K_H/K_M at the other extreme define

$$H^* = \frac{\overline{\rho' w}}{\left(\frac{g}{\bar{\rho}}\right)^{1/2} z^2 \left(\frac{d\bar{\rho}}{dz}\right)^{3/2}} = h \qquad (6.32)$$

where the denominator will be recognized as proportional to the heat flux in free convection (Priestley, 1959, p. 40) and the proportionality constant h has a value of approximately 0.9. Defining

$$K_H^* = \frac{K_H}{u_* z} = \frac{\overline{\rho' w}}{u_* z \frac{d\bar{\rho}}{dz}} \qquad (6.33)$$

$$L = \frac{\rho u_*^3}{g \overline{\rho' w}} \qquad (6.34)$$

and

$$Z = z/L \qquad (6.35)$$

Equation 6.32 can be written

$$H^{*2} = - K_H{}^{*3} Z^{-1} \tag{6.36}$$

If one substitutes Eqs. (6.33), (6.34), (6.35) and (6.36) into (6.31) an equation for R_f is produced in the form

$$R_f = \frac{K_H{}^{*3} K_M{}^{*}}{H^{*2}} \tag{6.37}$$

Now if it is assumed that both K_M and K_H are independent of u_* in free convection, i.e. all transport is a consequence of buoyant motion and independent of wind shear, then K_H/K_M must be constant. Therefore because the denominator of Eq. (6.37) is a constant, the flux Richardson number becomes

$$R_f \propto K_M{}^{*4} \tag{6.38}$$

A semi-empirical formula which embodies the limiting criteria outlined above is

$$\left(\frac{K_M{}^{*}}{k}\right)^4 = 1 - \frac{R_f}{R_{f_{crit}}} \tag{6.39}$$

which with some manipulation leads to an equation giving the ratio of K_H to K_M in free convection, namely

$$\frac{K_H}{K_M} = R_{f_{crit}}{}^{1/3} H^{*}{}^{2/3} k^{-4/3} \tag{6.40}$$

To derive an estimate for the value $R_{f_{crit}}$, $K_M{}^{*}$ is expanded in a power series (Monin, 1955)

$$\frac{K_M{}^{*}}{k} = 1 + \alpha_1 Z + \alpha_2 Z^2 \tag{6.41}$$

hence

$$\left(\frac{K_M^*}{k}\right)^4 = 1 + 4\alpha_1 Z + 6(\alpha_1 Z)^2 + \ldots \qquad (6.42)$$

and from Eqs. (6.39), (6.37) and (6.36)

$$\left(\frac{K_M^*}{k}\right)^4 = 1 - \frac{ZK_M^*}{R_{f_{crit}}} \qquad (6.43)$$

or for small Z

$$R_{f_{crit}} = \frac{K_M^*}{4\alpha_1} \qquad (6.44)$$

If $K_M^* \approx k = 0.4$ and $\alpha_1 = 0.6$ the value of $R_{f_{crit}}$ becomes 0.15 and from Eq. (6.40) the ratio K_H/K_M in free convection is 1.6*.

In summary, Ellison's model for the stability dependence of the ratio K_H/K_M requires

1. The existence of a limiting value for R_f in extreme stabilities; namely, $R_{f_{crit}}$.
2. The existence of a constant ratio K_H/K_M during free convection.

The uncertainty surrounding the true value of the ratio K_H/K_M has led many researchers to equate it to unity thus making R_f equal to R_i.

6.3.2.3 Equivalence of K_H and K_M - Businger's Paradox

The similarity theory approach, requiring as it does the pro-

*It is interesting to note that if the value of α_1 is 6.0 (Pasquill, 1962, p. 75) the asymptotic value for K_H/K_M is 0.82.

portionality of the diffusion coefficients, has been criticized by Businger (1958) on a novel basis. He shows that, if similarity is maintained, the diffusivities for heat and momentum, if equal for a short period average, must be unequal for a long period average, i.e., that the ratio K_H/K_M is a function of the observation period.

Consider an interval during which the average values of eddy viscosity and conductivity, wind gradient and temperature gradient are $\overline{K_M}$, $\overline{K_H}$, $\overline{du/dz}$ and $\overline{d\theta/dz}$ respectively and suppose that during the first half of this interval the wind is light and during the second half it is strong. Then indicating the first and second halves of the interval by subscripts 1 and 2 respectively the eddy diffusivity and wind gradient during the shorter periods will be

$$K_{M_1} = K_{H_1} = \overline{K_M}(1-\epsilon_1), \qquad K_{M_2} = K_{H_2} = K_M(1+\epsilon_1) \tag{6.45}$$

and

$$\left(\frac{du}{dz}\right)_1 = \left(\frac{d\bar{u}}{dz}\right)(1+\epsilon_2), \qquad \left(\frac{du}{dz}\right)_2 = \left(\frac{d\bar{u}}{dz}\right)(1+\epsilon_2) \tag{6.46}$$

because both the wind gradient and the diffusivity are linearly proportional to the wind speed. The potential temperature gradient, on the other hand, is inversely proportional to the wind speed near the ground and therefore

$$\left(\frac{d\theta}{dz}\right)_1 = \left(\frac{d\bar{\theta}}{dz}\right)(1+\epsilon_3), \qquad \left(\frac{d\theta}{dz}\right)_2 = \left(\frac{d\bar{\theta}}{dz}\right)(1-\epsilon_3) \tag{6.47}$$

Hence, averaging the values for the two halves of the interval one

finds the long period average will be

$$\left.\begin{aligned} \overline{K_M \frac{du}{dz}} &= \bar{K}_M\left(\frac{d\bar{u}}{dz}\right)(1+\epsilon_1\epsilon_2) \\ \overline{K_H \frac{d\theta}{dz}} &= \bar{K}_M\left(\frac{d\bar{\theta}}{dz}\right)(1-\epsilon_1\epsilon_3) \end{aligned}\right\} \qquad (6.48)$$

and it is apparent that the ratio of the eddy coefficients if equal to unity for the short period fluctuations cannot be so for the longer periods.

6.3.2.4 Equivalence of K_H and K_M - Radiational Influences

Near the ground the constancy of the ratio K_H/K_M requires wind and temperature profile similarity if the fluxes of heat and momentum can be assumed constant with height and if radiational fluxes are negligible compared to eddy fluxes. Under inversion conditions the effect of radiational heating and cooling is strong so that profile similarity is unlikely (Elliot, 1964). Under strongly unstable lapse conditions the eddy fluxes greatly exceed the radiational fluxes and therefore the existence of profile similarity is possible and the constancy of the ratio K_H/K_M is more readily checked. Observations appear to indicate an increase in the ratio K_H/K_M with increasing negative R_f (Priestley, 1959, p. 8).

6.3.2.5 Equivalence of the K's Assumed

From the evidence presented the eddy viscosity appears to differ

from the other exchange coefficients but, unfortunately due to conflicting observations and theory, no satisfactory relationship has been established. For simplicity the ratio K_H/K_M will be taken as unity. This assumption permits the computation of K_H and thus K, because these have been assumed equal, from observations of the wind and temperature profiles. From this point on the K's will be used interchangeably.

6.3.3 Classification of the Thermal Regime Near the Ground

When the lower atmosphere is unstable there is an interaction between thermally and mechanically induced eddies which tends to inhibit the growth of buoyant elements (Priestley, 1953). This is particularly true very near the ground in the layer of fully forced convection where the elements are small and the action of mechanical turbulence is sufficiently strong to mix them with environmental air before they can rise. At higher levels in the region of accelerative motion, buoyant elements begin to rise selectively, the rate of rise appearing to be independent of the wind shear, although somewhat inhibited by the presence of the ground. Still higher, in the region of natural convection (Thomas and Townsend, 1957), they became more completely organized and rise independently of the presence of the ground or of mechanically induced turbulence. Throughout this region continued mixing with environmental air by the action of self induced and residual turbulence causes the buoyant element to decelerate

slowly. Finally, on reaching a level where the potential temperature of the rising element equals that of the environmental air their upward motion ceases.

Webb (1958) has classified the three regions outlined above according to the dimensionless height $\zeta = z/L$ as follows:

$$\left.\begin{array}{lll} -0.03 \leq \zeta \leq 0 & \frac{\partial\theta}{\partial z} \propto z^{-1} & \text{forced convection} \\ -1.00 \leq \zeta < -0.03 & \frac{\partial\theta}{\partial z} \propto z^{-4/3} & \text{free convection} \\ \zeta < -1.00 & \frac{\partial\theta}{\partial z} \approx 0 & \text{natural convection} \end{array}\right\} \quad (6.49)$$

(Note that $\zeta \approx R_i$ when ζ is small)

This classification would suggest that in unstable air under all conditions of turbulence the temperature and wind structures are similar, with only the levels separating the three regimes changing.

6.3.4 The Vertical Component of Diffusivity Near the Ground

6.3.4.1 The Vertical Component of the Eddy Viscosity Near the Ground in Forced Convection

The height dependance of the eddy viscosity under neutral lapse conditions in the layer of constant momentum flux is derived directly from the well-known log-law wind profile and the stress equation (Sutton, 1953) and is written

$$K_M = u_* kz = k^2 z^2 \frac{\partial u}{\partial z} \quad (6.50)$$

Equation (6.50) has achieved general acceptance for neutral lapse conditions near the ground and is also assumed to apply in either stable or unstable conditions at heights less than about L/30. The latter corresponds in the unstable case to the region of forced convection in Webb's classification.

The height to which Eq. (6.50) is valid is not known. The only theoretical estimate for this level has been given by Rossby and Montgomery (1935) as

$$h = 2.28 \times 10^{-3} \frac{G}{f} \sin \alpha \qquad (6.51)$$

a function of the latitude α and geostrophic wind speed G. At 45°N with an angular deflection α of 20°

$$h \approx 7.8G \approx 100 \text{ m} \qquad (6.52)$$

under normal summer wind conditions.

6.3.4.2 The Vertical Component of Eddy Viscosity Near the Ground in a Stable Environment

Present knowledge concerning diffusion in a stable atmosphere is, as yet, incomplete and uncertain. The following paragraphs briefly outline current knowledge and specluation on this subject.

It has been postulated (Ellison, 1957) that, if $R_f = R_{f_{crit}}$ and the fluxes of heat and momentum are constant with height, K_M will be independent of height (see Eq. (6.31)). It follows from the definition of K_M that the wind, under these conditions, must increase lin-

early with height. Such a profile corresponds to laminar or Couette flow.

Linear wind profiles are rarely if ever observed.* Liljequist (1955), who measured wind profiles in the Antarctic under strong inversion conditions, never observed a linear wind profile.

Observations of the wind speed using sensitive Thornthwaite anemometers during extreme inversion conditions ($10 \leq R_i \leq 139$) over a snow surface in Michigan (Elder and Ryznar, 1964) failed to indicate a single linear profile; indeed, if the profiles are fitted by a power law, the greatest exponent is 0.5.

It appears likely, therefore, that Ellison's hypothesis is incorrect. Further support for this view comes from heat flux measurements in the Antarctic (Liljequist, 1955) which strongly suggest a value of unity for the ratio K_H/K_M under stable conditions.

A number of models for the eddy viscosity under stable stratification exist. When the stability is slight and the observation height chosen so that the ratio z/L is small the log-plus-linear profile leads to the following formula for K_M:

$$K_M = \frac{ku_*z}{1 + \frac{\alpha z}{L}} \approx ku_*z(1-\alpha R_i) \qquad (6.53)$$

---

*The oft quoted observations of Rider and Robinson (1951) were made in mean winds of 0.2 to 0.8 m sec^{-1} using Sheppard anemometers. As stated by the authors, "Some stopping of the anemometers occurred."

For greater stabilities Eq. (6.22) by Rossby and Montgomery (1935) may be used in the form

$$K_M = ku_*z(1+\sigma R_i)^{-1/2} \tag{6.54}$$

where σ is an empirically determined constant. For extreme stabilities K_M asymptotically becomes proportional to $z^{1/2}$, coinciding with the value given for extreme stability by Kohler (see Sutton 1953, p. 245) and observed by Elder and Ryznar (1965) and by Liljequist (1955).

Kohler assumes a power law for the wind profile

$$u = u_1\left(\frac{z}{z_1}\right)^{1-m} \tag{6.55}$$

which if the momentum flux is constant with height yields the Schmidt conjugate-power-law for the eddy viscosity in the form

$$K_M = K_1\left(\frac{z}{z_1}\right)^{m} \tag{6.56}$$

Kohler's equations and particularly his solutions for the friction layer wind seem to provide a reasonable fit to observations. Under any given regime both K_1 and m must be estimated.

A promising equation for the eddy viscosity has been derived by Swinbank (see Sect. 6.2.1.3.4), namely

$$K_M = ku_*L\left[1 - \exp\left(-\frac{z}{L}\right)\right] \tag{6.57}$$

From a good set of data Swinbank was able to show that L and u_* were constant over a limited height range. He also found good agreement between measured and computed heat flux. One difficulty in using

Eq. (6.57) is that u_* and L are themselves difficult to measure.

Finally, Ellison (1957) has suggested an equation for K_M of the form

$$K_M = ku_*z\left(1 - \frac{R_f}{R_{f_{crit}}}\right)^{1/4} \tag{6.58}$$

Equation (6.58) is highly speculative as mentioned earlier; in particular, for large stabilities it depends on the ratio K_H/K_M approaching zero. Support for Eq. (6.58) is presented in a recent paper by Webster (1964) which strongly suggests that K_H/K_M does decrease to zero for large R_i. Webster's work, however, was carried out in the wind tunnel with forced linear gradients of temperature and wind speed and under conditions which could hardly be considered steady. Even if true, Webster's results do not necessarily apply to the atmosphere where artificial wind and temperature gradients cannot be maintained. Even if Eq. (6.58) did hold, the application would still be of doubtful value due to ignorance of the correct value for $R_{f_{crit}}$.

A simple modification of Eq. (6.58) has been advanced (Panofsky, Blackadar, McVehil, 1960) in the form*

*Panofsky et al. (1960) have written Eq. (6.58) in a neat form. Define a non-dimensional eddy viscosity by

$$S = \frac{u_*kz}{K_M} \tag{6.60}$$

and substitute into Eq. (6.58). The resulting equation is

$$S^4 + \frac{1}{R_{f_{crit}}}\frac{z}{L}S^3 = 1 \tag{6.61}$$

The authors proceed to the assumption that K_H/K_M is a constant and thereby negate one of the prime assumptions in the development of Eq. (6.58). The entire argument is certainly highly controversial (Lumley and Panofsky, 1964, p. 112). Equation (6.61) may also be derived using dimensional arguments (Panofsky, 1961).

$$K_M = ku_*z(1 - 18\ R_i)^{1/4} \qquad (6.59)$$

where the constancy of the ratio K_H/K_M has been assumed. Equation (6.59) is obviously inapplicable to conditions of extreme stability.

6.3.4.3 The Vertical Component of Eddy Viscosity Near the Ground in an Unstable Environment

It is the object of this section to compare critically the great variety of equations which have been derived for the eddy viscosity in stable conditions. Each model must conform at least roughly to Webb's classification, Eq. (6.49), i.e., that K_H must increase linearly near the ground and roughly at $z^{-4/3}$ in the layer of free convection. The further assumption is made that K_M and K_H are equal. A brief summary of the equations follows:

1. Schmidt (see Sutton, 1953, p. 85)

$$K_M = K_1\left(\frac{z}{z_1}\right)^m$$

2. Holzman (1943)

$$K_M = ku_*z(1 - 10\ R_i)^{1/2}$$

3. Laikhtman (1944), Deacon (1949)

$$K_M = ku_*z\left(\frac{z}{z_o}\right)^{\beta-1}$$

4. Monin and Obukhov (1954)

$$K_M = ku_*z\left(1 - \frac{\alpha z}{L}\right) \qquad \frac{z}{L} \text{ small}$$

5. Ellison (1957)

$$K_M = ku_*z\left(1 - \frac{R_f}{R_{f_{crit}}}\right)^{1/4}$$

6. Panofsky et al. (1960)

$$K_M = ku_*z(1 - 18\ R_i)^{1/4}$$

7. Swinbank (1964)

$$K_M = ku_*L\left[1 - \exp\left(-\frac{z}{L}\right)\right]$$

8. Prandtl (1932)

$$K_H = hz^2\left(\frac{g}{T}\left|\frac{\partial\theta}{\partial z}\right|\right)^{1/2} \quad - 1.00 \leq \frac{z}{L} < - 0.03$$

It is indeed unfortunate that no set of data is available which will determine finally the correct form for the wind and eddy viscosity profiles. Of the equations above the first is incorrect near the ground because it fails to approach the logarithmic form and the fifth is impossible to use until more is known about Rf_{crit} and the ratio K_H/K_M. The fourth equation is derived under the assumption that z/L is small and therefore is unsuitable for use over a significant height range during periods of marked instability.

The third equation above has been used extensively and found to provide a reasonable fit to assorted data except under very stable conditions (Rider, 1954). The parameter β, however, must be derived empirically and therefore lacks universal applicability. As mentioned earlier in this chapter β is a function of the Richardson number and therefore of height so that in any given situation the third equation above gives at best only a crude approximation to the true eddy viscosity profile (see Priestley, 1959, p. 24).

The second and sixth equations have been shown to agree reasonably well with wind profile data over a broad range of stabilities. Both, however, have a dependence on R_i, which leads to some obviously erroneous conclusions concerning the temporal variation of the eddy viscosity during sunny calm weather (see App. C).

Seventh is Swinbank's equation, developed earlier, which, though it appears to fit most profile data well over a broad range of stabilities, shows systematic deviations from the Project Prairies Grass data (Barad, 1963). It should be borne in mind that the profile data themselves may contain systematic errors (MacCready, 1964) so that lack of agreement between model and observation is not necessarily proof that the model is wrong.

Prandtl's equation for free convection, the eighth above, applies within the appropriate range of z/L values in the free convective regime and has been found to agree well with observations during such periods (see App. C of this study).

6.3.5 The Vertical Component of the Diffusivity Within the Friction Layer Well Above the Surface

In a stable or adiabatic atmosphere the vertical component of the eddy viscosity can be estimated by the methods outlined in Sect. 6.2.2.3 and during free convection by the Prandtl method mentioned above. During natural convection, however, where $z/L < -1.00$, neither

of these methods is satisfactory; indeed, although much study has been devoted to the subject there is as yet no adequate description of the distribution of the vertical component of the diffusivity in the atmosphere. To clarify the problem a brief description of the fundamental nature of convection in a turbulent medium follows.

Consider first the convective motion of a buoyant bubble in a fluid at rest. It has been demonstrated that, in a still environment, the volume of a rising buoyant element increases by entrainment in exact proportion to the rate of ascent, resulting in a linear growth of the element with height (Morton, Taylor and Turner, 1956).

When the fluid is not at rest and turbulence exists independently of the motion of rising buoyant elements, the growth of such elements may not be a linear function of their rate of ascent. For example, recent observations of thermals in the atmosphere reveal that they do not necessarily expand with height (Warner, 1963). Warner suggests that turbulence existing outside the thermal may provide a mechanism for its erosion at a rate approximately equal to its self induced rate of growth. A theoretical treatment of a similar problem is given by Turner (1963).

The theory of buoyant motion in a turbulent atmosphere has been developed by Priestley in a series of papers on the subject (1953, 1954 (a); 1954 (b); 1957 and 1960). Because of its fundamental importance to the ideas being considered the first paper (Priestley, 1953) is reviewed here.

Consider the pair of equations

$$\left.\begin{aligned} \frac{dw}{dt} &= \frac{g}{T_e}(T-T_e) \\ \frac{dT}{dt} &= -w\,\Gamma \end{aligned}\right\} \qquad (6.62)$$

T_e being the environmental temperature and Γ the dry adiabatic rate of cooling. The first equation represents the acceleration of an element due to buoyancy, and the second the change in temperature due to adiabatic expansion. In the first equation the assumption is made that the environmental air is not accelerated.

Equations (6.62) are then treated by the standard perturbation technique and the equation of continuity subtracted giving

$$\left.\begin{aligned} \dot{\bar{w}} &= \frac{g}{T_e}(\bar{T}-T_e) - \frac{\partial}{\partial x}\overline{(u'w')} + \frac{\partial}{\partial y}(v'w') + \frac{\partial}{\partial z}(w'w') \\ \dot{\bar{T}} &= \bar{w}\Gamma - \frac{\partial}{\partial x}\overline{(u'T')} + \frac{\partial}{\partial y}(v'T') + \frac{\partial}{\partial z}(w'T') \end{aligned}\right\} \qquad (6.63)$$

where the dot represents partial differentiation with respect to time.

The next step is to apply an exchange coefficient hypothesis to the Reynold's stresses and their thermal counterparts, i.e.,

$$\left.\begin{aligned} \overline{u'w'} &= K_1 \frac{\partial w}{\partial x} \\ \overline{u'T'} &= K_2 \frac{\partial T}{\partial x} \end{aligned}\right\} \qquad (6.64)$$

and similar expressions for the terms in Eq. (6.63). The unfamiliar form of Eq. (6.64) may be explained by noting the following equality

$$K \frac{\partial u}{\partial z} = \frac{\tau_{xz}}{\rho} = \frac{\tau_{zx}}{\rho} = K_1 \frac{\partial w}{\partial x} \tag{6.65}$$

Making the isotropic assumption and substituting Eq. (6.64) in Eq. (6.63) one obtains

$$\left.\begin{aligned} \dot{\bar{w}} &= \frac{g}{T_e} (\bar{T}-T_e) + K_1 \overline{\nabla^2 w} \\ \dot{\bar{T}} &= - \bar{w}\Gamma + K_2 \overline{\nabla^2 T} \end{aligned}\right\} \tag{6.66}$$

Next, assume that the buoyant element is spherical, of radius R, that the interior vertical velocity is w and the exterior vertical velocity zero. Express the Laplacian in the finite difference form

$$\left.\begin{aligned} \overline{\nabla^2 w} &= \frac{C_1 \bar{w}}{R^2} \\ \overline{\nabla^2 T} &= C_2 \frac{(T-T_e)}{R^2} \end{aligned}\right\} \tag{6.67}$$

where the C's are form factors depending on the distribution of w and T within the buoyant element. Introducing Eq. (6.67) into (6.66) one finds that

$$\left.\begin{aligned} \dot{w} &= \frac{g}{T_e} (T-T_e) - k_1 w \\ \dot{T} &= - w\Gamma - k_2 (T-T_e) \end{aligned}\right\} \tag{6.68}$$

the bars indicating averages now being superfluous.

The parameters k_1 and k_2 may be considered as mixing rates for momentum and heat respectively. Intuitively one might expect the

rate of mixing of a buoyant element to be proportional to the ratio of its surface area to volume, i.e., to R^{-1}, yet the equation above yields

$$k_1 = \frac{C_1 K_1}{R^2}$$

If one considers the spectrum of turbulence, however, K_1 itself is proportional to $R^{4/3}$ (Richardson, 1926) so that $k_1 \sim R^{2/3}$ and the intuitive expectation is more or less confirmed.

In a steady environment the rising parcel will experience an environmental temperature change

$$\dot{T}_e = w \frac{\partial T_e}{\partial z} \tag{6.69}$$

Combining Eq. (6.68) and Eq. (6.69) yields a second order equation in the vertical velocity

$$\dddot{w} + (k_1+k_2)\ddot{w} + \left(\frac{g}{T_e}\left(\frac{\partial T_e}{\partial z} + \Gamma\right)+k_1k_2\right) w + \frac{1}{T_e}\frac{\partial T_e}{\partial z} w(\dot{w}+k_1 w) = 0 \tag{6.70}$$

which can be solved numerically, or, with certain simplifying assumptions, analytically.

In general, Priestley finds that, depending on the values of K and R and on the stability, the buoyant element will follow one of three modes of motion, absolute buoyancy, asymptotic ascent or oscillatory motion.

The essence of Priestley's contribution is his proof that absolute buoyancy is not simply the result of a superadiabatic lapse rate but

depends also upon wind shear and the size of the buoyant element. By way of illustration Table 6.1, reproduced from Priestley's paper (1953), indicates the critical radius necessary for absolute buoyancy under a particular set of circumstances. Noteworthy is the large element size needed to achieve buoyancy when the lapse rate is small.

TABLE 6.1

CRITICAL ELEMENT SIZE

(Under a particular set of conditions)

$-\frac{\partial T_e}{\partial z} + \Gamma$ (°C cm^{-1}):	10^{-5}	10^{-4}	10^{-3}	10^{-2}	10^{-1}	1
R(m):	1500	250	40	8	1.5	0.25

The picture of the field of turbulence in superadiabatic conditions which emerges is as follows: For $-0.03 \leq z/L \leq 0$ forced convection dominates and the eddy conductivity, if equal to the eddy viscosity, is

$$K_H = ku_*z \quad \text{i.e.,} \quad K_H \propto z \tag{6.71}$$

In the region $-1.00 \leq z/L < -0.03$ free convection dominates, but the damping effect of the ground is marked. The equation for the eddy conductivity is

$$K_H = hz^2 \left(\frac{g}{T}\frac{\partial\theta}{\partial z}\right)^{1/2} \quad \text{i.e.,} \quad K_H \propto z^{4/3} \tag{6.72}$$

Still higher, in the region of natural convection $z/L < -1.00$, the

temperature gradient drops to zero and the eddy conductivity loses its meaning. In this region heat is transported, without the need of a continuous temperature gradient, by buoyant elements which rise from the region of free convection with a surplus of heat and continue upward until the loss of buoyancy due to mixing and adiabatic expansion brings them to rest. The layer of natural convection must therefore be a region of decelerating motion and decreasing diffusivity.

As mentioned in an earlier chapter the exchange coefficient hypothesis can be applied to the region of natural convection since pollen and other pollutants do spread upward continuously. In the case of heat one may assume a value of K_H equal to K which would be equal to the heat flux per unit temperature gradient were a temperature gradient to exist. As yet there is no body of knowledge for the determination of the eddy diffusivity in natural convection.

Figure 6.5 is an aircraft sounding, reproduced for illustrative purposes from the results of the in-season experiment of 1962 conducted at Willow Run Airport. The value of L computed from the low level wind and temperature profile data shows reasonable agreement with the height at which the potential temperature gradient becomes zero. An approximate value for H is selected as the height at which the potential temperature increases sharply. An indication of this height, the upper limit of convection, is provided by the presence of cloud. From 2 to 8 tenths of thin scattered cumulus clouds were based at from 3800 to 4500 feet with tops at 5500, indicating that weak con-

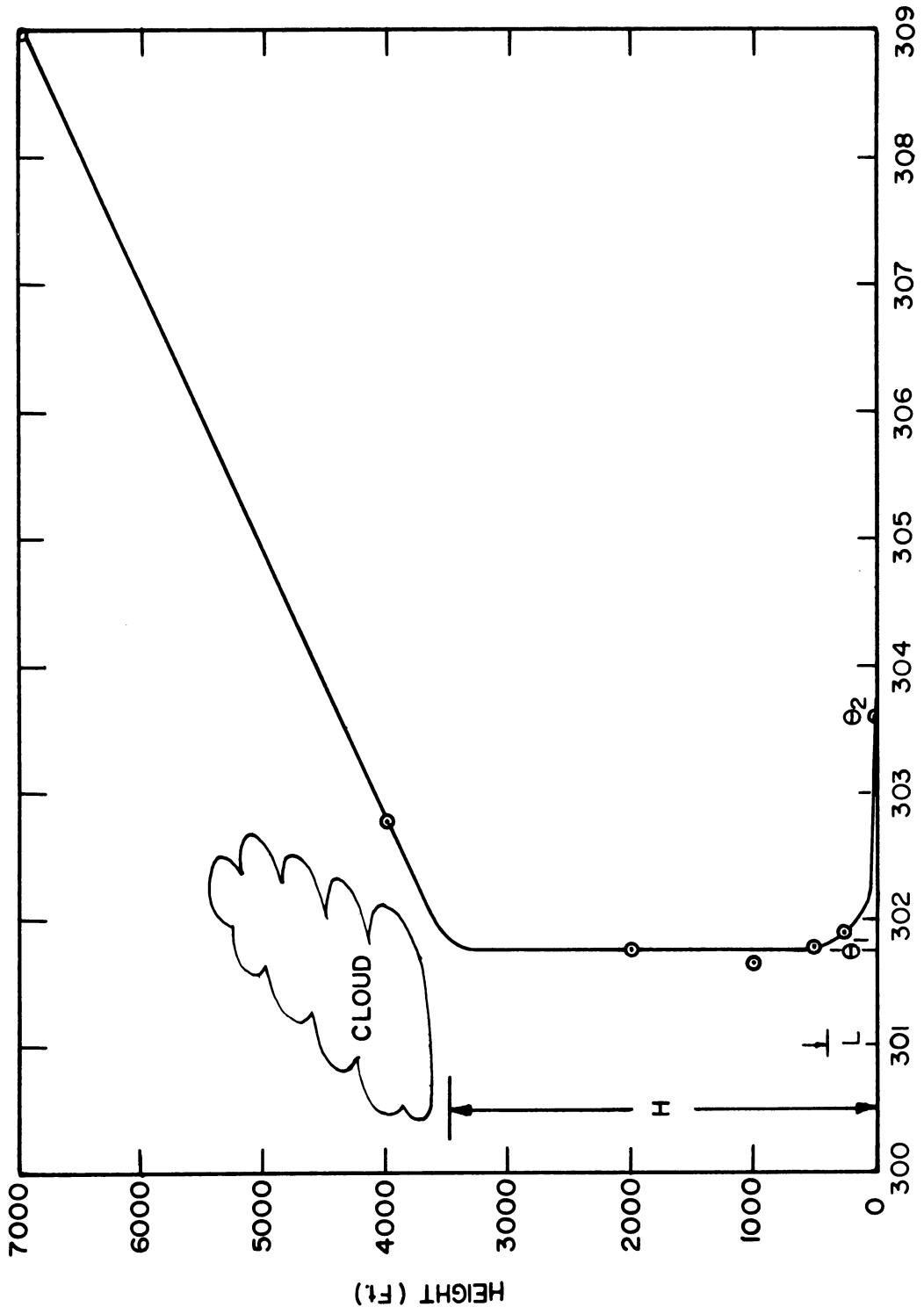

Fig. 6.5. Potential temperature vs. height. Aircraft sounding - August 1962.

vection was penetrating to about 4000 feet.

Because no adequate model is available for the computation of the eddy diffusivity in natural convection, and because some model is necessary for the solution of the parabolic diffusion equations, the simplest possible distribution which does not conflict with current knowledge is used. In particular, during periods having super adiabatic lapse rates, Eqs. (6.71) and (6.72) are used in their appropriate regions while at higher elevations a linear decrease of eddy diffusivity to the top of the convective layer is assumed.

In concluding this section it should be remarked that a great deal of work has been done on the theory of free or natural convection of which only a small fraction has been reviewed here. Because none of the theories have been able to accommodate the combined effects of self induced turbulence, environmental turbulence, and the subsiding return flow, they cannot be used to determine a satisfactory distribution for the eddy diffusivity and therefore have been omitted.

6.3.6 The Measurement of the Vertical Component of the Eddy Diffusivity

Aside from the indirect methods outlined above there are several direct methods by which the eddy diffusivity for mass and heat or the eddy viscosity may be measured. A brief outline of these methods follows.

6.3.6.1 Eddy Correlation Technique

The success of the eddy correlation technique depends on the ca-

pacity of the measuring instruments to record the correlation between the vertical wind and the entity under consideration in the significant range of eddy sizes. It is also necessary to have an accurate vertical profile of the entity over the time period during which the eddy correlation is made. If E represents the quantity of the entity per unit mass of air then the transport coefficient will be

$$K = \frac{\overline{E'w'}}{\frac{d\bar{E}}{dz}} \qquad (6.73)$$

Insurmountable practical difficulties prevent the utilization of this technique in measuring the eddy diffusivity of pollens or spores. The problem especially near the ground lies in the relative scarcity of pollen and the difficulty in acquiring an adequate sample in the short time period of importance to diffusive processes. There is some hope that the technique may be useful in the layer of natural convection, since in this region the significant eddy size is comparatively large.

The most frequent course is to measure either K_H or K_M by the eddy correlation technique and then to assume that K has the same value.

6.3.6.2 Profile Measurement Technique

Under a steady-state condition in the atmosphere wherein the upward particle flux due to diffusion is everywhere balanced by the downward flux due to gravitational settling the eddy diffusivity can be computed from the equation

$$K = - \frac{q\chi}{\frac{\partial \chi}{\partial z}} \tag{6.74}$$

6.3.6.3 Continuity Technique

Assuming a uniform homogeneous source, not necessarily steady, the diffusivity at a given level may be computed from the continuity equation

$$K_{z_2} = \frac{\frac{\partial}{\partial t} \int_{z_1}^{z_2} \chi \, dz + \left(K \frac{\partial \chi}{\partial z} \right)_{z_1} + q(\chi_{z_1} - \chi_{z_2})}{\left(\frac{\partial \chi}{\partial z} \right)_{z_2}} \tag{6.75}$$

which is derived by taking a single integration of Eq. (4.14) and re-arranging terms.

6.3.6.4 The Hodograph Technique

Within the friction layer under steady conditions and no horizontal temperature gradient the balance between frictional and Coriolis force yields the equation

$$\frac{\partial}{\partial z} \left(K_M \frac{\partial u}{\partial z} \right) = - fv$$

or

$$\left(K_M \frac{\partial u}{\partial z} \right)_{z_2} - \left(K_M \frac{\partial u}{\partial z} \right)_{z_1} = - \int_{z_1}^{z_2} fv \, dz$$

If z_2 is chosen at the top of the friction layer where $\partial u/\partial z$ is zero then the eddy viscosity at z_1 may be written

$$K_M(z_1) = f \int_{z_1}^{z_2} v \, dz \Big/ \left(\frac{\partial u}{\partial z}\right)_{z_1} \qquad (6.76)$$

From a double or triple theodolite pilot balloon ascent under atmospheric conditions which satisfy the assumptions leading to Eq. (6.76) it is possible to evaluate K_M. This equation was first derived by Rossby (1935).

6.3.6.5 Spectral Technique

The eddy correlation technique for measuring the eddy viscosity (Sect. 6.3.6.1) requires the cross correlation of the high frequency components of two variables and therefore sophisticated instrumentation. For eddies which lie within the Kolmogoroff inertial subrange, another technique is available (MacCready, 1953) which in neutral conditions requires the measurement of only one variable or, in a diabatic environment, of two variables independently.

Defining $F(K)$ to be the one dimensional energy density of atmospheric turbulence in wave number space and ϵ to be the rate of energy dissipation, then in the inertial subrange it can be shown by dimensional reasoning that

$$F(K) = \text{const } \epsilon^{2/3} K^{-5/3} \qquad (6.77)$$

The rate of dissipation ϵ in an adiabatic atmosphere is

$$\epsilon = \overline{uw} \frac{\partial u}{\partial z} = K_M \left(\frac{\partial u}{\partial z}\right)^2 \qquad (6.78)$$

or in a diabatic atmosphere it is

$$\epsilon = K_M\left(\frac{\partial u}{\partial z}\right)^2 + K_H \frac{g}{\theta}\frac{\partial \theta}{\partial z}$$

which, assuming equality of the K's, may be written

$$\epsilon = K_M\left[\left(\frac{\partial u}{\partial z}\right)^2 + \frac{g}{\theta}\frac{\partial \theta}{\partial z}\right] \qquad (6.79)$$

The eddy viscosity is found from Eqs. (6.78) or (6.79) and (6.77) by substituting into the equations the measured wind and temperature gradients and the energy density at a particular wave number. The energy density is found from the wind speed autocorrelation coefficient using the relation

$$F(K) = \beta\,\overline{u^2}\sqrt{\frac{\pi}{2}}\int_0^\infty R_E(t)\cos Kt\,dt \qquad (6.80)$$

which has been described in Chapt. 2 (see Eq. (2.22)).

6.3.6.6 Mixing Length Technique

The eddy viscosity may be expressed in the form (see Eq. (2.5))

$$K = \beta\,\overline{w^2}\int_0^t R_E(t)\,dt \qquad (6.81)$$

where $R_E(t)$ is the autocorrelation coefficient of the vertical velocity measured at a point in space.

The maximum length and period of eddies in the vertical direction are limited by the presence of the ground and therefore the integral

on the right of Eq. (6.86) has a limiting value I, where

$$I = \int_0^{\infty} R_E(t)\,dt = \int_0^{T} R_E(t)\,dt$$

and T is the time at which the autocorrelation coefficient becomes zero. A mixing length may be defined by the relation $\ell = I\sigma_w$, where σ_w is the standard deviation of the vertical windspeed, and therefore Eq. (6.81) may be written as

$$K = \beta\sigma_w\ell \qquad (6.82)$$

Both σ_w and ℓ can be found from measurements of the vertical component of the wind speed (Pasquill, 1963). Within the lower 100 m the mixing length is a linear function of height and therefore Eq. (6.82) can be written (Panofsky, 1961) in the form

$$K = \text{const}\ \sigma_w z \qquad (6.83)$$

where the constant must be evaluated.

6.3.6.7 Energy Budget Technique

The energy budget at the earth-air interface may be expressed by the equation

$$R_o + G_o + LE_o + H_o = 0 \qquad (6.84)$$

where R_o is the net radiation, G_o the soil heat flux at the interface, L the latent heat of vaporization, E_o the rate of evaporation or condensation and H_o the sensible heat flux. If R_o, G_o and E_o are measured H_o may be calculated. From H_o, if the temperature gradient above

the ground is measured, the eddy conductivity may be calculated using the equation

$$H_o = \rho\, c_p\, K_H \left(\frac{\partial \theta}{\partial z}\right)_o \tag{6.85}$$

6.4 THE LATERAL COMPONENT OF THE EDDY DIFFUSIVITY

6.4.1 The Influence of Eddy Scale on Diffusion

Consider Taylor's (1921) equation for the lateral component of the eddy diffusivity, which is written

$$K_y = \frac{1}{2}\frac{\partial \sigma_y^2}{\partial t} = \overline{v^2} \int_o^t R(\xi)\, d\xi \tag{6.86}$$

Substitute the Fourier transform of the power spectrum function for $R(\xi)$ in Eq. (6.86), reverse the order of integration and integrate. The resulting equation is

$$K = \overline{v^2} \int_o^\infty F(n)\, \frac{\sin 2\pi n t}{2\pi n}\, dn \tag{6.87}$$

where n is the eddy frequency (Batchelor, 1949). When the travel time t is small Eq. (6.87) becomes

$$K = \overline{v^2}\, t \int_o^\infty F(n)\, dn \tag{6.88}$$

and all eddies contribute to the diffusion in proportion to their en-

ergies. For large t, however, Eq. (6.87) shows that the components of the eddy spectrum play a decreasing role as their frequencies increase.

What is usually observed, however, is not the diffusion about the true mean wind direction (if such can be defined) but about a mean direction defined over a finite sampling interval or about the instantaneous center of a puff. By this means all eddies having periods longer than the sampling time or larger than the puff are effectively filtered out (see Eq. (2.27)).

It can be clearly seen from the discussion above that the type of diffusion described in Eq. (6.87) is inapplicable to the problem of diffusion about the center of a moving puff where the effective eddy size continually increases with the downwind distance.

A very clear discussion of the mechanism of lateral diffusion about a moving center and the complexity of describing it mathematically has been given by Richardson (1926) in a noteworthy paper entitled "Atmospheric Diffusion on a Distance-Neighbor Graph." The following brief discussion brings out the more pertinent arguments in relation to the present analysis.

The value taken by the lateral component of the eddy diffusivity depends to a large extent upon the scale of the phenomenon being studied. Table 6.2 taken from Richardson's paper, shows the enormous range of values as we pass from the molecular to the synoptic scale. Figure 6.6 is a graphical representation of the same data with the

TABLE 6.2

EDDY DIFFUSIVITY AND MIXING LENGTH AFTER RICHARDSON (1926)

References	K(cm^2 sec)	ℓ(cm)
Molecular diffusion of O_2 into N_2	1.7×10^{-1}	5×10^{-2}
At 9 m from anemometers at 2, 16, 32 m (W. Schmidt)	3.2×10^{3}	1.5×10^{3}
Anemometers at 21-305 m (Akerblom)	1.2×10^{5}	1.4×10^{4}
Pilot balloons at heights 100 and 800 m (Taylor, Hesselberg and Svendrup)	6×10^{4}	5×10^{4}
Tracked balloons manned or unmanned (L. F. Richardson)	10^{8}	2×10^{6}
Volcanic ash (L. F. Richardson)	5×10^{8}	5×10^{6}
Diffusion due to cyclones regarded as deviations from the mean circulation (Défant)	10^{11}	10^{8}

diffusivity plotted against the length of the eddies involved or, in the case of molecular motion, against the mean free path of the molecules. From these data Richardson devised the empirical equation.

$$K = 0.2\, \ell^{4/3} \tag{6.89}$$

where ℓ is in cm and K in $cm^2 sec^{-1}$, an equation whose basic form has been corroborated in the Kolmogoroff inertial subrange by dimensional reasoning (Batchelor, 1950). The agreement, however, must be somewhat fortuitous because virtually all the points on Richardson's graph are well outside the inertial subrange and because other curves could have been drawn which fit his data equally well.

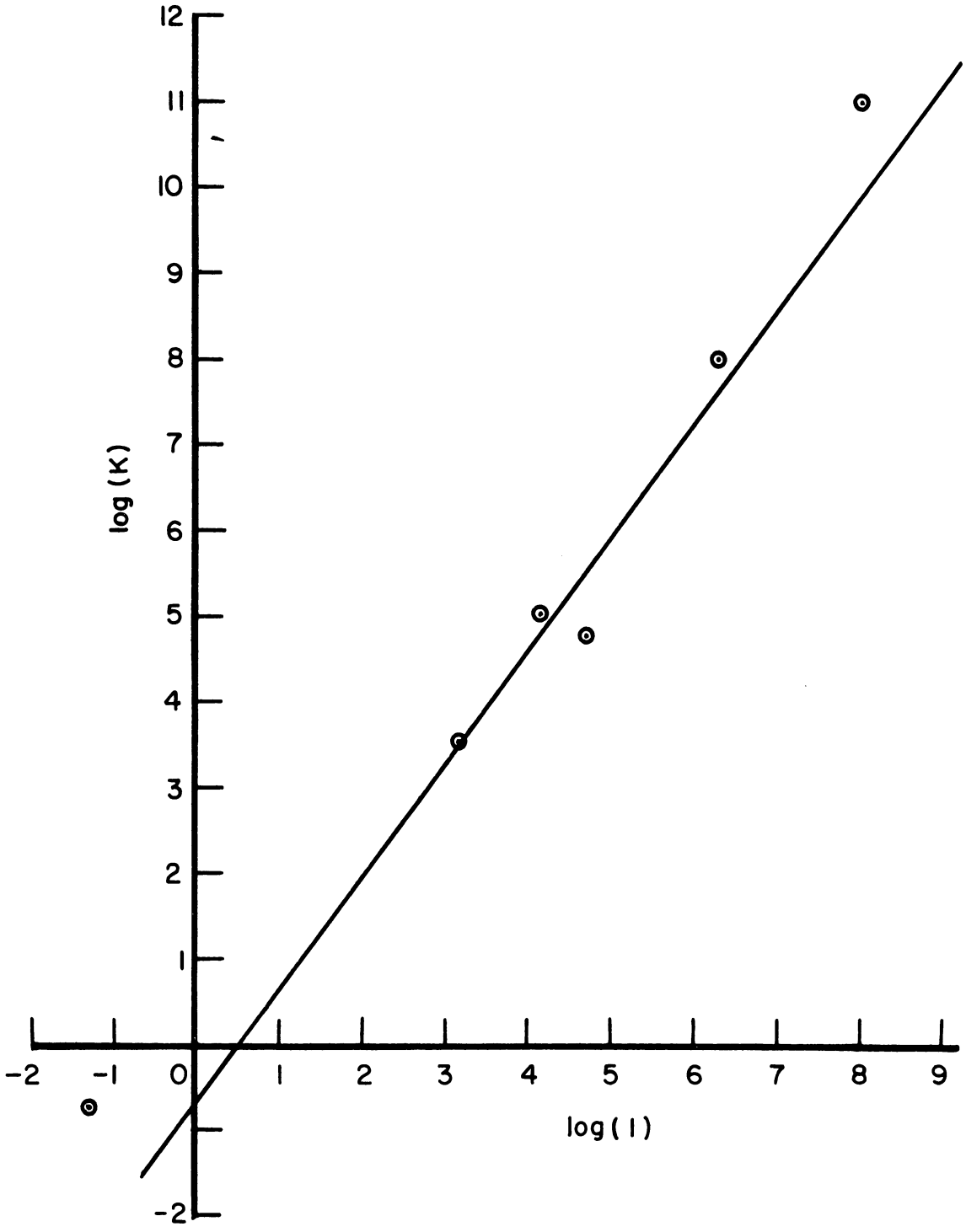

Fig. 6.6. Diffusivity as a function of the mixing length - the straight line represents the equation $K = 0.2\ell^{4/3}$ (Richardson, 1926).

The fact that the diffusivity increases with the scale of the turbulence means that the rate of separation of two particles increases with increasing separation. Therefore, it is not possible to specify the lateral component of the diffusivity at a point without also specifying the separation distance of the particles concerned To illustrate consider two equally sized puffs of smoke emitted a distance d apart. The resultant downstream distribution is not on the average simply the sum of two similar distributions separated by a distance d but rather the sum separated by a distance d', where d' minus d is the additional separation due to diffusion of one puff from the other. The same is true for puffs emitted serially.

A continuous plume may be treated as a series of puffs, each element of which grows with time in accordance with the energy available in eddies of its own size. The individual puffs separate at a rate determined by the lag between their times of emission. Since there is virtually no limit to the size of the horizontal eddies there is presumably no limit to the increase of diffusivity with increasing emission time.

The discussion of the paragraphs above has two important applications to the problem of the estimation of the cross wind component of diffusivity over an urban area. First, the magnitude of the diffusivity will increase with the sampling time in a manner analogous to the increase of diffusivity with emission time mentioned in the preceding paragraph. Second, the cross wind or lateral component of diffusivity

will be constant with the downwind distance except for a negligible reduction caused by the damping of the effect of the high frequency components of turbulence.

6.4.2 The Estimation or Measurement of the Lateral Component of Diffusivity and Its Distribution with Height

The lateral component of the diffusivity is dependent upon eddies some of which are related to local phenomena such as wind speed, surface roughness and thermal instability and some of which are a consequence of larger scale phenomena such as the breakdown of synoptic scale eddies and flow over large scale features of the terrain. As a consequence of the diversity of generating processes the lateral eddy structure is difficult to predict, especially its larger components.

When the dispersion of a plume is measured on a stationary array all eddy frequencies are involved as noted in the discussion of the preceding section, but, because the sampling is conducted over a short period and the mean wind direction is measured over this period, eddies whose periods are much larger are filtered out. Eddies whose periods are of the same order as the sampling period, however, will contribute to the dispersion as shown by Eq. (2.27). These eddies cause the observed distributions of particulates to be non-normally distributed, i.e. to be skewed, bimodal, have trends, etc. as noted by Lumley and Panofsky (1964, p. 154). Therefore, at the same site with the same wind and the same stability, it is not only possible but likely that the measured diffusivity on two occasions will be

different.

In the future it may be possible to predetermine the eddy power spectrum for a large body of air on the basis of its history and a sequence of spectral measurements. Until then it will not be reasonable to expect to predetermine a value for the lateral component of the diffusivity which will successfully predict the lateral dispersion in any continuous source experiment.

On the other hand, the method of Hay and Pasquill (1959) in which the variance of the wind is measured during the course of the experiment has some promise. Here at least the actual wind variance is measured, and this may be related to the particle variance by methods outlined in Chapt. 2. Even this method is not completely satisfactory because the distribution of pollutant is unlikely to be normal and therefore more of the statistics of the wind fluctuations are needed than simply the standard deviation. (see Eq. (2.42)).

The interference by larger eddies in the attainment of a normal distribution of concentration in the lateral direction has led many researchers to look for a gap in the eddy spectrum. No such gap has been proven to exist, although there does appear to be a dip at periods near one hour (Panofsky, 1964, p. 126).

Practically nothing is known concerning the vertical variability of the cross wind component of the eddy diffusivity. However, a few comments may be made with respect to eddy diffusivities measured over periods of an hour or more. Such eddies are so large that they

most probably extend throughout the depth of the friction layer. Observations at Brookhaven at night at 23, 46, and 91 m (Lumley and Panofsky, 1964, p. 179) indicate no change of eddy energy with height for values of the dimensionless frequency $f = nz/\bar{u}$ less than 0.1. Assuming reasonable values for n,z and v of $1/3600$ sec^{-1}, 360 m and 10 m sec^{-1} respectively, f takes a value of 10^{-2}, an order of magnitude less than the limiting Brookhaven value, suggesting that the lateral component of diffusivity over periods of an hour or more is constant with height.

There is certainly a considerable diurnal variation in the turbulent spectrum at wave lengths of the order of one kilometer or less due to the development of thermals during the day, but there is no evidence to indicate any diurnal change in the energy contained in eddies of the order of 20 km, a value which might be considered typical of a one hour observation period. Therefore, without evidence to the contrary, it will be assumed that for sampling periods of one hour or more the lateral component of diffusivity K_y is a function of neither time nor height.

Three methods by which K_y may be estimated or measured are outlined as follows:

1. If the scale length is known K_y can be estimated from Eq. (6.89). For example, if the sampling interval is one hour and the wind speed 5 m sec^{-1} the largest eddy which can completely pass a station is 18 km in diameter. Using this value for the scale length leads to an estimate of K_y equal to $4 \times 10^{+3}$ m^2 sec^{-1}.

2. By integrating the steady three-dimensional diffusion equation with respect to height a new equation may be derived in the form

$$\frac{\partial}{\partial x}\int_0^\infty u\chi \, dz = \left[K \frac{\partial \chi}{\partial z} + q\chi \right]_0^\infty + K_y \frac{\partial^2}{\partial y^2}\int_0^\infty \chi \, dz \qquad (6.90)$$

The term in brackets is obviously zero at the upper limit and, if small downwind distances are assumed, will be small at the lower limit. Indicating integration in the vertical by the symbol $\wedge$ K_y may be found from the equation

$$K_y = \frac{\partial}{\partial x}(\widehat{\chi u}) \Big/ \frac{\partial^2 \hat{\chi}}{\partial y^2} \qquad (6.91)$$

A number of practical difficulties attend the use of Eq. (6.91): first, the lateral distributions are rarely smooth; second, the spacing of observations in the downwind direction is rarely close enough to allow good estimates to be made of $\partial(\widehat{u\chi})/\partial\chi$; third, the use of finite differences (which must be used in any practical setting) to estimate derivatives is notoriously inaccurate. Estimates of K_y using this technique may be found in App. B.

3. From Eq. (2.5)

$$K_y = \frac{1}{2}\frac{\partial \hat{\sigma}_y^2}{\partial t} = \frac{1}{2}\frac{\partial \hat{\sigma}_y^2}{\partial x} \qquad (6.92)$$

where $\hat{\sigma}_y^2$ is the variance of the vertically integrated particle distribution. Equation (6.92) is derived on the basis of a homogeneous field of turbulence, and therefore is strictly inapplicable near the ground. If, however, measurements are made over small distances and the particles are confined to a narrow height range, Eq. (6.92) should provide a reasonable estimate of K_y. Estimates of K_y using this technique may be found in App. B.

The problem of selecting an appropriate model for K_y has not been answered satisfactorily in this section. Lacking a satisfactory model, and feeling intuitively that the value given by Method 1 above is too large, the author assumed the following model:

1. The lateral component of diffusivity for sampling periods of one hour or more is not a function of height.

2. Eddies having periods of one hour or more are principally caused by the breakdown of synoptic scale systems and by large scale features of the terrain. Their energies are assumed to be extremely variable and, as yet, an unpredictable function of the history of the air in which they occur.

3. These large eddies are assumed to be formed independently of the wind strength at the point at which they are observed and therefore their contribution to the diffusivity is expected to be inversely proportional to the wind speed.

4. Because of the necessity for making some estimate of the lateral component of diffusivity for a sampling period of one hour, the author has given K_y the value 10 m^2 sec^{-1} in summer and 5 m^2 sec^{-1} in winter.

6.5 CONCLUDING REMARKS

With the completion of this chapter, models for the meteorological variables and boundary conditions necessary to solve the diffusion equations of Chapt. 4 have been outlined and the assumptions leading to their development examined. The following chapter is a summary of the results of computations performed using these models or, in many cases, simplified versions of them.

7. RESULTS, CONCLUSIONS AND SUGGESTIONS FOR FURTHER STUDY

7.1 INTRODUCTION

The work undertaken in this study may be divided into two major divisions as follows:

1. Theoretical developments including

   1.1 the development of adequate diffusion models,
   1.2 the specification of initial and boundary conditions,
   1.3 the selection of appropriate models for the meteorological variables and finally
   1.4 the solution of the diffusion equations by numerical methods; and

2. The planning, operation and analysis of diffusion experiments used to corroborate or negate the theoretical models.

The result of the analysis under the first division are given in this chapter and the experimental results are reported in three appendices each of which is devoted to a single experiment.

7.2 SOLUTIONS TO THE UNSTEADY ONE-DIMENSIONAL DIFFUSION EQUATION

7.2.1 An Outline of the Problem

The unsteady one-dimensional diffusion equation is written (see Eq.(4.14))

$$\frac{\partial \chi}{\partial t} = \frac{\partial}{\partial Z}\left(K_z(z)\ \frac{\partial \chi}{\partial Z} + q\chi\right) \tag{7.1}$$

with boundary conditions (see Eqs. (4.17) and (4.18))

$$\left.\begin{aligned} \left[K\frac{\partial\chi}{\partial Z} + q\chi\right]_{\ell+} &= -P(t) + F\chi(\ell) \qquad z = \ell \\ \chi &= 0 \qquad\qquad\qquad\quad z > H \end{aligned}\right\} \tag{7.2}$$

where ℓ is the height of the top of the vegetation and H is the level of the top of the convective layer.

As a matter of convenience, for use in testing the accuracy of the solution to Eq. (7.1) the parameters q, $K_z(z)$, P(t) and F are chosen as follows:

1. q is set equal to 0.012 m sec^{-1};
2. $K_z(z)$ is increased linearly to a value of 20 m^2 sec^{-1} at $z = H/40 = h$ and decreased as the square of the height to a value of zero at z = H, as specified approximately by the Rossby-Montgomery model;
3. P(t) is assumed to have a Gaussian distribution for which the time of peak emission, standard deviation and total emission are specified; and
4. F is taken to be equal to q.

The solution of Eq. (7.1) is readily achieved by the method given in Sect. 4.4. Care must be exercised, however, in establishing the proper boundary conditions if major computational problems are to be avoided. A brief discussion of three such possible errors encountered by the author are discussed in the following sections.

7.2.2 Initially Unbalanced Boundary Conditions

If the initial pollen profile does not satisfy the condition at the lower boundary the solution of Eq. (7.1) will contain an error

which oscillates with a slowly decreasing amplitude as the solution proceeds in time. The same effect occurs in the solutions of the equations of motion in the atmosphere when initial conditions are unbalanced (Wiin-Nielsen, 1964).

The type of error caused by an imbalance in the initial condition is illustrated in Fig. 7.1 where solutions are obtained at ten minute intervals for an example in which the production term P is constant while the initial pollen concentration is everywhere zero. It will be noted that the ground level dimensionless pollen concentration S is greatly overestimated at 10 minutes, underestimated at 20 minutes, overestimated at 30 minutes and so forth, the oscillation gradually damping out with increasing time. Even after 1 hour and 40 minutes, however, the oscillation is still significant.

The error may be eliminated by ensuring that conditions are balanced at the initial time. In the example illustrated above this can be done by setting $P = 0$ at $t = 0$.

7.2.3 Zero Concentration as the Upper Boundary Condition

In solving the one-dimensional diffusion equation it is possible to create an unstable situation in which the computed pollen concentration can increase idenfinitely at the level just below the boundary if the concentration at the upper boundary is equated to zero while the diffusivity is allowed to remain non zero.

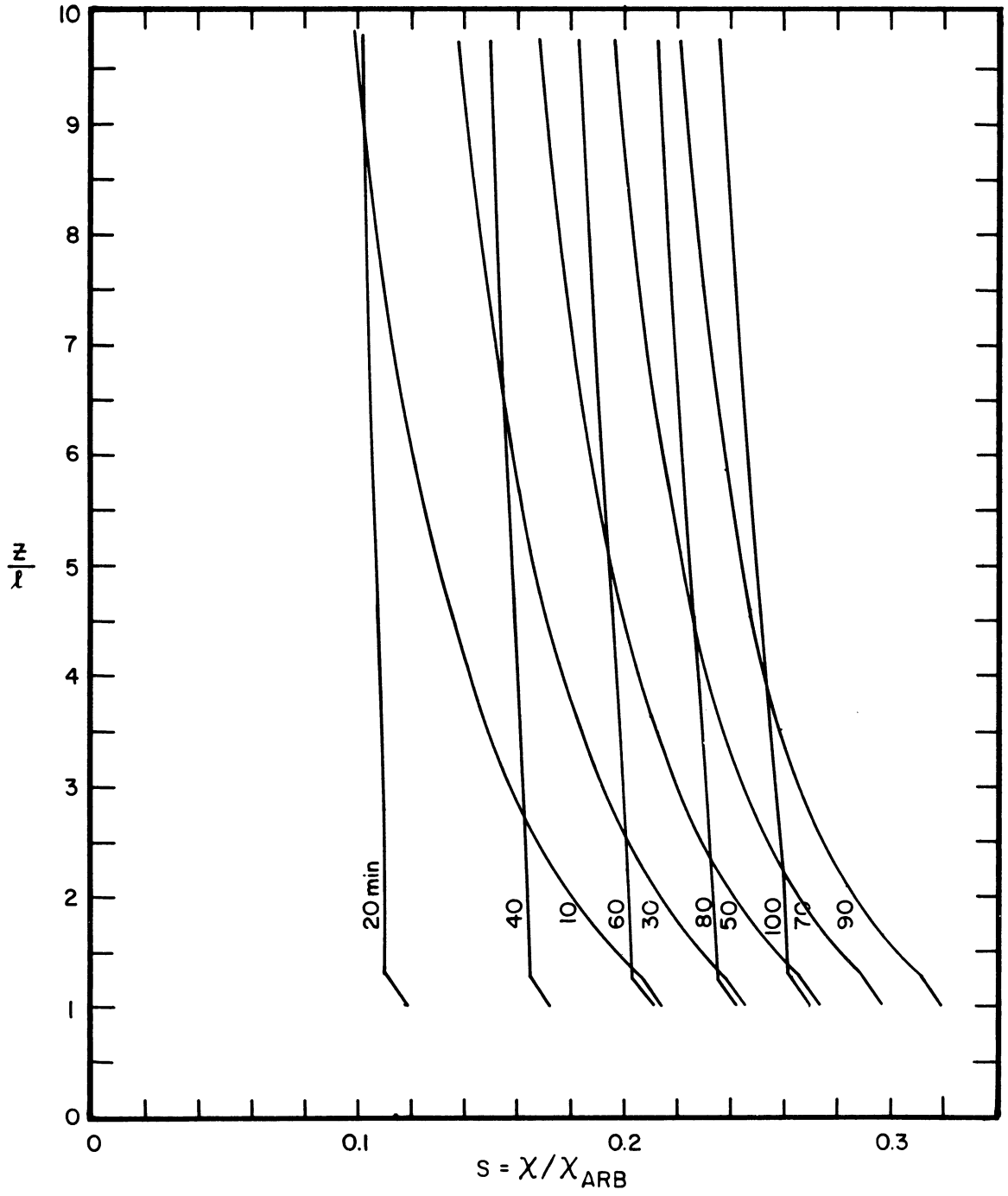

Fig. 7.1. Solutions to the unsteady one-dimensional parabolic diffusion equation for unbalanced initial conditions. Here $\chi(z) = 0$ at $t = 0$, $P(t) = \text{const}$ and $\ell = 1.0$ m.

This type of error may be eliminated either by equating the concentrations at the top two levels of integration, i.e. the zero flux boundary condition, or by allowing the diffusivity to become zero at some point below the boundary. The second method is preferred because the first is somewhat artificial.

To illustrate, consider an example in which Eq. (7.1) is solved subject to the initial distribution shown in Fig. 7.2,* the downward flux at the lower boundary equal to the gravitational settling rate, the concentration at the upper boundary equal to zero and the diffusivity constant with height. It will be noted that the solution proceeds smoothly until the computed pollen concentration reaches a significant value at the level H after which the concentration gradient becomes finite between levels 14 and 16 causing pollen to accumulate at the level 15 and finally causing the entire solution to become unstable. In Fig. 7.2 the first sign of an instability appears as a small positive slope at level 15 on the 5527.5 sec concentration profile and by 8921.6 sec the entire profile has developed a positive slope.

7.2.4 Forward Differencing and the Lower Boundary Condition

The lower boundary has a special significance in the problems under consideration here because all the computed pollen enters and

*It will be noted that the ordinate in Fig. 7.2 is on a logarithmic scale with $z = \ell$ and $z = H$ for the value on the ordinate set equal to 0 and 15 respectively.

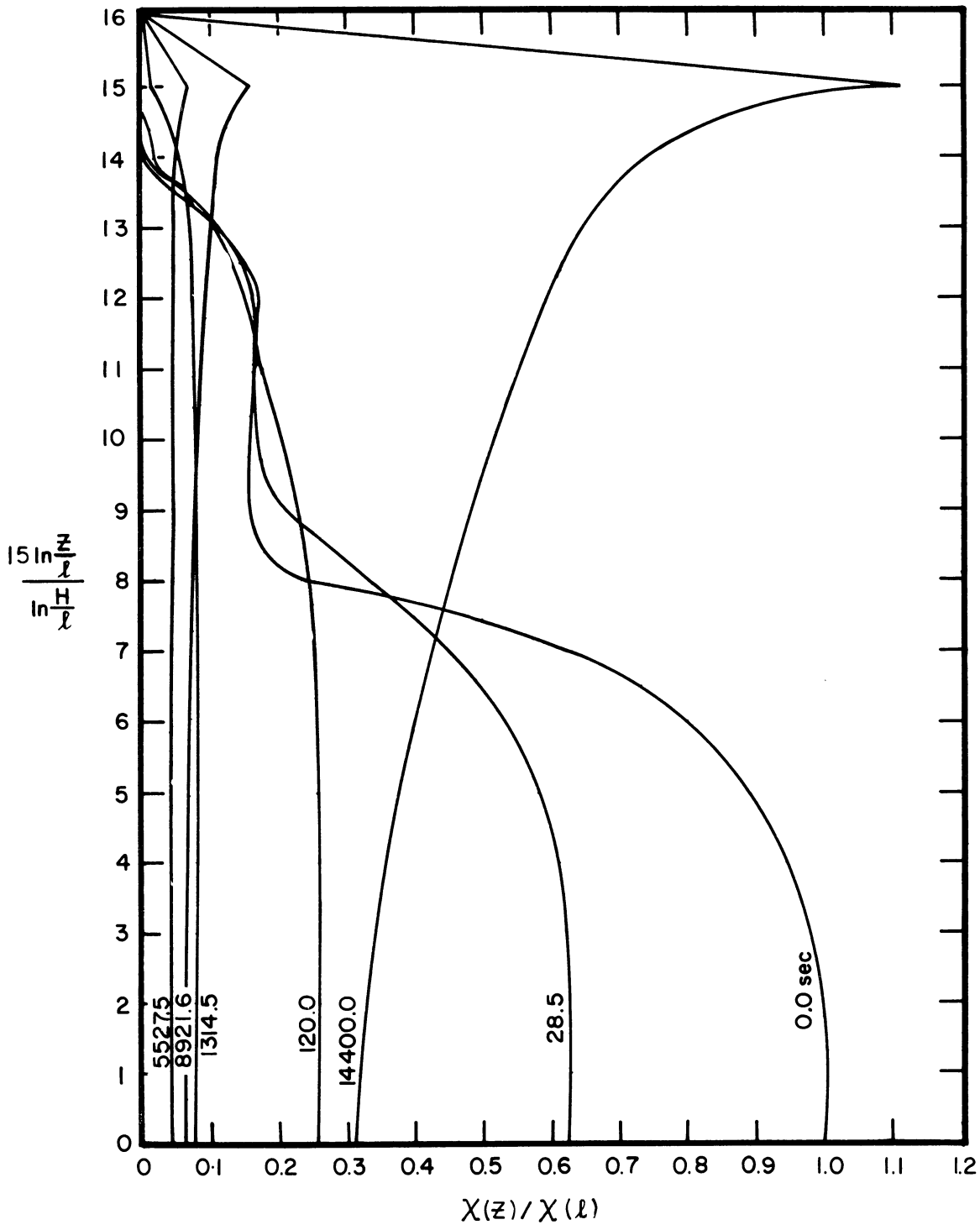

Fig. 7.2. Solutions to the unsteady one dimensional parabolic diffusion equation for eddy diffusivity constant with height and the boundary condition $\chi(H) = 0$.

leaves the system at this level. The following paragraphs discuss a serious error resulting from improper care in selecting a finite difference method at the lower boundary.

Suppose that the forward difference is used to express the derivative in Eq. (7.2), so that

$$\left(\frac{\partial \chi}{\partial Z}\right)_{\ell} = \frac{\chi(z_1)-\chi(\ell)}{z_1-\ell} = \frac{\chi(z_1)-\chi(\ell)}{\Delta z} \qquad (7.3)$$

where the subscript 1 refers to the first nodal level above ℓ. As shown in Sect. 4.4 the error in Eq. (7.3) is of order Δz whereas had the central difference been used the error would have been of order $(\Delta z)^2$.

To improve the accuracy of the finite difference expression for the forward difference consider the MacLaurin series expansion for $\chi(z_1)$, which is written

$$\chi(z_1) = \chi(\ell) + \Delta z\chi'(\ell) + \frac{(\Delta z)^2}{2!}\chi''(\ell) + \frac{(\Delta z)^3}{2!}\chi'''(\ell) \qquad (7.4)$$

where the primes denote differentiation with respect to height. The derivative at the lower boundary can be accurately represented by the equation

$$\chi'(\ell) = \frac{\chi(z_1)-\chi(\ell)}{\Delta z} - \frac{\Delta z}{2!}\chi''(\ell) - \frac{(\Delta z)^2}{3!}\chi'''(\ell) \qquad (7.5)$$

The second term on the right, evaluated from the derivative of Eq. (7.2) with respect to height is

$$\chi''(\ell) = -\frac{(K'(\ell)+q-F)}{K(\ell)}\chi'(\ell) \tag{7.6}$$

On substituting Eqs. (7.2) and (7.6) into Eq. (7.5) the expression for $\chi'(\ell)$ becomes

$$\chi'(\ell) = \frac{[\chi(z_1)-\chi(\ell)]\Delta z}{1-\frac{\Delta z}{2!}\frac{(K'(\ell)+q-F)}{K(\ell)}} \tag{7.7}$$

if the third and higher derivatives of χ at ℓ are insignificant. The fractional error E in $\chi'(\ell)$ committed by ignoring the second derivative term of Eq. (7.5) is then

$$E = \frac{\Delta z}{2!}\frac{(K'(\ell)+q-F)}{K(\ell)} \tag{7.8}$$

An error in $\chi'(\ell)$ is reflected in an apparent error in the pollen emission term P (see Eq. (7.2)).

The magnitude of the error represented by Eq. (7.8) may not be trivial; in one particular problem it was 23% while the term containing the third derivative was 2%. It is extremely important to minimize such errors because, as can be seen from Eq. (7.2), the error in $\chi'(\ell)$ is reflected in an apparent error in the pollen emission term P and therefore changes the entire flux of pollen into the system.

Two different methods have been utilized to minimize the error at the lower boundary in the solutions which follow; the first method is to use the central difference at the boundary as shown in Modern Comput-Methods (Natl. Phys. Lab., 1961, p. 97), and the second method is to use the more accurate expression for the forward difference which in-

cludes the term in $\chi''(\ell)$ given in Eq. 7.5.

7.2.5 Computational Results

The accuracy of the solutions to Eq. (7.1) as indicated by the correction terms of the finite difference approximations in Eqs. (4.26) and (4.27), depends upon the height spacing chosen. In this study the degree of error is assessed in two ways: first, by comparing solutions computed for different numbers of nodal points, and second by carrying out a pollen continuity calculation as discussed in the following paragraph. The error due to finite differencing in time is minimized by taking small time steps, 10 minutes in the examples given.

The accuracy of the condition on the lower boundary can be tested by computing the total pollen in the atmosphere, adding the loss due to the downward flux at the lower boundary and comparing the result with the total pollen input. Mathematically this can be expressed in the following way. The unsteady one-dimensional diffusion equation is integrated with respect to height giving

$$\frac{\partial}{\partial t}\int_{\ell}^{H} S\,dz = \left[K\frac{\partial S}{\partial Z} + qS\right]_H - \left[K\frac{\partial S}{\partial Z} + qS\right]_{\ell} \qquad (7.9)$$

where the first term on the right is zero. Integration of Eq. (7.9) with respect to time gives

$$\left[\int_{\ell}^{H} S\,dz\right]_{t=t} - \left[\int_{\ell}^{H} S\,dz\right]_{t=0} = -\int_{o}^{t}\left(K\frac{\partial S}{\partial Z} + qS\right)_{\ell} dt \qquad (7.10)$$

where the second term on the left is zero if no pollen is in the air at

the initial time. Introducing the boundary condition of Eq. (7.2) into the right hand side of Eq. (7.10) and rearranging terms the equation becomes

$$\left[\int_{\ell}^{H} S\,dz\right]_t + \int_0^t FS\,dt = \int_0^t P(t)\,dt \qquad (7.11)$$

where the first term is the total pollen in the air, the second is the total loss to the ground and the third is the total input or production.

Pollen budget computations are given in Table 7.1 for vegetation depths ranging from 0.02 to 10 m and for 10 to 40 nodal points. The particular solutions given are computed under the following conditions:

1. The deposition velocity F is set equal to the particle fall speed q.

2. The pollen emission rate P is given by

$$P(t) = P_{MAX} \exp\left[-\frac{1}{2}\left(\frac{t-t_m}{\sigma}\right)^2\right] \qquad (7.12)$$

   where the time of maximum emission t_m is 4 hrs, the standard deviation of the emission curve σ is 1 hr and the total emission from $-\infty$ to t_m is 54.15 x P_{MAX}.*

3. The time step is 10 minutes.

The values given in the right hand colume of Table 7.1 (see following page) represent the sum of the pollen in the atmosphere and the total loss of pollen by deposition and should be equal to the total

*The value 54.14 results from the nondimensionalization of the equations. The integral of the right hand side of Eq. (7.12) from $t = -\infty$ to $t = t_m$ is $P_{MAX}\ \sqrt{\pi/2}\cdot\sigma$. In the conversion to nondimensional form a division by $\chi_{ARB} = P_{MAX}/q$ is performed and the integral becomes $\sqrt{\pi/2}\cdot\sigma\cdot q$, which for σ = 3600 sec and q = 0.014 m sec^{-1} is equal to 54.14.

TABLE 7.1

THE RAGWEED POLLEN BUDGET

Number of Nodal Points	Height of Vegetation (m)	Ratio of Pollen in the Air P_{MAX}	Ratio of Pollen Deposition P_{MAX}	Ratio of Total Pollen P_{MAX}
10	1.0	23.71	6.61	30.32
20	1.0	40.07	10.71	50.77
30	1.0	42.60	11.43	54.02
40	1.0	43.45	11.68	55.13
40	10.0	45.34	0.32	54.65
40	5.0	44.84	9.99	54.82
40	0.5	42.86	12.34	55.20
40	0.1	41.10	13.83	54.92
40	0.05	40.17	14.39	54.55
40	0.02	38.91	15.06	53.97

emission, 54.14. It will be seen that when fewer than 30 nodal points are used the solutions are inaccurate and when more than 30 nodal points are used, the solutions are satisfactory over a wide range of vegetation heights.

The effect of nodal spacing on the accuracy of the solutions to Eq. (7.1) is illustrated in Fig. 7.3 where the first and fourth examples from Table 7.1 are compared. The column at the right of the figure shows at different heights the ratios of the concentrations illustrated by curves A and B. It will be noted that the two curves are approximately similar. Because the diffusion equations do nothing more than redistribute the computed pollen concentration, the difference in the two curves must be the result of dissimilar boundary conditions, i.e. a greater pollen input in the case of curve A.

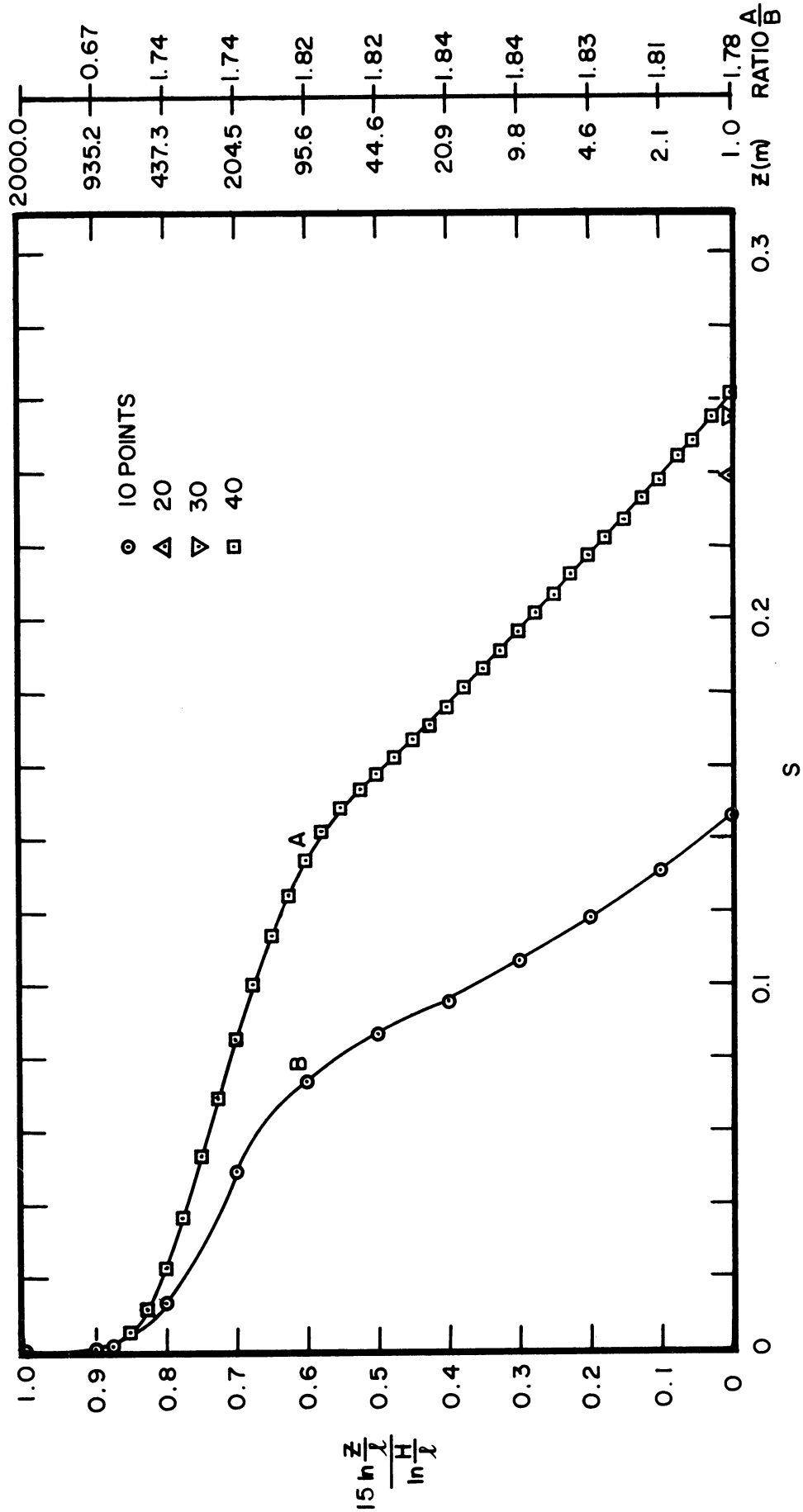

Fig. 7.3. Solutions to the unsteady one-dimensional parabolic diffusion equation for 10 and 40 nodal points for a vegetation height of 1.0 m.

It is, therefore, more profitable to improve the accuracy of the solution at the lower boundary than to increase the number of nodal points. Logical first steps in that direction would be to maintain a small step size and use central differences at the lower boundary and to carry as many terms in the MacLaurin series expansion as possible.

A set of solutions obtained under the same conditions as those used in the computation of the values in the fourth row of Table 7.1 (see points 1 to 3 including Eq. (7.12)) are illustrated in Fig. 7.4. The following characteristics of the solutions should be noted:

1. The slope of the curve at the lower boundary reflects the rate of pollen flux at that level. At the peak emission time, 4 hrs, the curve has a maximum negative slope, whereas at 4 standard deviations from the peak emission period, 8 hrs, the curve has effectively a zero slope. (Note that the independent variable is graphed in the direction of the ordinate.)

2. During the period of peak emission the pollen concentration profile is sharply curved near the lower boundary and at the upper limit of pollen penetration, but is of nearly constant slope between these levels.

3. After the period of peak emission pollen continues to diffuse rapidly upward and the profile slowly adjusts to a condition in which the concentration is constant with height.

4. Very little pollen reaches the top of the convective layer. This is a result of the decreasing diffusivity with height above the level L, the scale height.

To test the ability of the solutions of Eq. (7.1) to adequately duplicate dispersion in the real atmosphere one should substitute observed values of the various parameters into the equation and compare the resulting computed profiles with observed profiles. This has not yet been accomplished; however, it is possible to compare the general

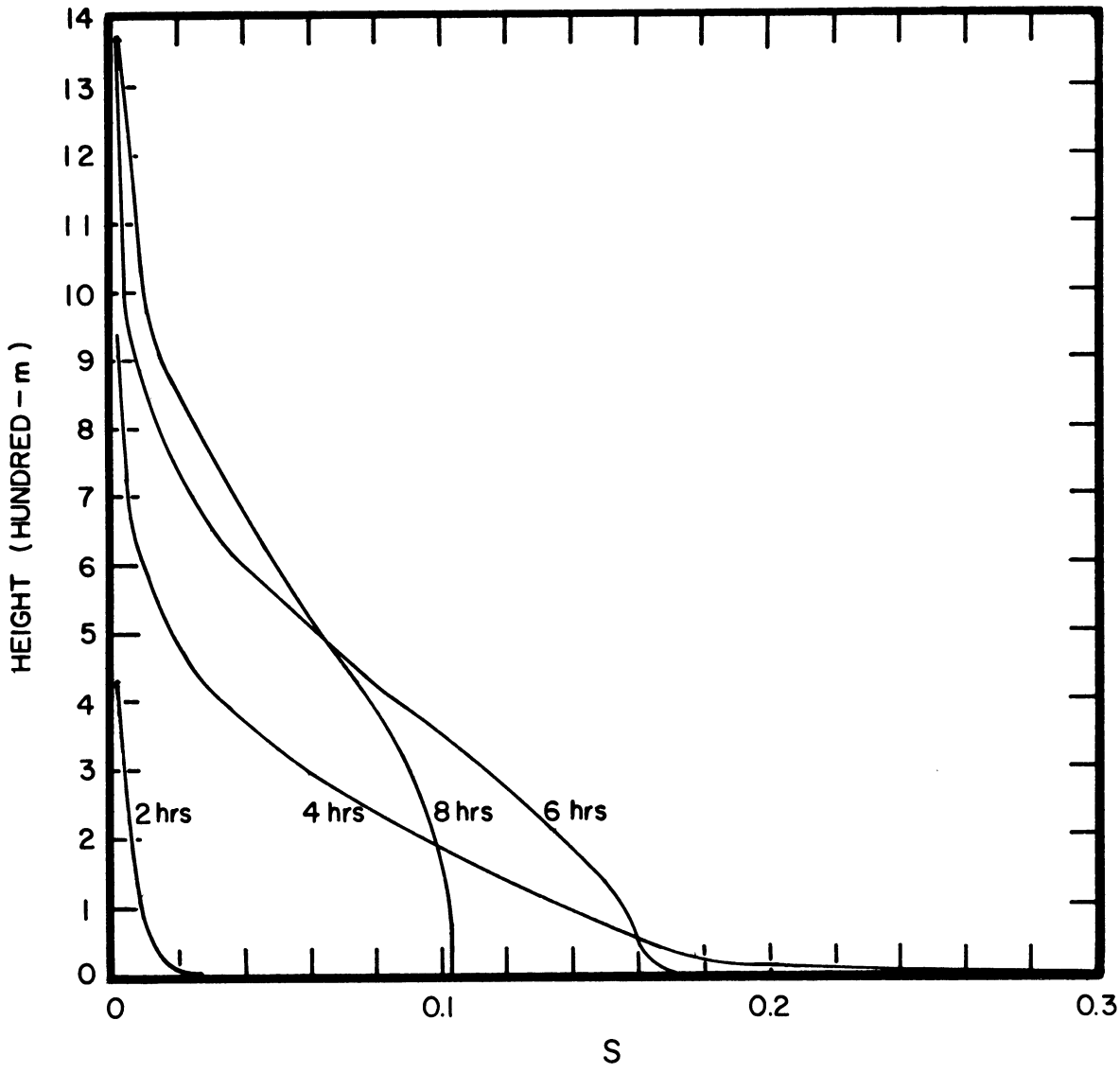

Fig. 7.4. Solution to the unsteady one-dimensional parabolic diffusion equation for $P(t) = \exp\left[-\frac{1}{2}\left(\frac{t-4}{1}\right)^2\right]$, F = q, K a function of height and 40 nodal points.

characteristics of the curves in Fig. 7.4 with the profiles reported in App. C and shown in Figs. C.22.1-6. To facilitate comparison Fig. C.22.4 is reproduced here as Fig. 7.5. The general similarity of the two sets of profiles is apparent.

7.2.6 Solutions of the Steady Two-Dimensional Diffusion Equation

The solutions obtained for the steady two dimensional parabolic diffusion equation are very similar to those described above and were carried out using essentially the same program. Only one set of solutions is given and that appears in App. A below.

7.3 POLLEN CONCENTRATION OVER AN URBAN AREA

7.3.1 Parameter Values, Boundary and Initial Conditions

The culmination of the work reported in the first six chapters and Sect. 7.2 of this chapter is presented in this section. Ideally, the solution over the urban area should be found from the complete parabolic diffusion equation, but as discussed in Chapt. 4 it has been found necessary to deal with a simplified version of the steady three-dimensional model as given by Eq. (4.48).

The following parameter values and boundary conditions are used.

1. The wind speed profile is assumed to follow the 1/7 power law, i.e.

$$u(z) = u(\ell)(z/\ell)^{1/7}$$

2. The profile of the vertical component of diffusivity is assumed to be as follows

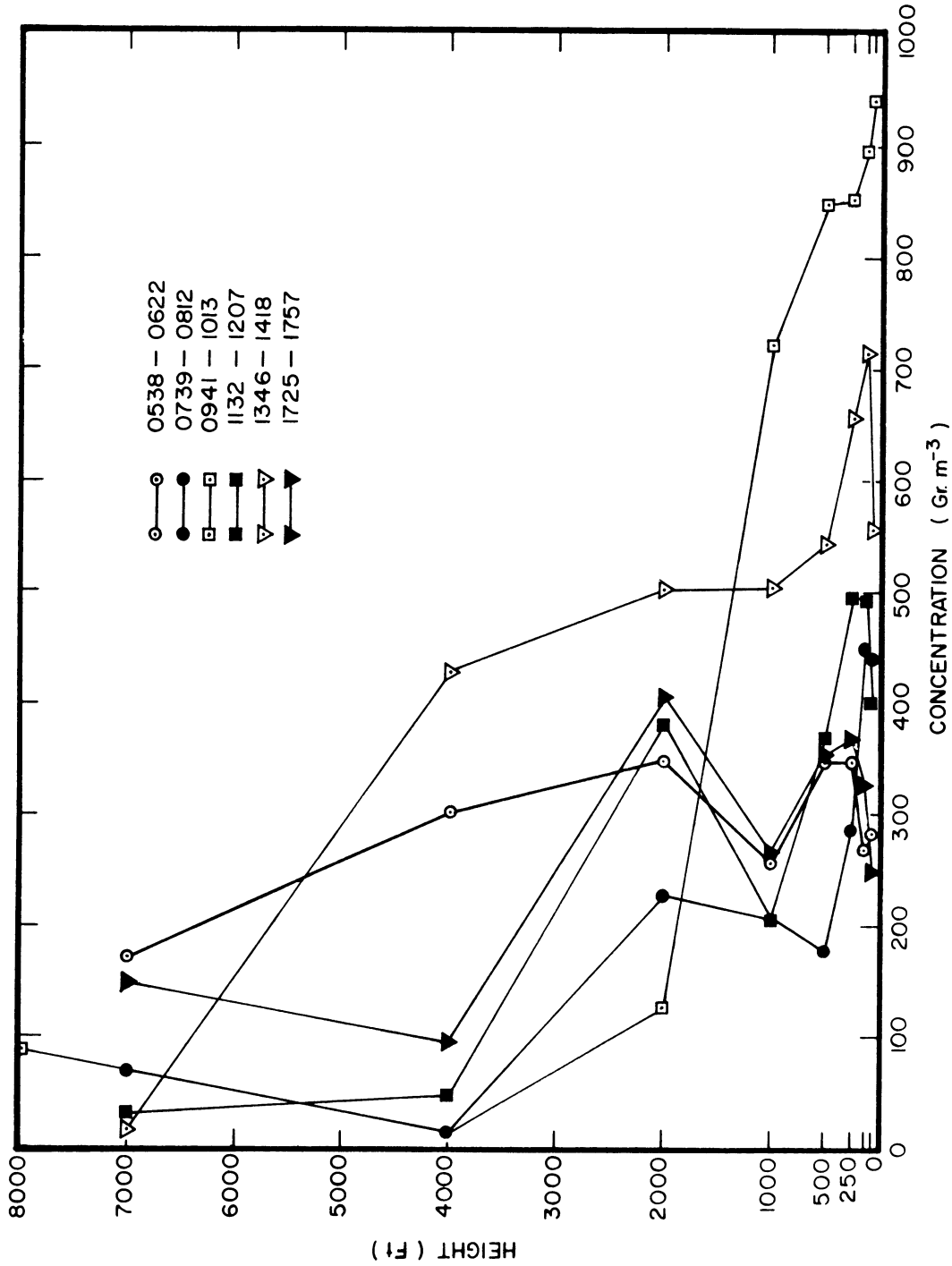

Fig. 7.5. Observed ragweed pollen profiles measured by aircraft over Willow Run Airport in Michigan August 29, 1962.

$$K_z(z) = K_z(h)\ z/h \qquad \ell \leq z \leq h$$

$$K_z(z) = K_z(h) \left(\frac{H-z}{H-h}\right)^2 \qquad h \leq z \leq H$$

where many combinations of values would fit the nondimensional variables used, but a reasonable set satisfying the conditions under which the problem is solved is H = 1500 m, h = H/40, $H_z(h)$ = 20 m^2 sec^{-1} and ℓ = 0.1 m.

3. The lateral component of the diffusivity is assumed to be constant with height, and under the conditions given above has a value of 10 m^2 sec^{-1}.

The initial conditions pertaining to the upwind boundary of the urban area depend primarily upon the time of day relative to the time of peak emission. The initial condition used here is the solution to the one-dimensional diffusion equation, given in the preceding section, at the time of peak emission strength as shown in Fig. 7.4. This choice should permit a reasonable comparison to be made between the contribution to the concentration from small local sources within the urban area and that from the surrounding countryside.

One important question for which there is no definitive answer at present concerns the relative strengths of the local and external sources. The local source is assumed to be an area of relatively dense ragweed growth whereas the external source is an area of mixed vegetal cover; only a small portion of which has a significant ragweed population. The Washtenaw county agent reports that 48% of the land in the Ann Arbor area is cultivated and 29% of that is in cereal crops other than corn; this means that approximately 1/7 of the total land area

contains strong pollen sources. A small concentrated source in an urban area may therefore be assumed to have a strength about seven times greater than the average country source. Confirmation for this figure comes from a comparison of the estimates of large scale sources strength given in Sect. C.6.4.2 and measurements reported using a whirling arm sampler (Sheldon and Hewson, 1960, p. 84) around a concentrated source (Harrison, 1965). In the results which follow the urban area source is given a strength seven times greater than that over the rural area.

The boundary conditions are exactly as described in Eq. (4.56); over the urban area the pollen emission term P is equated to zero; outside the urban area and over the small area source within the urban area P is given a finite value; the pollen loss at the ground is computed from Eq. (5.3).

7.3.2 A Comparison of the Contributions to Urban Pollen Concentrations by Internal and External Sources

The equations describing the diffusion of pollen into an urban area from an infinite external source have been solved using the methods given in Sect. 4.7, and those describing the diffusion of pollen from a small area source by the methods given in Sect. 4.8.

The substitution of reasonable values for the components of the dimensionless parameters permits the presentation of the results in a more concrete form. Values of the dimensions of the urban area, small local source, and increments in the grid network compatable with the parameter values of Sect. 7.3.1 are given below.

	Urban Area	Small Area Source
Downwind Increment	100 m	5 m
Crosswind Increment	100 m	5 m
Width	4800 m	50 m

The results comprise two three-dimensional tables containing several thousand concentration values. As such they are too voluminous to be reported here. Instead the results will be shown in a series of cross sectional, plan and one-dimensional figures.

The first, Fig. 7.6, is a traverse at ground level in the downwind direction through the heart of the city measured from the upwind edge. The small local source is shown at 1 km in the downwind direction although comparisons at other distances can be made by transposition of the curve. Curve A shows the concentration at ground level through the center of the city resulting from pollen advected into the city from an infinite external source. Curve B shows the concentration at ground level over and downwind of a 50 x 50 m square area source located within the city.

Under the particular but realistic set of conditions noted above the following tentative conclusions are drawn:

1. The concentration of ragweed pollen during periods of pollen emission decreases rapidly with distance from the upwind boundary of the ragweed free urban area, reaching a concentration equal to one half and one third of its value on the upwind boundary at a distance of 0.2 and 1 km downwind respectively.

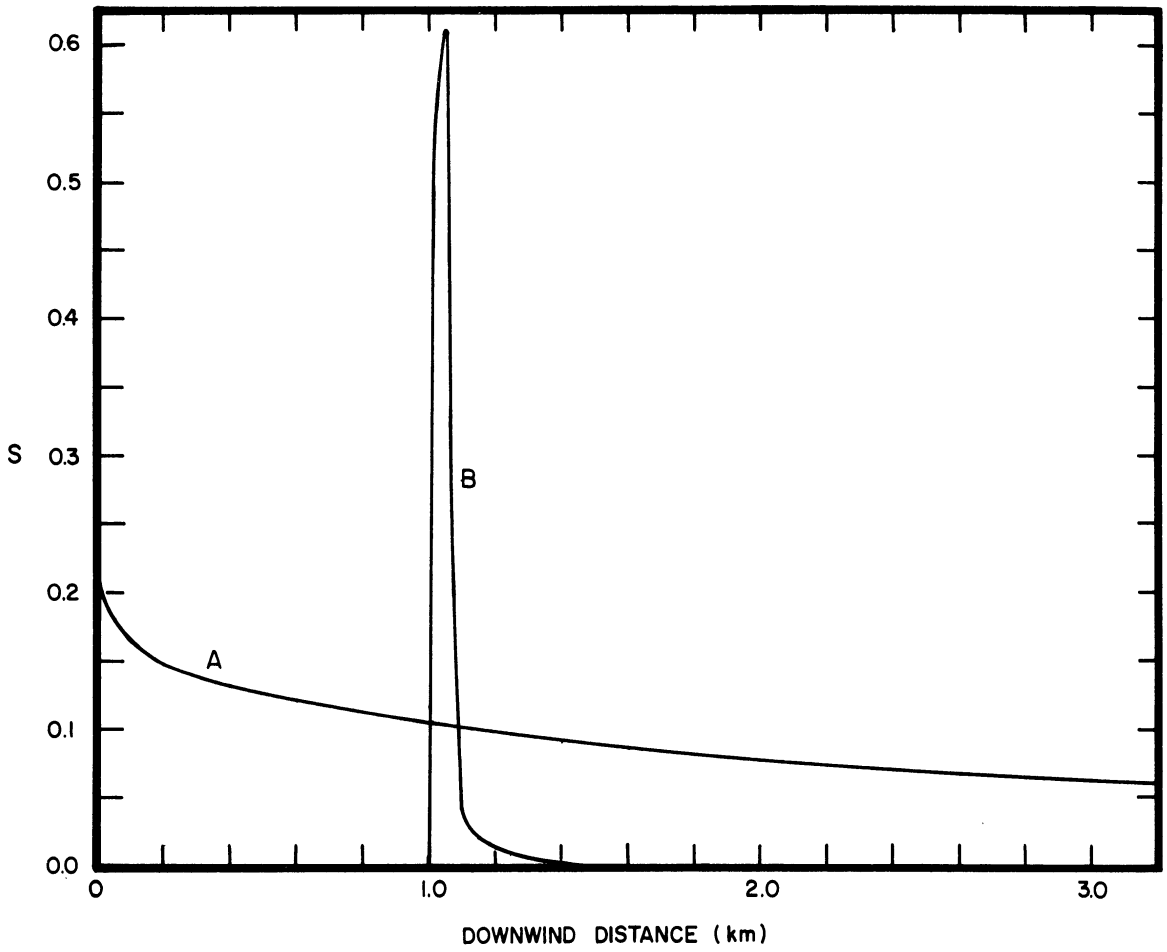

Fig. 7.6. The ragweed pollen concentration at ground level along a traverse in the downwind direction across an urban area. The distance from the upwind edge of the city is given along the abscissa and the dimensionless concentration $S = \chi/\chi_{ARB}$ as given along the ordinate. Curve A represents pollen advected into the urban area from an infinite external source and curve B represents pollen from a 2500 m^2 area source located 1 km from the upwind edge of the urban area.

2. Over and immediately downwind from a small local ragweed pollen source the concentration may be higher than its average value in rural areas.

3. The contribution to the urban pollen concentration by a local source of small diameter becomes insignificant relative to the pollen carried into the city from the surrounding countryside at distances of more than a few source diameters downwind. In the example illustrated in Fig. 7.6 the fractional concentration contributed by the local source decreases to less than 10% at a downwind distance of 4 times its diameter.

The results shown in Fig. 7.6 apply only to a particular portion of the day, namely the period of peak pollen emission. Earlier in the day the relative effect of the local source will be greater, whereas after the period of peak emission it will decrease to insignificance.

The rate of decay of pollen concentration with distance downwind from the area source may be compared with the calculations performed on the basis of Sutton's equations (see Eq. (1.1)) by Yang (1959). For an area source extending to infinity in the cross wind direction Yang's model gives concentrations of 8, 4 and 3% of the peak value at 2, 3 and 4 source widths downwind. Comparable figures taken from curve B of Fig. 7.6 are 7, 3 and 2% respectively.

The ground level pollen concentration in the vicinity of the local source is compared with the concentration of pollen from the external source in a plan view illustrated in Fig. 7.7. The area over which the local source causes an appreciable increase in pollen concentration is seen to be relatively small.

Figure 7.8 shows the manner in which the pollen profile changes with increasing distance across an urban area. Curve A is the profile

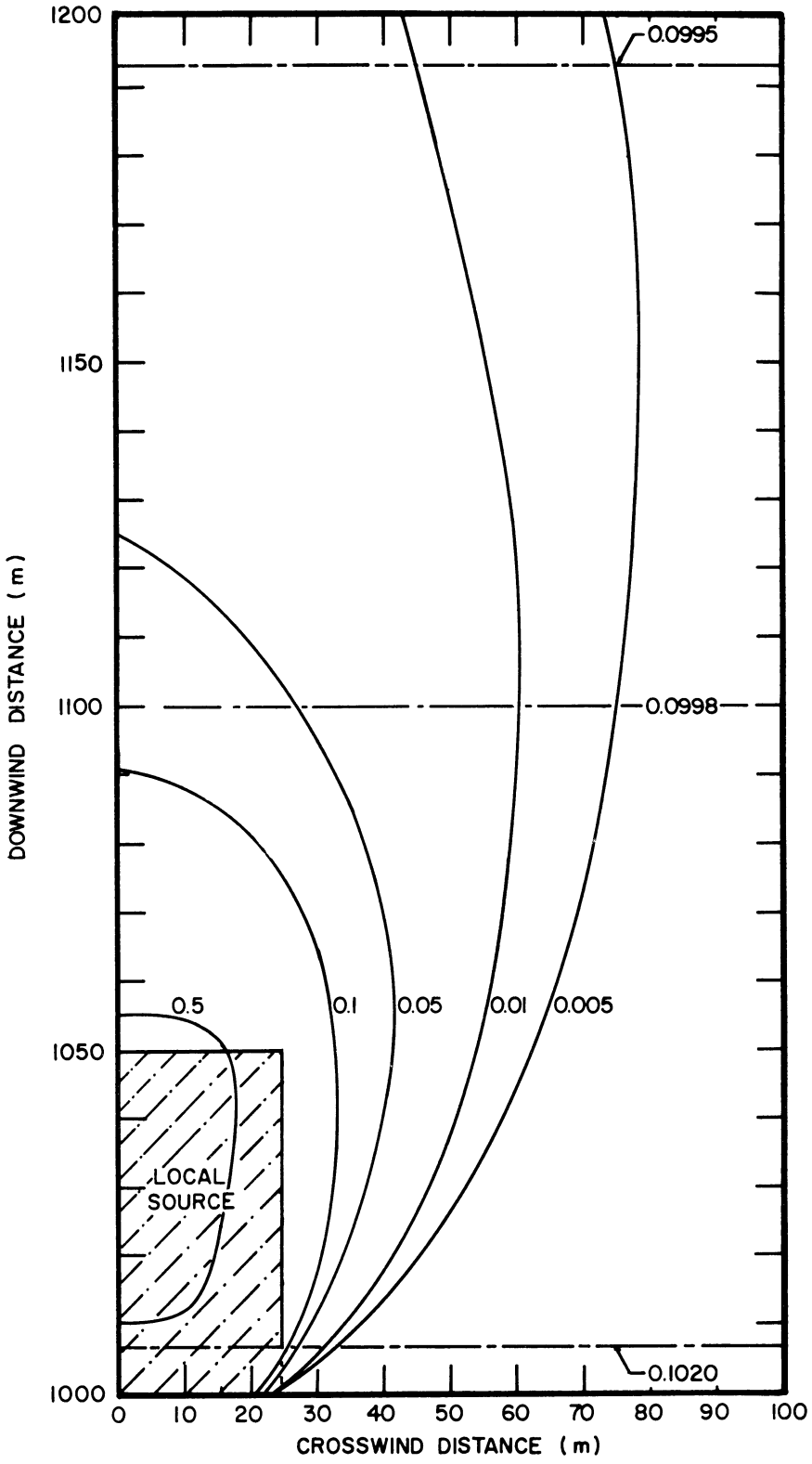

Fig. 7.7. A plan view of the computed ground level distribution of the dimensionless concentration S resulting from 1, a local source within an otherwise ragweed free urban area - solid lines, and 2, advection from the surrounding rural areas - dot dash lines. Details of the problem are outlined in the text.

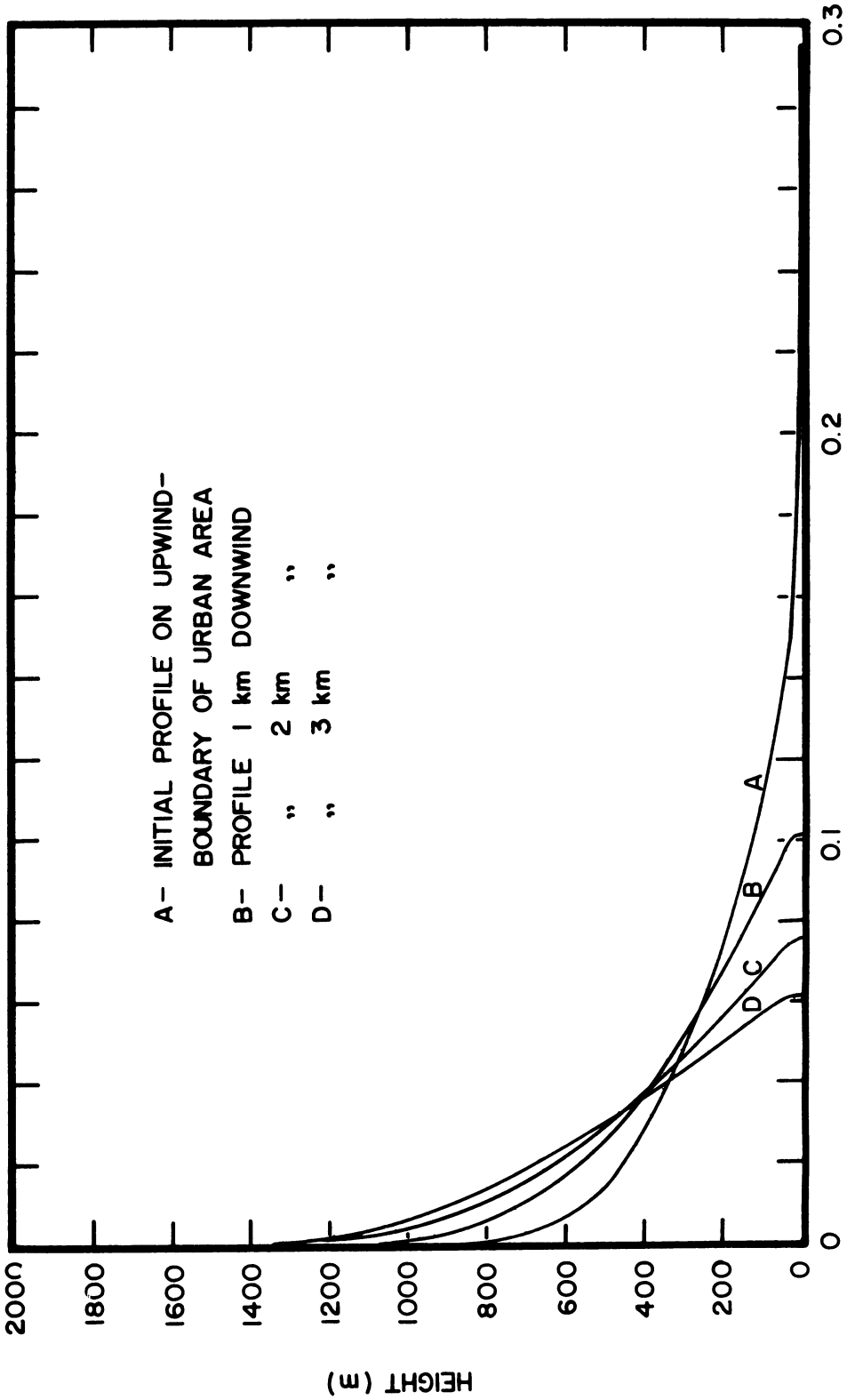

Fig. 7.8. The computed vertical profile of the dimensionless pollen concentration S resulting from the advection of ragweed pollen into an urban area from an infinite homogeneous rural source. Solutions are given at distances of zero, 1, 2 and 3 km downwind from the city's boundary.

computed by means of the unsteady one-dimensional diffusion equation under the conditions outlined earlier. The extreme slope of the profile near the ground is a consequence of the high pollen emission rate occurring at the peak emission period of the day. Although it is not easily seen in the figure the concentration at ground level is 0.295. Downwind from the city's boundary the pollen profile becomes constant with height very near the ground and begins the adjustment toward a constant value aloft.

The crosswind distribution of pollen is illustrated in Fig. 7.9 at x = 0, 100 and 4000 m downwind from the city's boundary and for z = ℓ, 100 and 1000 m in elevation. Note that the crosswind boundary of the city occurs at 2300 m in the figure. One surprising aspect of this figure is the extremely sharp demarcation between urban and rural pollen concentrations. Even at x = 4 km the transition from urban to rural values occurs over a distance of only 1/2 km. The question arises, is the value of the lateral component of the diffusivity used in this solution, i.e. K_y = 10 m^2 sec^{-1}, too small?

It may be recalled that measured values of K_y over a 1 hr period in November of 1960 during the out-of-season experiment were of order 1 m^2 sec^{-1} (see Tables B-14 and B-15). From the discussion of Sect. 6.4.2 the summer values should be considerably larger as a result of the lower wind speed during that season. Therefore the value 10 m^2 sec^{-1} seems entirely reasonable. The only estimate of K_y which would appreciably alter the pattern shown in Fig. 7.9 is Richardson's (see Sect. 6.4.2),

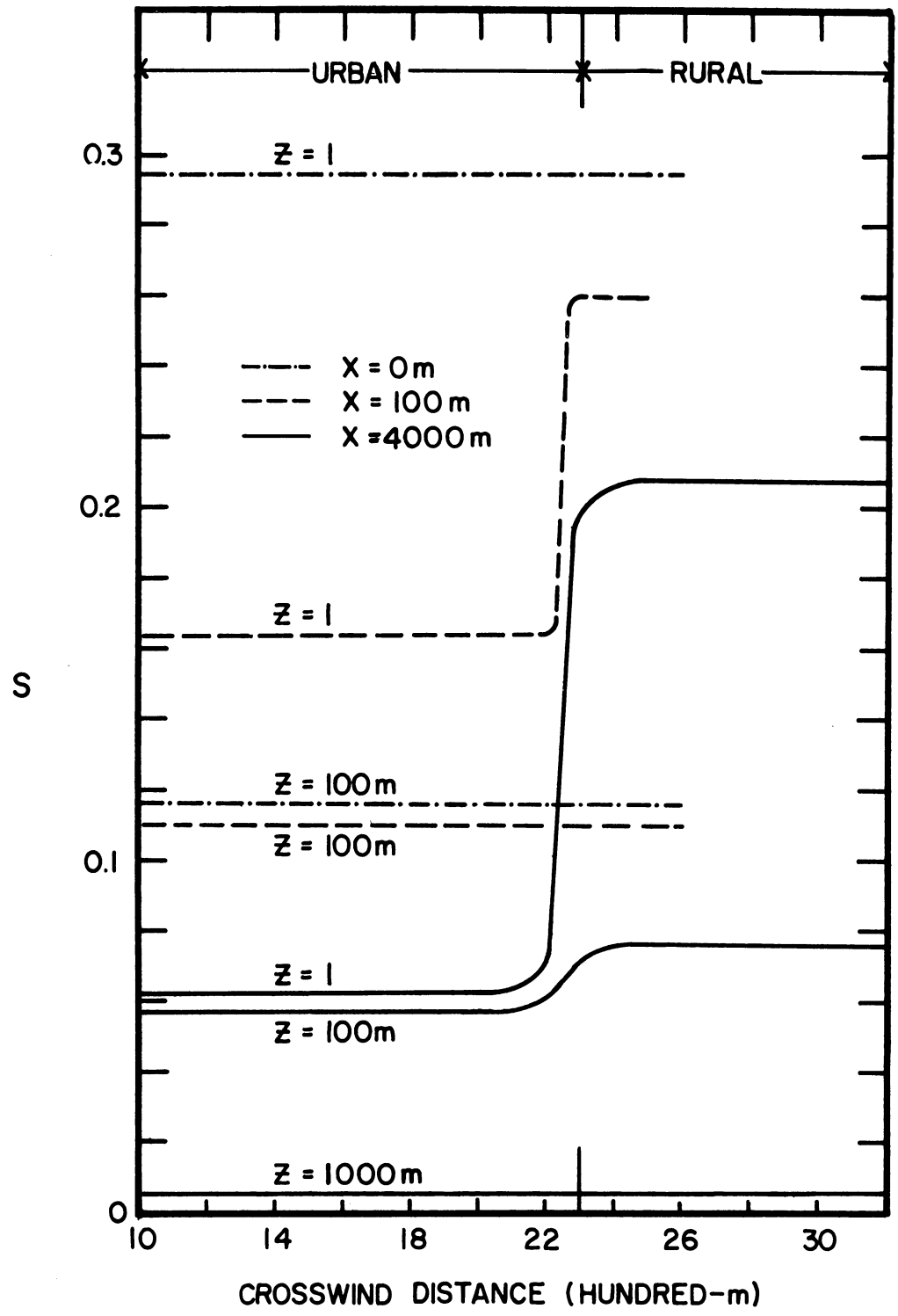

Fig. 7.9. The crosswind distribution of pollen concentration across an urban area at distances of zero, 100 m and 4000 m downwind from the city's boundary. Conditions are the same as those of the previous figures.

which is of order 10^3 m^2 sec^{-1}.

7.4 CONCLUSIONS

The conclusions which follow are divided into sections: first, those which pertain directly to the solution of the parabolic diffusion equations and the computation of pollen concentrations over an urban area; and second, those which apply to the atmospheric parameters, boundary conditions and other peripheral findings.

7.4.1 Primary Conclusions

The agreement between the forms of the theoretical solutions to the unsteady one-dimensional and steady two-dimensional parabolic diffusion equations and those of the experimental observations presented in App. A and C suggest that these equations satisfactorily represent the diffusion of ragweed pollen in the atmosphere.

Solutions of the steady three-dimensional parabolic diffusion equation show that small isolated ragweed sources within an urban area have little influence on the pollen concentration in the city except in their immediate vicinity. Unless a city contains a relatively dense ragweed population, the major portion of the pollen within its borders is advected from the surrounding farmland.

The highest pollen concentrations within a ragweed free area which adjoins a ragweed source area occur within a relatively narrow strip downwind from the source. Under the particular conditions outlined in

Sect. 7.3 the strip is approximately 500 m wide. If one can consider this to be a typical figure, then the residents of a city may be afforded some protection from high pollen concentration by ensuring that a 1/2 km strip of land around the margin of the city is kept free from ragweed. This may be accomplished most simply by having all cereal grain fields bordering a city plowed in early August before ragweed pollination begins.

7.4.2 Secondary Conclusions

A number of conclusions have been reached throughout the body of this study. The relevance of some of these is more obvious within the context of the chapters in which they occur. A brief summary, however, is given in the following paragraphs.

7.4.2.1 Pollen Flux into the Plant Canopy

The condition on the lower boundary, i.e. at the top of the vegetative canopy, if one exists, or otherwise at the earths surface, can in the case of ragweed pollen be adequately and realistically expressed by the equation

$$\left(K \frac{\partial \chi}{\partial z} + q\chi\right)_{\ell+} = - P + F\chi(\ell)$$

(see Eq. (1.18)), where P is the upward flux of pollen at the boundary caused by pollen emission and F is a deposition velocity.

The deposition velocity F may be computed from the equation

$$F = \left(\frac{K}{\chi}\frac{\partial \chi}{\partial Z} + q\right)_{\ell}$$

(see Eq. (5.2)). The gradient of pollen downward from the top of vegetation at ℓ can be computed only on the basis of a detailed knowledge of conditions within the plant canopy (see Chapt. 5).

Computed profiles of pollen concentration within a plant canopy can be made to agree with the presumed correct distribution according to the theories proposed here only if the adhesive efficiency of the plant surface is extremely low, of order 0.01. The spruce tree, according to the theory presented in Chapt. 5, should be the most efficient natural air cleanser for ragweed pollen.

7.4.2.2 Inferences from Pollen Profiles

In the absence of strong advective influences the profiles of aerosols in the atmosphere indicate the flux condition at the lower boundary. A concentration which increases with increasing height indicates that the aerosol is being absorbed faster than the rate at which it would deposit by gravitational settling alone; a concentration which decreases with height indicates emission at the boundary and a constant concentration with height indicates deposition by gravity.

Aerosol profiles aloft under steady-state conditions may be used to infer the diffusivity; however, steady-state conditions rarely occur in the atmosphere and therefore such inferences must be made with extreme caution (see Chapt. 3).

7.4.2.3 Solution of the Parabolic Diffusion Equations

The unsteady one- and the steady two- and three-dimensional parabolic diffusion equations may be readily solved using the methods of Chapt. 4 if certain precautions at the boundaries are observed. The unsteady two- and three-dimensional equations present some serious computational problems which have not as yet been overcome.

7.4.2.4 Atmospheric Parameters

Models for the atmospheric parameters needed to solve the diffusion equations, namely the vertical profiles of the wind and diffusivity, are still only crude approximations to the true values in the atmosphere; this is particularly true above 50 m. A thorough discussion of various models is given in Chapt. 6 and the most appropriate, in the judgement of the author, selected for use in the diffusion models.

The conclusions reached regarding one's ability to make meaningful estimates of the lateral component of the diffusivity deserve special mention. It is shown by means of Eq. (2.37) and in the discussion in Sect. 6.4 that under apparently identical atmospheric conditions and surface roughness characteristics the lateral component of the diffusivity may vary markedly from one observation period to the next. Serious consideration should be given to this problem when planning diffusion experiments.

7.4.2.5 The Field Experiments

From the results of field experiments reported in App. A to C it

is concluded that, at least over the vegetal cover experienced at Willow Run Airport in Michigan, the deposition velocity of ragweed pollen at the ground is equal to its gravitational settling velocity. This produces a loss of pollen at the ground much smaller than has been suggested by other authors.

From the same experiments it is concluded that the lateral distribution of pollen emitted from a point source is not likely to be Gaussian, and the vertical distribution if the source is near the ground will be skewed positively toward higher elevations. The diffusivities inferred from the pollen distributions agree well with diffusivities measured by other methods.

The pollen profiles measured by aircraft during 1962 provide a reasonable confirmation of the reliability of the parabolic diffusion equation model. During that season pollen was carried to between 1500 and 2000 m in considerable concentrations. From this it may be inferred that ragweed pollen is carried many hundreds of miles before being completely deposited on the ground. A crude estimate from Eq. (C.19) of the distance pollen may travel in a 10 mph wind before it is depleted to 5% of its initial average concentration is 1200 miles.

7.5 SUGGESTIONS FOR FURTHER RESEARCH

Questions are raised within the body of this study which apply to every facet of micrometeorological research; only those directly involved in the central problem are considered in this section.

The unsteady one-dimensional diffusion equation should be solved using a variety of realistic parameter values and boundary conditions in an attempt to match the pollen profiles reported in App. C.

An attempt should be made to produce an accurate fit to the pollen profiles reported in App. A using the steady two-dimensional diffusion equation.

The solutions of the steady three-dimensional diffusion equation should be tested by means of an adequate sampling program upwind of and across an appropriate urban area.

Methods of solving the unsteady two- and three-dimensional diffusion equations should be found, because most real diffusion problems in the atmosphere are unsteady.

The pollen, wind and diffusivity profiles in vegetation should be measured and compared with theoretical profiles. Many measurements should be made of the distribution of the various types of vegetation and the spectrum of element sizes. The sampling efficiency of various kinds of vegetation should be measured.

Equations (A.4) and (C.19) relating to the long distance transport of pollen should be checked by means of an adequate observational program. The results will be of particular interest to paleontologists and others interested in the atmospheric transport of pollen and other substances over large distances.

Although the problems mentioned above are important, they are overshadowed in terms of urgency by unsolved problems of a purely micro-

meteorological or mesometeorological nature. Of particular value to those interested in pollen transport would be the determination of the vertical distributions of the components of the wind and diffusivity in the convective layer.

APPENDIX A

THE 1959 IN-SEASON EXPERIMENT

A.1 INTRODUCTION

The 1959 in-season experiment was designed to investigate the rate of diffusion and deposition of ragweed pollen emanating from a natural ragweed source. Theoretical analysis was facilitated by the use of a rectangular source sufficiently long that it could be considered infinite in extent in one dimension, and sufficiently large that its effect was distinct from that of the general ubiquitous ragweed population.

A.2 DESCRIPTION AND PREPARATION OF THE EXPERIMENTAL SITE

The experiment was carried out in an area lying between four runways and the east parking apron of The University of Michigan's Willow Run Airport as shown in Fig. A.1. A preseason survey revealed that the experimental site, which previously had been subjected to cultivation, had not been disturbed during the 1959 season and, consequently, was covered by a uniform growth of ragweed. The remainder of the airfield was mowed at frequent intervals and contained only occasional isolated patches of ragweed. Thus it was possible, through eradication of weeds from selected areas, to produce a rather uniform and well defined source of ragweed pollen in an otherwise ragweed free area. The site was also well suited to the experiment because of the

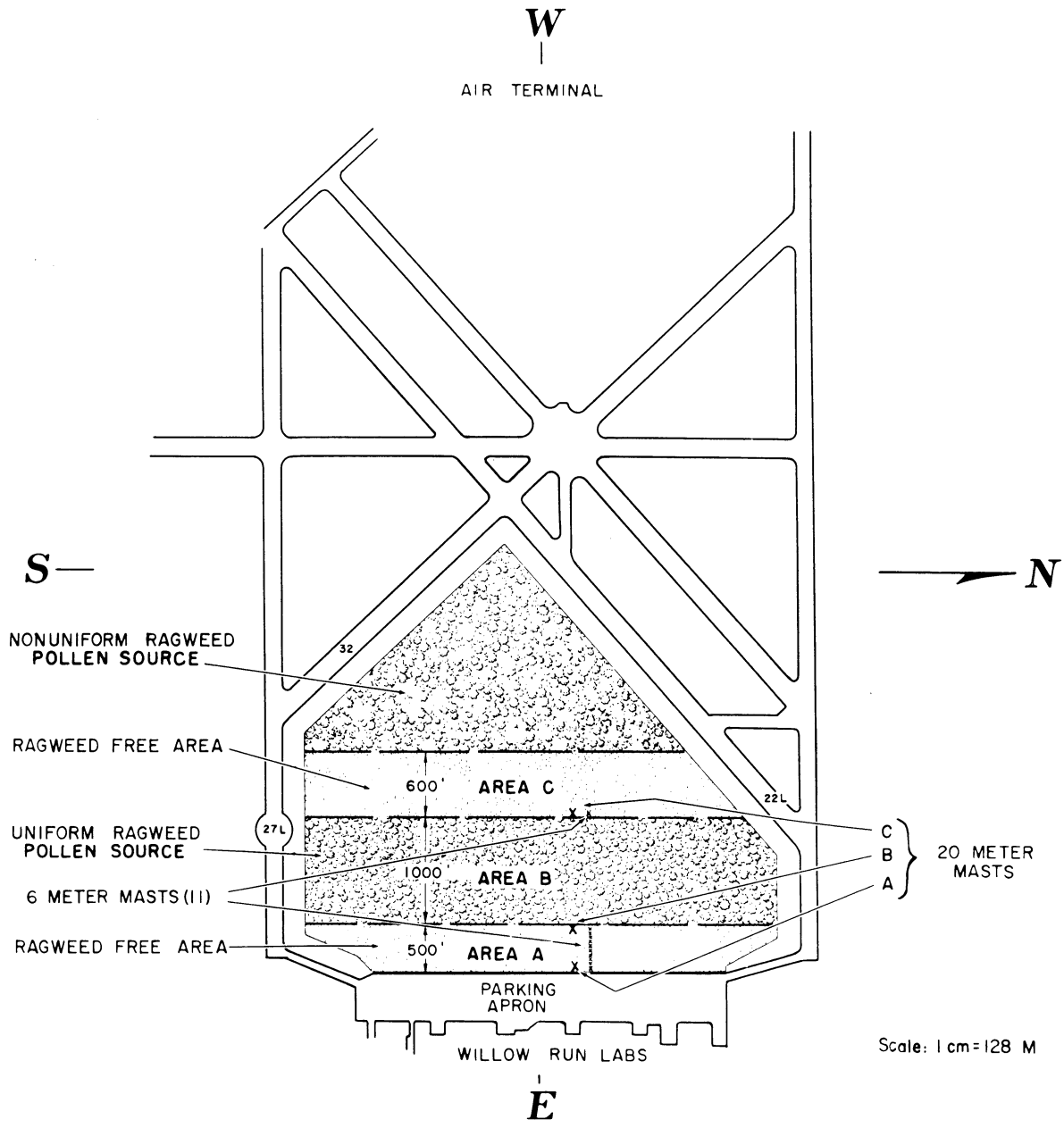

Fig. A.1. 1959 in-season pollen sampling site.

uniformity of the terrain over a long upwind fetch.

A strip 500 ft wide adjacent to the concrete apron at the east end of the field, area A, was sprayed with 2-4-D (Esterone 1010) on two separate days to kill all ragweed. Earlier in the season the area had been mowed so that a uniform growth of relatively low grass remained after all broad-leafed plants had been killed.

No chemical treatment was applied to area B, a nearly rectangular plot 1000 x 4500 ft in dimension between masts B and C, shown in Fig. A.1. A dense and uniform growth of ragweed in this area intermingled with various varieties of grass provided a uniform source of pollen.

Of the remaining area enclosed by airport runways 32, 27L, and 22L, a 700 ft wide strip area C adjacent to the area B, mentioned above, was sprayed once with 2-4-D prior to the measurement program. A survey of the area showed that plants were stunted and that male inflorenscence did not develop.*

A discontinuity in the source was noted after the experiment was in operation. The area north of an east-west line 50 ft north of the line of sampling towers shown in Fig. A.1 had a mixture of quack grass and ragweed while south of the line the cover was bunch grass and ragweed. The discontinuity was very distinct due to the variation

*It was observed that one application of 1 lb of active 2-4-D per acre at the time the plants are beginning to flower will satisfactorily restrict pollen production. A second application of 2-4-D at a later date effects a complete kill. All 2-4-D chemicals required for this program were donated by the Dow Chemical Company, Midland, Michigan.

in color of the grass. North of the line the density of ragweed plants was about a third of that to the south.

A.3 SAMPLING INSTRUMENTATION

A.3.1 Mounting of Instrumentation

Three 21 m towers were erected; tower A at the edge of the concrete apron, tower B on the line separating areas B and C and tower C on the upwind edge of the source area (see Fig. A.1). Ten 6 m masts, labelled A-J proceeding from east to west, were erected at intervals of 50 ft along a line 50 ft north of the large towers. An additional 6 m mast H was located adjacent to mast C, west of the source. Figure A.2 is a photograph of the array of masts, and shows also the uniformity of the terrain.

A.3.2 Rotobar Samplers

Battery powered rotobar sampling units (see Harrington et al., 1959) shown in the insert in Fig. A.3 were located at heights of 0.61, 1.83, 4, 8, 12, 16, and 20 m on each of the large masts. By reversing the polarity of the applied voltage it was possible to reverse the direction of rotation of the rotobars, so that samples could be collected on the two bars of each unit for two distinct periods of time.

Two governed DC motors were considered: the Barber Colman types AYOM 2013 (6V) and BYQM 2020 (12V). Over the range of voltages and loads which might be anticipated in field use, the BYQM 2020 proved

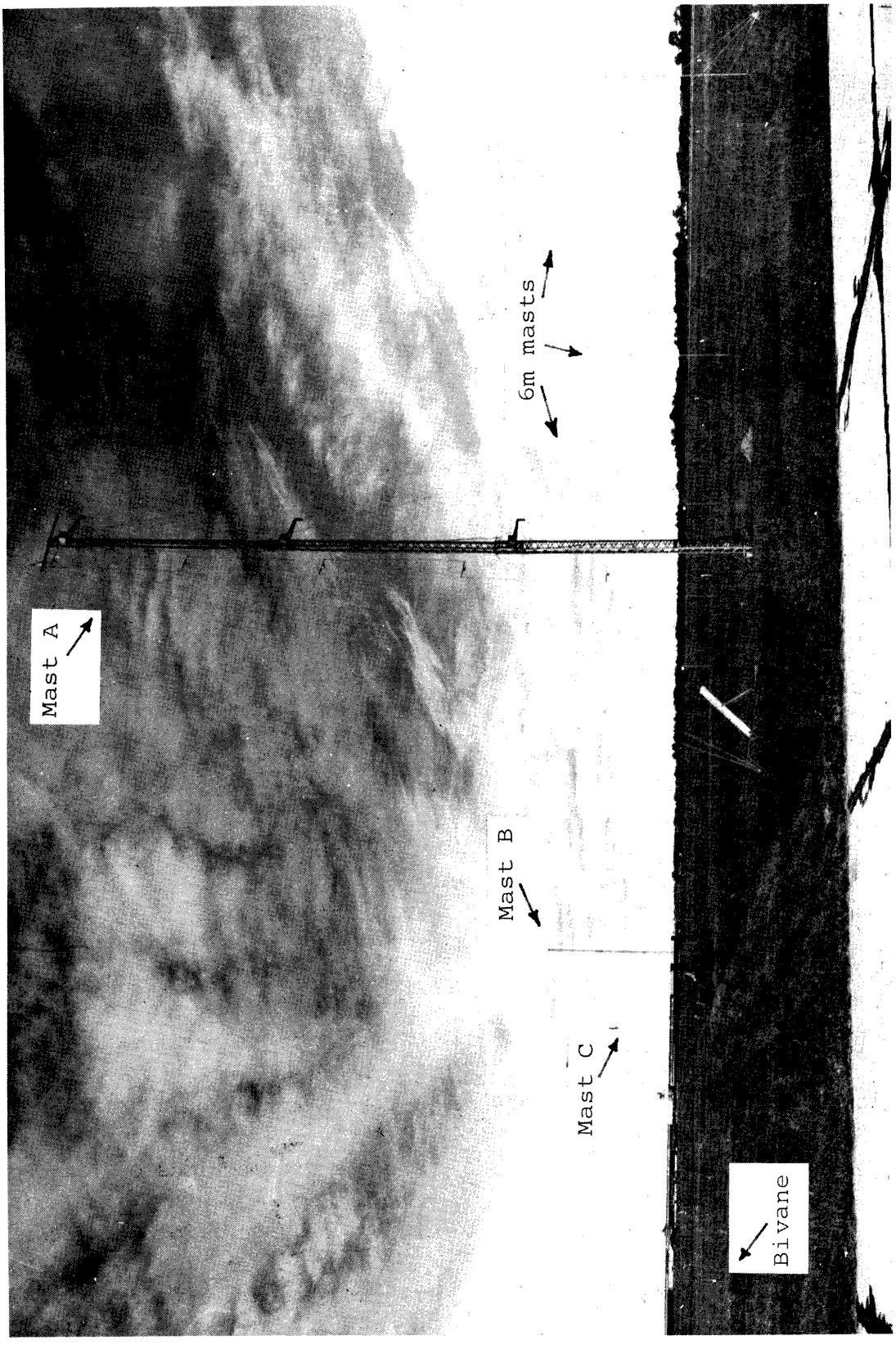

Fig. A.2. Sampling mast array, in-season experiment, 1959.

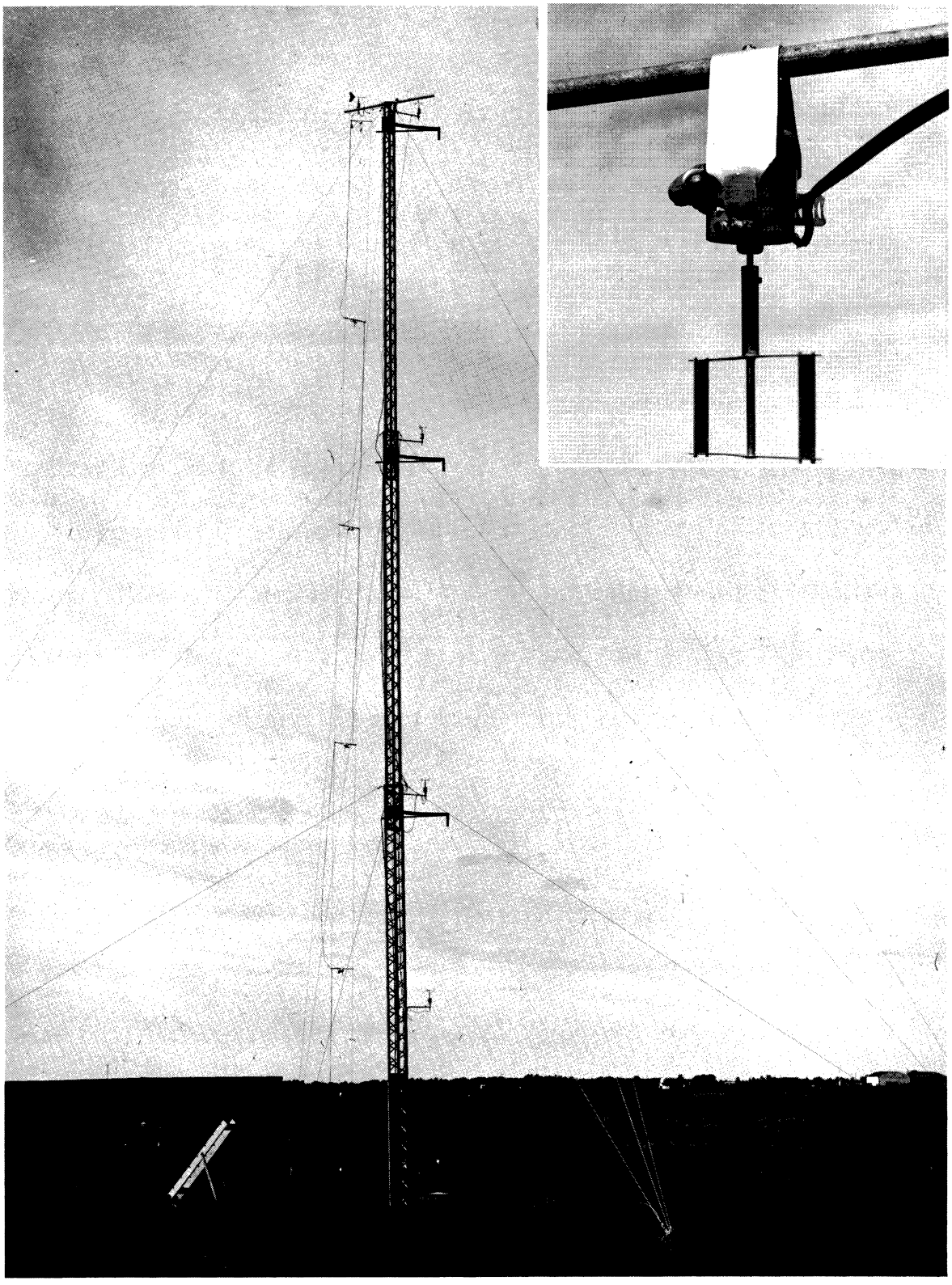

Fig. A.3. Instrumentation on 21 m mast A. Anemometers and thermocouple aspiration tubes shown to right of tower, wind vane at the top and rotobar samplers to the left. Inset: detail of rotobar sampler.

to have a speed more nearly constant as shown in Fig. A.4.

The sampler and sampling technique are the same as those described elsewhere (Harrington et al., 1959), except that the radius of the sampling arm was increased to 3.56 cm, providing a peripheral speed of 20 mph at 2400 rpm, and a volume rate of sampling of 1 m^3 per hr.

A.3.3 Multilevel Rotobar Sampler

A multilevel rotobar sampler was devised to provide a pollen concentration profile for the lowest two feet of the atmosphere. The samplers were mounted on a vertical shaft driven by a 1725 rpm 1/3 hp motor.* The motor was mounted on a heavy steel stand and the shaft supported near the top by an angle-iron-mounted bearing as shown in Fig. A.5. The samplers were fastened to the shaft at heights of 0, 3, 6, 12, and 24 in. above its base. The sampler mounting was similar to that of the standard rotobar sampler except that the radius of rotation was increased to 5 cm to compensate for the slower rotational rate. Each bar swept out 0.828 m^3 per hr and two bars were mounted, diametrically opposed, at each of the sampling levels.

In operation, the sampler was set in a trench so that the lowest sampling bar was at ground level. The trench was covered with plywood and soil to simulate the natural surface, and the two ends of the trench were left open to allow air circulation around the motor.

*General Electric model 5KH35KG122.

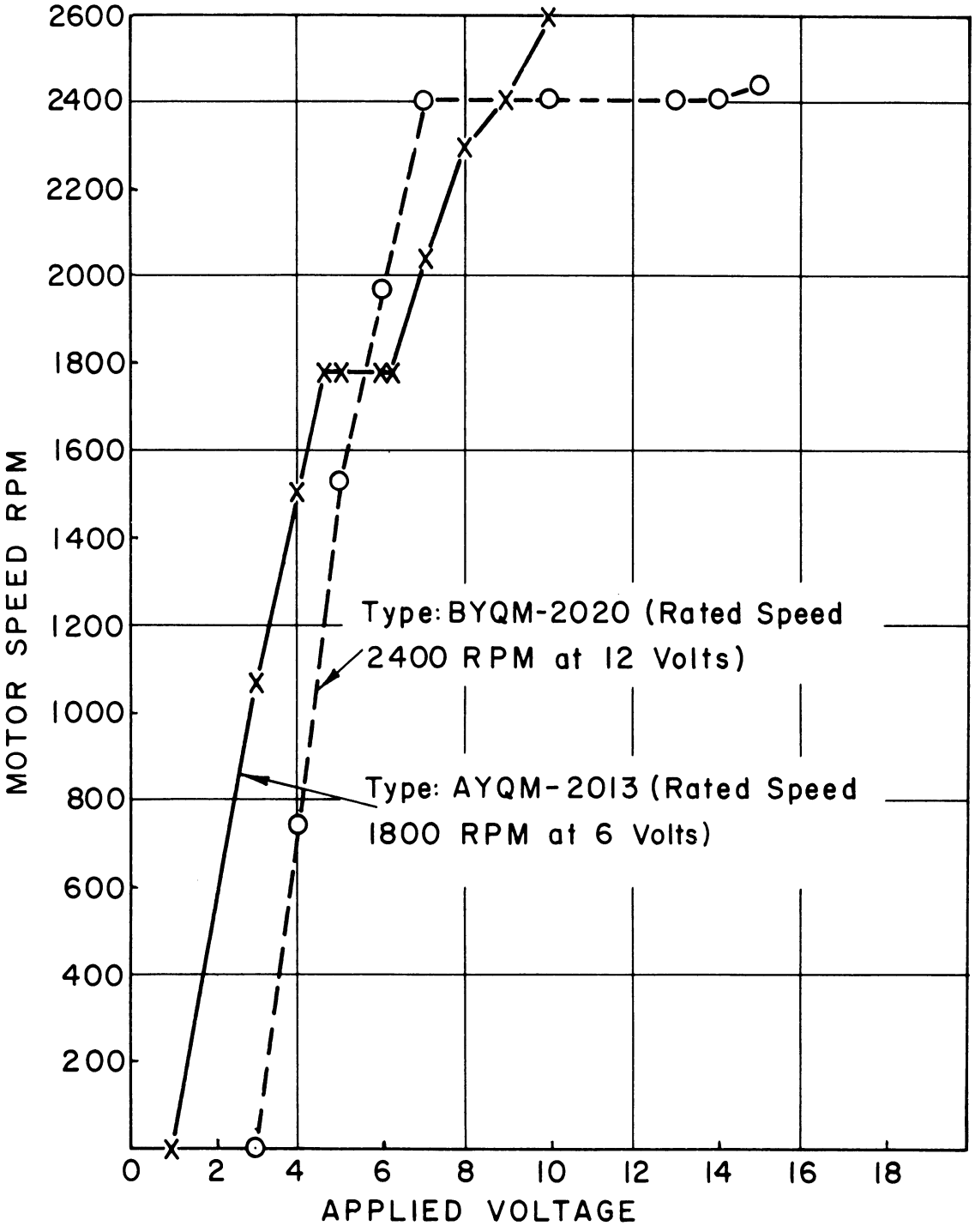

Fig. A.4. Motor speed versus applied voltage for Barber-Colman governed-speed DC motors.

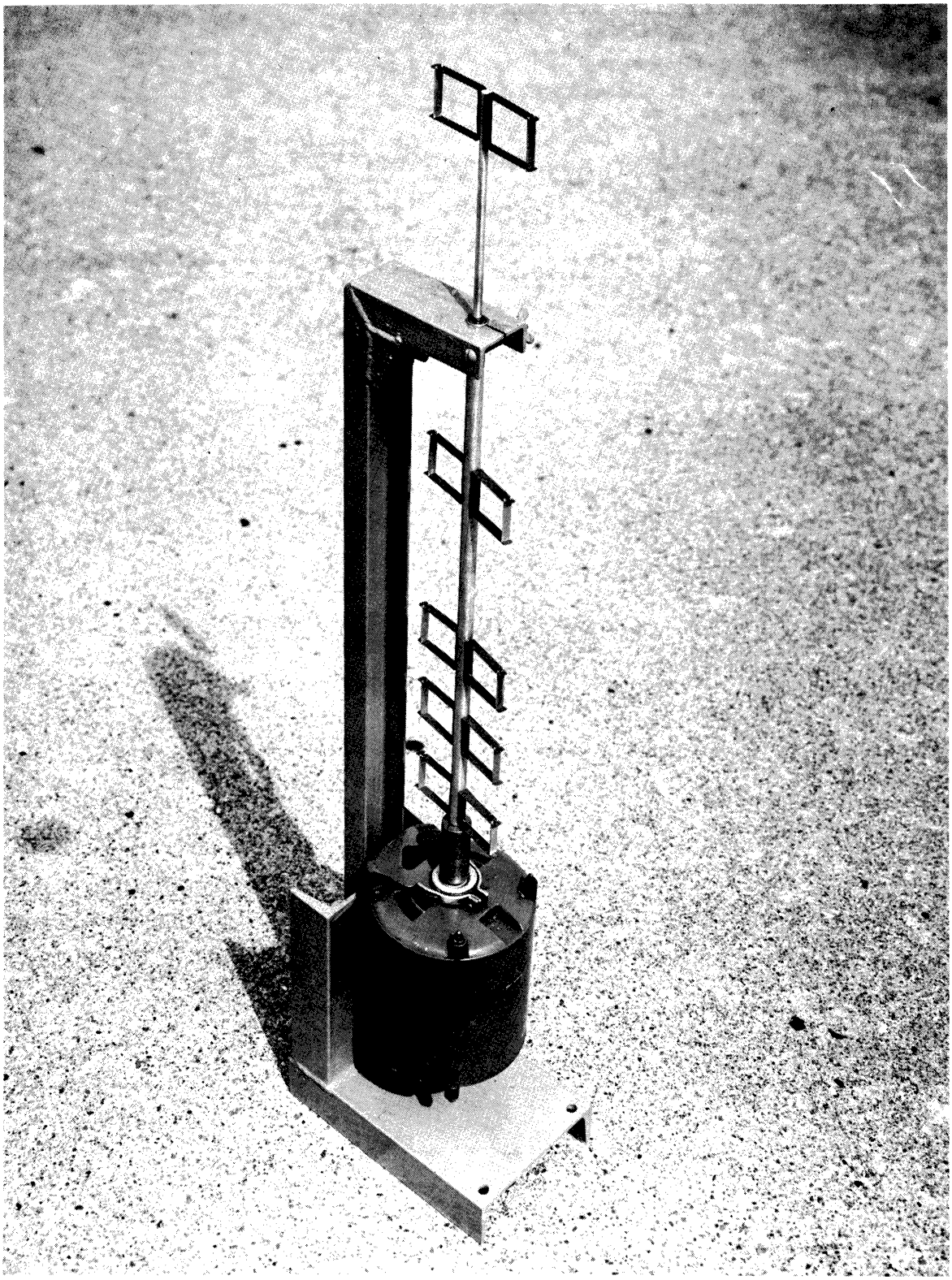

Fig. A.5. Low-level pollen profile sampler.

A.3.4 Flag Samplers

Standard flag samplers (Harrington et al., 1959) (the flag sampler is a Scotch Tape wrapped two in. bank pin placed in a glass bearing) were mounted on the 6 m masts at heights of 0.3, 0.6, 1.2, 1.8, 2.4, 3.7, 4.9, and 6 m as shown in Fig. A.6.

A.4 METEOROLOGICAL OBSERVATIONS

Meteorological observations were operated simultaneously with the pollen concentration determinations. These observations were in addition to the standard U.S. Weather Bureau observations which were made routinely on the west side of Willow Run Airport.

A.4.1 Wind Measurements

The vertical gradient of wind speed was measured by a system of 8 low-inertia, 3-cup Beckman and Whitley anemometers supported on 2-ft arms mounted at 5, 7.5, and 11 m and at the top of the 21 m tower A. The wind speed was recorded by use of digital counters and an Esterline Angus recorder.

Wind direction was measured by a Beckman and Whitley vane also mounted on top of tower A and recorded using a standard Esterline Angus strip chart recorder.

A.4.2 Temperature Lapse Rate Measurements

The vertical temperature gradient was measured by slow response, aspirated copper-constantan thermocouples mounted at 6.5, 12.6, and

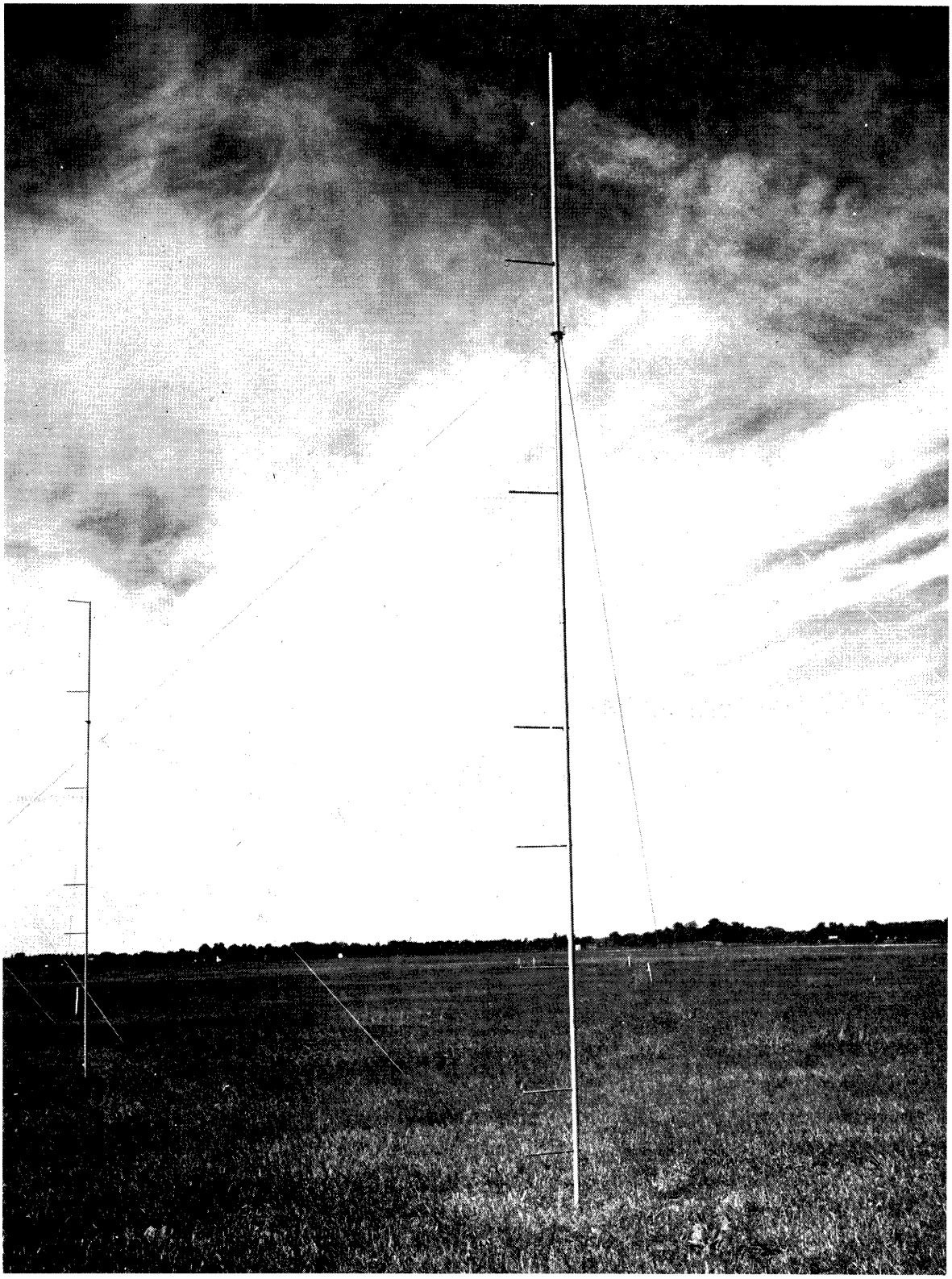

Fig. A.6. Flag sampler exposure, 6 m masts.

19.1 m on tower A. Sequential recording was performed once each minute with an accuracy of about 0.2°C. Instrumentation detail on tower A is shown in Fig. A.7.

A.5 EXPERIMENTAL PROCEDURE

Because the ragweed pollen source was oriented in a north-south direction, meaningful sampling could be accomplished only with westerly winds. Accordingly, sampling was carried out only when the wind was in the sector from 230 to 300°; the south westerly sector was preferred owing to the source discontinuity mentioned earlier.

The routine adopted was as follows. On arrival at the field the recorders were started and time marked, the instruments were set in operation and the rotobar samplers were mounted and set in operation by a team of two men, while the flag samplers were set up by a second team of two. The time required to mount the rotobar samplers was 25 minutes while the flags took 15-20 minutes to mount.

The flag samplers were exposed for a 2-hr period; the direction of rotation of the rotobars was changed after 1 hr and the bars replaced after 2.

The pollen sampling program thus provided for measurements to a height of 21 m of the 2-hr mean vertical pollen concentration profiles upwind, immediately downwind, and 500 ft downwind from the source of pollen. Measurements of the profile to a height of 6 m were also made at 50-ft intervals downwind from the source. The

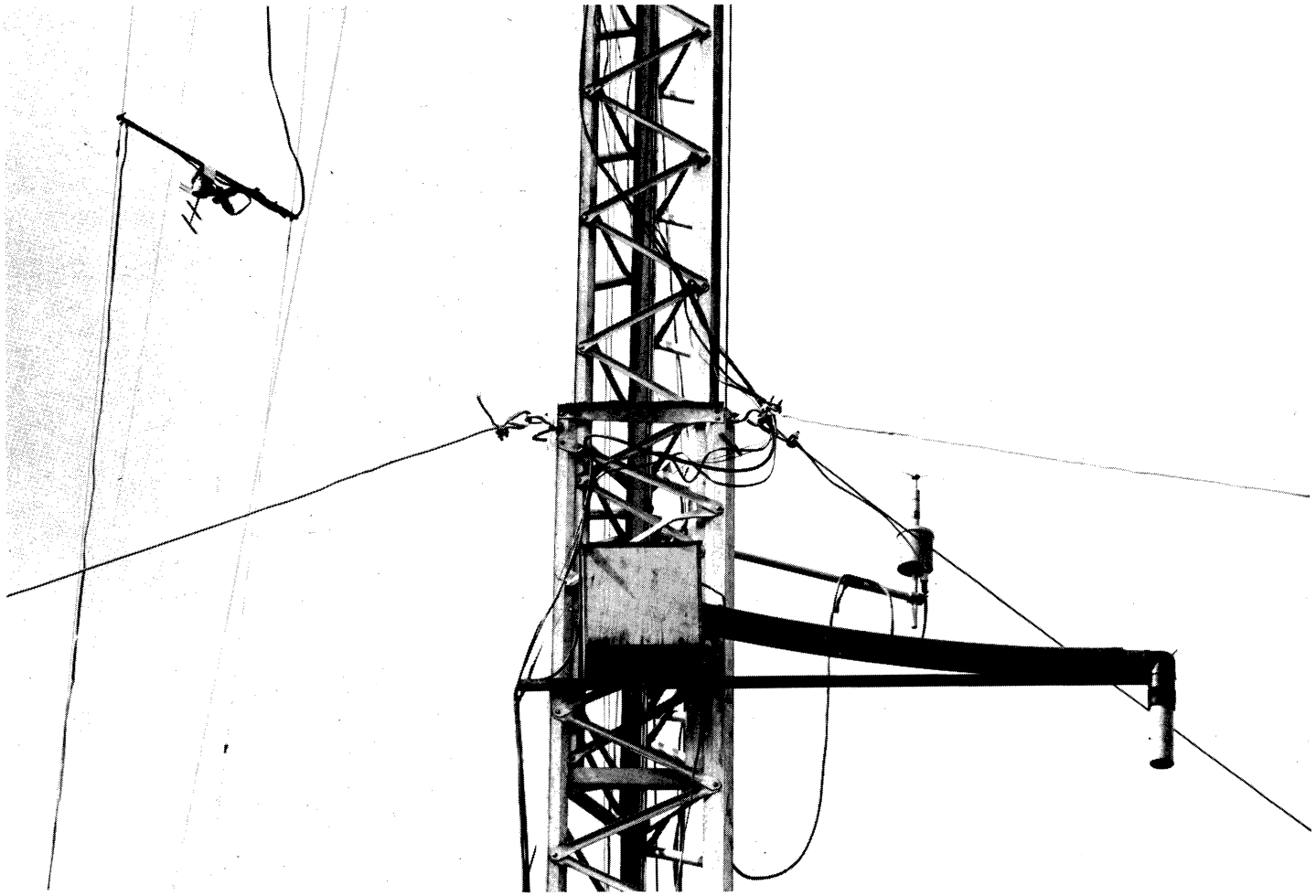

Fig. A.7. Instrumentation detail, mast "A". Anemometer and aspirated thermocouple on right, rotobar pollen sampler on left.

upwind measurements were intended to provide necessary information on the background level of pollen concentration. The downwind measurements could then provide a measure of the rate of dilution due to diffusion and deposition. A total of eight periods of observations were obtained during the 1959 ragweed season.

A.6 ANALYSIS

The rotobar and flag samples were mounted in a shelter in the field. Mounting consisted of removing the Scotch Tape from the sampler, placing it on a clear glass slide with the previously exposed side facing upward, covering it with a cover slip and labeling it. Later the ragweed pollen were counted under a microscope at 100X magnification.

Ten-minute average wind speeds, wind directions and temperatures were abstracted from the records at 10 minute intervals beginning on the hour. These, in turn, were averaged over the appropriate sampling periods.

Wind profiles, graphed and extrapolated or interpolated to find the wind at each flag sampler level, were used to compute the flag sampler efficiency and sampling volume.

A.7 RESULTS

A.7.1 Observation Periods

The dates and time periods during which observations were car-

ried out are shown in Table A-1.* It will be noted that as a consequence of the difference in time required to set up the flag and rotobar samplers, and of a shortage of personnel, the two types of samplers were not operated simultaneously.

A.7.2 Wind Speed and Direction

Table A-2 contains a record of the wind speed on the 20 m tower and Tabel A-3 contains a record of the wind direction measured at the top of the 20 m tower.

A.7.3 Pollen Profile Measurements

Table A-4 contains a record of the pollen counts on the flag samplers and computed concentrations, Table A-5 contains a record of the rotobar pollen counts and Table A-6 contains a record of the ground level profile sampler pollen counts.

The pollen profiles from towers A and B for the series of observations of Thursday, September 3, are reproduced in Fig. A.8. One set of flag profiles for the period 0800-1000 on September 3 is shown in Fig. A.9. Because the observation times for the flag and rotobar samples did not generally coincide, it is difficult to compare the resulting profiles; however, there is reasonable agreement between the first two rotobar periods and the first flag sampling period during the September 3 run. These with the flag concentrations multiplied by

*Tables not included in this Appendix will be found in Volume III.

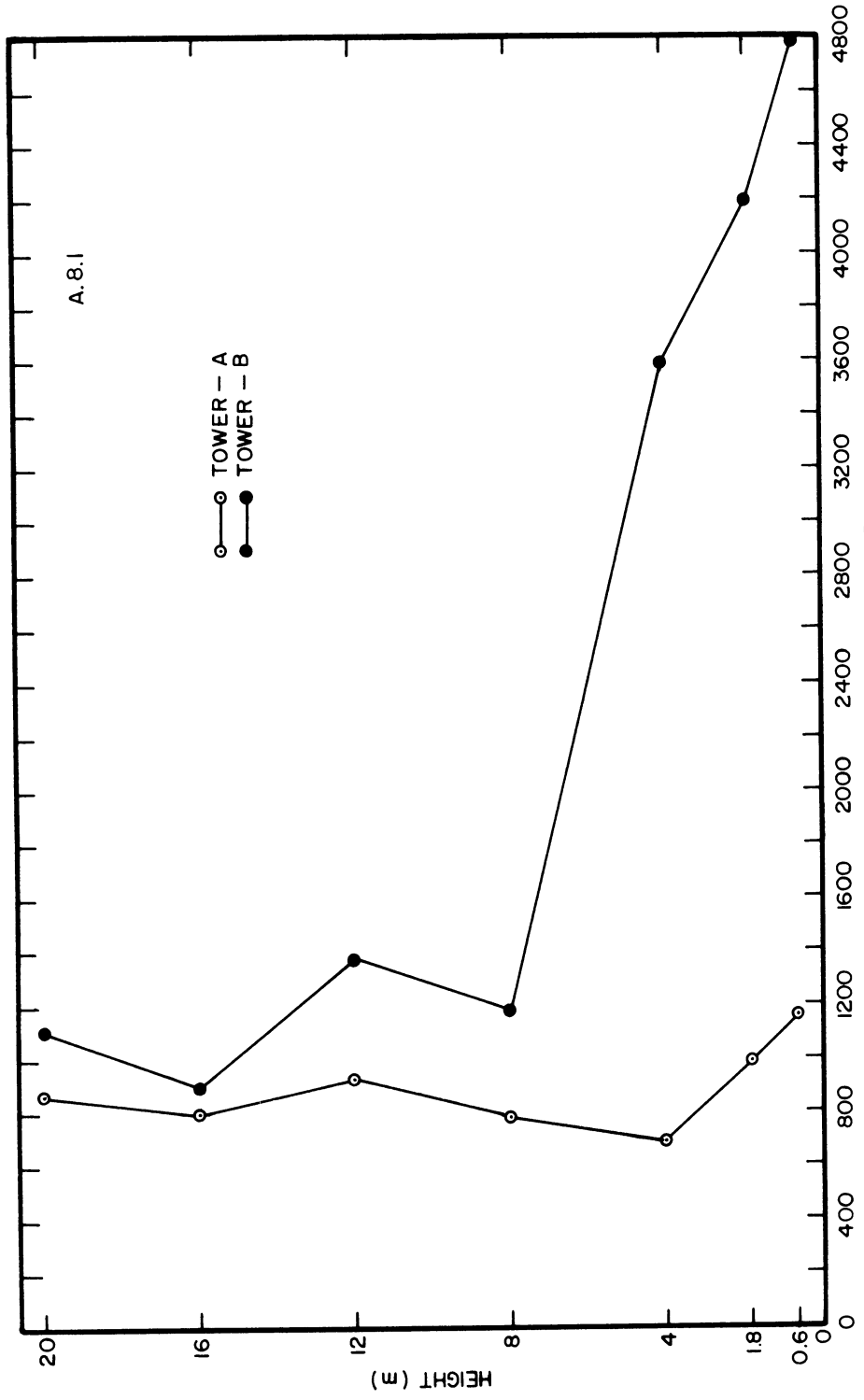

A.8.1 0815-0915

Fig. A.8. Ragweed pollen profiles observed September 3, 1959 during in-season experiment on towers A and B at the times shown. The concentrations are given in grains per cubic meter.

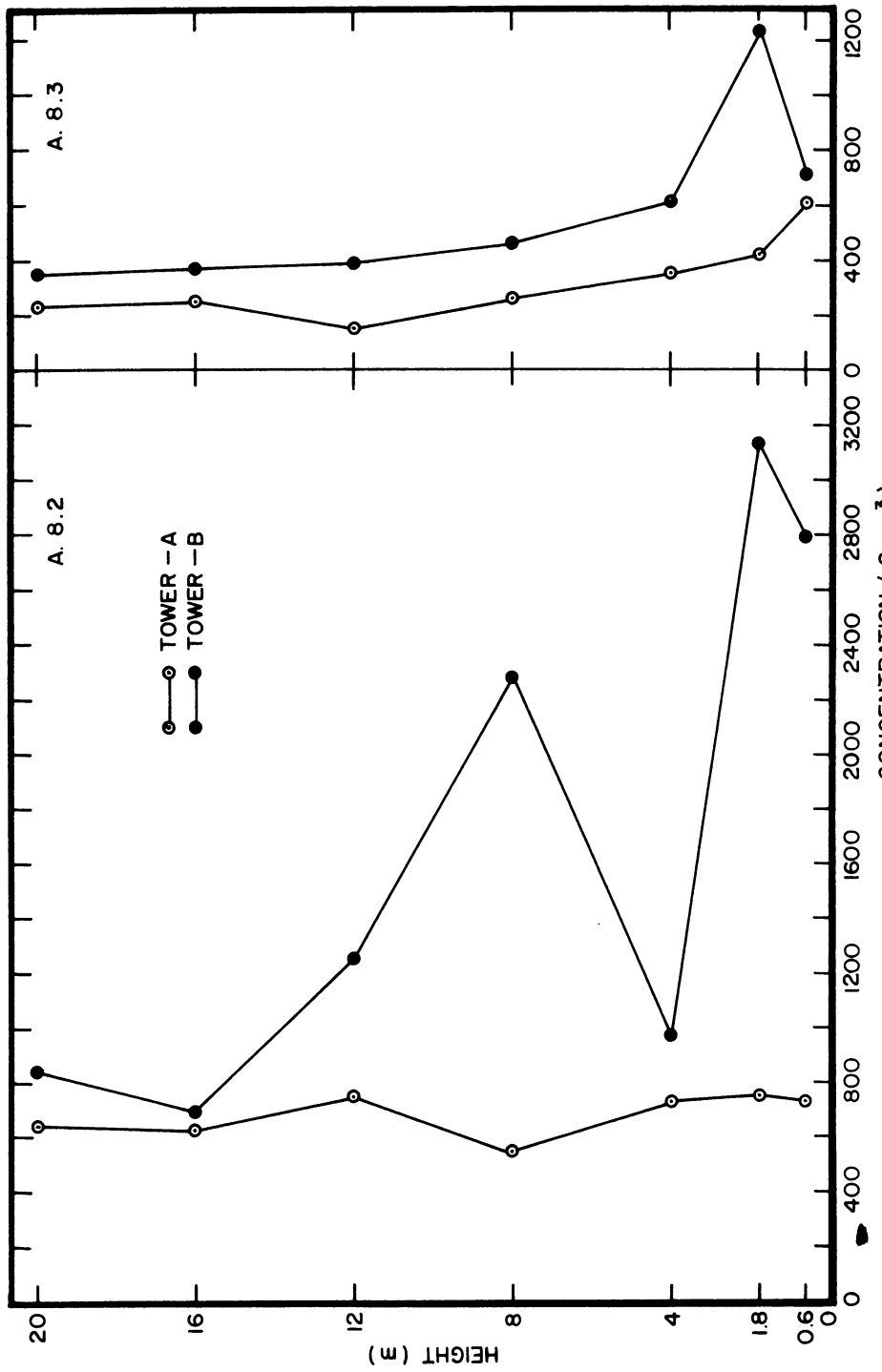

A.8.2 0915-1015 A.8.3 1030-1130

Fig. A.8. Continued

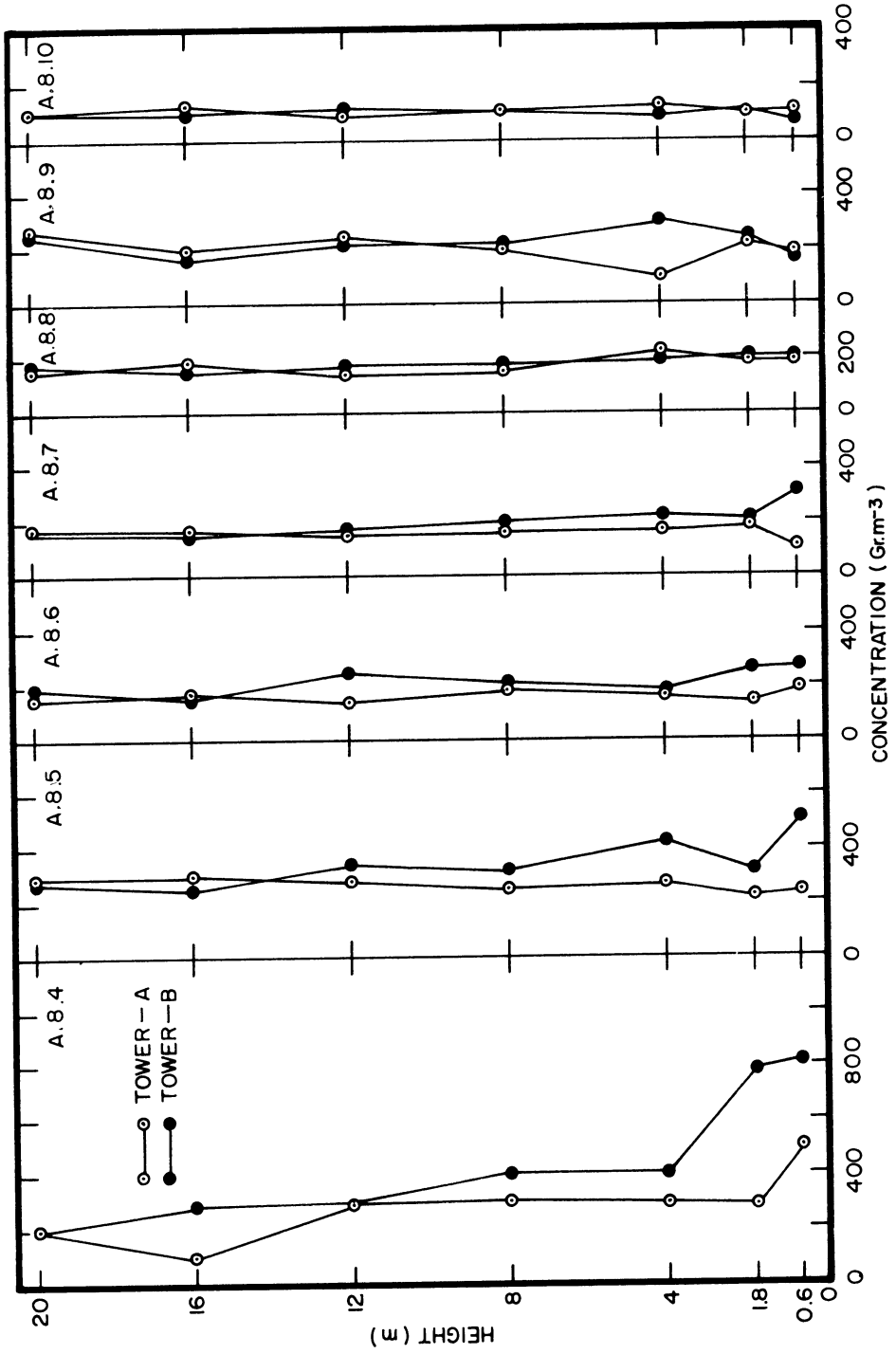

A.8.4 1130-1230
A.8.8 1627-1727

A.8.5 1246-1405
A.8.9 1742-1945

A.8.6 1405-1505
A.8.10 1945-2022

A.8.7 1523-1627

Fig. A.8 Concluded

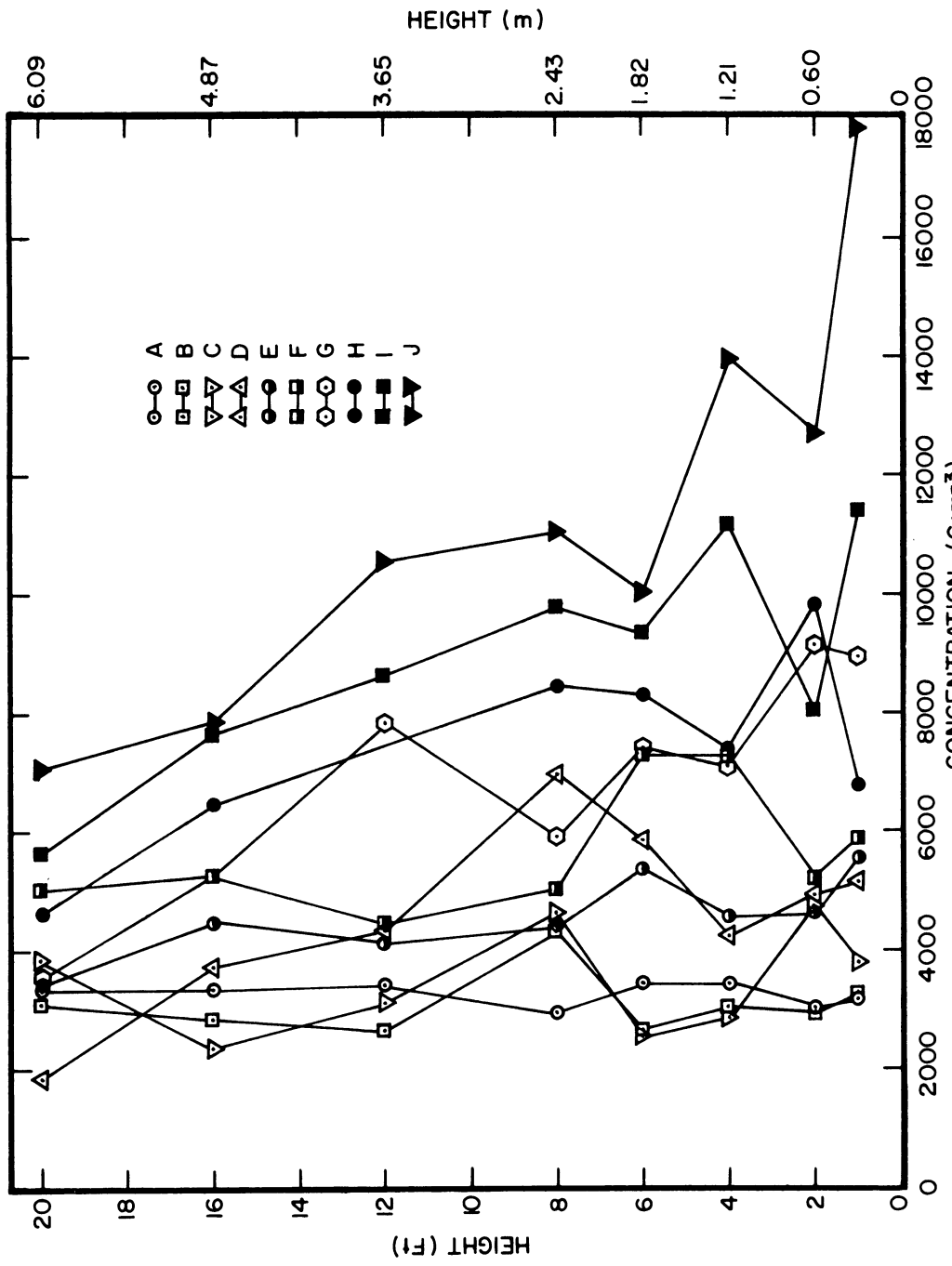

Fig. A.9. Ragweed pollen concentration from flag samplers on masts at 50 ft intervals across a ragweed free area; 0800-1000 September 3, 1959.

a factor to make them coincide with the rotobar concentrations at tower A, are reproduced in Fig. A.10.

A.8 SOURCES OF ERROR

A.8.1 Introduction

In outline the 1959 in-season experiment was a good one and the results, which appear in the following section, provide a considerable insight into both the magnitude of the diffusion process and the mechanism of surface deposition. The experiment was performed, however, by workers with inadequate instrumental capability, with the consequence that the meteorological observations are inadequate for the theoretical computations of such parameters as the eddy diffusivity.

A.8.2 Non-Uniformity of the Source

As mentioned in Sect. A.2 there was a sharp discontinuity in source strength along an E-W line 50 ft north of the sampling stations. From Table A-3 it will be noted that the wind direction was usually south of west so that for the most part the effect of the discontinuity on the profiles could be neglected.

A.8.3 Rotobar Samplers

Frequent tests of the rotobar samplers in a wind tunnel (unpublished) indicated a coefficient of variation of about 11%, an unknown fraction of which was due to actual variations of pollen concentrations in the tunnel. It could be expected, therefore, that the

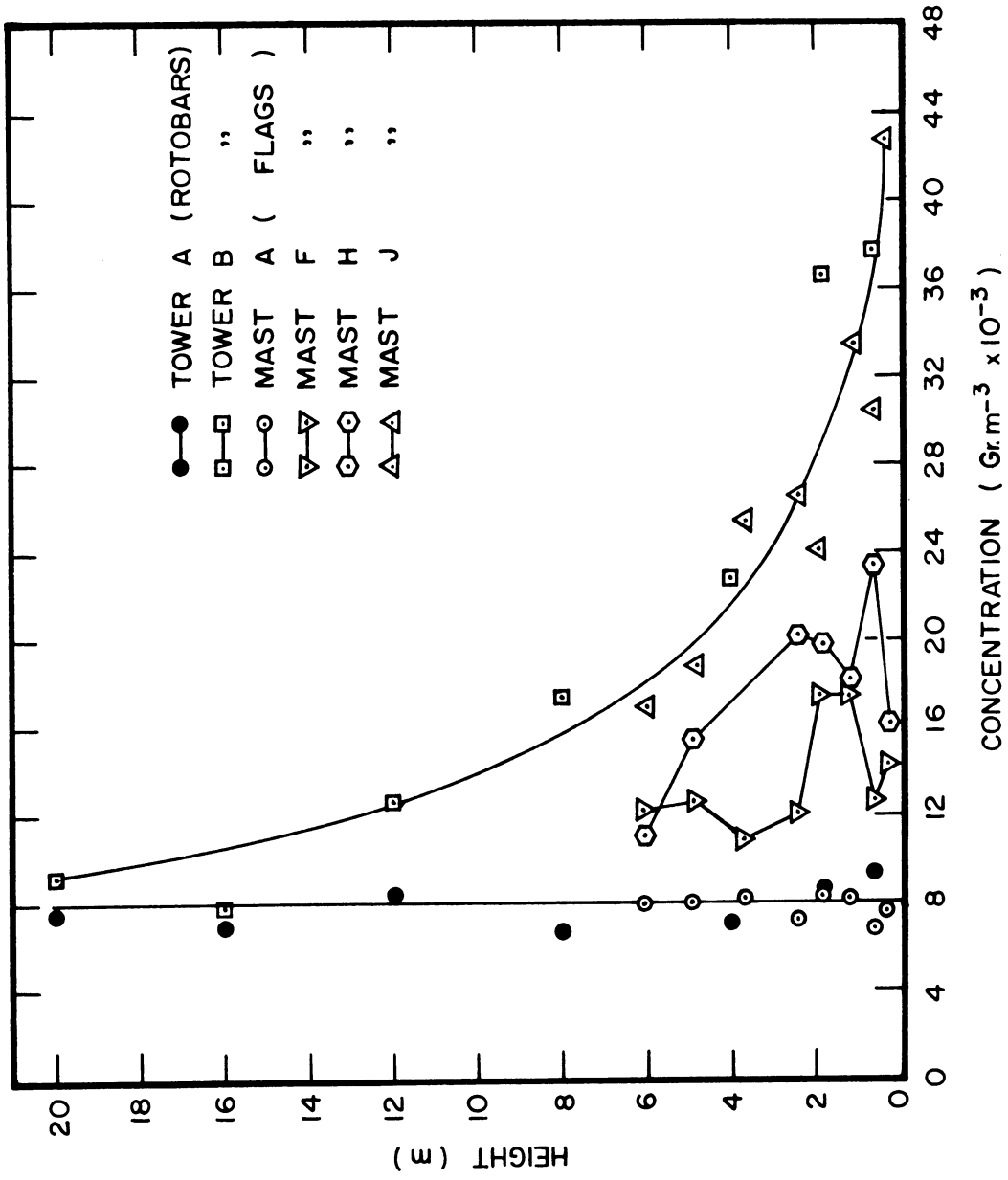

Fig. A.10. A comparison of pollen profiles measured by flag and rotobar samplers across a 450 ft wide ragweed free area on the downwind side of a 1000 ft wide ragweed pollen source; 0800-1000, September 3, 1959.

rotobar measurements have a coefficient of variation caused by factors other than the variability of pollen concentration in the air of no more than 11%.

The theoretical impaction efficiency for ragweed pollen on a cylinder having the same diameter as the rotobar is about 90%. An additional loss of pollen occurs owing to the lack of perfect adhesiveness of the sampling surface. This additional loss is estimated from wind tunnel measurements to be of the order of 20%, reducing the overall efficiency to 70%. These two sources of error have not been accurately evaluated.

A.8.4 Flag Samplers

In the construction of the flag sampler a length of double coated Scotch Tape is sealed together around a 2 in. pin. Tension in the tape eventually causes the portion of the tape next to the pin to separate, thus widening the sampling surface. The occurrence of this possible source of error during a given experiment depends upon the age of the tape and the mode of preparation of the flag as well as the time elapsed since preparation; the fact that flags were exposed for 2 hrs intensified the problem. Increases in diameter of as much as 35% were observed, and errors of the same or occasionally greater magnitude are expected.

The theoretical efficiency of the flag sampler (Harrington, et al., 1959) computed using Brun and Mergler's curves is a function of

the wind speed. All flag counts are reduced to concentration using the equation:

$$\chi = \frac{C}{E_i V} \qquad (A.1)$$

where C is the observed pollen count, E_i is the impingement efficiency and V is the volume sampled. The flag adhesive efficiency is not known, but because of lower air speeds across the sampling surface it is assumed to be much higher than that of the rotobar. This assumption is borne out by comparisons between the two samplers (Harrington et al., 1959).

The winds at flag sampler height were estimated by extrapolating the tower winds to ground level, assuming a logarithmic profile. Because most of the samples were collected during the day, this technique resulted in an under-estimation of the low level winds and an over-estimation of the concentrations.

A.8.5 Beckman and Whitley Anemometers

Compared on a horizontal bar for periods of an hour, the four Beckman and Whitley anemometers recorded average winds which were within 1% of their mean indicated speed. This is more than sufficient accuracy for the purpose of the experiment.

The exposure of the instruments upwind of the tower (see Figs. A.2, A.3, and A.7) minimized the error due to the deflection of the wind around the tower. The magnitude of the tower-caused error is

assumed to be less than 2%.

A.8.6 Beckman and Whitley Vane

The recorded wind direction was averaged over a period of 1/2 hr. The maximum error is estimated at being 3-4°.

A.8.7 Aspirated Thermocouples

During the dismantling of the tower the thermocouple wires were discovered to have become bared as a result of pinching and were in contact with the aluminum of the tower in several places. For this reason the temperature profiles are deemed completely unreliable.

A.9 DISCUSSION OF RESULTS

A.9.1 Introduction

The observations of September 3, beginning at 0800 E.S.T. before pollen emission started and ending at 2022 E.S.T. comprise the most interesting and complete set of data from the 1959 in-season experiment. While much could be done with the remaining data, the following discussion will be concerned almost entirely with the observations from September 3. The day was sunny with steady west-south-west winds having speeds of 2.5 to 6 m sec^{-1}.

A.9.2 Deposition Rate Inferred

It will be observed that late in the day the pollen concentration as shown in Fig. A.8 is, within measurable limits, constant with height.

According to the discussion of Sect. 3.4.2 this means that over the short grass surface of the observation site pollen deposition is approximately at the gravitational rate. This finding is confirmed by observations on all the observation days as shown by the records contained in Tables A-4 and A-5. This is one of the major findings of the 1959 in-season experiment.

A.9.3 Rate of Decay of Concentration After Emission

Late in the day the pollen should approach a constant value with height over a broad height range as shown in App. C. If the height to which the constant pollen profile extends is H, and the concentration is χ grains m^{-3}, then the total pollen in a column one meter square and H meters high will be equal to N where

$$N = \chi \cdot H \qquad (A.2)$$

The rate of change of N with time will be

$$\frac{dN}{dT} = - \chi q \qquad (A.3)$$

and therefore if the pollen is kept uniformly mixed

$$\chi = \chi_{t=0} e^{-qt/H} \qquad (A.4)$$

and the concentration should decay exponentially with time. Considering only that portion of the day when the profile can be expected to be roughly constant with height, i.e., afternoon, and assuming the depth of the constant layer to be about 1500 m (see App. C), the ratio $\chi/\chi_t = 0$ for a 1 hr period should be approximately 0.97 and for 10 hrs 0.75.

The average concentration between the 12 and 16 m levels on tower A shown in Fig. A.11 should be representative of the concentration at higher levels during the afternoon because, as noted above, the pollen is evenly distributed with height at that time. A straight line fitted by eye to the afternoon data indicates that the ratio $\chi(t+10\ \text{hr})/\chi(t)$ equals 0.77, in good agreement with the figure 0.75 computed above. It must be admitted, however, that the data leave considerable latitude for maneuver.

It should be remarked that the so-called "box model" which leads to exponential decay depends upon the presence of strong mixing in the full depth of the layer involved. During the night much of the upper level turbulence dies out and strong mixing may be confined to a shallow region near the ground. When this occurs, according to the model, pollen is replaced in the mixing layer by gravitational settling from aloft at the same rate as it is being deposited on the ground. The concentration near the ground should remain constant during this period until all the pollen has settled out of the air, or until a new turbulent regime or new emission occurs the next morning.

A.9.4 Diffusivity Inferred

The diffusion of pollen a short distance in the lee of an infinitely long area source can be represented by the steady two-dimensional diffusion equation if, during the short period in which the pollen is in transit over the sampling network, the rate of pollen

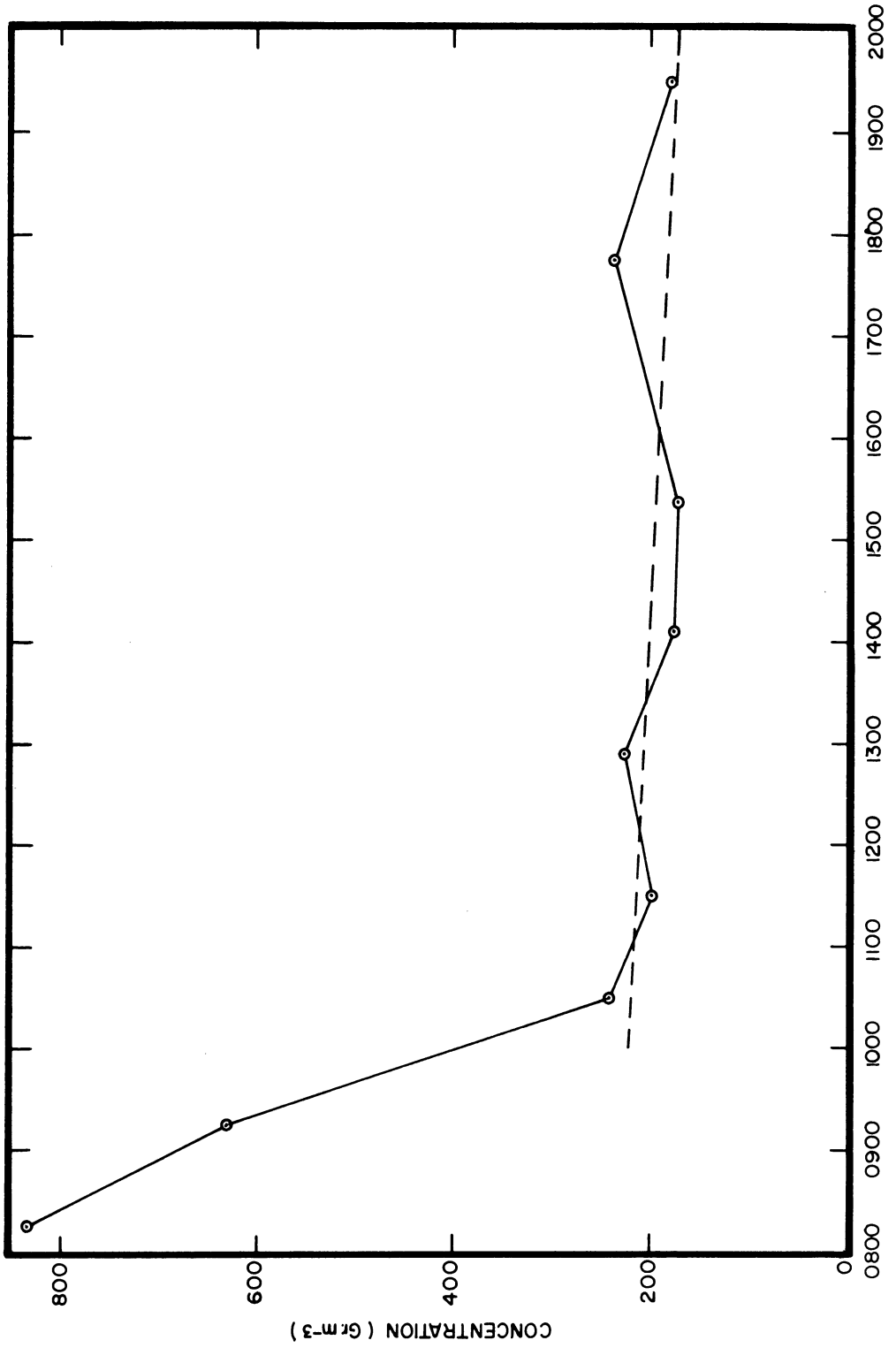

Fig. A.11. The average concentration between 12 and 16 m on tower A at Willow Run Airport September 3, 1959.

emission and the meteorological parameters are steady. During the 1959 pre-season experiment, for example, the width of the ragweed free area was 500 ft or 152 m and therefore, a wind as low as 1 m sec^{-1} traversed the sampling array in only 2-1/2 mins. Because the average emission and atmospheric conditions do not change markedly over such a short period the assumption of steadiness is a reasonable one.

The steady two-dimensional diffusion equation (Eq. (4.41)) is written

$$u(z)\,\frac{\partial \chi}{\partial X} = \frac{\partial}{\partial Z}\left[K_z(z)\,\frac{\partial \chi}{\partial Z} + q\chi\right] \qquad (A.5)$$

A thorough discussion of the equation and its method of solution is given in Sect. 4.5. It can be seen from Eq. (A.5) that, if the vertical distribution of the horizontal wind and diffusivity and the pollen fall speed are known, the concentration can be computed. Likewise, if the pollen distribution at two distances downwind and the wind speed and fall speed are known, the diffusivity can be found.

Figure A.12 shows an example of a solution to Eq. (A.5) for the following conditions:

1. $\ell = 0.1$ m
2. $u(\ell) = 0.8$ m sec^{-1}
3. $K_z(\ell) = 0.5$ m^2 sec^{-1}
4. The initial pollen distribution is set equal to the distribution observed on tower B during the 0815-0915 sampling period, September 3, 1959. To normalize the initial distribution all concentrations were divided by the value $\chi(\ell)$ which was found by extrapolation of the observed profile to the level ℓ.

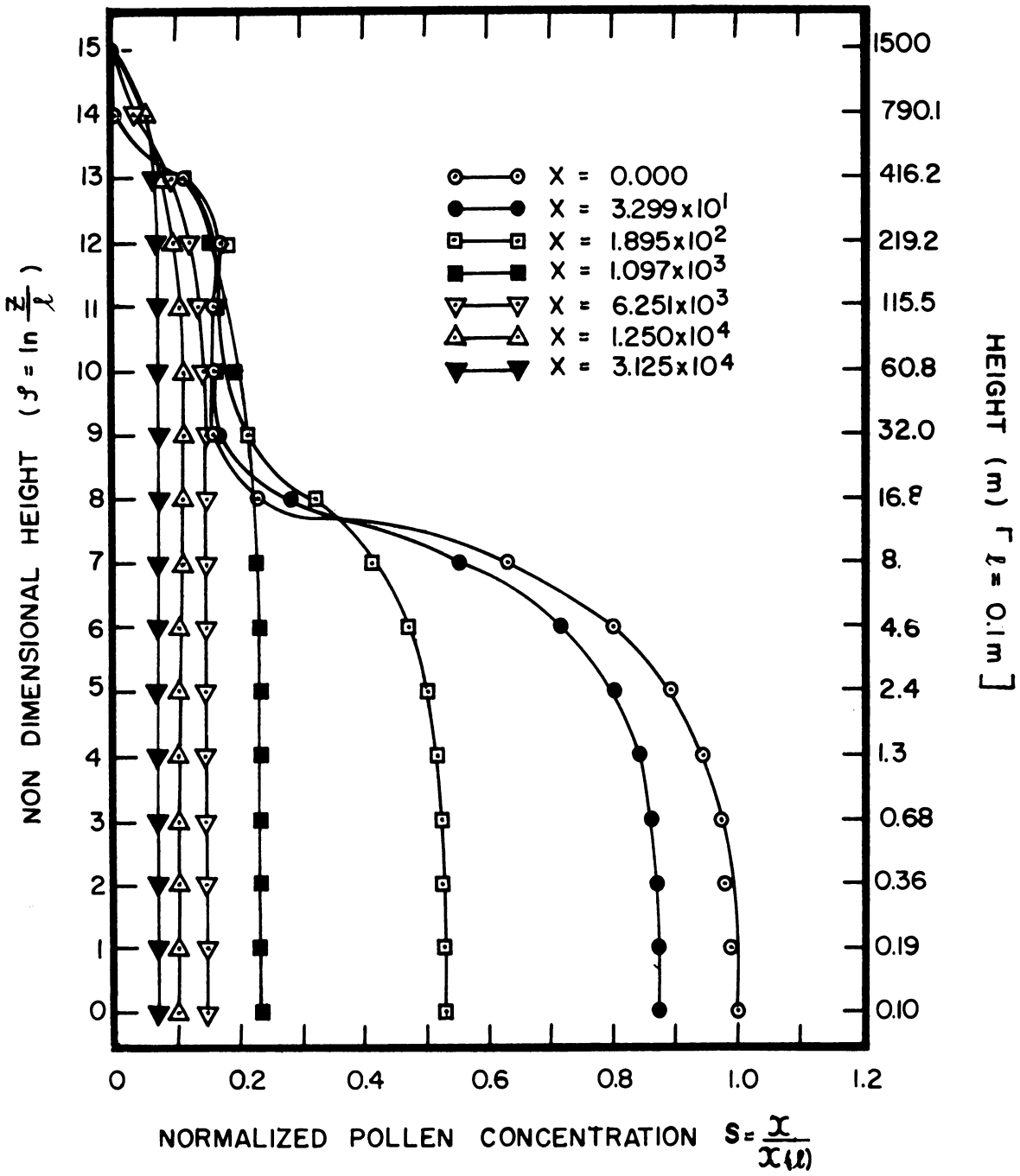

Fig. A.12. A solution of the steady two-dimensional diffusion equation for the parameter values ℓ = 0.1 m, $u(\ell)$ = 0.8 m sec^{-1}, $K_z(\ell)$ = 0.5 m^2 sec^{-1} and the pollen profile on the upwind boundary given by the total grains column of Table A-5, September 3, 1959, run no. 1, tower B. The nondimensional distance is given by $X = K(\ell)x/u(\ell)\ell^2$.

The non-dimensional distance X in Fig. A.12 is given by the equation

$$X = \frac{K(\ell)x}{u(\ell)\ell^2} \qquad (A.6)$$

Let us compare the observed and computed change in pollen profile across the interval separating towers A and B. From the observed pollen concentration data for the 0815-0915 observation period on September 3, 1959, shown in Fig. A.8, the value of the ground level dimensionless concentration S may be seen to decrease from unity at tower B to 0.15 at tower A, a distance of 137 m. Reference to Table A-3 shows that the wind during the observation period was south west and therefore the distance 137 m corresponds to approximately 200 m in the direction of the wind. The computed values of S indicate a value of 0.15 at a distance X = 5750 (see Fig. A.12) which, for the parameters given above, corresponds to a distance of only 92 m. The value $K_z(0.1\ m) = 0.5\ m^2\ sec^{-1}$ is therefore much too large.

The observed pollen profile at tower A is compared in Fig. A.13 with profiles obtained from the solution of Eq. (A.6) using the initial profile from tower B shown in Fig. A.8 and values of $K_z(\ell)$ of 0.01, 0.05, and 0.1 $m^2\ sec^{-1}$. It is seen that the value of $K_z(0.1\ m)$ which best explains the observed profile is 0.1 $m^2\ sec^{-1}$. This value is somewhat large, judging by the data given by Vaughan (1961), but is certainly of the right order of magnitude. An independent measurement of the eddy diffusivity was not obtained.

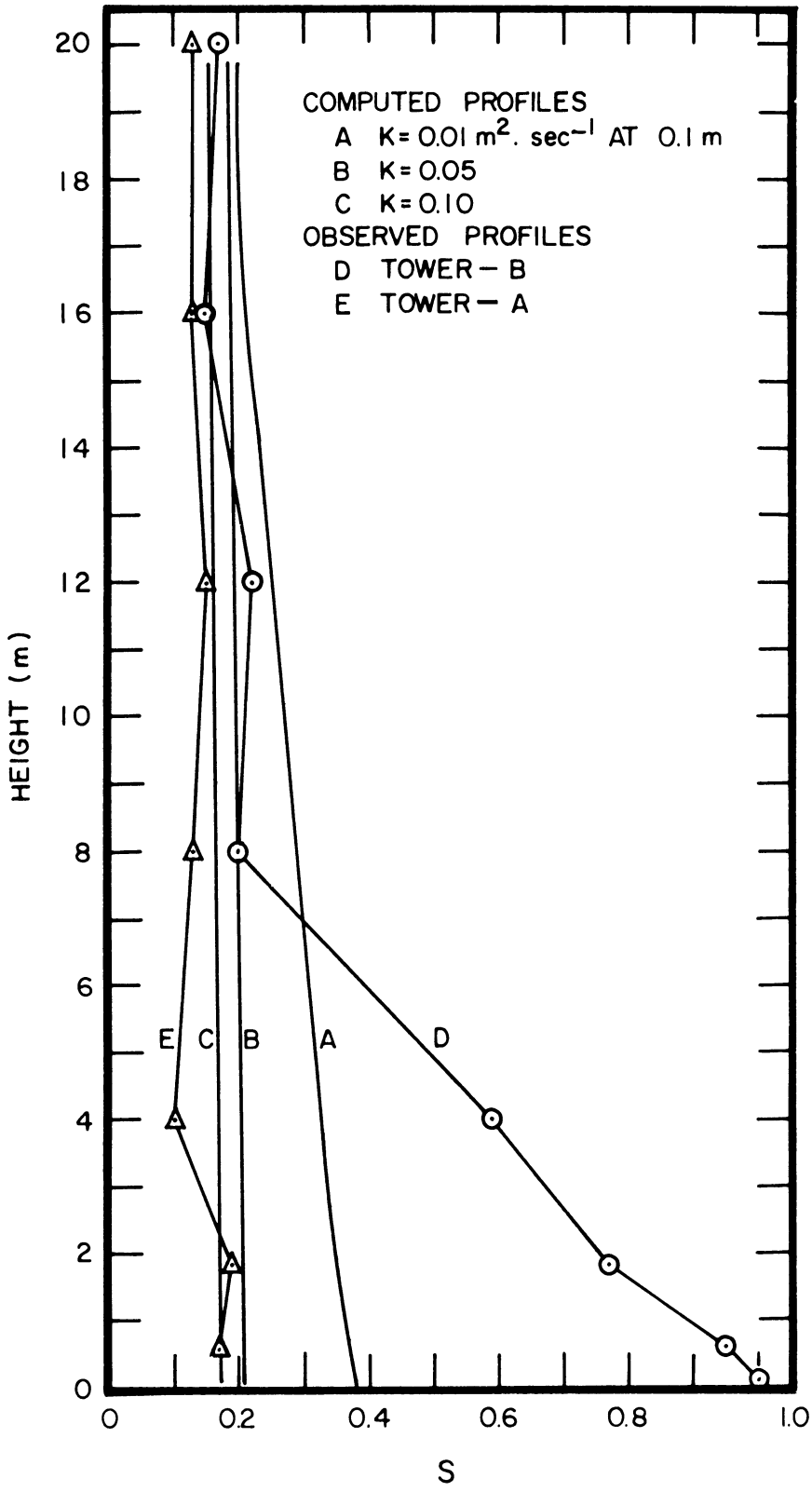

Fig. A.13. Computed and observed pollen profiles. For an initial profile the same as that observed on tower B the profiles computed at a distance of 200 m downwind using values of $K_z(0.1\ m) = 0.01$, 0.05, and 0.1 are compared to the observed profile at tower A.

There is little doubt that the numerical solution of the steady two-dimensional parabolic diffusion equation produces results which agree well with observations of pollen concentration in the atmosphere. A more positive affirmation of the method, however, would require an extensive sampling program combined with an independent means of measuring the eddy diffusivity.

APPENDIX B

THE 1960 OUT-OF-SEASON EXPERIMENT

B.1 OBJECTIVES

The 1960 out-of-season experiment was designed primarily to find out how the rate of pollen deposition is related to wind speed, lapse rate, eddy diffusivity and the shape of the ragweed pollen profile. A secondary aim was to relate the variances of the lateral and vertical pollen distributions to the variances of wind speed and direction.

B.2 THE EXPERIMENTAL SITE

B.2.1 Introduction

In earlier out-of-season pollen experiments the uncontrolled nature of the source had led to complications. In those experiments ragweed plants which had been forced to early maturity in the greenhouse well before the regular ragweed pollen season began were used as a pollen source. The use of such a natural source creates several problems: first, since pollen is emitted in continuously varying quantities it is imperative that any sampling array be erected rapidly in order that the samplers all operate at the same time; second, the strength of the source and its dependence on wind speed and time are unknown; and third, the natural source covers a finite area, which complicates the mathematical modelling of dispersion of pollen from it. On the other hand, a natural source is a necessity if one wishes to know how real plants behave in a natural environment.

The objectives of the 1960 out-of-season experiment were such that they could be achieved most satisfactorily using a controlled

point source. The use of a controlled source allowed time for the operation of a complex array consisting of 2128 samplers, a number which was sufficient for the accurate estimation of plume statistics.

The accurate measurement of the surface deposition of aerosols over a natural terrain including vegetation is an extremely difficult undertaking. On the suggestion of a staff member (Dingle, 1959) the natural vegetation was removed from the sampling site and replaced by fine sand. It was also planned to use sand in containers as ground level samplers, however, another method, to be discussed in a later section, was finally adopted.

B.2.2 The Sampling Array

The sampling array was located at the same site at Willow Run Airport as was used in the 1959 in-season experiment (see App. A).

A 50 m square area was prepared by mowing the grass, killing the grass chemically, covering with a layer of fine sand and levelling.*

The array itself consisted of three grids at distances of 6, 12 and 18 m from a central point source as shown in Figs. B.1-B.3. The open side of the array faced approximately south-west, the direction of the prevailing wind at Willow Run in the early fall. At 25.7° intervals along the three arcs, 6.1 m posts were placed and guyed. Eyelets were affixed to each post at heights 1/4, 1/2, 1, 1-1/2, 2 m, etc. to a height of 3, 4, and 5 m at the 6, 12, and 18 m arcs, respectively. Wires were strung parallel to the ground through the eyelets and tightened so that the sag between masts was no more than 2 cm.

Small glass bearings (see Harrington et al., 1959) were affixed to

*The levelling was not perfect, a maximum difference in elevation between the emission point and array being 1/3 m as shown in Fig. B.1.

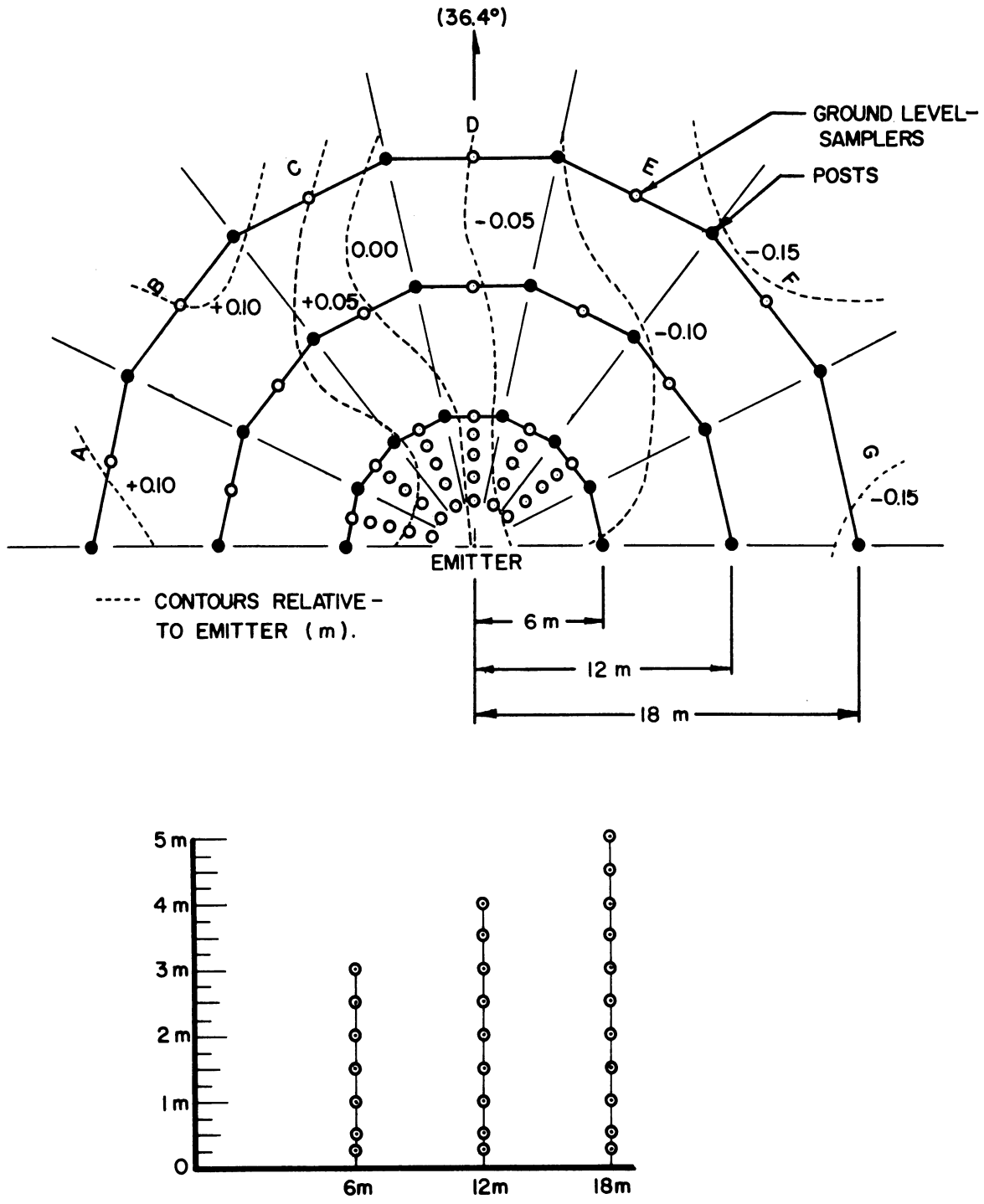

Fig. B.1. Plan view and vertical section through the 1960 out-of-season pollen sampling array. Flag samplers are mounted at 1/2 m intervals on wires located at three radial distances at the heights shown in the vertical section. The land contours relative to the emission point are also known.

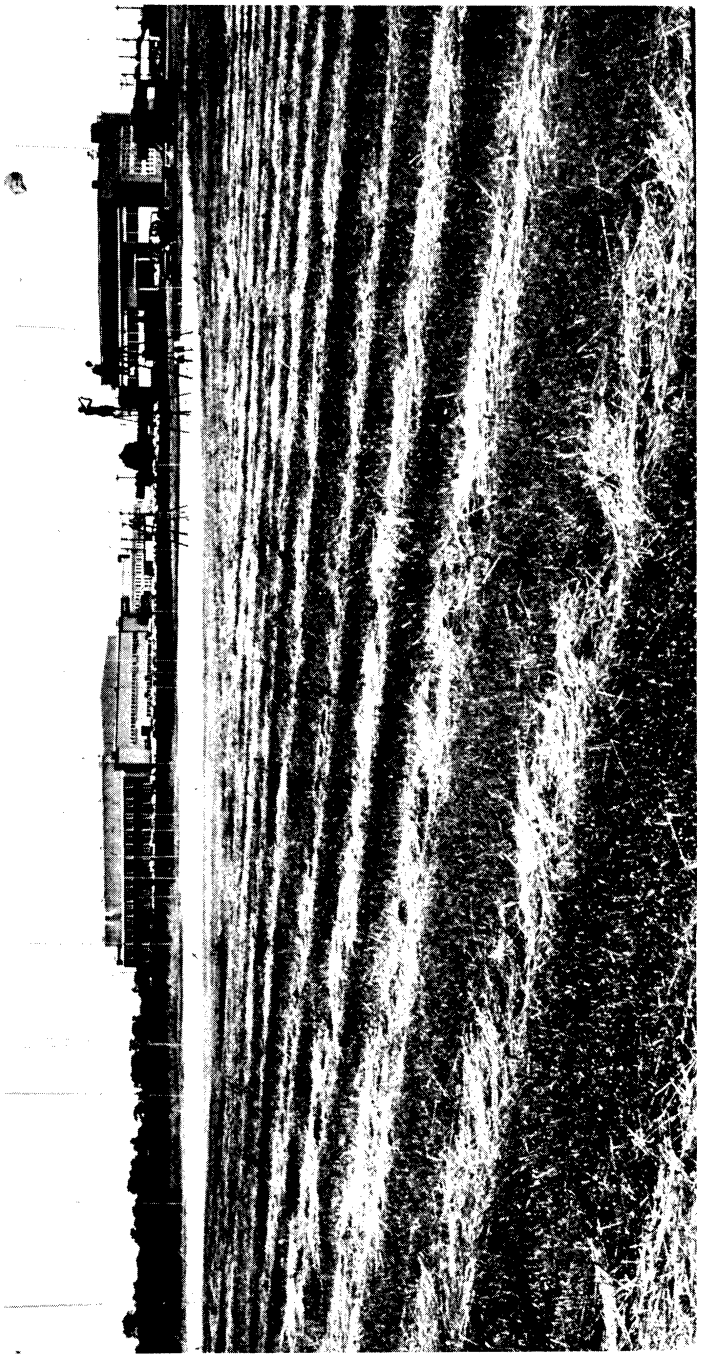

Fig. B.2. The 1960 out-of-season experimental site during construction of the pollen sampling array. The camera was facing north-east.

Fig. B.3. The 1960 out-of-season experimental site during construction showing the sand surface and ground level samplers. During observation periods the sand was smoothed and flush with the upper edge of the samplers. The stub of pipe marks the location of the center of the array.

each wire at 1/2 m intervals, using small rubber ligatures and Duco household cement. The bearings at each position were arranged vertically using a theodolite. Table B-1 gives the number of samplers in each section.

Ground level samplers were located on six radii extending outward from the emitter at 2, 3, 4, 5, 6, 12, and 18 m as shown in Fig. B.1. At each location a 26 m diameter microfilm can filled with light concrete to within 1.3 cm of the lip was sunk in the sand so that its lip was even with the sand surface.

The pollen emitter was located on a 3 m metal post located at the center point of the array (see Figs. B.1 and B.3).

During the experiment it was found that when the wind blew parallel to the wires they began to vibrate with increasing amplitude. To dampen the oscillation, one vertically oriented wire was fixed loosely to each wire at the center of each section of the 12 m array. At 18 m, two such damping wires were located at 1/3 and 2/3 the distance between the posts. With these wires affixed, it was possible to sample with winds up to 10 m sec^{-1} without losing any flag samplers.

TABLE B-1

THE NUMBER OF SAMPLES PER ARC SECTION

Arc Section	6 m	12 m	18 m
A	5	10	15
B	5	11	16
C	5	10	16
D	6	11	16
E	5	11	16
F	5	10	16
G	5	11	15

B.3 EQUIPMENT

B.3.1 The Pollen

The pollen used was from Ambrosis artemisiifolia and collected in 1955 by Greer Drug in Lenoir, North Carolina. It was dried but not defatted. The density, carefully measured using a gas pycnometer (Harrington and Metzger, 1963), was found to be 0.83. The size of the grains was determined by mixing thoroughly a small quantity from the jar, placing a tiny amount of the mixed sample on a dry slide and sizing the grains under a microscope using a Whipple disc. The size distribution of several 100 grain samples is given in Table B-2.

TABLE B-2

RAGWEED POLLEN SIZE--OUT-OF-SEASON EXPERIMENT 1960

Treatment	Origin	Diameter (μ)			S.D.
		Mean	Max	Min	
In Water	(Greer Drug)	20.2	24	17	1.4
Dry	(Greer Drug)	21.7	26	17	1.7
Dry	(Greer Drug)	21.9	25	16	1.6
Dry	(Greer Drug)	22.4	28	18	1.6
Dry	(Greer Drug)	22.3	25	14	1.6
In Oil	(Greer Drug)	21.3	25	17	1.5
In Oil	(Greer Drug)	21.0	25	10	2.1
On Scotch Tape	(Greer Drug)	21.5	25	17	1.6
On Scotch Tape	(Natural Pollen)	20.3	25	17	1.3

The uniformity of the grain size is evident. Their mean diameter is 21.4μ and mean standard deviation is 1.6μ. The ragweed pollen grain is nearly but not exactly spherical, the mean difference between minimum and maximum axes, as viewed in the microscope, being about 1μ.

The gravitational fall speed of ragweed pollen in air can be computed by Stokes' Law since 20μ lies near the middle of the range of particle sizes for which Stokes' Law is valid. Because the ragweed pollen

grain is spherical and of diameter 21.4μ its fall speed is

$$v = \frac{\rho_p g d^2}{18\eta} \qquad \text{(B.1)}$$

where ρ_p the particle density is 0.83 gm cm^{-3}; g the acceleration of gravity is 981 cm sec^{-2}, d the particle diameter is 21.4 x 10^{-4} cm and η the viscosity of air is 1.845 gm cm^{-1} sec^{-1}. Using these values the gravitational settling velocity v of the pollen is about 1.4 cm sec^{-1}. (It should be noted that in all the work in this analysis d was assumed to be 20μ so that v becomes 1.2 cm sec^{-1}).

B.3.2 The Dispenser

The dispenser was a glass tube fitted with a porous plug of fritted glass and corked at each end as shown on the upper left of Fig. B.4. A tube inserted through the lower cork led by means of a long rubber hose to a dry nitrogen cylinder located downwind of the array. A small metal disc baffle was located inside the tube 2 cm below the upper cork. A glass exit tube extended through the upper cork to a height of 5 cm or so above the cork. The upper end of the tube was sealed and a small hole made in the side about 2 cm below the sealed end.

In operation, pollen was placed on the fritted glass plug and the corks adjusted firmly. The nitrogen pressure was increased until the pollen was violently fluidized. Large clusters of pollen were prevented from entering the exit tube by the metal disc baffle mentioned above. A further breakdown of pollen clusters was effected by having the exit

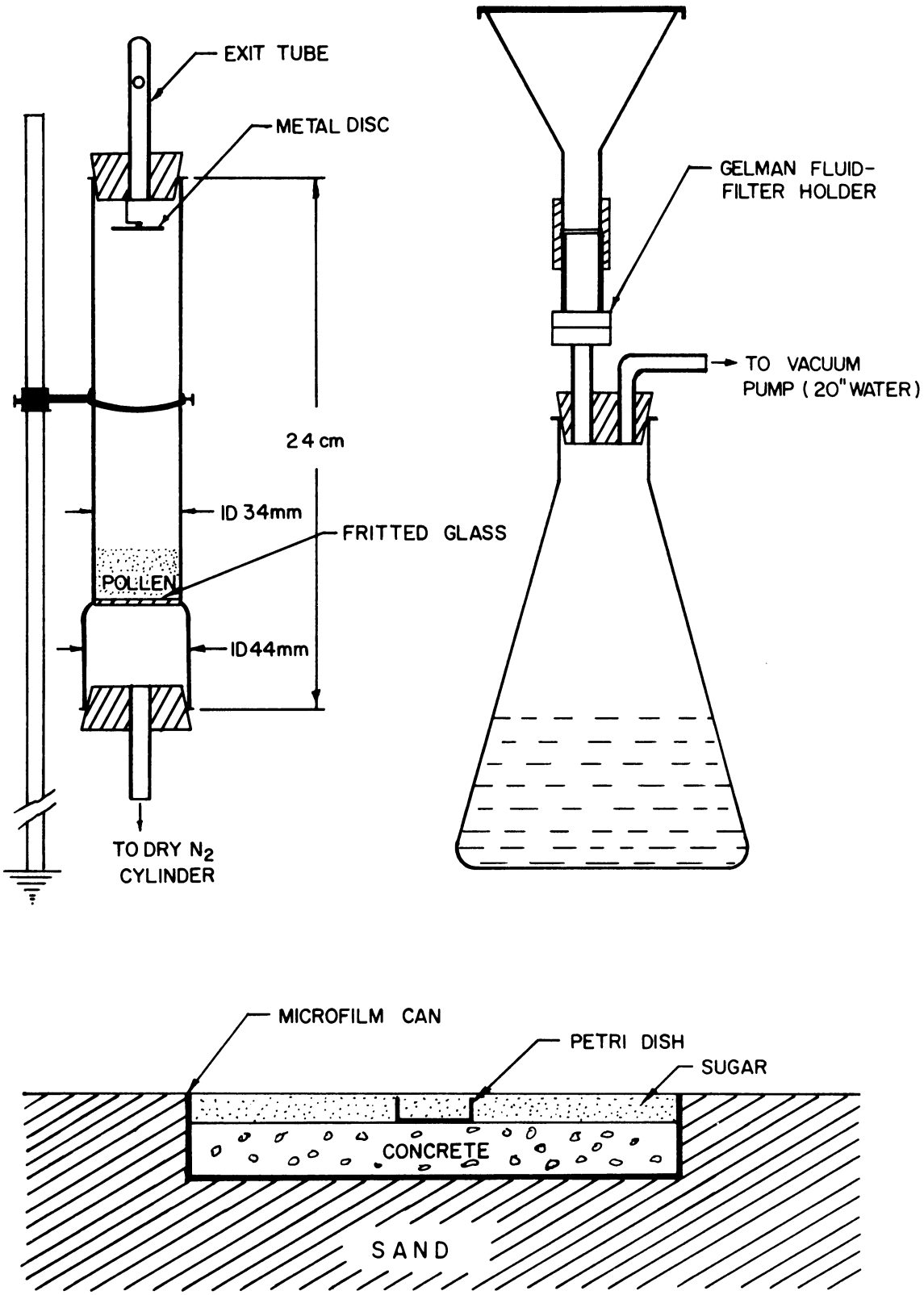

Fig. B.4. Upper left, the pollen emitter; upper right, the pollen filtration mechanism; lower center, the ground level sampler.

hole in the side of the exit tube, a technique which had been found after much experimenting, to provide the best means of producing an output of single grains.

B.3.3 The Array Sampler

Standard flag samplers were used during the experiment (see Harrington et al., 1959). Two seemingly minor, but actually very important changes, were made in the preparation of the flags. First, the flag was tightly rolled, ensuring a snug contact of the Scotch Tape behind the pin and preventing the separation mentioned in App. A. Second, the flags were sprayed with dilute rubber cement (1 part of cement to 10 parts of thinner), ensuring a uniform coat. Because of the changes in preparation, it is believed that the coefficient of variation for a set of flags sampling in a uniform concentration would be no greater than 10%.

B.3.4 The Ground Level Sampler

As noted earlier, the ground within the sampling array was covered with a layer of sand. The grain size of the sand was fairly uniform but had a few pebbles as large as 0.6 cm in diameter intermixed. It was hoped to use as a sampling material some soluble substance of about the same grain size as the sand, so that it would collect pollen at the same rate as the surrounding sand and so that the pollen could easily be removed by filtration techniques. A number of chemicals were tried but most were either insufficiently soluble or contained

impurities which masked the pollen. Refined sugar was most satisfactory, being highly soluble and completely lacking in insoluble impurities.

The ground level sampler consisted of a 10 cm diameter 1.11 cm deep petri dish placed in the center of the micro-film can mentioned above and shown in Fig. B.4. The upper edge of the dish came 0.16 cm below the lip of the can. The sampling surface of refined sugar was poured into the can and levelled with a straight edge. The lip of the petri dish was just visible through a fine layer of the semi-transparent sugar. The excess sugar was levelled into the surrounding sand using a meter rule. The sampler therefore consisted of a petri dish full of sugar set level with the surrounding terrain and protected from accidental pollution by an annulus of sugar 8 cm wide.

Aside from problems of accidental pollution of the ground level sampler few operating difficulties were encountered. At first it was thought that ants might be a problem, but in fact the extremely rich diet sickened or sated most of them so that they were no problem at all. Rain or dew did cause a problem by dissolving the sugar in the area surrounding the sampler. The subsequent crusting made it difficult to prepare the site for the next experiment.

After sampling, the top half of the petri dish was pressed into the sugar over its bottom half, sealing the pollen inside. The dish was removed, labelled and sealed with masking tape. Later, the seal was removed, the sugar dissolved and filtered through a Gelman AM-1

millipore filter using the apparatus illustrated in Fig. B.4. After filtration, the filter was dried, stained and the pollen on it counted under a microscope at 100 x.

B.3.5 Temperature Profile Measurement

The thermocouple arrangement was similar to that used in the 1959 in-season experiment (see App. A). Four shielded aspirated thermocouples were mounted on a 7.3 m tower at heights of 6.1, 3.1, 1.5, and 0.42 m.

Each thermocouple unit consisted of a 16 gauge copper-constantan junction soldered into a brass well 0.95 cm in diameter and 3.17 cm long. The thermocouple was mounted inside a radiation shield consisting of two concentric Formica tubes 3.17 cm and 5.08 cm in diameter respectively, and 15 cm in length. The entire arrangement, mounted facing downward on a tower, was provided with ventilation by means of a high voltage low pressure centrifugal fan.

Temperature differences between the lowest level and higher levels were recorded sequentially, using a Bristol Dynamic Recorder, Model 1PH560-51-B7-T664-T89-T98, serial number 638425 with a range of 0 to 1 mV. Accuracy was estimated at 0.02° Celsius.

B.3.6 Wind Speed Measurement

Four Thornthwaite anemometers were mounted on a 5 cm^2 aluminum mast at heights of 0.75, 1.5, 3.0, and 6.0 m. Recording was accomplished by photographing the digital counters of the Thornthwaite

indicator system at 5 sec intervals (see Fig. B.5). Timing was accomplished by positioning a clock with a digital indicator within the field of view of the camera. Tests on a horizontal bar indicated that the anemometers read within 3% over a 40 min test period.

B.3.7 Wind Direction Measurement

The wind direction was measured at an elevation of 6 m at the top of the square aluminum mast which supported the anemometers. The vane was a 9 in. square flat plate aluminum unit centered 22 in. from the axis of rotation. The maximum overshoot was 13% and the distance constant was 14 ft (Gill, 1965).

The direction transducer was a Fairchild 746 ANB117 20 kohm potentiometer, linear within 1/2%. The recorder was a Texas Instrument Rectilinear Recorder with ± 0.5 ma full scale deflection. The power supply to the potentiometer was adjusted to provide ± 0.5 ma for a 90° deflection of the vane. The overall accuracy of the system with a steady wind was assumed to be ± 2% over the full scale.

B.4 PROCEDURE

B.4.1 Preliminary Run

One run, on November 13, 1960, was undertaken to enable an estimate of the efficiency of the sampling array to be made. A weighed quantity of pollen was emitted at a height of 1.5 m and sampled on only the 6 m array. The number of grains emitted were computed from the known

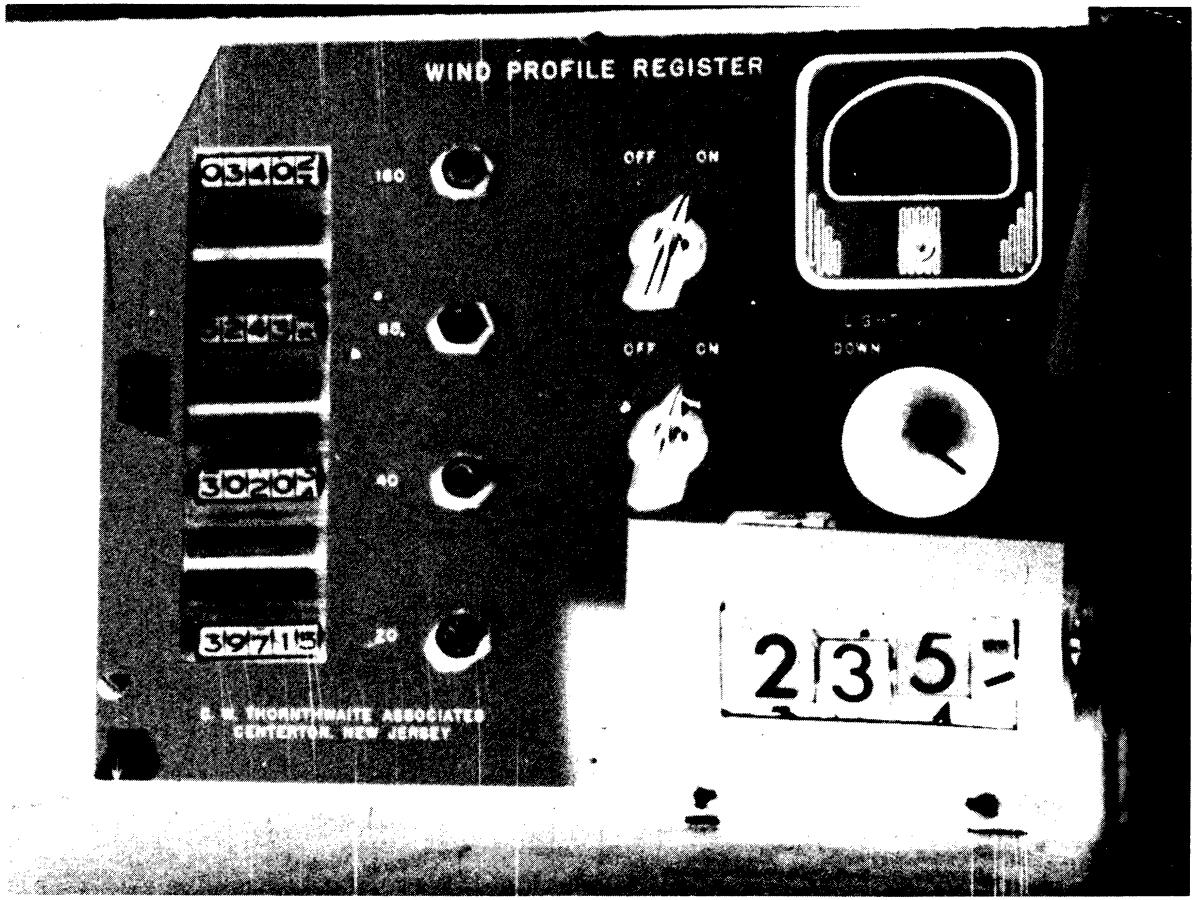

Fig. B.5. A typical photographic record of the Thornthwaite wind system counters and the time. Air pollution by aeroallergens. Out-of-season experiment 1960.

weight, density and size of the pollen and compared with the integrated catch over the array to provide an estimate of the array efficiency.

The procedure was as follows: the emitter was cleaned and weighed. Pollen was added and the weighing repeated. The emitter was attached to the post in the center of the array at a height of 1.5 m and connected to the nitrogen cylinder. The 6 m array was loaded with flag samplers taken from numbered locations in specially prepared double bottom cardboard boxes. The Thornthwaite anemometers were installed, and the camera started. The wind direction recorders and the Bristol recorder were started. When all recorders were operating well, the pressure gage on the nitrogen cylinder was opened until the pollen boiled violently (the exact pressure setting was not recorded).

After sampling, the emitter was sealed and returned to the laboratory for weighing, the flag samples were replaced in their boxes and returned to the laboratory for mounting and counting and the chart rolls and film from the meteorological instrumentation were collected for analysis.

B.4.2 Complete Runs

Three complete runs were carried out on November 14, 17 and 28, 1960. The procedure was similar to that outlined above. The emitter during these tests was mounted at 1/2 m. The ground was prepared by carefully raking, smoothing and finally resmoothing the area around each ground level sampler with the edge of a meter stick. The flags

were mounted only in the sectors which were expected to receive pollen. The petri dish and sugar were then placed in the ground level samplers and leveled.

After a 1-hr sampling period, the ground level samplers were sealed, the flags removed, and the procedure outlined in B.4.1 above followed.

The ground level samplers were given special treatment to prevent loss of pollen or contamination since in preliminary tests it was found difficult to dissolve and filter pollen from a sugar solution without loss or gain of pollen from polluted surfaces. The following procedure was found to be satisfactory:

1. The exterior of the sealed petri dish was carefully washed, the seal broken and the larger half, or top, carefully removed.

2. The sugar in the bottom section was thoroughly saturated with alcohol and the top section moistened with alcohol to prevent the pollen from becoming airborne.

3. The sample and top were then inverted over a large funnel, leading into a flask and carefully washed, using distilled water. The walls of the funnel were wetted with alcohol and washed.

4. The suspension in the flask was then filtered through a Gelman AM-1 1-in membrane filter (Fig. B.4) and once again the funnel was carefully washed first with alcohol, then distilled water. Note: Care must be exercised since the filter dissolves in pure alcohol.

5. The filter was removed and dried in a sealed desiccator, then mounted, clarified with acetic acid, covered and counted.

B.5 RESULTS

B.5.1 Preliminary Run Results

This run was carried out on November 13, 1960 from 1322 to 1543 hr, a sampling duration of 2 hr and 21 min.

The number of pollen grains emitted is computed below:

Clean weight of emitter with attachments	223.243 g
Weight after loading with pollen	239.490 g
Weight of pollen	16.247 g
Weight of emitter, plus pollen after the run	237.190 g
Weight of pollen emitted	2.300 g

The weight of one pollen grain W is given by

$$W = \frac{\pi d^3}{6} \rho_p \qquad (B.2)$$

Assuming $d = 21.4 \times 10^{-4}$ cm, $\rho_p = 0.83$ gm cm^{-3} then $W = 4.259 \times 10^{-9}$ gm/grain and the total number of grains N is given by

$$N = \frac{\text{wt. pollen}}{W} = 0.5400 \times 10^9 \qquad (B.3)$$

The number of grains passing through the 6 m array is found in the following way:

1. The flag pollen count is integrated horizontally along each height, using Simpson's Rule.

2. From the measured wind speed the flag efficiency is computed for each level (see Harrington, et al., 1959).

3. The integrated flag counts from 1. above are divided by the product of the flag area and the efficiency giving the number of grains per meter in the vertical direction as shown in Table B-3* and Fig. B.6.

*Tables not included in this Appendix will be found in Volume III.

4. The resulting numbers are integrated vertically, using Simpson's Rule to find the total number of grains passing through the array as shown in the last row of Table B-3.

TABLE B-3

COMPUTATION OF TOTAL POLLEN PASSING THROUGH THE 6 m ARRAY

November 13, 1960

Height (m)	Integrated Pollen Count	Wind Speed (mph)	Impaction Efficiency	Number of Grains Per Meter in Vertical
0.25	$170.3\overline{3}$	6.3	0.83	621.7×10^4
0.50	$717.1\overline{6}$	7.2	0.85	2553.1×10^4
1.00	$4389.3\overline{3}$	8.3	0.87	15274.9×10^4
1.50	$4564.1\overline{6}$	8.8	0.875	15792.0×10^4
2.00	$1929.6\overline{6}$	9.2	0.88	6638.0×10^4
2.50	$522.6\overline{6}$	9.5	0.885	1787.5×10^4
3.00	$118.6\overline{6}$	9.8	0.89	403.4×10^4

Total pollen passing through the array - 0.2164×10^9 grains.

The ratio of the total pollen passing through the array to the total pollen emitted gives a measure of the array efficiency E. The array efficiency for the preliminary run is

$$E = \frac{0.2164 \times 10^9}{0.5400 \times 10^9} \approx 0.40$$

which may be considered as a measure of the adhesive efficiency of the samplers. The value $E_a = 0.4$ is surprisingly low in view of the fact that values near unity had been estimated previously. Part of the low array efficiency may be the result of having the concentration peak fall

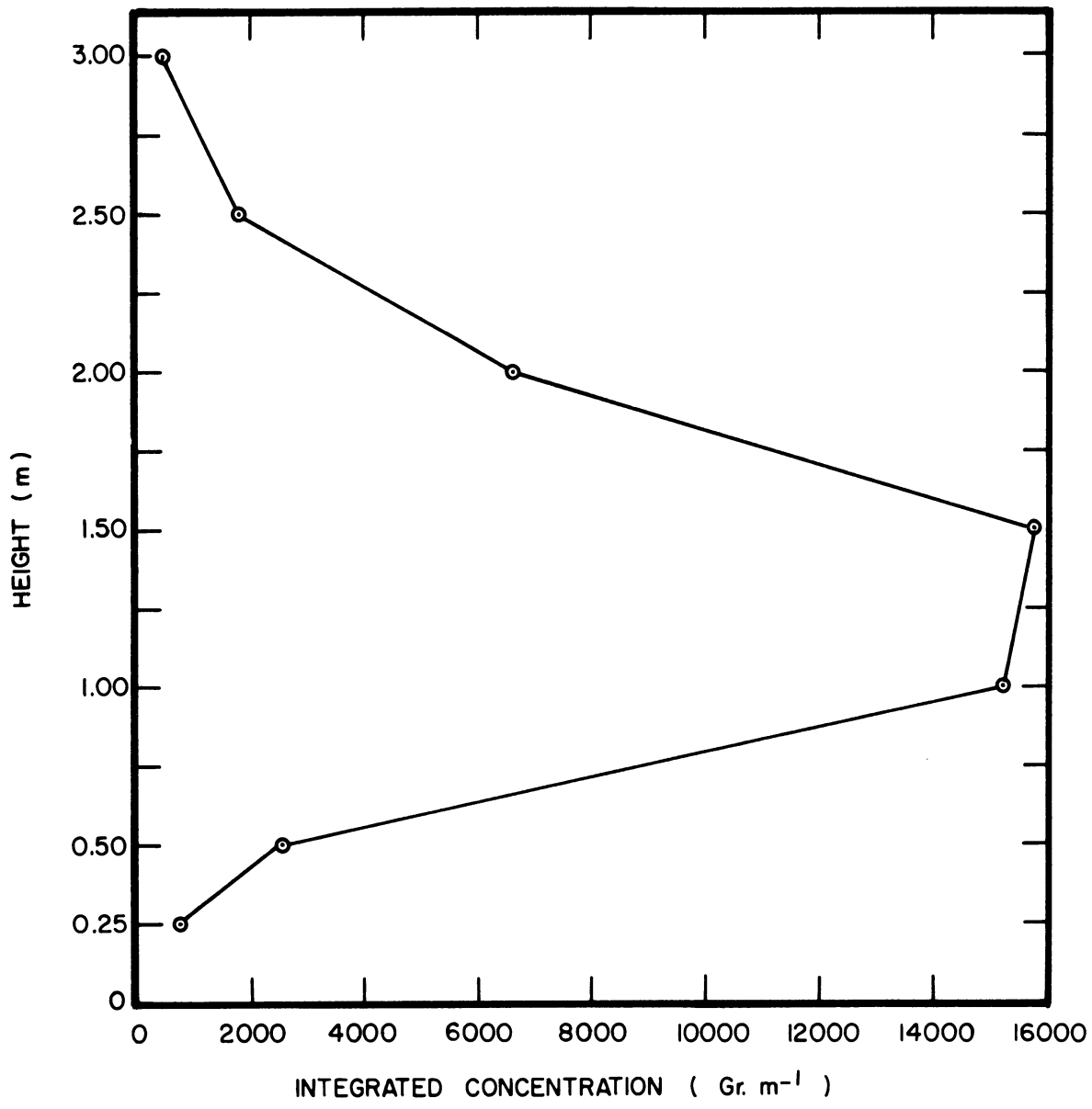

Fig. B.6. The crosswind integrated ragweed pollen capture. Preliminary run, out-of-season experiment November 13, 1960.

between two levels but it is evident that losses over the top of the array and deposition at the ground are negligible (see Fig. B.6).

The vertical distribution of the crosswind integrated pollen capture illustrated in Fig. B.6 demonstrates a positive skewness with height as shown in Fig. B.7. The skewness appears to be more than can be accounted for by the downwind displacement of the pollen peak and is possibly a consequence of the increase in diffusivity with height.

The horizontal distribution of vertically integrated pollen capture is shown in Fig. B.8 and Fig. B.9. In view of the discussion of Sect. 6.4.2 it is surprising to find a distribution so nearly Gaussian, especially when it is considered that the duration of the run was 2 hr and 21 min. As will be seen later, this distribution is not typical.

B.5.2 Full Scale Run Results

B.5.2.1 General

Full scale runs were conducted on November 14, 17 and 28. The pollen counts for those dates and for the preliminary run of November 13 are tabulated in Table B-4. The pollen counts from the ground level samplers are tabulated in Table B-5.

The temperature records for the three full runs are entered in Table B-6. The wind direction, abstracted every 5 sec to the nearest degree, and the 5 sec averages are given for the runs of November 14 and 28 in Table B-7 whereas only the 5 sec average is given for November 17. The vane was not operative during the preliminary run of

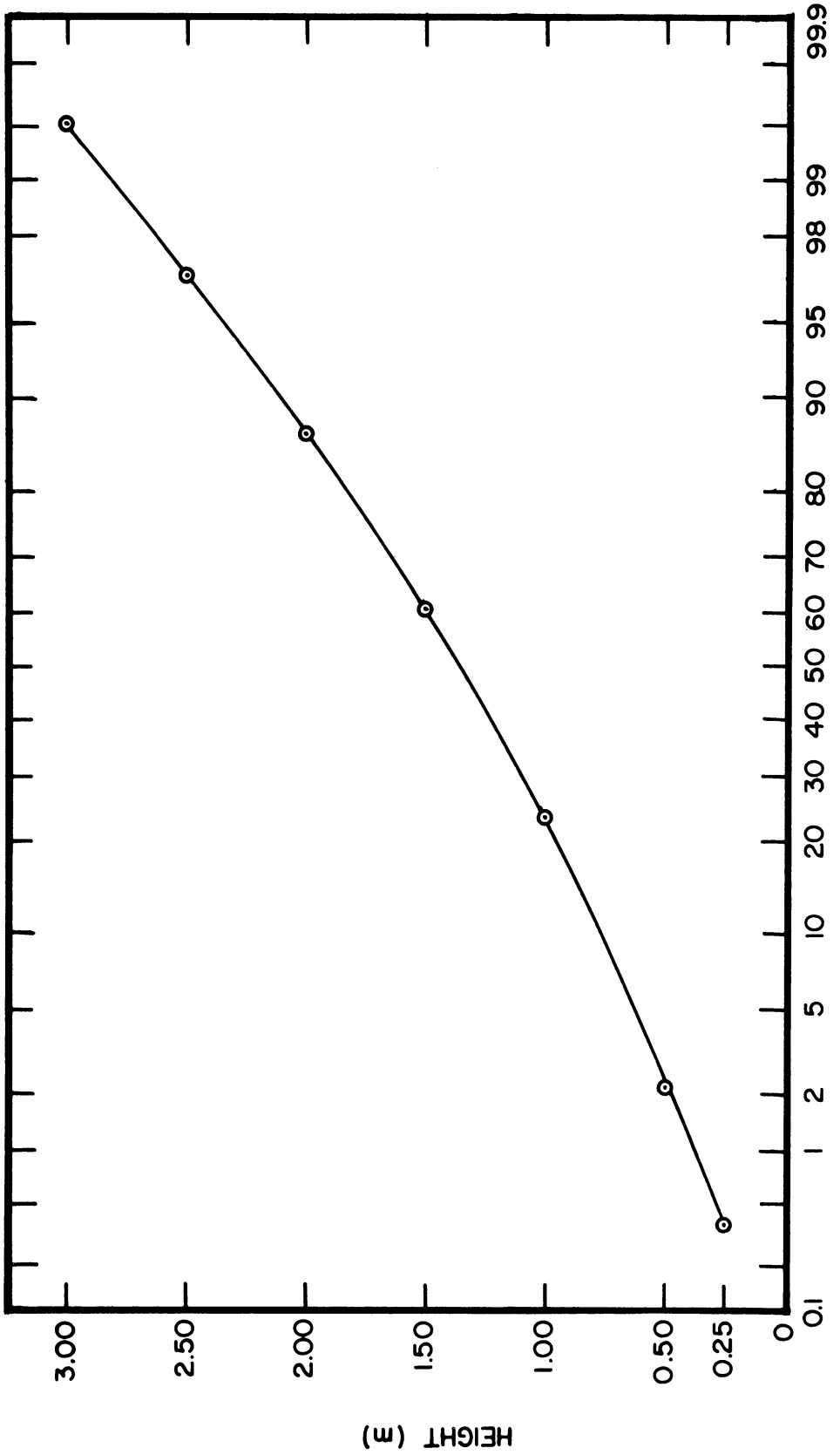

Fig. B.7. The cumulative vertical distribution of horizontally integrated pollen capture shown on probability paper. An upward curvature signifies positive skewness with increasing height. Out-of-season experiment November 13, 1960.

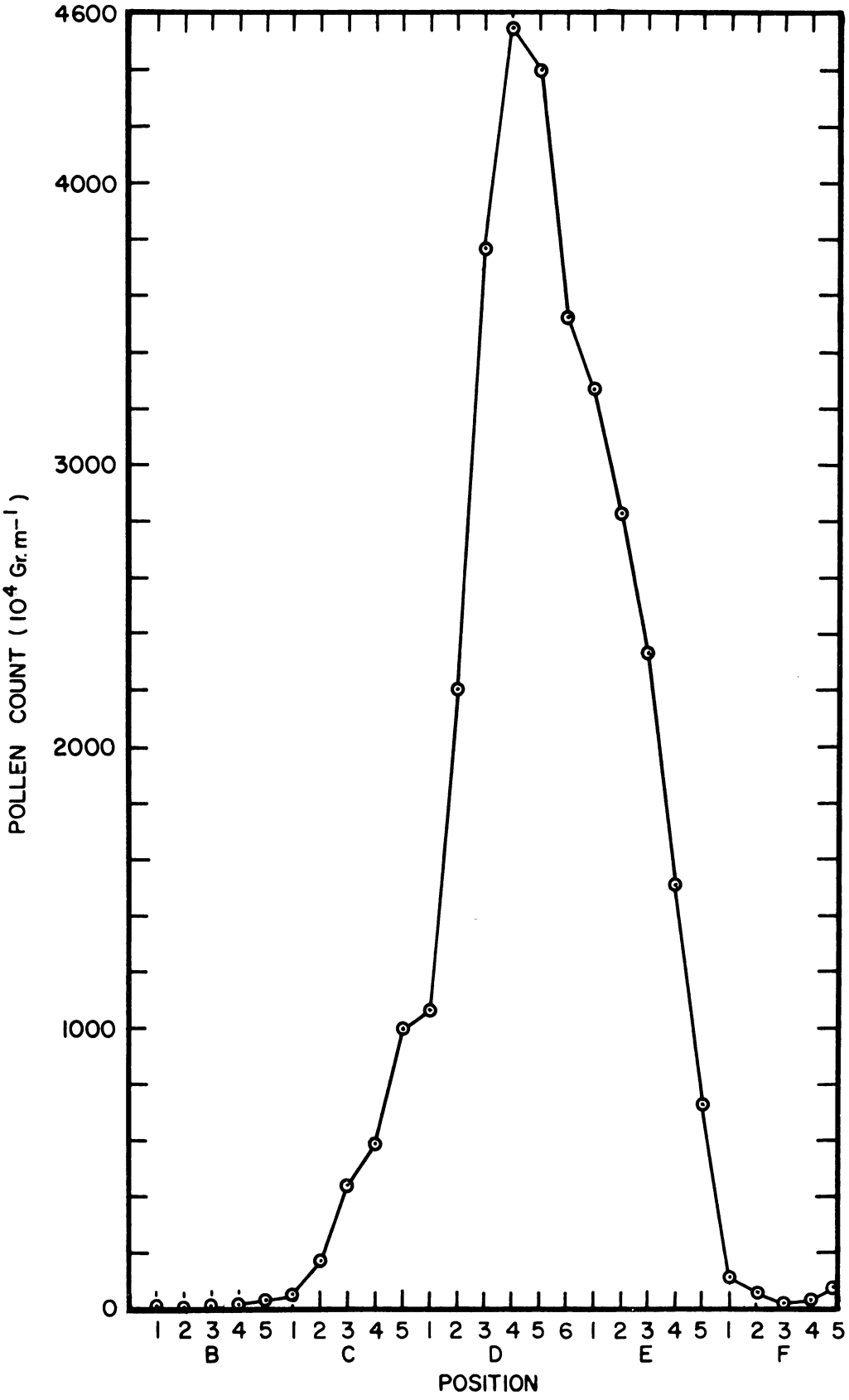

Fig. B.8. The horizontal distribution of vertically integrated pollen capture. Out-of-season experiment November 13, 1960.

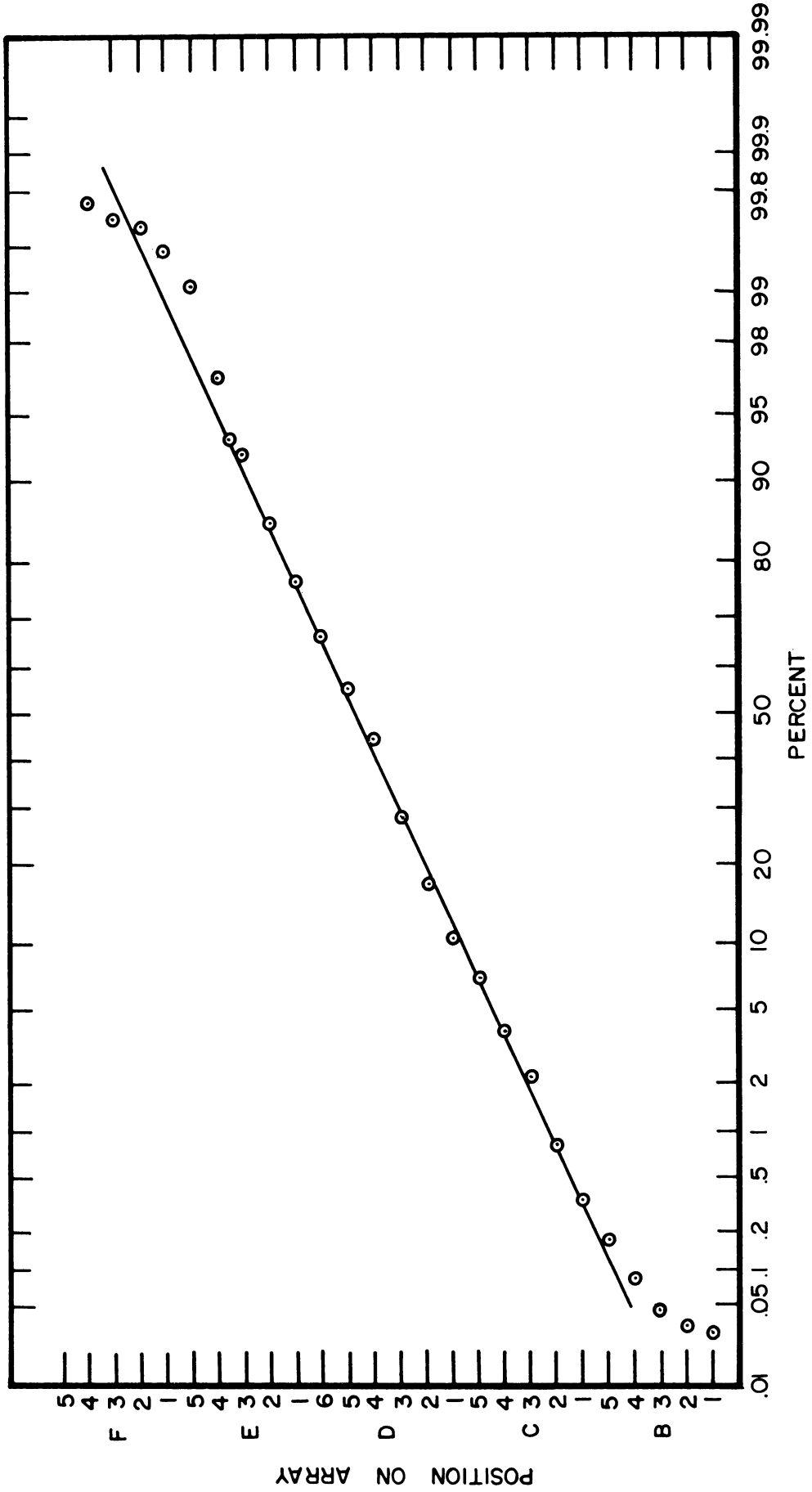

Fig. B.9. The cumulative horizontal distribution of vertically integrated pollen capture shown on probability paper. Preliminary run, out-of-season experiment November 13, 1960.

November 13. The wind speed records were abstracted every 5 sec, but only the average speeds over the sampling periods are reproduced in Table B-8.

B.5.2.2 Operational Data

Run of November 14

Period of emission	1451 - 1551
Weather	Broken to overcast cloud
Pollen emitted	0.486 g
Number of grains emitted	0.1141×10^9

Run of November 17

Period of emission	1602 - 1704
Weather	Clear to scattered cloud
Pollen emitted	2.902 g
Number of grains emitted	0.6814×10^9

Run of November 28

Period of emission	1452 - 1552
Weather	Overcast
Pollen emitted	3.150 g
Number of grains emitted	0.7396×10^9

B.5.2.3 Pollen Distribution

The statistical description of the crosswind distribution of a diffusing substance is sometimes employed to determine the lateral component of the eddy diffusivity, an important meteorological parameter. When used for this purpose, however, the distributions, whether measured on a rectilinear grid or on the arcs of circles, lead to serious problems in analysis whenever the total angular width of the distribution is large.

Suppose first that sampling stations are arranged in planes normal to the mean wind direction, and that the dispersion of particles from a point source is measured. Consider first the travel or dispersion time, which is usually taken to be equal to the normal distance from the source to the plane divided by the mean wind speed. It is obvious that the actual travel time of a particle from the source to a point on the plane is a function of the angular displacement of the point from the mean wind direction. In the case of a 90° deflection the travel time will be infinite. It must be concluded, therefore, that the value of the diffusivity which applies to the dispersion measured on a plane is not a constant over the plane and, indeed, at great distances from the center of the plume it approaches infinity. To apply a constant value of K_y or for that matter of K_z to a given level on a plane is only valid when the dispersion angle is small.

Second, consider a sampling network composed of arcs of circles. In this case, assuming that the wind speed is equally strong in all observed directions, the travel time and, therefore the lateral and vertical components of diffusivity will, at a given level, be constant with angular displacement around the grid. Unfortunately, the statistics which apply to circular distributions such as the circular normal distribution described by Gumble et al. (1953) have not been adapted for use in the diffusion equations. It is necessary, therefore, to assume that angles are small, and that measurements on a circular grid approximate those on a plane. When the angular spread of a diffusing

plume is large, such as often occurs in summer with light winds, no presently available theory adequately describes the diffusion process.

During the full scale runs of the 1960 out-of-season experiment the distribution was neither so compact that the linear approximation could be made without error nor so disperse that the error was intolerable. Throughout most of the following analysis the arcs are regarded as straight lines normal to the mean wind direction. During a part of the analysis a projection between the arcs onto planes normal to the mean wind was carried out; the corrections, however, were small relative to the sampling variance. No estimate of the magnitude of the error is made.

Figures B.10 are the vertically integrated crosswind distributions of pollen on the 6, 12 and 18 m arrays observed during the observation periods of November 14, 17, and 28 respectively. The abscissas of the nine graphs conserve the angle subtended at the source by successive samplers.

It is immediately apparent from the figures that the standard deviation of the angular displacement is nearly constant with distance over the short distances involved, as suggested by Taylor (1921), and Hay and Pasquill (1959). It is also apparent that the crosswind distribution is not necessarily Gaussian. Tables B-9 and B-10 compare the standard deviation of the wind direction trace to the standard deviation of the angular distribution of the particles.

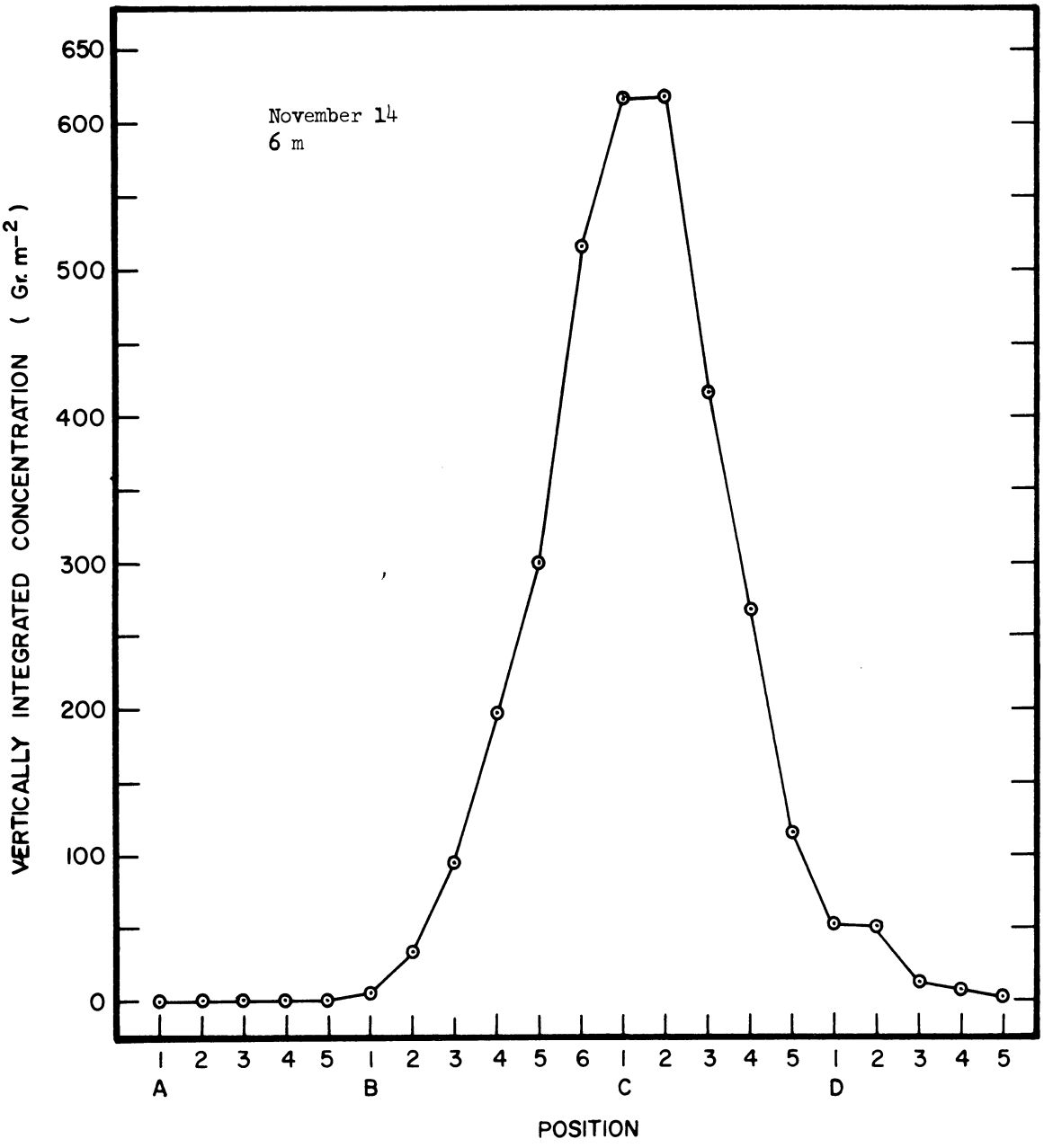

Fig. B.10. The horizontal distribution of vertically integrated pollen concentration. Out-of-season experiment 1960.

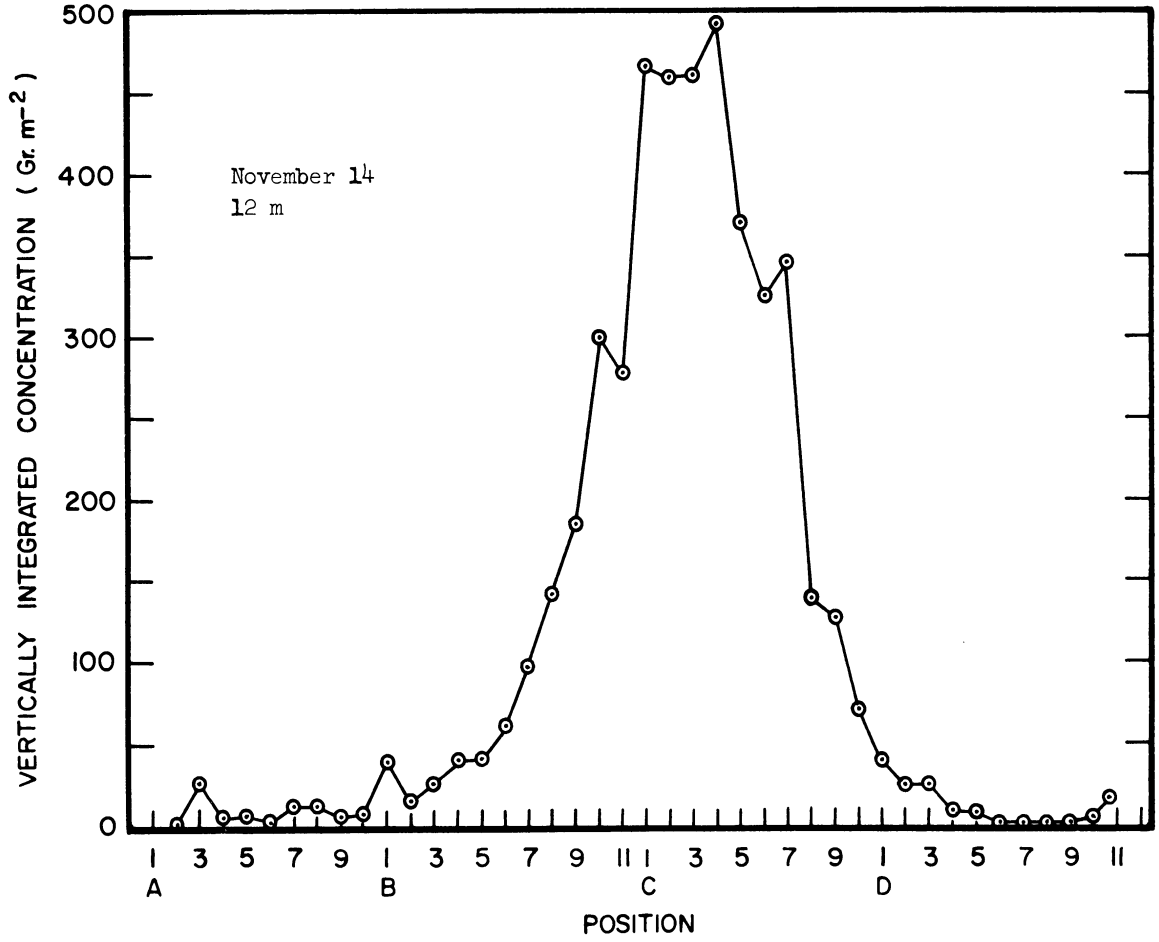

Fig. B.10 (Continued)

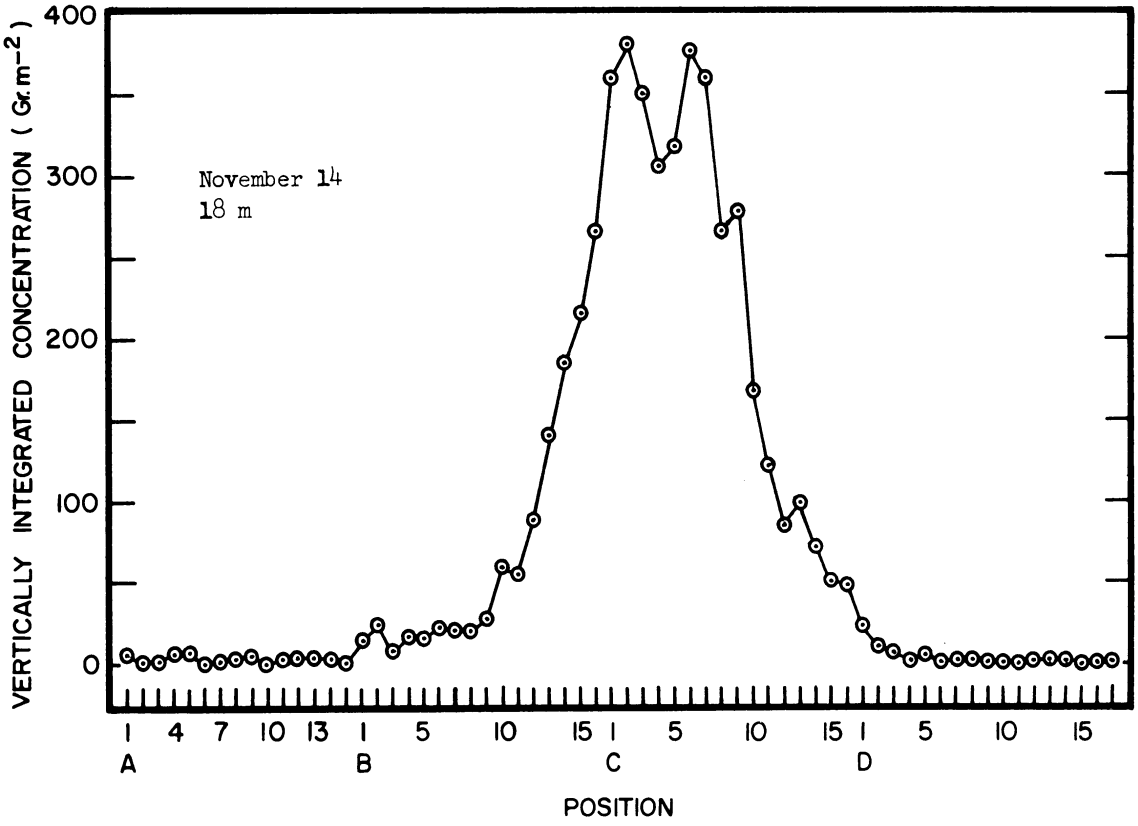

Fig. B.10 (Continued)

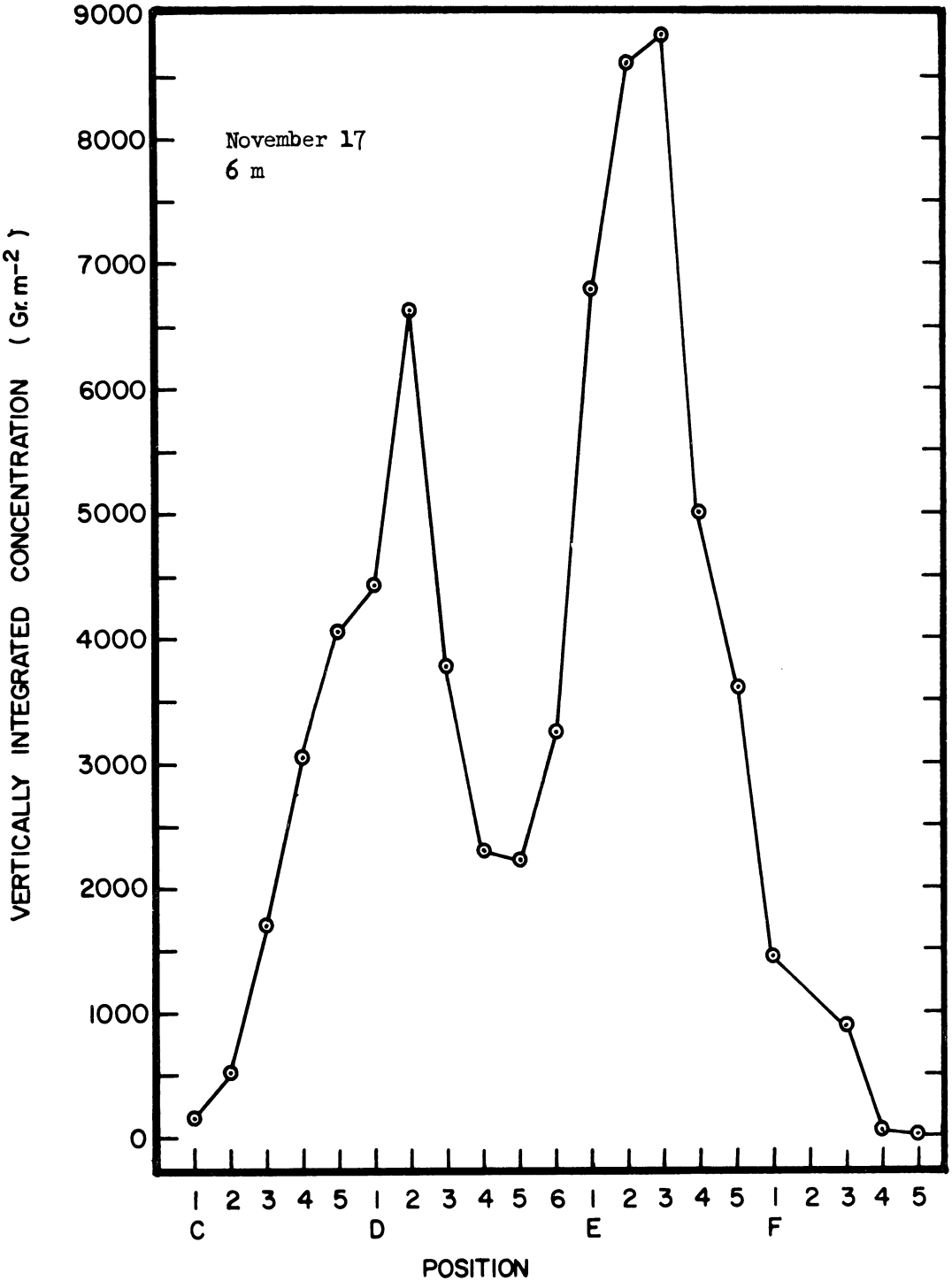

Fig. B.10 (Continued)

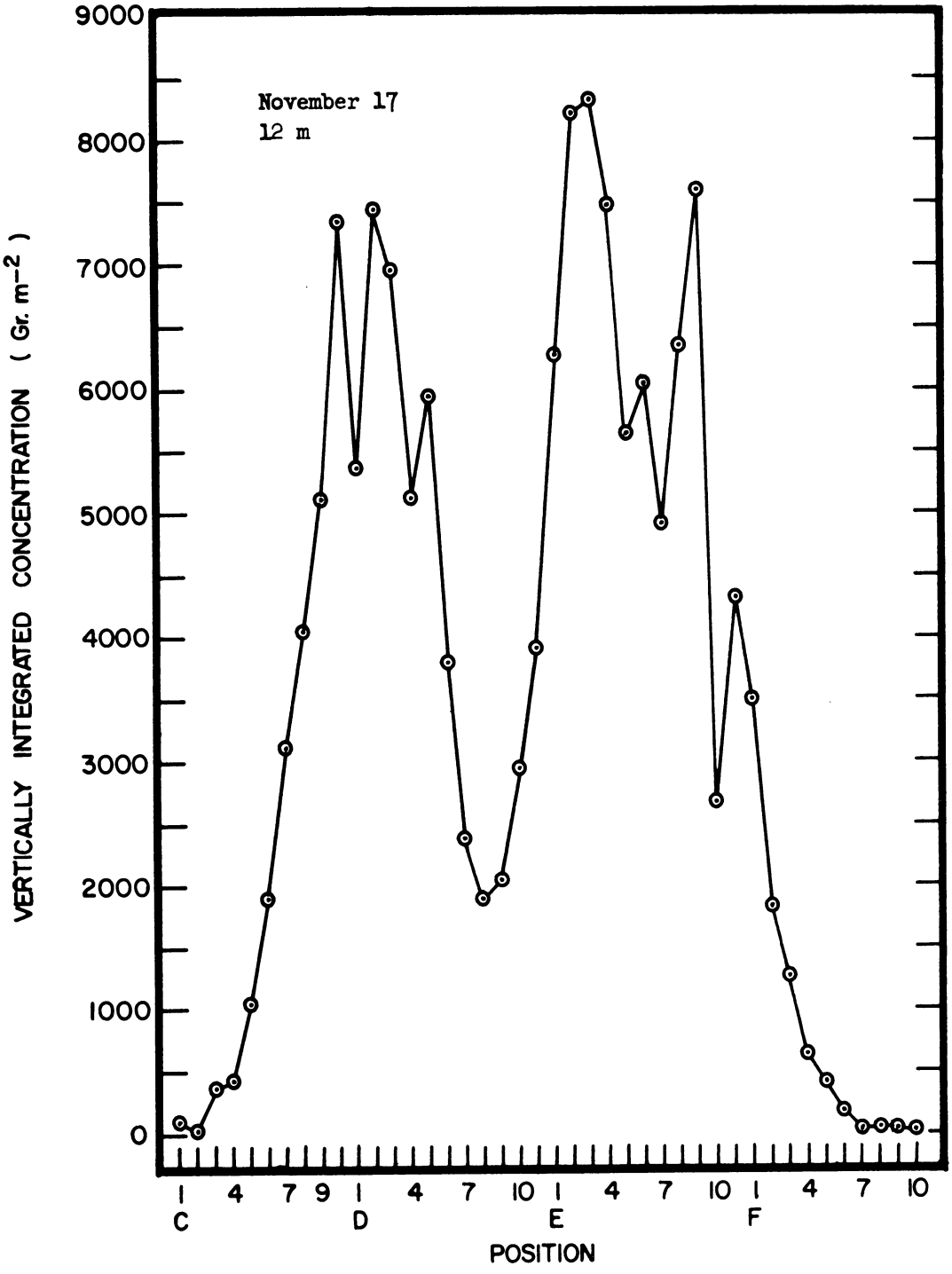

Fig. B.10 (Continued)

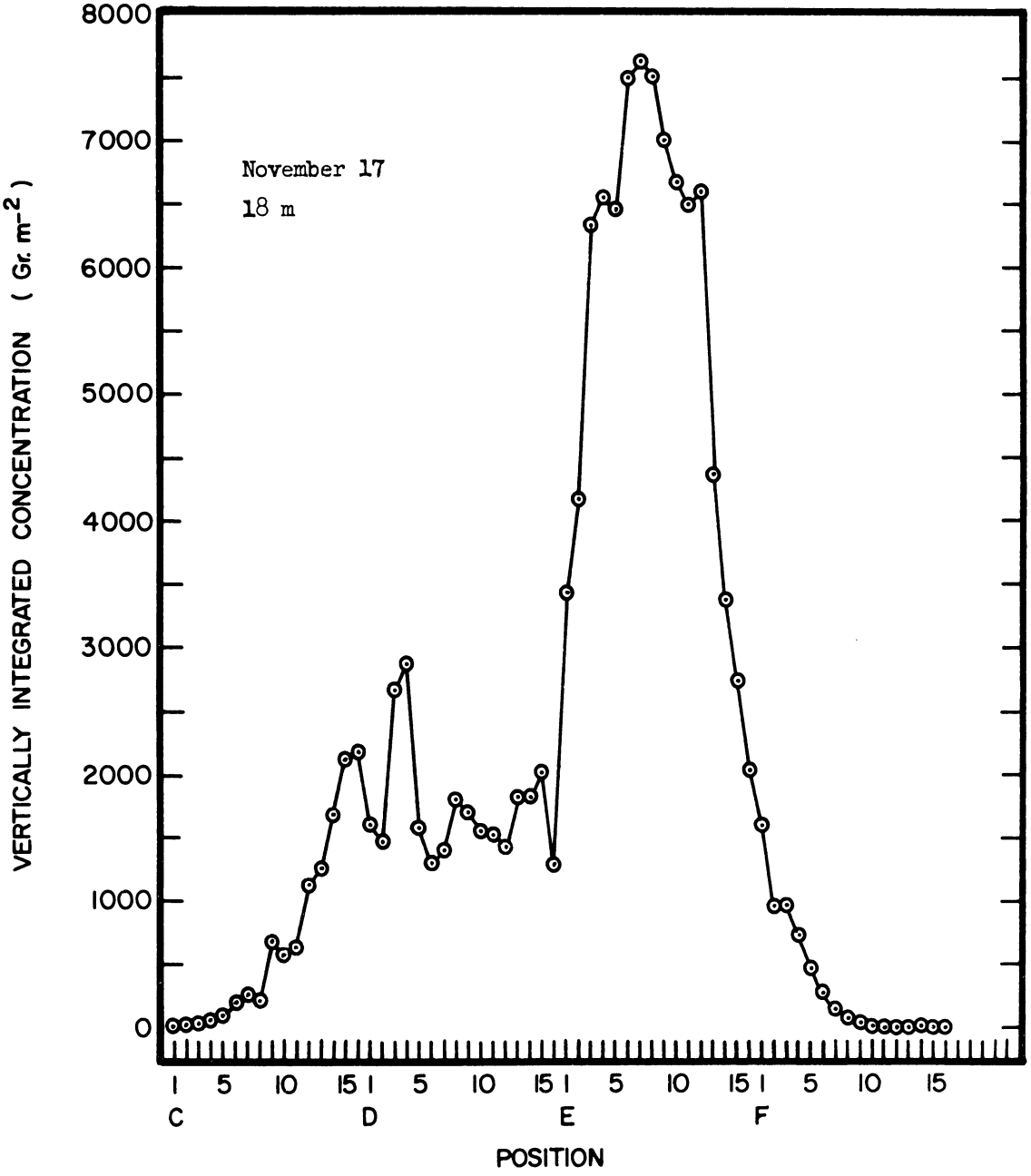

Fig. B.10 (Continued)

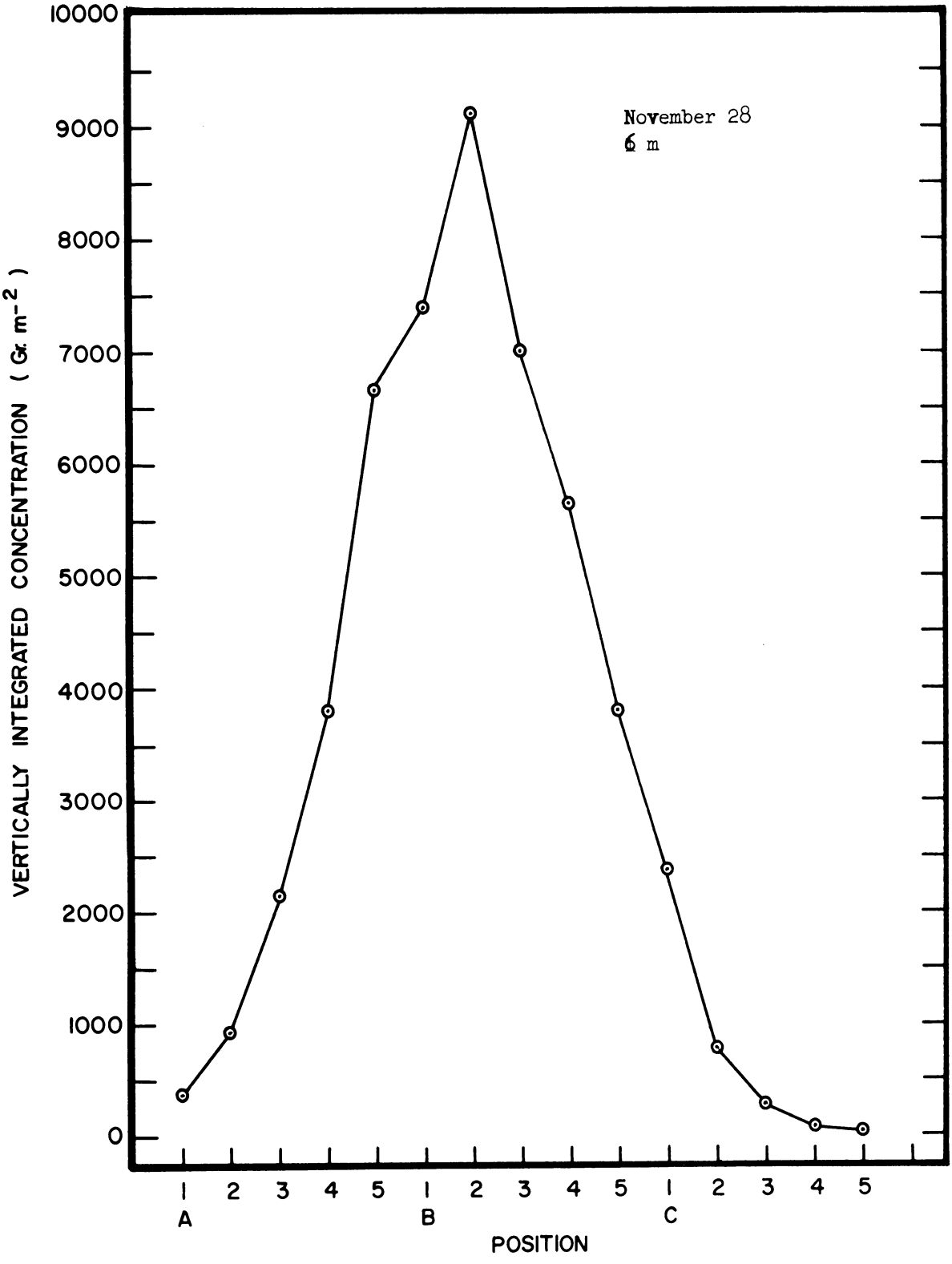

Fig. B.10 (Continued)

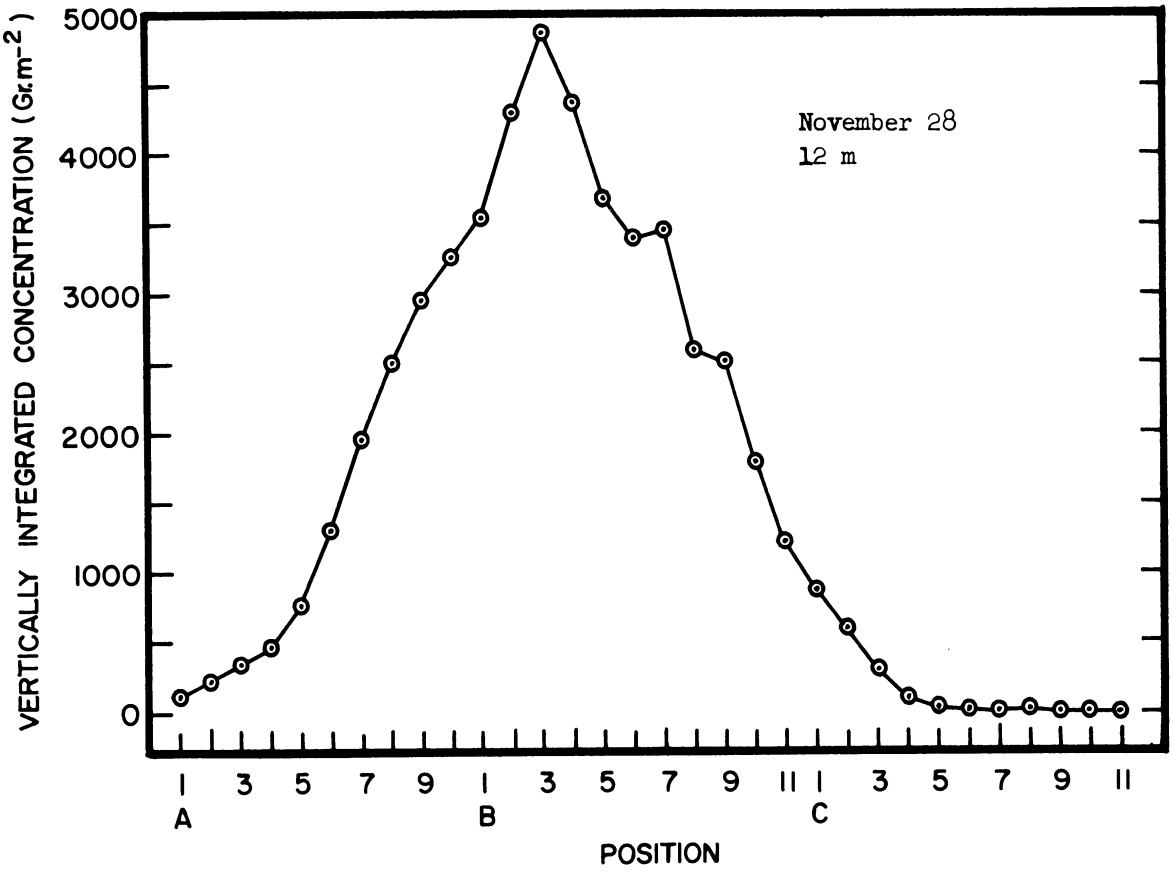

Fig. B.10 (Continued)

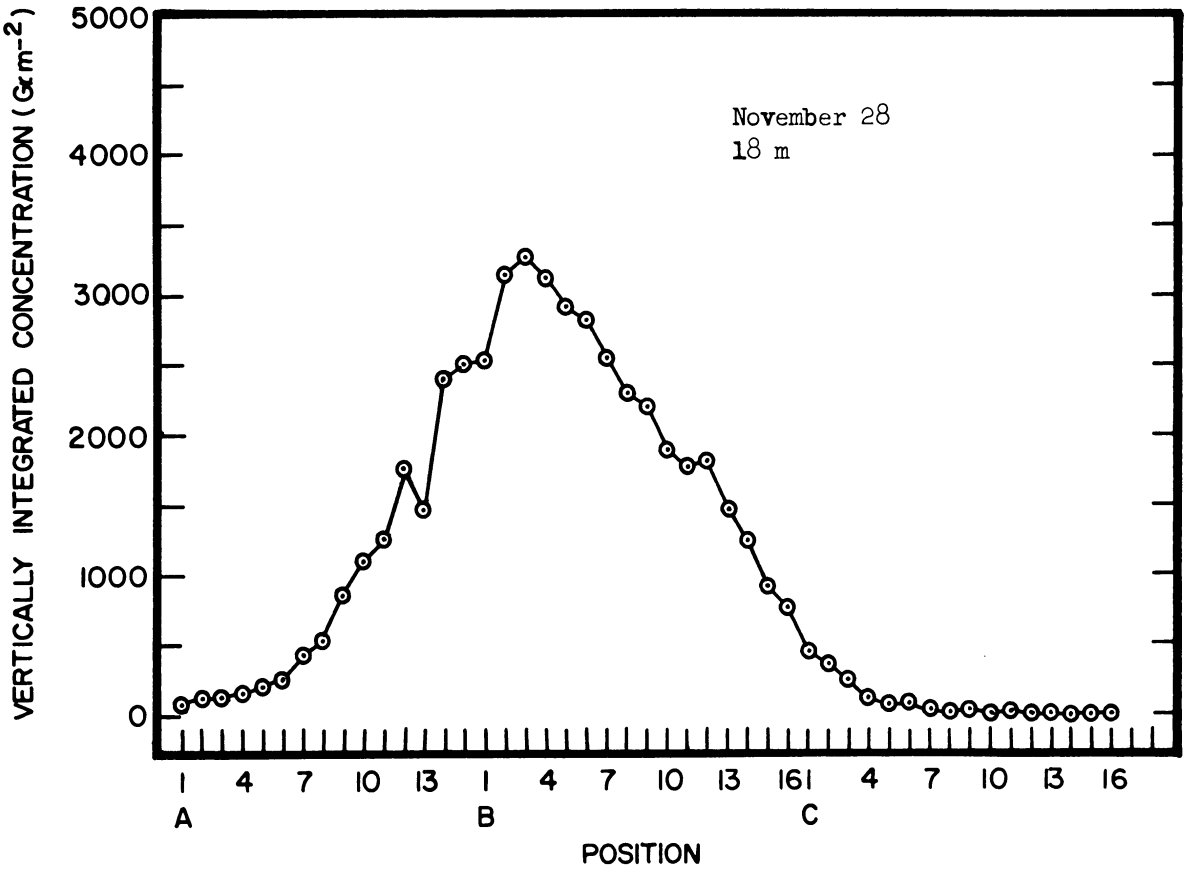

Fig. B.10 (Concluded)

TABLE B-9

THE MEAN, VARIANCE, AND STANDARD DEVIATION OF THE HORIZONTAL DISTRIBUTION OF POLLEN CONCENTRATION—OUT-OF-SEASON EXPERIMENT 1960

November 14

Arc	Height	Mean (deg.)	Variance (m^2)	Variance (deg.^{2})
6 m	0.25	4.93	1.11	103.39
	0.50	4.62	1.10	101.97
	1.00	6.78	1.73	160.94
	1.50	5.70	1.94	179.78
	2.00	14.72	8.89	824.83
	2.50	45.15	7.06	655.50
	3.00	38.89	5.94	551.32
12 m	0.25	4.81	3.81	88.36
	0.50	4.01	3.89	90.24
	1.00	3.72	5.38	124.78
	1.50	2.20	6.08	141.02
	2.00	1.00	1.07	24.80
	2.50	0.73	4.53	105.06
	3.00	353.01	9.16	212.32
	3.50	340.91	1.94	44.87
	4.00	351.99	1.44	33.35
18 m	0.25	2.87	7.88	81.29
	0.50	3.64	8.73	90.06
	1.00	2.91	8.27	85.32
	1.50	3.02	7.63	78.72
	2.00	359.52	8.49	87.59
	2.50	357.75	29.43	303.63
	3.00	358.17	7.08	73.04
	3.50	359.50	12.04	124.21
	4.00	353.23	13.29	137.11
	4.50	0.83	24.89	256.79
	5.00	350.38	16.95	174.87

TABLE B-9 (Continued)

November 17

Arc	Height	Mean (deg.)	Variance (m^2)	Variance (deg.^{2})
6 m	0.25	48.47	4.36	405.10
	0.50	51.65	4.31	400.46
	1.00	46.42	4.10	380.94
	1.50	46.57	4.91	456.21
	2.00	44.63	4.97	461.78
	2.50	57.59	5.67	526.82
	3.00	18.67	1.39	129.15
12 m	0.25	50.69	15.12	350.69
	0.50	48.53	16.01	371.33
	1.00	43.02	17.08	396.15
	1.50	48.60	18.97	440.00
	2.00	51.61	14.82	343.73
	2.50	48.23	20.68	479.65
	3.00	53.36	13.92	322.86
	3.50	60.88	10.59	245.62
	4.00	47.92	8.12	188.35
18 m	0.25	50.90	31.13	321.17
	0.50	50.85	31.86	328.70
	1.00	53.69	26.56	274.02
	1.50	55.97	23.14	238.73
	2.00	44.66	21.52	222.73
	2.50	43.10	26.00	268.24
	3.00	41.47	23.80	245.54
	3.50	42.31	33.65	347.18
	4.00	39.91	26.59	274.33
	4.50	37.37	33.02	340.66
	5.00	40.28	22.08	227.80

TABLE B-9 (Concluded)

November 28

Arc	Height	Mean (deg.)	Variance (m^2)	Variance (deg.^{2})
6 m	0.25	341.56	1.25	116.02
	0.50	340.74	1.44	133.65
	1.00	339.31	1.27	117.87
	1.50	339.68	1.65	153.14
	2.00	339.14	2.05	190.27
	2.50	341.33	1.87	173.56
	3.00	339.64	1.39	129.01
12 m	0.25	339.23	5.08	117.82
	0.50	339.19	4.88	113.18
	1.00	338.50	5.32	123.39
	1.50	339.13	5.41	125.48
	2.00	338.86	5.47	126.87
	2.50	337.72	5.41	125.48
	3.00	335.60	6.98	161.89
	3.50	339.90	1.39	32.24
	4.00	333.35	1.56	36.18
18 m	0.25	337.31	9.35	96.46
	0.50	337.43	9.93	102.45
	1.00	338.25	10.30	106.26
	1.50	337.92	10.24	105.64
	2.00	337.44	10.78	111.22
	2.50	337.51	10.30	106.26
	3.00	336.60	10.94	112.87
	3.50	338.17	14.14	145.88
	4.00	336.93	18.29	188.70
	4.50	336.27	20.80	214.59
	5.00	340.26	14.93	154.03

TABLE B-10

WIND DIRECTION STATISTICS

Date	Average Wind Direction	Variance (deg.^{2})
November 14	186.96	48.68
November 17	246.07	79.64
November 28	288.08	127.46

Figure B.11 is the horizontally integrated vertical distributions of pollen observed on November 14, 17, and 28 respectively. All nine curves are found to be strongly positively skewed with increasing height as would be expected in a region of strong diffusivity gradient. It will be noted that the peak of the pollen profile is well below the level of emission (0.5 m). This effect is not a consequence of gravitational settling as might be supposed, but the result of pollen storage in the region of small diffusivity near the ground. It is shown below that the depositional loss to the ground is relatively small.

B.5.2.4 Surface Deposition

The original purpose of the 1960 out-of-season experiment was to compare the measured rate of pollen deposition to the rate computed by means of Eq. (5.3). Later insight into the problem, however, led the author to believe that pollen deposition over a sand surface should be independent of the meteorological parameters and should occur at about the gravitational rate; consequently, it was decided to compare computed gravitational deposition with that measured using the sugar samplers.

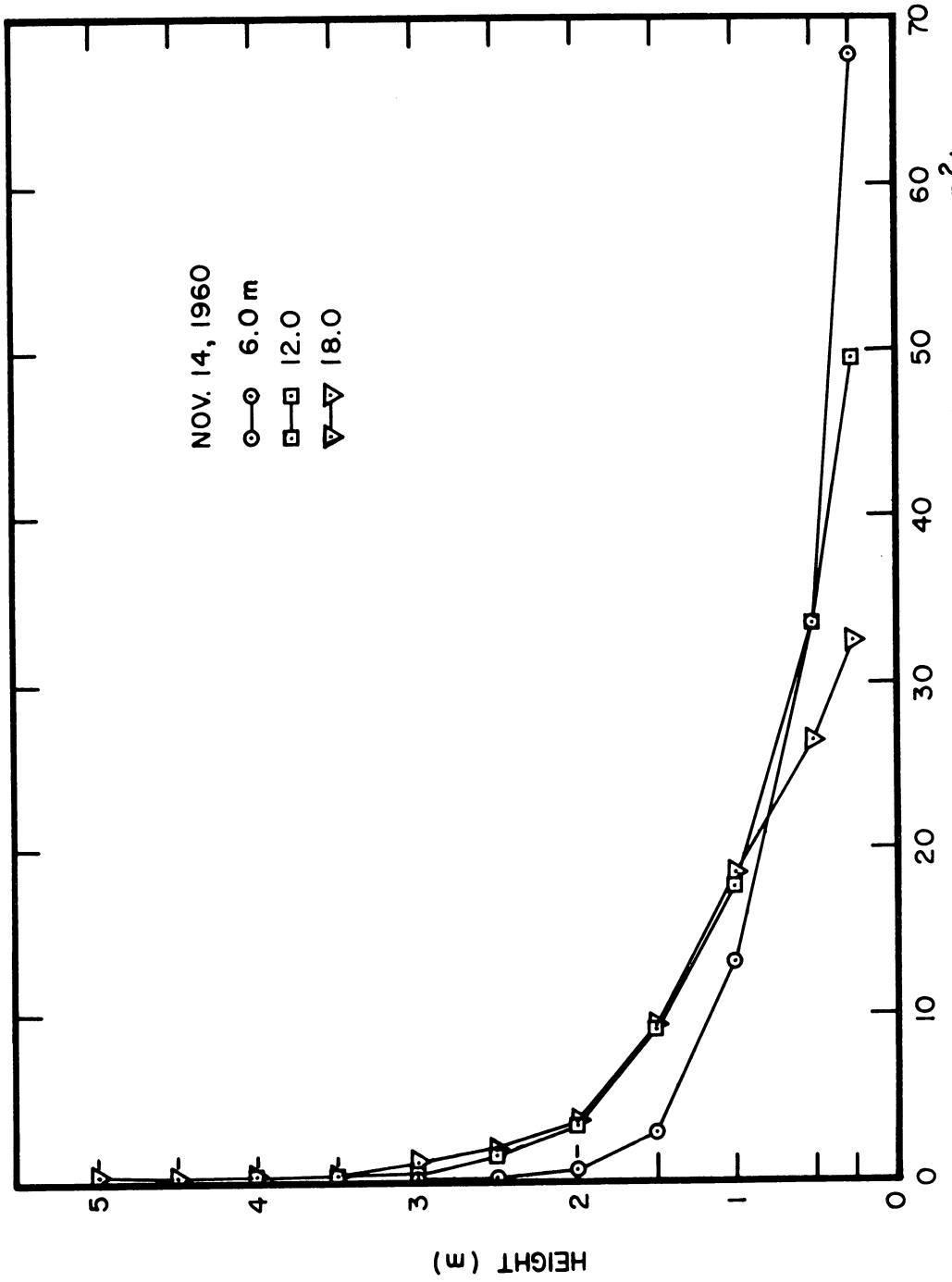

Fig. B.11. The vertical distributions of horizontally integrated pollen concentration. Out-of-season experiment 1960.

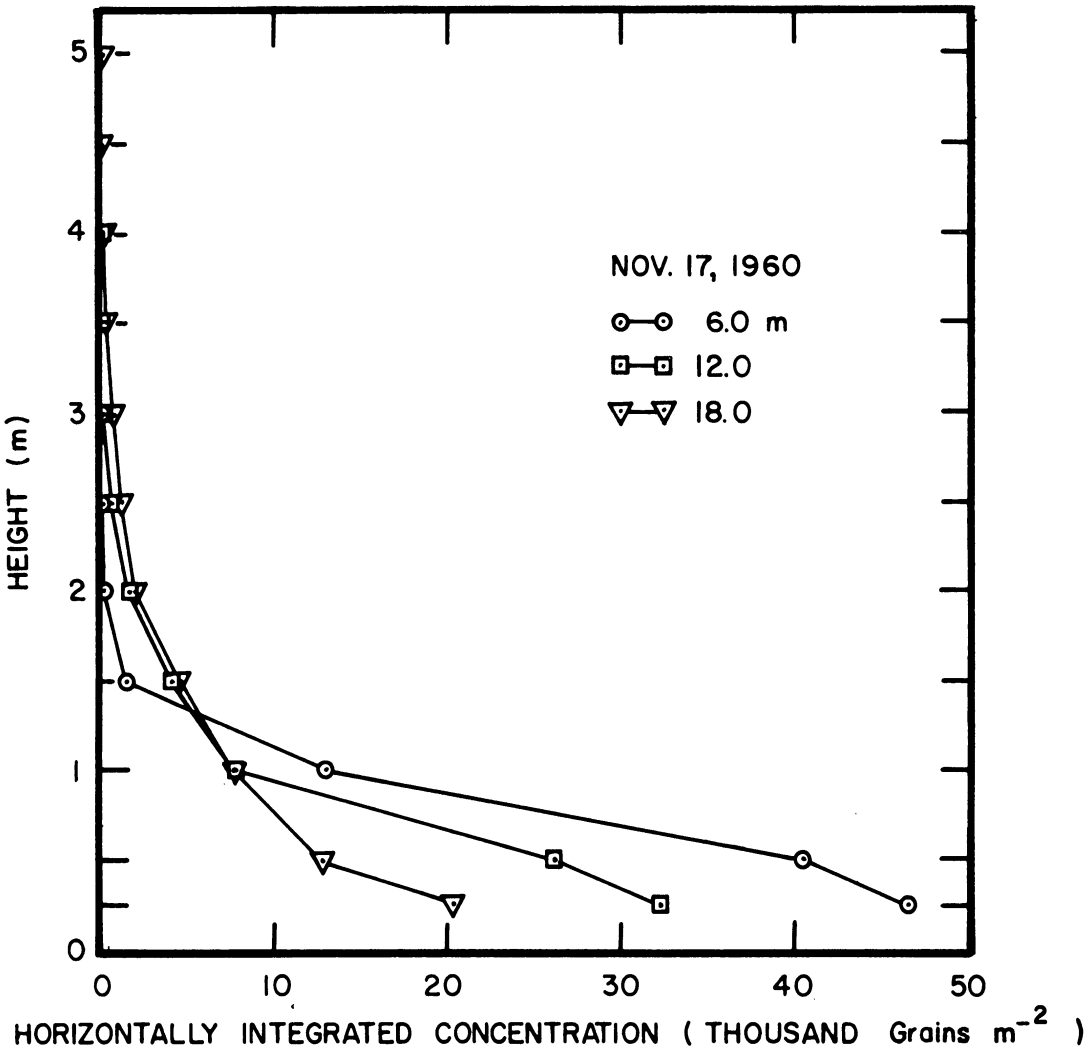

Fig. B.11 (Continued)

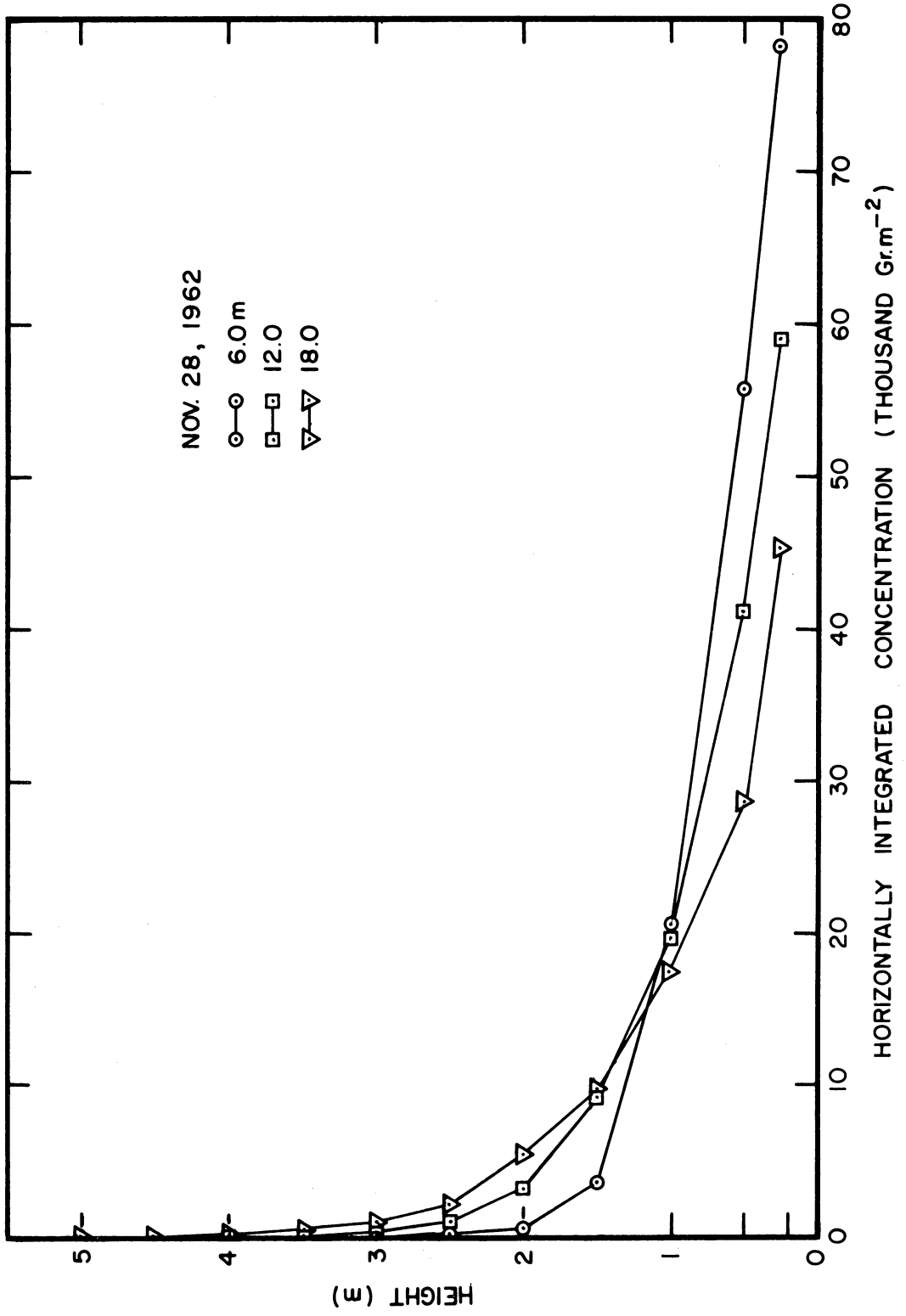

Fig. B.11 (Concluded)

The total number of pollen grains caught in each sugar sampler is given in Table B-5. The counts, converted to the number of grains deposited per square meter,* is compared with the deposition by gravitational settling in Table B-11. The numerical value of the deposition was determined from the equation

$$D_G = \chi_{0.25\ m} \cdot q \cdot t$$

where $q = 0.014\ m\ sec^{-1}$, $t = 3600$ sec and $\chi_{0.25\ m}$ was assumed to be representative of the ground level concentration.

The comparison shown in Table B-11 (pages 281 and 282) reveals unsatisfactory agreement, but that for November 28 shown in Table B-11 (page 283) is better. The results in the first two runs are believed to be due to errors which will be discussed in a later section. The results for November 28 support the conclusion that pollen deposition does occur at the gravitational rate.

B.5.2.5 The Pollen Budget

The method used to compute the total pollen passing through the array given in Sect. B.5.1 may be applied to the observations of November 14, 17, and 28. In addition, if the pollen budget is desired, the pollen loss by deposition must be estimated or measured.

Integration of the pollen counts over the array was undertaken in much the same way as in the preliminary run. First an integration was

*The petri dish area was $0.636 \times 10^{-2}\ m^2$.

TABLE B-11

RAGWEED POLLEN DEPOSITION

(gr m^{-2})

November 14, 1960

Sector Distance (m)	B		C		D		E	
	Measured	Computed	Measured	Computed	Measured	Computed	Measured	Computed
2	48,100		98,400		89,283		30,337	
3	62,247		125,909		35,682		58,946	
4	50,300		243,015		28,922		27,665	
5	62,876		222,266		31,909		30,809	
6	59,103	9,752	166,621	126,252	53,130	1,285	28,294	252
12	53,287	2,293	178,253	46,066	47,628	76	6,444	
18	20,120	60	89,441	20,034	29,708	101	20,120	

TABLE B-11 (Continued)

November 17, 1960

Sector Distance (m)	C		D		E		F	
	Measured	Computed	Measured	Computed	Measured	Computed	Measured	Computed
2	3,458		78,595		236,885		12,103	
3	50,457		160,176		408,536		21,220	
4	96,357		429,600		777,933		196,487	
5	308,563		443,432		717,419		38,831	
6	270,366	96,264	346,761	265,003	600,151	533,383	96,514	21,420
12	134,711	27,418	305,105	73,534	259,926	248,926	51,872	2,621
18	32,381	11,189	68,220	16,985	130,153	99,036	97,772	403

TABLE B-11 (Concluded)

November 28, 1960

Sector Distance (m)	A		B		C	
	Measured	Computed	Measured	Computed	Measured	Computed
2	52,501		264,550		6,601	
3	123,394		503,951		8,173	
4	218,651		1,024,721		29,237	
5	279,483		1,044,213		25,779	
6	217,865	307,692	608,639	1,302,386	32,066	32,206
12	125,437	116,928	566,041	432,583	38,197	3,326
18	58,789	69,199	165,735	185,170	20,120	907

performed horizontally along each wire using Simpson's rule, then a vertical integration was performed, assuming that the count at ground level was equal to that at one meter. The resulting number was divided by the area of the sampler to give the total number of pollen grains passing through the array.

A comparison between the integrated flux through each arc and the total emission is shown for each of the three experiments (Table B-12).

TABLE B-12

TOTAL POLLEN PASSING THROUGH THE ARRAY

Date	No. Grains Emitted	Total Pollen Flux Through Arcs		
		6 m	12 m	18 m
November 14	0.1141×10^9	0.0392×10^9	0.0416×10^9	0.0392×10^9
November 17	0.6814×10^9	0.3321×10^9	0.2455×10^9	0.1985×10^9
November 28	0.7396×10^9	0.6694×10^9	0.5882×10^9	0.5308×10^9

There are several reasons why the measured pollen flux shown in Table B-5 should not be equal to the total emission:

1. Surface deposition has not been accounted for.
2. The adhesive efficiency of the flag sampler is less than unity.
3. Pollen may escape from the top or sides of the sampling array.
4. Pollen may be removed from the air by the wires and samplers of the array.

Each of these possible pollen losses will be considered in the following

paragraphs.

The rate of deposition was measured during each of the full runs, but only the run of November 28 is considered to be sufficiently reliable for use in pollen budget computations.

The deposition measurements given in Table B-11 (page 283) were made at the center of each segment at radial distances of 2, 3, 4, 5, 6, 12 and 18 m from the pollen source. To find the total deposition over the area lying between the source and a given downwind arc, it is necessary first to integrate along each arc, and then to integrate radially outward over the desired distance. Because the array flag samplers were much more closely spaced than the ground level samplers the lateral flag sampler distributions at 1/4 m were used to aid in interpolation between ground level samplers.

The results of the arcwise integration are shown in Fig. B.12. One notes the rapid increase in deposition with distance near the source reaching a peak about 10 source heights downwind then decreasing approximately linearly with radial distance.

The total pollen deposition to various distances from the source is computed by means of a progressive integration under the curve of Fig. B.12. The cumulative fractional deposition is shown in Fig. B.13 as a function of distance from the source. It can be seen that the depositional loss is small, amounting to only 6.3% at a distance of 18 m. This should be contrasted with the much larger values computed by Gregory (1961; see Fig. 24, p. 171).

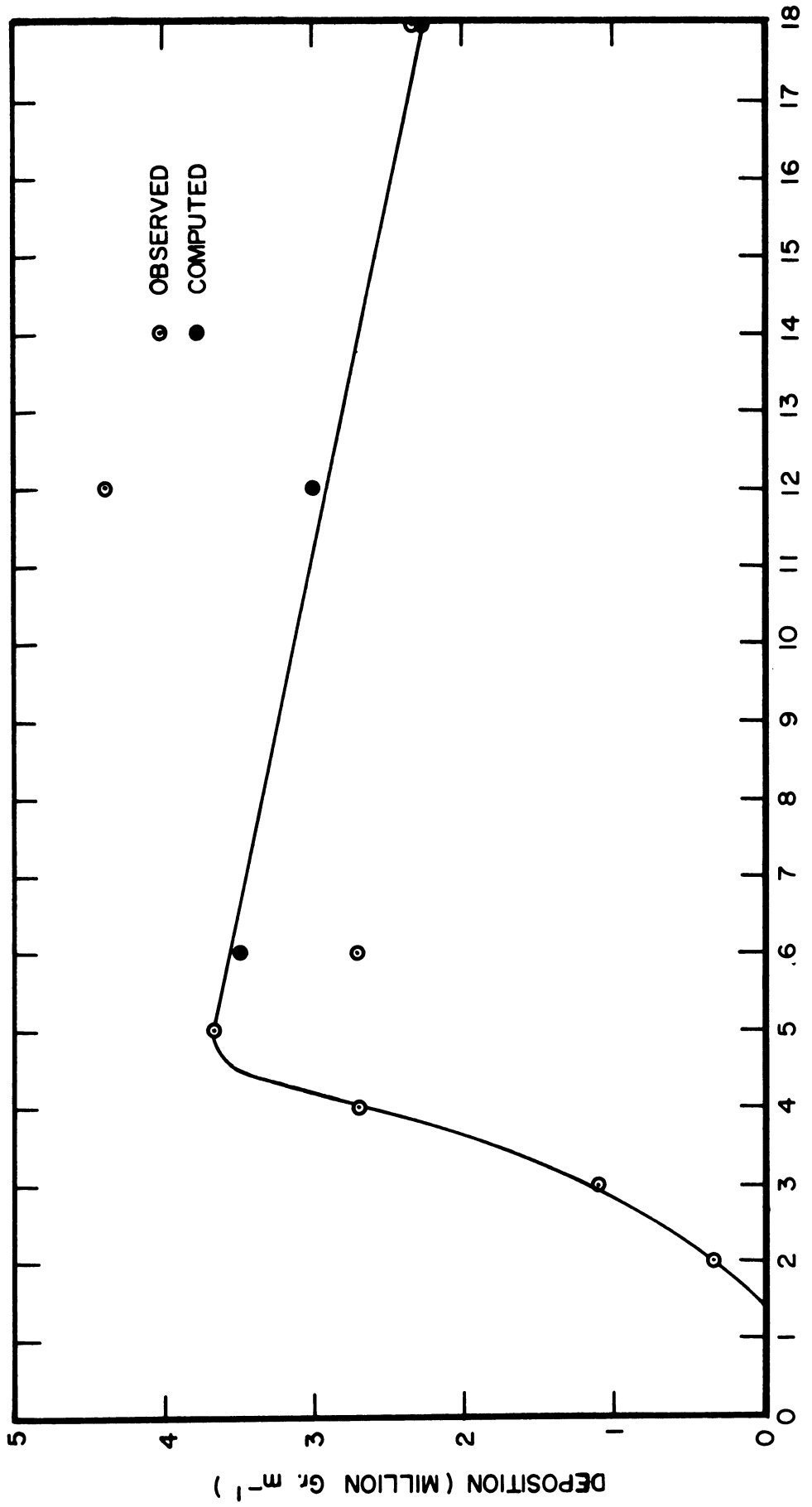

Fig. B.12. The ragweed pollen deposition as a function of distance from a point source. Out-of-season experiment November 28, 1960.

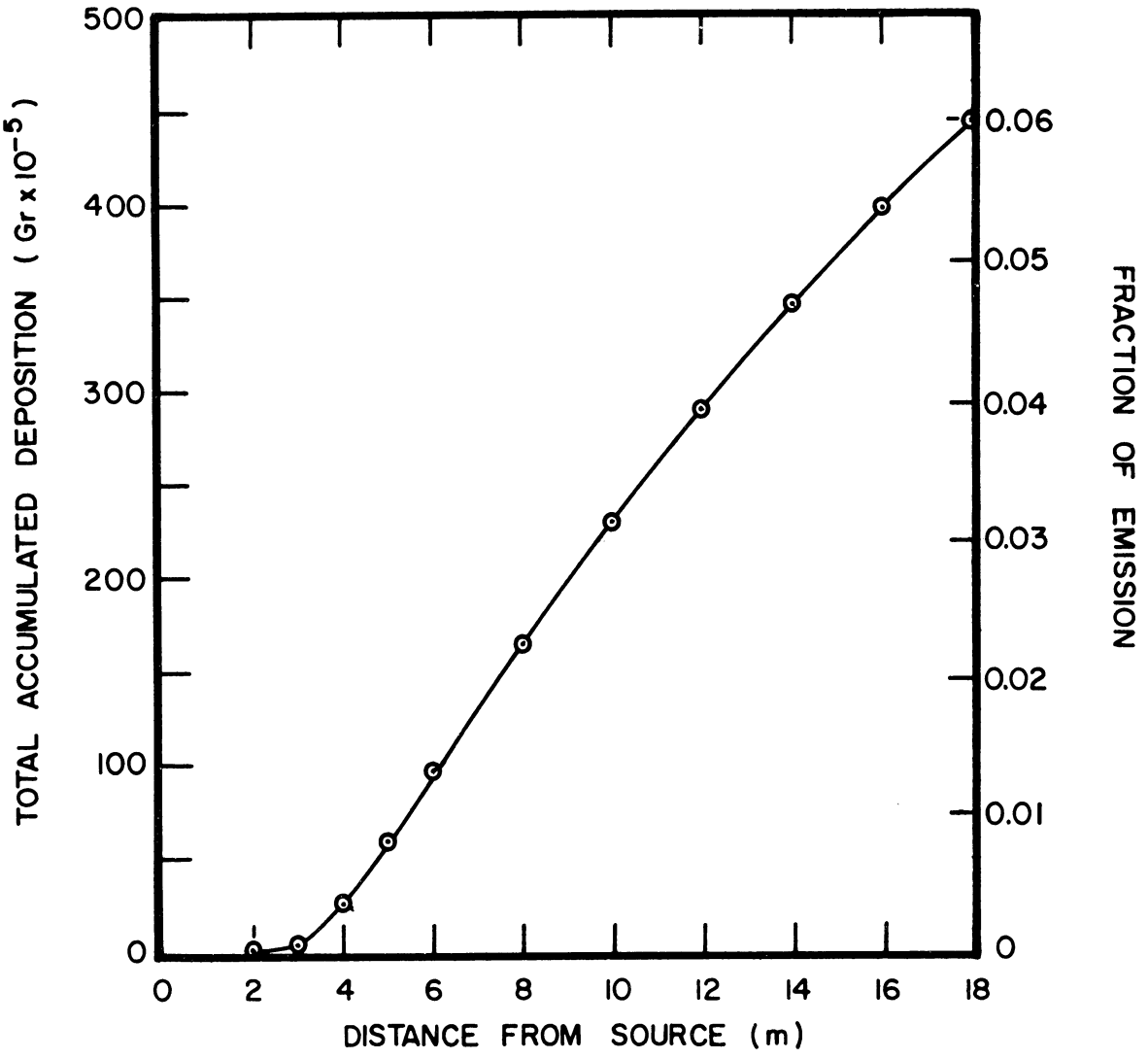

Fig. B.13. The cumulative frational ragweed pollen deposition as a function of distance from a point source. Out-of-season experiment November 28, 1960.

The computation of pollen deposition permits a more complete estimate of the pollen budget to be made. The budget for the experiment of November 28, 1960 is shown in Table B-13 below. At the 6 m

TABLE B-13

THE POLLEN BUDGET

November 28, 1960

Total pollen emitted	0.7396×10^9 grains
Total pollen through 6 m array	0.6694×10^9 grains
Total deposition to 6 m array	0.0096×10^9 grains
	0.6790×10^9 grains
Total pollen through 12 m array	0.5882×10^9 grains
Total deposition to 12 m array	0.0290×10^9 grains
	0.6172×10^9 grains
Total pollen through 18 m array	0.5308×10^9 grains
Total deposition to 18 m array	0.0465×10^9 grains
	0.5773×10^9 grains

arc the number of grains computed by means of the pollen budget shows surprisingly good agreement with the number of grains emitted, the ratio of the two being 0.92. Further downwind the ratio progressively decreases, being 0.83 and 0.78 at 12 and 18 m respectively.

The author has no adequate explanation of the apparent loss of pollen with downwind distance. If the loss were attributable to an error in the deposition rate the latter would have had to be five times greater than the values observed and computed, a conclusion which is not justified.

The discrepancy is not explained by losses of pollen above or around the array. In both cases the top and edges of the array contain only the extreme tails of the pollen distribution which, because it is approximately Gaussian, constitutes a negligible fraction of the total pollen.

The wires of the array and samplers remove no more than 1% of the pollen from the air because they occupy no more than that fraction of the array area. Their effect is therefore insufficient to account for the observed loss.

It is of interest to compare the efficiency of the array (adhesive efficiency of the sampler) for the full experiments with the value 0.4 computed for the preliminary experiment of November 13. The array efficiencies for the three full experiments of November 14, 17, and 28 are 0.4, 0.5, and 0.9 respectively; the last value requires some explanation.

Until recently it has been assumed that the sampler efficiency is not a function of its age. This assumption seemed to be corroborated by early wind tunnel tests by the author in which rubber cement coated flag samplers of age 30 days to a few minutes appeared to have equal efficiencies. More recent tests, however (Stohrer, 1964) suggest that the earlier results may have been in error. No conclusive experiment has been performed.

The more recent results seem to be supported by the 1960 experimental data. The flags for the November 13, 14, and 17 experiments

were prepared well in advance whereas those for November 28 were hurriedly prepared the day prior to the experiment. No records of the exact time of flag preparation were kept.

In conclusion it should be remarked that the pollen budget estimate of November 28 is satisfactory; there have been few estimates in the past which so satisfactorily account for the mass of aerosol emitted.

B.5.2.6 Computations of Eddy Diffusivity

B.5.2.6.1 The Continuity Equation Method

The method of Eq. (6.91) is used to compute the lateral component of the eddy diffusivity from the array data of the 1960 out-of-season experiment. Equation (6.91) is written

$$K_y = \frac{\frac{\partial}{\partial X}(\hat{\hat{\chi}}u)}{\frac{\partial^2 \hat{\hat{\chi}}}{dy^2}} \qquad (B.6)$$

where the "double hat" represents integration in both the x and z coordinate directions.

The values of the first and second derivatives were found at the central point of each arc in the following way:

1. At the intersection of the mean plume direction and the 6, 12, and 18 m arcs the tangent to each arc was drawn.
2. The values of $\hat{\hat{\chi}}$ were obtained and interpolated or extrapolated linearly onto the tangents to the arcs.
3. The resulting values were smoothed graphically.
4. A difference table was computed, finding the values δ^2, δ^4, δ^6, and δ^8 where

$$\delta \hat{\hat{\chi}}(y) = \hat{\hat{\chi}}\left(y + \frac{h}{2}\right) - \hat{\hat{\chi}}\left(y - \frac{h}{2}\right)$$
$$\delta^n \hat{\hat{\chi}}(y) = \delta^{n-1}\left(y + \frac{h}{2}\right) - \delta^{n-1}\left(y - \frac{h}{2}\right) \qquad \text{(B.7)}$$

where h is the distance between samplers. The second derivative is computed from the relation

$$\frac{\delta^2 \hat{\hat{\chi}}}{\delta y^2} = \frac{1}{h^2}\left[\delta^2 - \frac{\delta^4}{12} + \frac{\delta^6}{90} - \frac{\delta^8}{560} + \ldots\right] \qquad \text{(B.8)}$$

5. The first derivative was computed, using forward central and backward differences at the 6, 12, and 18 m arcs respectively.

$$\left(\frac{\partial \hat{\hat{\chi}}}{\partial X}\right)_{6\ m} = \frac{1}{h}\left(-\frac{\hat{\hat{\chi}}_{18}}{2} + \frac{2\hat{\hat{\chi}}_{12}}{2} - \frac{3\hat{\hat{\chi}}_{6}}{2}\right)$$
$$\left(\frac{\partial \hat{\hat{\chi}}}{\partial X}\right)_{12\ m} = \frac{\hat{\hat{\chi}}_{18} - \hat{\hat{\chi}}_{6}}{2h} \qquad \text{(B.9)}$$
$$\left(\frac{\partial \hat{\hat{\chi}}}{\partial X}\right)_{18\ m} = \frac{1}{h}\left(\frac{3\hat{\hat{\chi}}_{18}}{2} - 2\chi_{12} + \frac{\hat{\hat{\chi}}_{6}}{2}\right)$$

The values of $\hat{u}$, $\partial^2\hat{\hat{\chi}}/\partial y^2$, $\partial\hat{\hat{\chi}}/\partial X$ and K_y are given in Table B-14. No computations are given for the November 17 run since the distribution is bimodal and no estimate of the second derivative could be made.

The considerable variation in the estimate of K_y made at each of the three arcs should be noted. The value on the central arc is most reliable because the forward and backward difference estimates of $\partial\hat{\hat{\chi}}/\partial X$ at the 6 and 18 m arcs are not as accurate as the central difference used at 12 m.

TABLE B-14

THE COMPUTATION OF THE LATERAL COMPONENT OF EDDY DIFFUSIVITY FROM PROFILE MEASUREMENTS—OUT-OF-SEASON EXPERIMENT 1960

Date	Arc (m)	$\hat{u}$ (m sec^{-1})	$\partial^2\hat{\hat{\chi}}/\partial y^2$ (gr m^{-3})	$\partial\hat{\hat{\chi}}/\partial x$ (gr m^{-2})	K_y (m^2 sec^{-1})
November 14	6	2.890	-117	- 18.6	0.46
	12	3.055	- 65	- 19.7	0.93
	18	3.117	-112	- 20.7	5.38
November 28	6	2.970	- 20,960	-930	0.13
	12	2.995	- 5,084	-489	0.29
	18	3.121	- 824	48	0.18

B.5.2.6.2 Taylor's Method of Computing Eddy Diffusivity

The method of Eq. (6.92) gives for the lateral and vertical components of the diffusivity

$$K_y = \frac{1}{2}\frac{d}{dt}(\sigma_y^2)$$

and (B.10)

$$K_z = \frac{1}{2}\frac{d}{dt}(\sigma_z^2)$$

where σ_y^2 and σ_z^2 are the variances of the particle distributions in the lateral and vertical directions respectively.

Table B-15 shows the lateral and vertical components of the eddy diffusivity computed by Taylor's method. It will be noted that at 1/2 m K_y is 10 to 30 times as large as K_z.

TABLE B-15

THE EDDY DIFFUSIVITY COMPUTED BY TAYLOR'S METHOD—
OUT-OF-SEASON EXPERIMENT 1960

Date	Eddy Diffusivity (m^2 sec^{-1})	Arcs		
		6-12 m	12-18 m	6-18 m
November 14	K_y	0.865	0.727	0.794
	K_z	0.080	0.074	0.076
November 17	K_y	2.708	2.420	2.585
	K_z	0.047	0.101	0.074
November 28	K_y	0.975	1.252	1.109
	K_z	1.039*	-0.937*	0.076

*Obvious error in the 12 m array variance.

B.5.2.6.3 Profile Method of Computing Eddy Diffusivity

As indicated in Sect. 6.3 there are a number of ways by which the vertical component of the eddy diffusivity can be computed. Here, only the method based on the log-law profile is used, i.e.

$$K(z) = u_* kz \qquad \text{(B.11)}$$

The log-law should be valid under the atmospheric conditions of the three out-of-season experiments because, first they were conducted in November when insolation was weak and the wind was strong and second, either the time of observation was late in the day when adiabatic lapse conditions could be expected, or the sky was overcast. It should be noted that the temperature profile data were unreliable on November 14, and 17 but that the measured lapse rate was adiabatic on November 28 as shown in Table B-6.

From the log-profile equation

$$u_* = k \frac{u(z_2) - u(z_1)}{\ell n(z_2/z_1)} \tag{B.12}$$

and therefore

$$K_z(z) = k^2 \frac{[u(z_2) - u(z_1)]z}{\ell n(z_2/z_1)} \tag{B.13}$$

Table B-16 shows the values of $K(z)/z$ and $K(1/2\ m)$ for the three observation periods. The good agreement with the values of Table B-15 should be noted.

TABLE B-16

COMPUTATIONS OF THE EDDY DIFFUSIVITY
BY THE LOGARITHMIC PROFILE METHOD

Date	$K(z)/z$ ($m\ sec^{-1}$)	$K(1/2\ m)$ ($m^2\ sec^{-1}$)
November 14	0.114	0.057
November 17	0.119	0.060
November 28	0.151	0.076

B.6 SOURCE OF ERROR

B.6.1 Introductory Comments

The accuracy of the various instruments used in the 1960 out-of-season experiment is given in Sect. B.3; therefore, only additional sources of error not covered in that section are discussed here.

B.6.2 Thermocouples

After completion of the experiment of November 17 several of the Bristol recorder tubes were found to be weak. No confidence should be placed in the temperature profile data for the observation periods of November 14 and 17. The data for the 28th should be accurate within the limits specified in Sect. B.3.5.

B.6.3 Flag Samplers

As noted earlier, the coefficient of variation of the samplers owing to differences in their size and adhesiveness should be no more than 10%. An additional error caused by the tilt of the flag sampler bearings on their wire support would result in a 6 and 13% reduction in catch for a tilt of 20 and 30° respectively.

During the placing of the flag samplers in their bearings, an attempt was made to reduce all bearing tilts to less than 20°. During the experiment itself, however, a very few shifted to tilting angles of as much as 30°.

B.6.4 Ground Level Sugar Samplers

Extreme care was needed at all times to minimize accidental pollution of the ground level samplers. During the full scale runs of November 14 and November 17 the procedure was not perfected and accidental pollution of unknown magnitude may have occurred. By November 28, a number of modifications in procedure were made to minimize the errors. The November 28 data can be considered to be the most reliable.

B.6.5 Slope of the Array Site

The maximum slope of the array site was 15 cm in 18 m as shown in Fig. B.1. The slope does not introduce a serious source of error if it is assumed that the air moves parallel to the ground. It has been suggested, however (Jacobs, 1965), that the streamlines do not lie parallel to the ground, but actually approach the ground over upward sloping terrain. No quantitative calculations have been made.

B.6.6 Change of Roughness

As can be seen in the photographs of the site (Figs. B.2-4) an abrupt change of roughness occurred at the sampling site, from rather rough mown grass to fine grain sand. It is not known to what extent the change of roughness affected vertical motion in the array area.

Another feature of the array site which may have been responsible for peculiarities in the flow pattern was a small drop in ground level just west of the dispenser, a consequence of attempting to level the site. It is possible that a standing wave was established near the dispenser.

APPENDIX C

THE 1962 IN-SEASON EXPERIMENT

C.1 INTRODUCTION

The 1962 in-season experiment was designed for two purposes: first, to observe the vertical profile of pollen concentration during the ragweed season; and second, from profile observations of temperature, humidity and pollen to compute the vertical components of the eddy diffusivities for heat and mass as functions of time and height.

The observations were conducted at one observing site in one dimension, the vertical, and therefore it was not possible to measure horizontal fluxes of the variables. For this reason it was important to find a site centered within a large region over which each of the measured variables was horizontally homogeneous. The failure to find a perfect site was responsible for the major sources of error in the experiment.

The vertical component of the diffusivity can be determined from profile measurements by the method given in Sect. 6.3.6.3. The diffusivity is computed from Eq. (6.75) which is

$$K_z(z_1) = \frac{-\frac{\partial}{\partial t}\int_{z_1}^{z_2} \chi dz + \left(K_z \frac{\partial \chi}{\partial z}\right)_{z_2} + q(\chi_{z_2}-\chi_{z_1})}{(\partial \chi/\partial z)_{z_1}} \qquad (C.1)$$

where the symbol χ refers to any conservative entity in the air. By choosing z_2 at a height such that χ becomes zero, Eq. (C.1) can be

reduced to the equation

$$K_z(z_1) = \frac{-\left[\frac{\partial}{\partial t}\int_{z_1}^{z_2} \chi dz + q\chi_{z_1}\right]}{(\partial\chi/\partial z)_{z_1}} \qquad (C.2)$$

Equation (C.2) shows that two measurements of the vertical profile of χ separated by a short interval of time are sufficient to estimate K_z.

The serious errors which may occur when the condition of horizontal homogeneity is not fulfilled may be avoided in some cases if the horizontal concentration gradient can be estimated. For example, two of the three variables measured during the 1962 experiment, namely temperature and humidity, are observed and charted synoptically so that their rate of advection can be estimated and hence eliminated. The third variable, ragweed pollen concentration, has an unknown horizontal variability so that homogeneity is a requisite to the accurate use of Eq. (C.2).

The vertical profiles should be measured, ideally, at one point and one instant of time, but in practice small scale inhomogeneities in concentration, low concentrations and sampling limitations necessitate either space or time averaged observations. During the 1962 in-season experiment airborne drum samplers were used above 60 ft and tower mounted rotobars were used at ground level. Thus, spacial averages were obtained from 60 ft upward, and temporal averages from 60 ft downward.

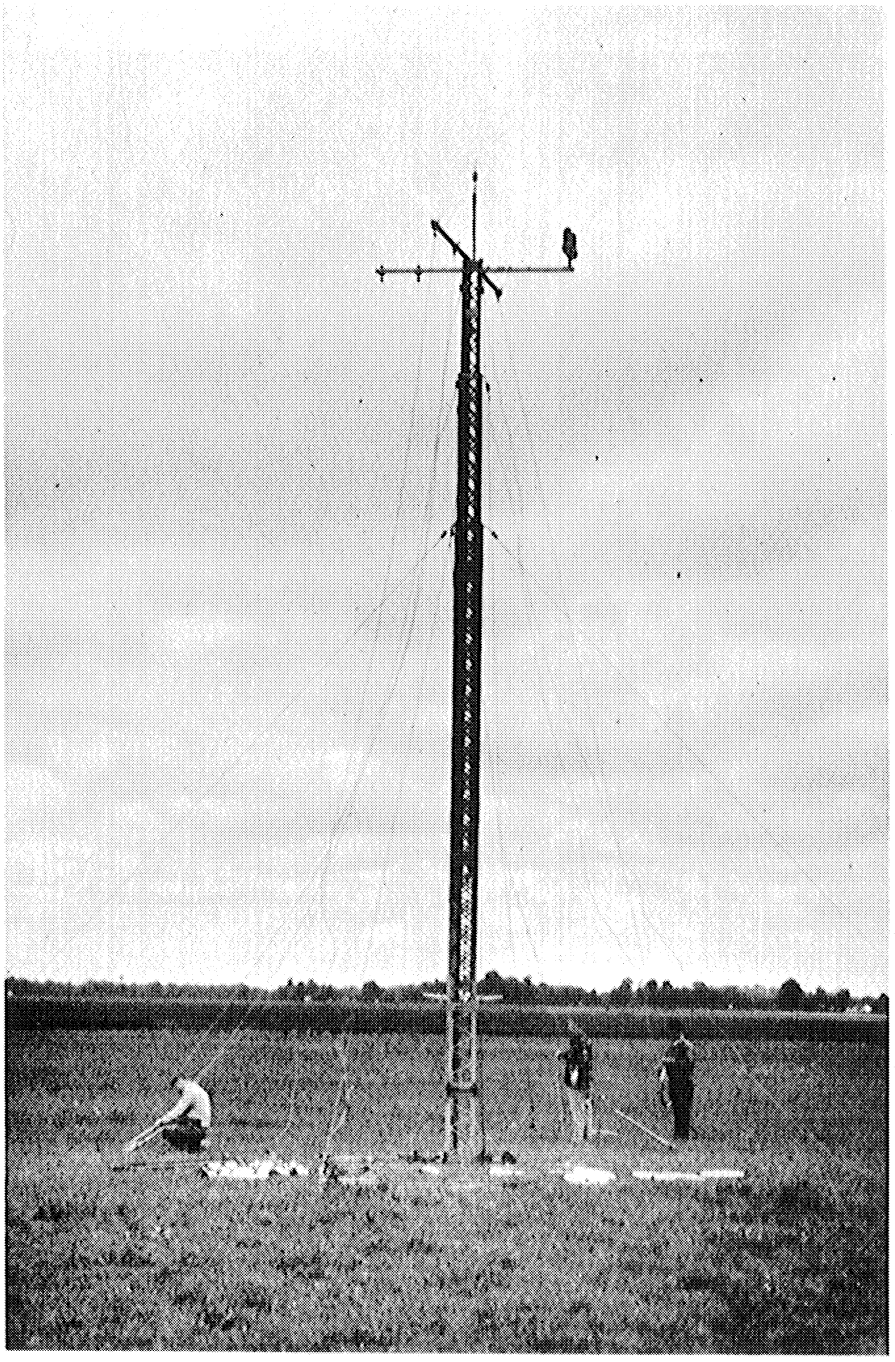

Fig. C.1. The meteorological tower in the process of erection. The view is across Willow Run Airport looking north-west. In-season experiment August 1962.

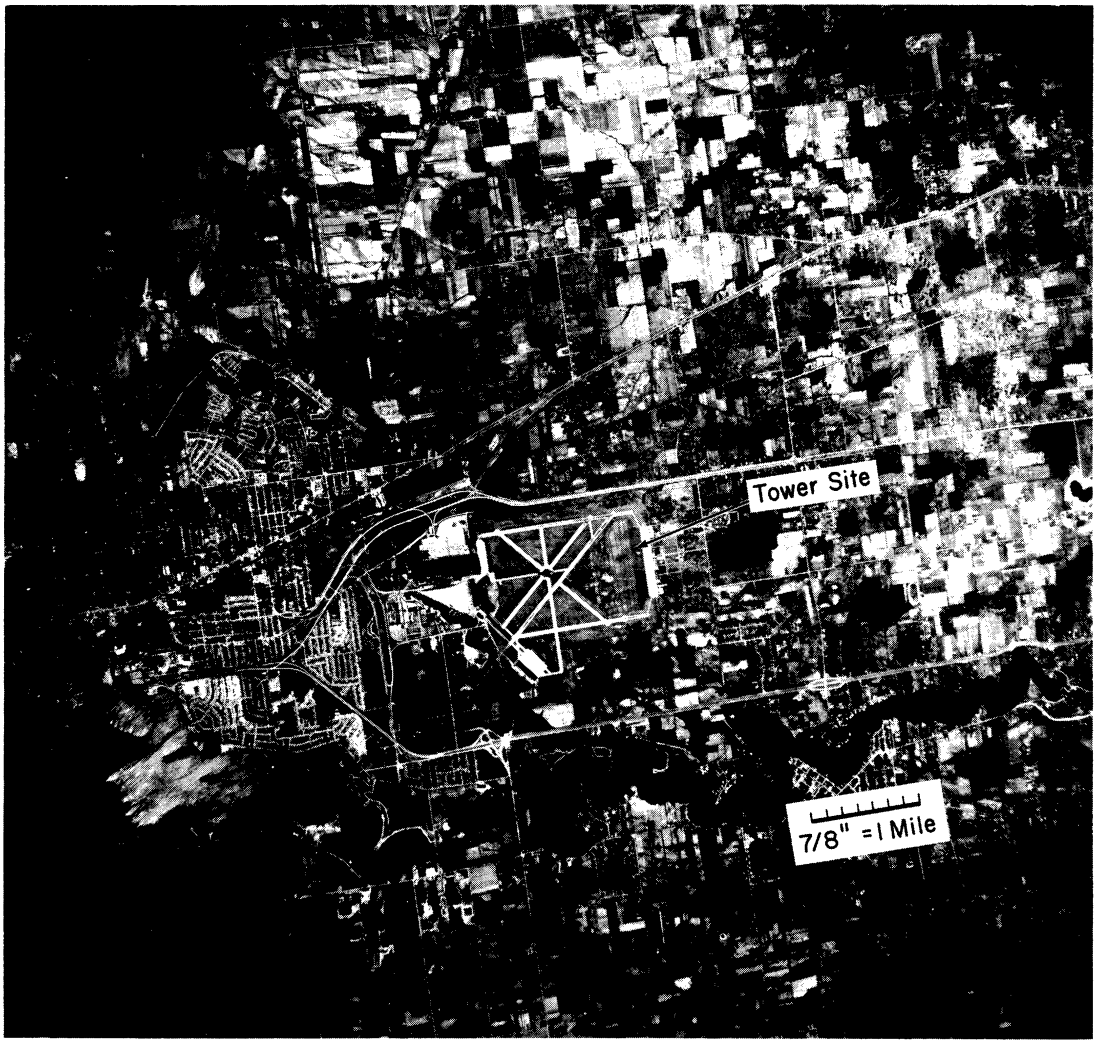

Fig. C.2. An aerial view of Willow Run Airport and the surrounding countryside. (Courtesy of 127th Tactical Reconnaissance Wing of the Michigan Air National Guard.)

C.3 GROUND EQUIPMENT

C.3.1 The Tower

A telescopic 18 m aluminum tower was erected on a wooden platform 37.8 m west of the parking apron on the grassy strip mentioned above. Figure C.3 is a view of the instrumented tower taken from the southwest. Two sets of rotobar samplers were hung from pulleys located at the ends of a cross beam at the top of the tower. The samplers were mounted at 4, 7, 10, 13 and 16 m and an additional two samplers were located at 1/2 m on posts driven into the ground a short distance west of the tower (Fig. C.4). One Beckman and Whitley three cup anemometer was installed at 20 m on a stand erected at the top of the tower. A line of wet and dry temperature sensors located at 1/2, 4, 7, 10, 13, and 16 m were hung from a pulley attached to a second cross beam atop the tower. To minimize the influence of the tower the two sets of rotobar samplers were located to the northwest and southeast of the tower and the temperature sensors to the southwest.

C.3.2 The Samplers

The standard D.C. rotobar described in App. A and mounted as shown in Fig. C.5 was used to sample pollen at the tower site. In previous experiments the sample bars had been wrapped in double coated Scotch Tape and sprayed with dilute rubber cement (Harrington et al. 1959). During the 1962 experiment the sampling surfaces of the bars were painted black and sprayed directly with dilute rubber cement. To

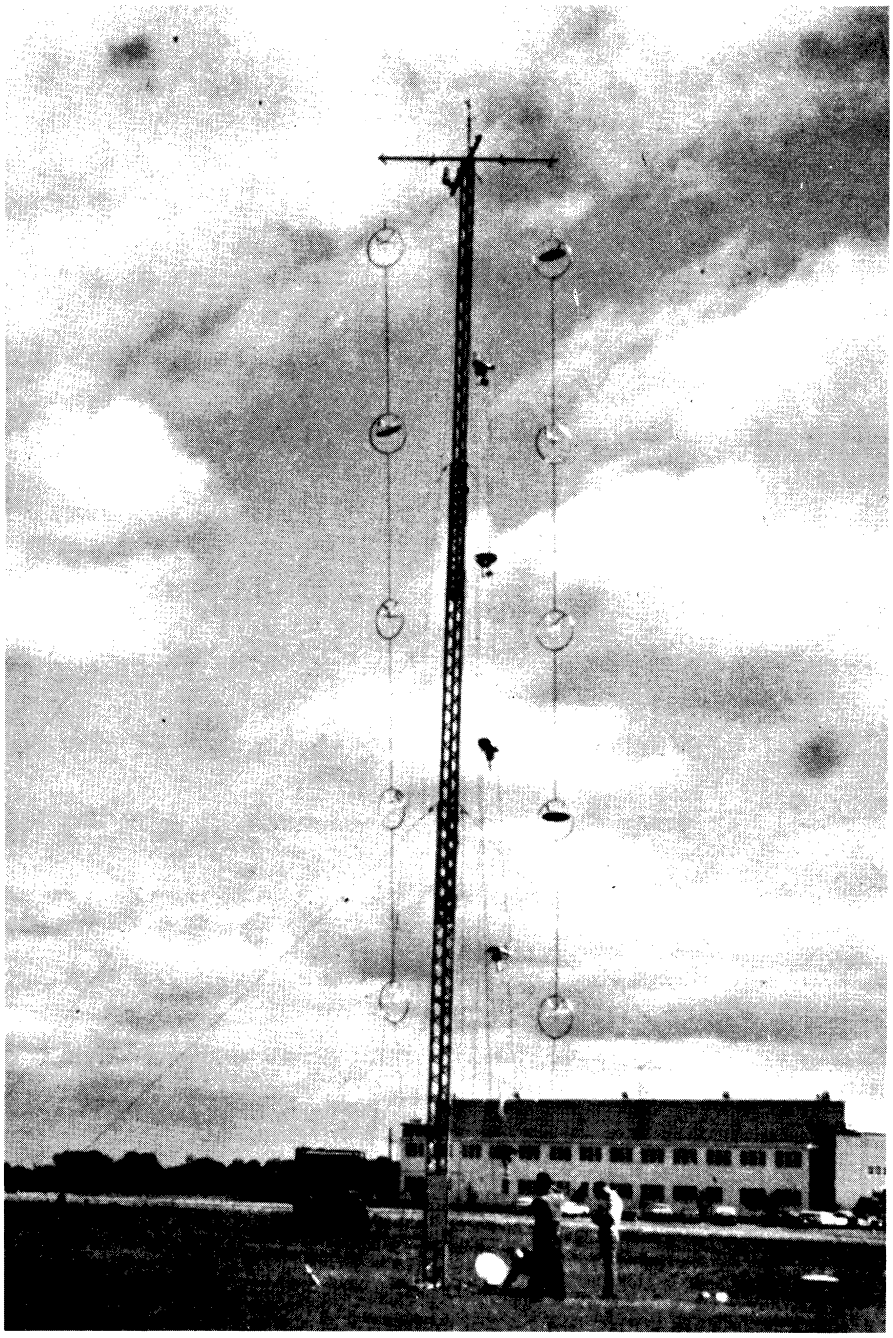

Fig. C.3. The meteorological tower showing the two lines of rotobar samplers at either side and the wet and dry thermocouple instrumentation just to the right of the tower. One of the 1/2 m rotobar samplers appears on the ground to the right of the tower. An anemometer atop the tower is not quite visible in the photograph. In-season experiment 1962.

Fig. C.4. The rotobar sampler at 1/2 m above ground. The view is toward the north-west across Willow Run Airport. In-season experiment 1962.

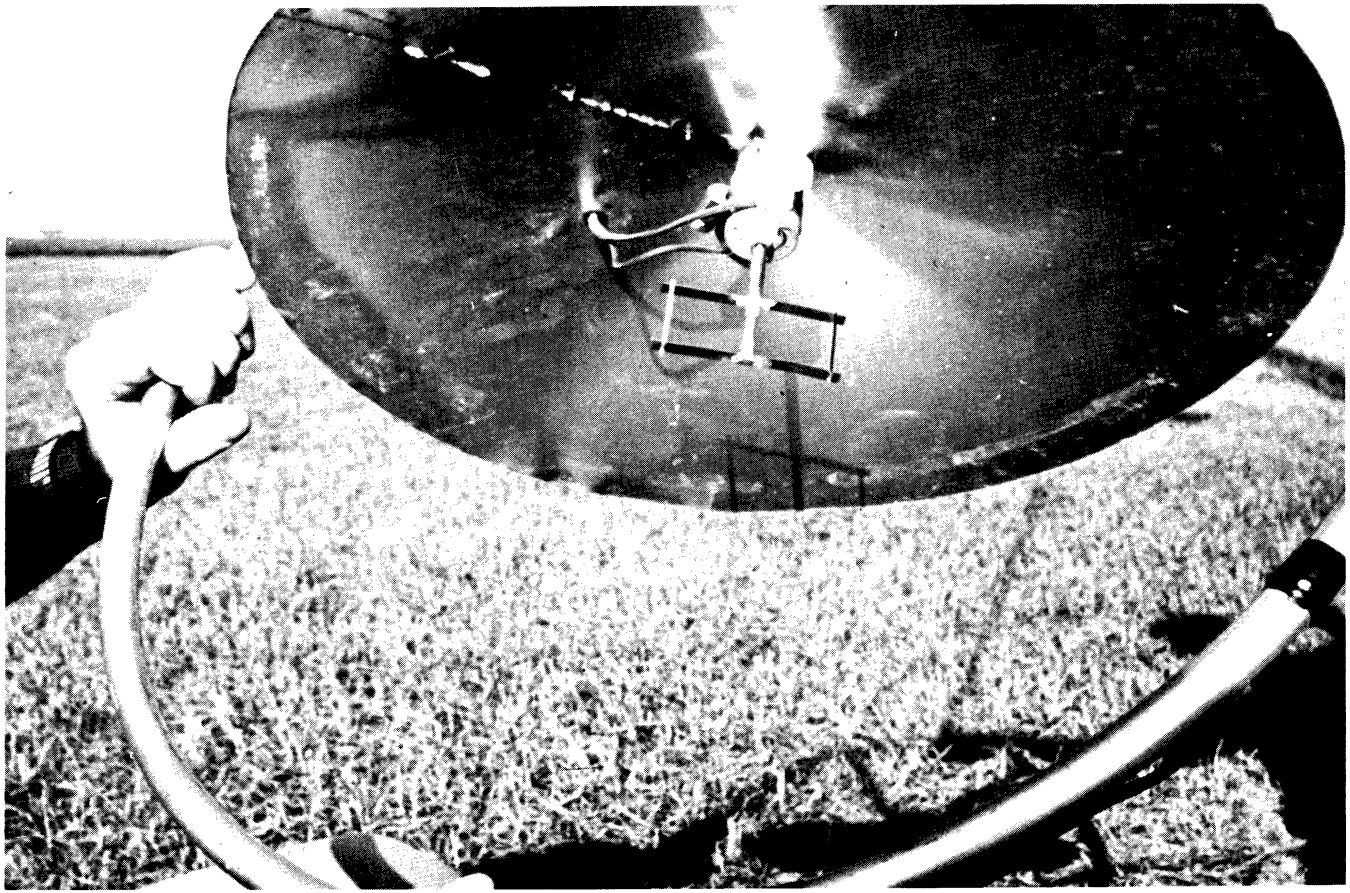

Fig. C.5. The rotobar sampler mounted under a metal coolie-hat rain shield. In-season experiment 1962.

prevent accidental contamination, a special bar box was constructed as shown in Fig. C.6 in which the bars were kept with their sampling edge face down and free of contact with any surfaces.

C.3.3 The Wet and Dry Thermocouples

Wet and dry thermocouples composed of copper-constantan 16 gauge, polyvinyl over polyvinyl extension wire (Brown Inst. Div.) were soldered in brass wells 5/16 in. in diameter by 1-1/4 in. in length to provide slow response wet and dry thermocouple temperature measurements.

The thermojunctions were held by set screws on either side of a silvered fiber-glass tube 1-1/4 in. in diameter by 6 in. in length separated down the center by a plastic plate. The dry junction was positioned below the level of the wet junction to minimize cooling effects. The assembly was then held by set screws within a chromed metal cylinder 6 in. in length and 2 in. in diameter.

Continuous moistening of the wet thermojunction was maintained by a wick which passed through a plexiglass tube extending through both cylinders to a small plexiglass constant water level vessel. The water level was accurately maintained by means of an immersed inlet tube. Water was supplied to the inlet tube from an 8 oz plastic wash bottle reservoir mounted so as to be in the discharge path of air from the aspiration fan. The aspiration fan was calibrated using an Alnor velometer for a flow rate of 1450 fpm with the complete assembly in

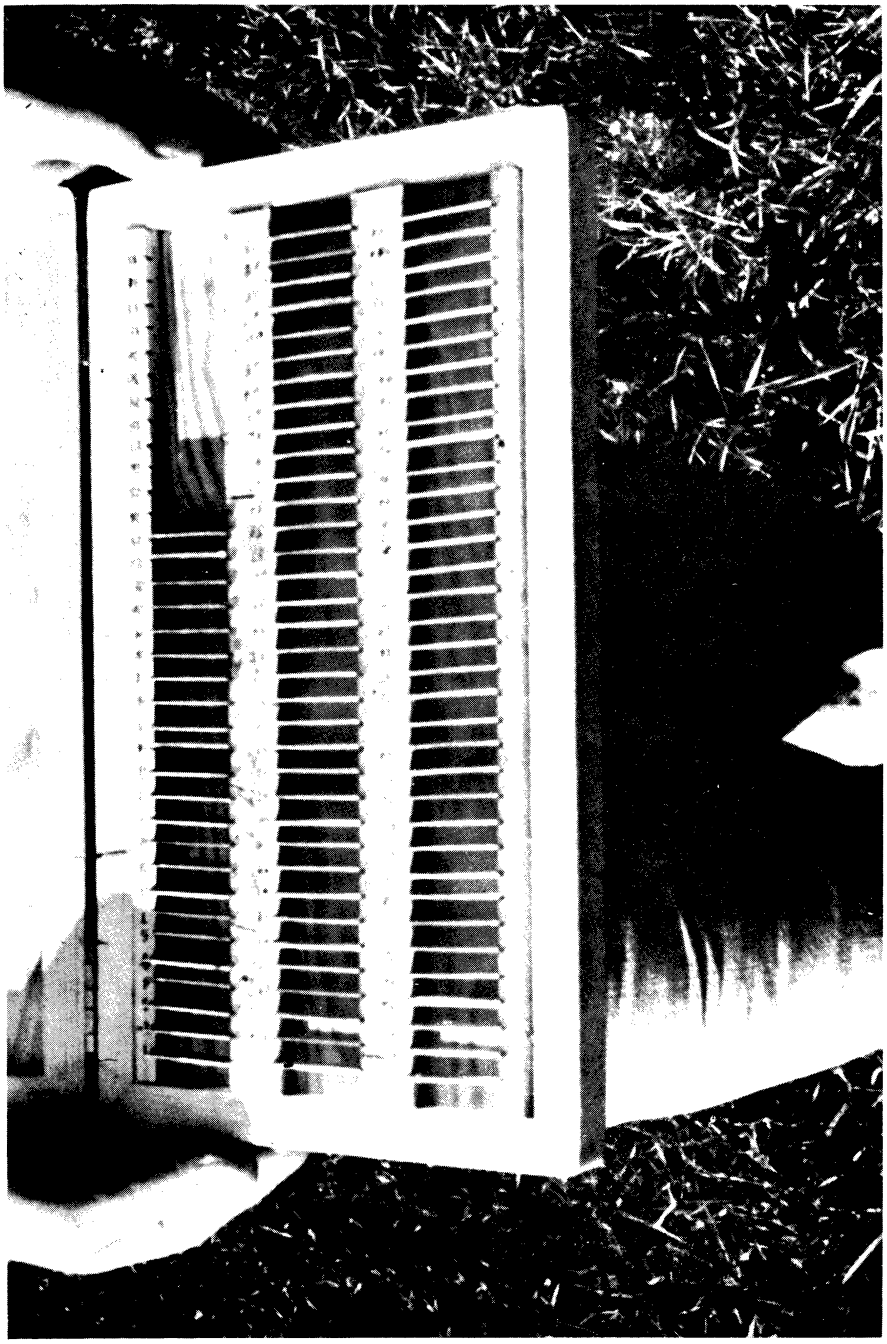

Fig. C.6. The rotobar sampler box. In-season experiment 1962.

place. The entire unit, shown in Fig. C.7, was shielded from the sun by an aluminum coolie hat.*

The temperatures were recorded on a Brown Electronik 20 point recorder of range -25°F to 125°-F and having a cycle time of 10 min. Cycling was arranged so that all the dry thermocouples were recorded sequentially followed by the wet, thus minimizing errors due to temporal changes in the lapse rates.

C.3.4 The Anemometers

One Beckman and Whitley model 170-2 anemometer was installed on the top of the tower at a height of 19.30 m. The remaining anemometers were installed on a separate 10 m aluminum mast located 138 ft to the south of the sampling tower and 124 ft west of the concrete parking apron as shown in Fig. C.8.

Beckman and Whitley anemometers were located on the 10 m mast at 4, 6, and 10 m and Thornthwaite anemometers (model 102) at 1/4, 1/2, 1 and 2 m.

The Thornthwaite anemometers have a starting speed of 0.3 mph, a range up to 32 mph and a specified accuracy of ±5%. The Beckman and Whitley anemometers have a starting speed of 0.6 mph, a range up to 24 mph and a specified accuracy of ±5%. Each set of units were matched so that results within each set are comparable within 2%.

*The wrinkles in the coolie hat were caused accidentally.

Fig. C.7. The wet and dry thermocouple mounting, showing the centrifugal aspiration fan, the radiation shield, the water supply bottle, the constant level water supply, and the silvered metal radiation shield for the thermocouples. In-season experiment, 1962.

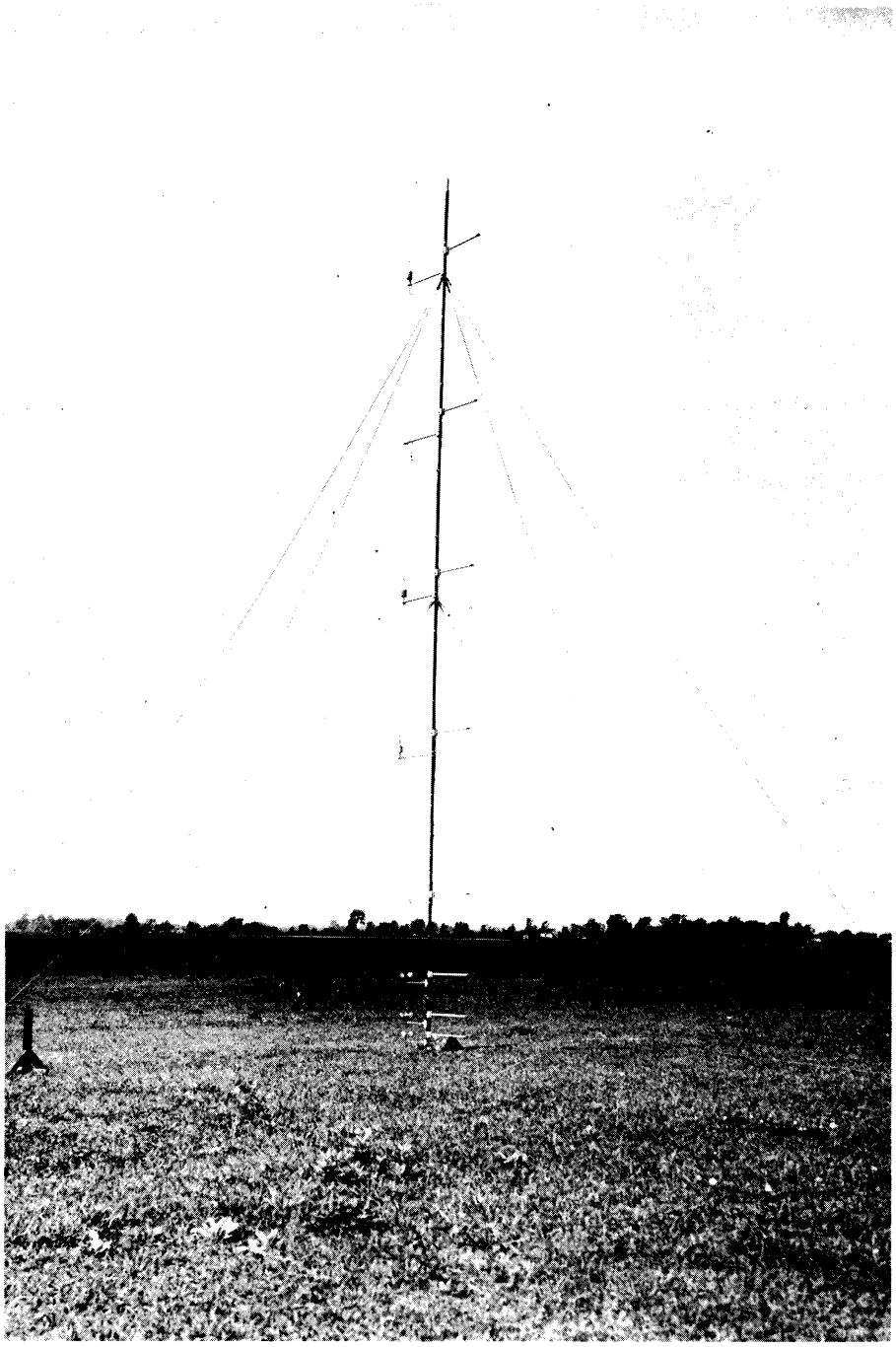

Fig. C.8. The aneomometer mast. (Courtesy D. J. Portman.) In-season experiment 1962.

Recording of the anemometer pulses was accomplished by Veeder Root counters with decade output in parallel with an Esterline Angus 20 pen operations recorder.

C.4 AIRCRAFT EQUIPMENT

C.4.1 The Aircraft

The Cessna 172 stock model, single engine, light utility aircraft shown in Fig. C.9 was used to carry out the upper level sampling. The engine was rated at 145 HP giving the aircraft a maximum load capacity of 2200 lbs. The following weights were recorded; the aircraft, 1370 lb; the fuel supply, 252 lbs; and the personnel, 320 lbs, leaving only 258 lbs available for equipment. The loaded climb rate of the aircraft was 500 ft min^{-1} near the ground, reducing to 200 ft min^{-1} near 8000 ft.* The fuel supply provided for four hours of flying time.

Figure C.10 shows the pilot and a scientist seated in the aircraft. Immediately behind the scientist one can see a battery box and behind his head a water supply bottle for the wet thermocouple. Figure C.11 is a sketch of the position of various pieces of equipment as they were fastened into the aircraft.

C.4.2 The Power Supply

Two sources of D.C. power were used to operate the sampling and

*There was some question as to whether the pilot was getting the best performance from the aircraft.

Fig. C.9. The Cessna 172 aircraft. One drum sampler can be seen under the wing at the right. In-season experiment 1962.

Fig. C.10. Pilot and scientist in the Cessna 172 aircraft. In-season experiment 1962.

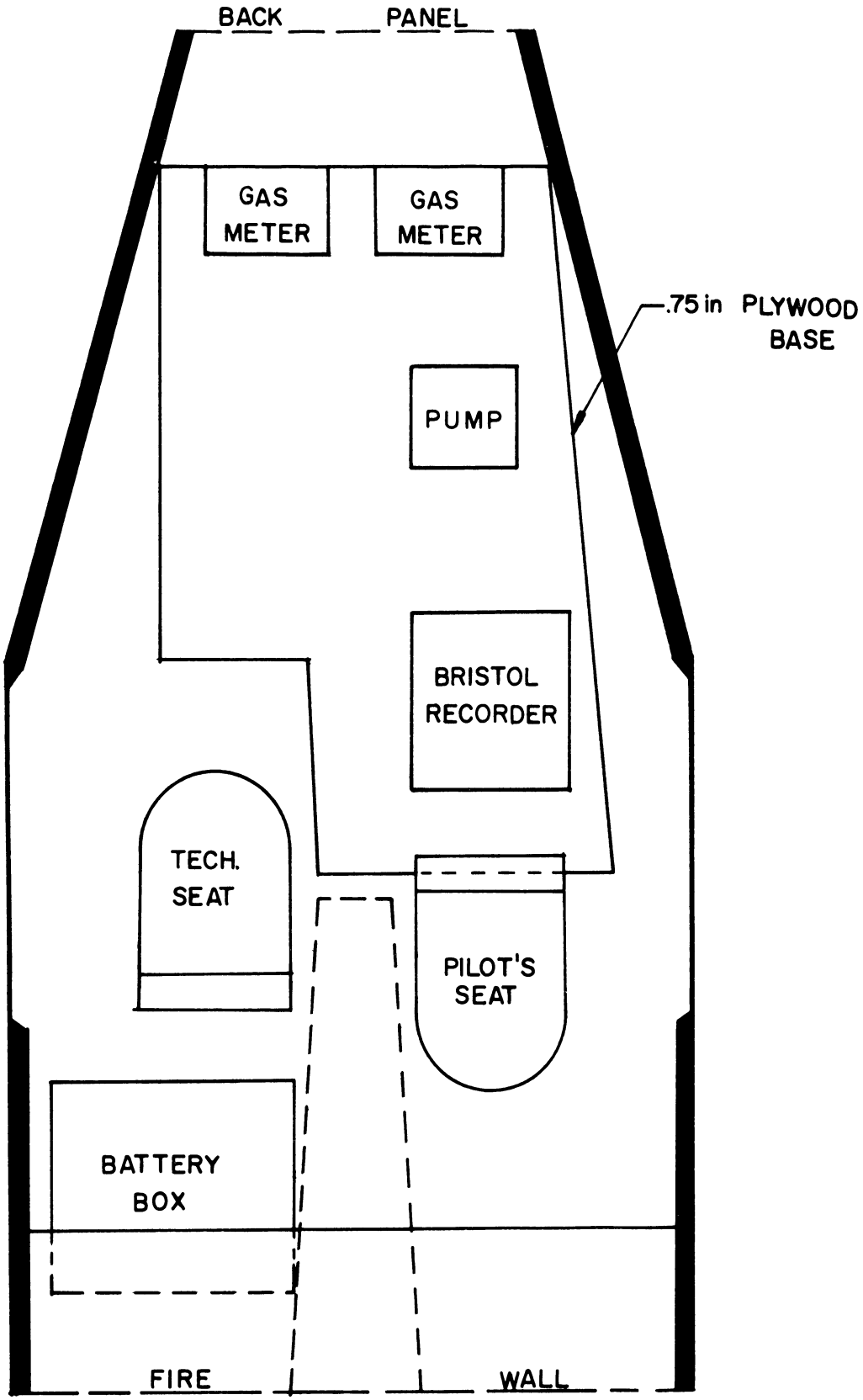

Fig. C.11. Plan view of the instrument location within the aircraft. In-season experiment 1962.

recording equipment in the aircraft. First the aircraft itself has a 12 volt, 35 amp system which can be tapped through the cigarette lighter. Second, two heavy duty Delco 12 volt batteries were connected in series to provide 24 volts. Six batteries were used in all, four attached to a quick charge unit on the ground and two in the aircraft.

C.4.3 The Pollen Sampler

Two drum samplers (Metronics Associates) were carried by the aircraft, one attached to the struts below each wing as shown in Fig. C.12. The details of the sampler have been described fully elsewhere (Sheldon and Hewson, 1960) and will not be repeated in detail. In Fig. C.12 the back of the sampler enclosing case is open exposing the drum.

The drum sampler was originally designed for use with a fluorescent tracer of about 2μ mean diameter. Ragweed pollen is one order of magnitude larger and, for efficient collection requires certain modifications in the sampler. According to the manufacturer a particle the size of ragweed pollen is retained with 100% efficiency if the intake velocity is 20 liters min^{-1} and the nozzle to drum separation 0.080 in., whereas at higher speeds or smaller separation distances some pollen may be blown off the drum. Details of the modified nozzle design are given in Fig. C.13.

In sampling, one must be concerned about two efficiencies, collection and retention. With a sampling rate of 20 liters min^{-1} the

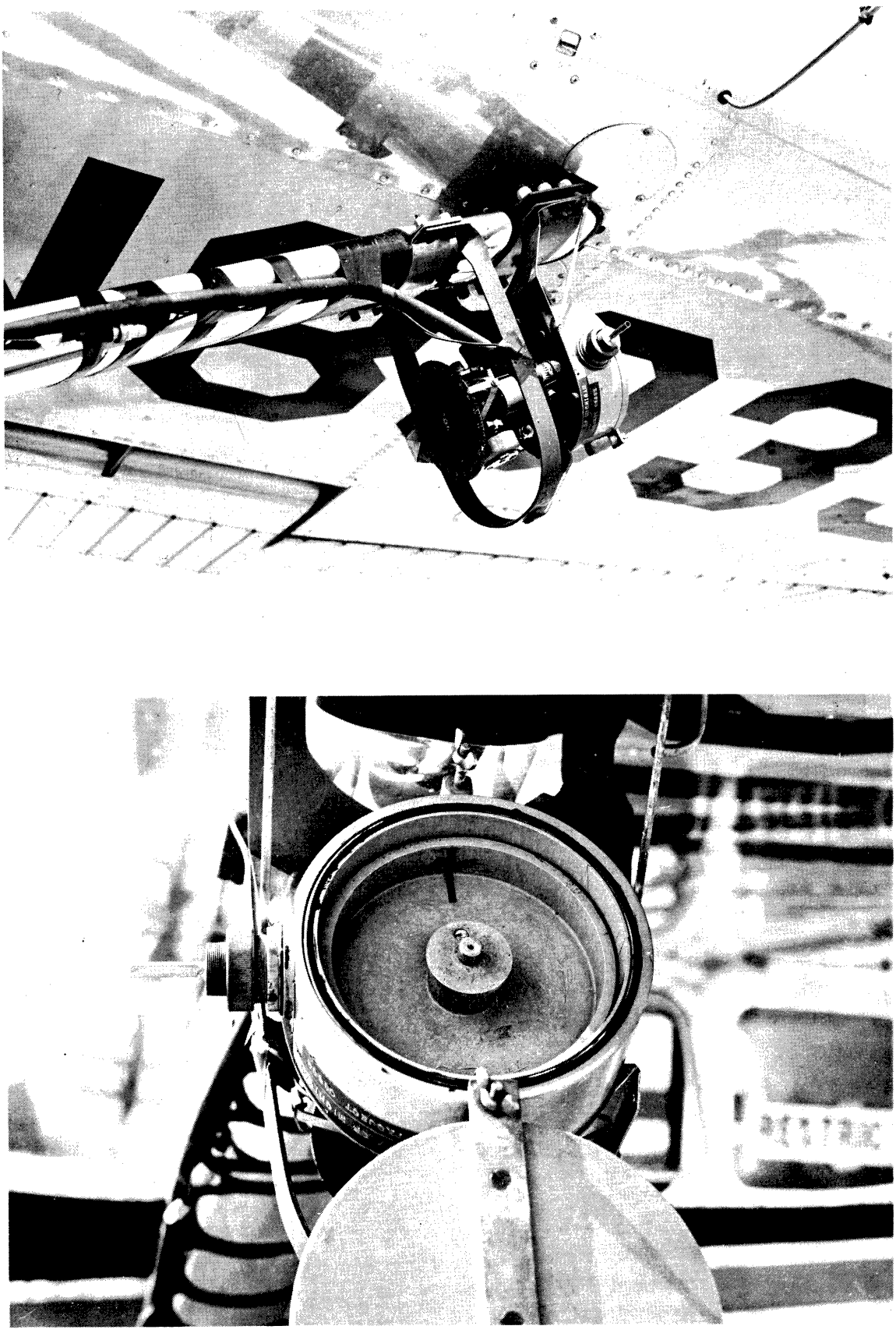

Fig. C.12. Detail of the drum sampler mounting and interior view of the drum sampler. In-season experiment 1962.

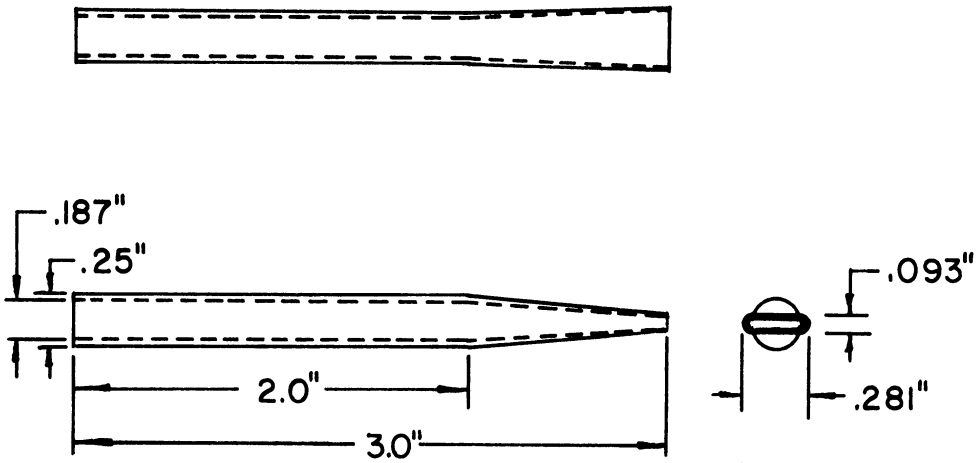

Fig. C.13. Schematic diagram of the drum sampler entrance tube. In-season experiment 1962.

intake velocity is only 40 mph or half the speed of the aircraft. This means that the sampler will indicate a concentration higher than that actually experienced. It was decided that the error due to aniso-kinetic sampling could be estimated more readily than the lack of retention and therefore the sampler was run at the rate suggested by the manufacturer. The ratio of the measured to true concentrations was estimated to be about 1.22 (Watson, 1954).

The sampling surface of the drum was spray painted black to facilitate identification and counting of the pollen. A layer of dilute rubber cement (1 part cement to 10 parts thinner) was sprayed over the paint. After sampling, the drums were stored in sealed cans and later counted using reflected light under an especially adapted microscope.

Vacuum for the sampler system was supplied by a 24 volt D.C. motor driven Leiman Bros. centrifugal air pump. A Stewart Warner vacuum meter measured the pressure drop across the pump. Two Rockwell Synthetic-V gas meters, accurate to 1%, were used to measure the volume flow to the drum samplers.

C.4.4 The Temperature Measurement

Wet and dry copper-constantan thermocouple units were installed in a 2 in. diameter T shaped chromium plated cylindrical radiation shield attached first to the step and later to a wing strut of the aircraft as shown in Fig. C.14. The wet thermocouple was located downwind of the dry. Water was conducted from an inverted plastic bottle

Fig. C.14. The wet and dry thermocouple mounting. In-season experiment 1962.

reservoir by a rubber hose to a shoe lace wick covering the wet thermojunction.

The temperature difference between the exposed thermojunctions and a standard temperature maintained in a thermos flask was recorded on a Bristol 0-1 mv Dynamic Recorder. The temperature in the thermos was read by means of a mercury in glass thermometer installed in the thermos through the cork. The water temperature of the standard was quite constant, varying less than 0.1°C hr^{-1}. To record the full range of temperatures the input from the thermocouples was fed through a five range positioning potentiometer to the recorder. Wet and dry thermocouple readings were made alternately at three second intervals by means of an automatic timer switch.

C.5 PROCEDURE

Observations were conducted on six days during the peak of the 1962 ragweed season: August 25 and August 27-31. The weather maps at 0600 GMT for the period August 25 through August 31 are shown in Fig. C.15.

C.5.1 Ground Observations

On all regular observation days, August 27 to 31 the meteorological equipment was started at 0500 or 0600 and stopped at dark. Charts were time marked each half hour. A sling psychrometer was used to check the wet and dry bulb temperature at a height of about 1/2 to 1 m and this value recorded on the chart as a crude check on the thermocouple meas-

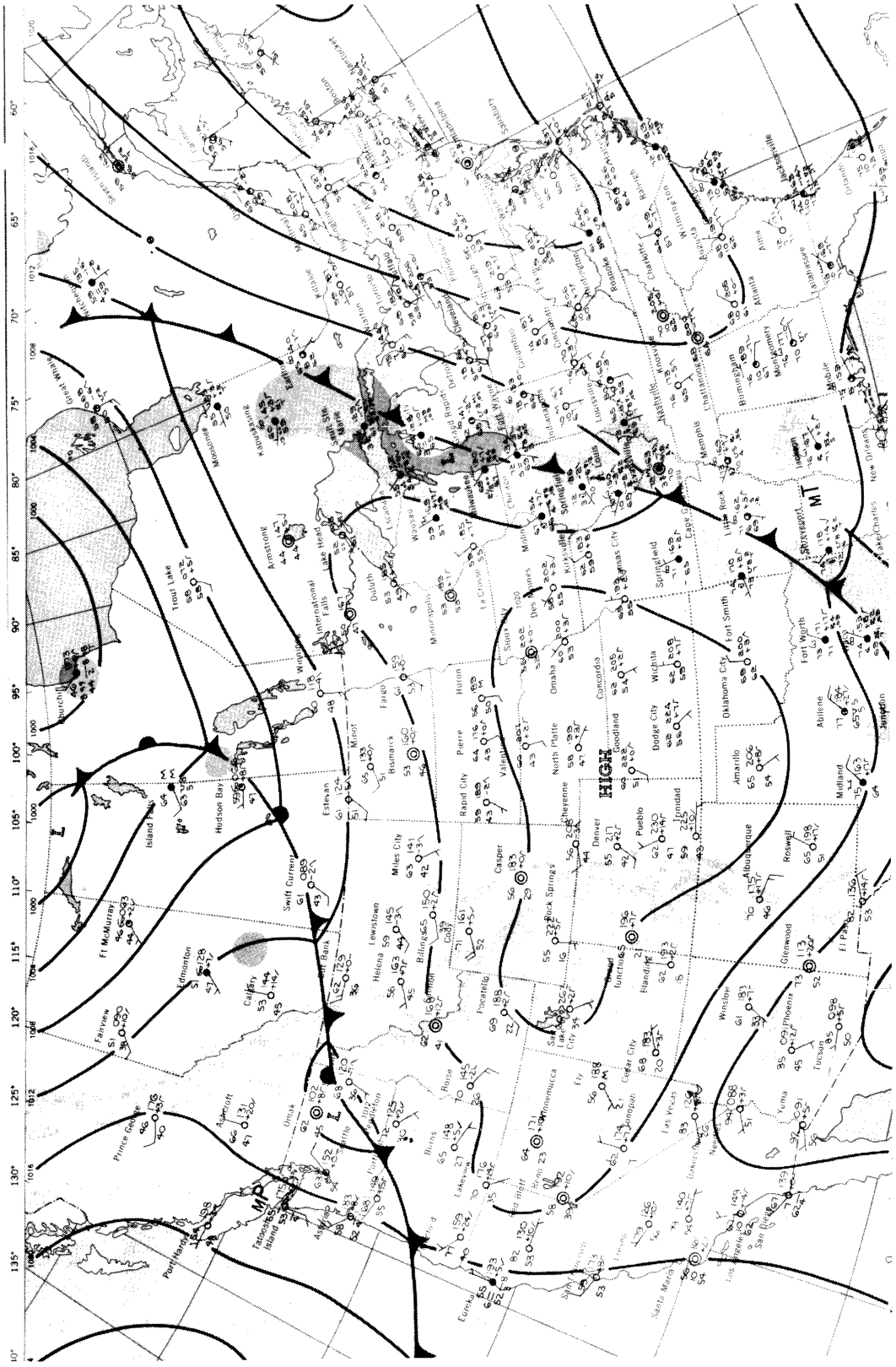

August 25, 1962.

Fig. C.15. U. S. Weather Bureau sea level weather maps 0600 GMT.

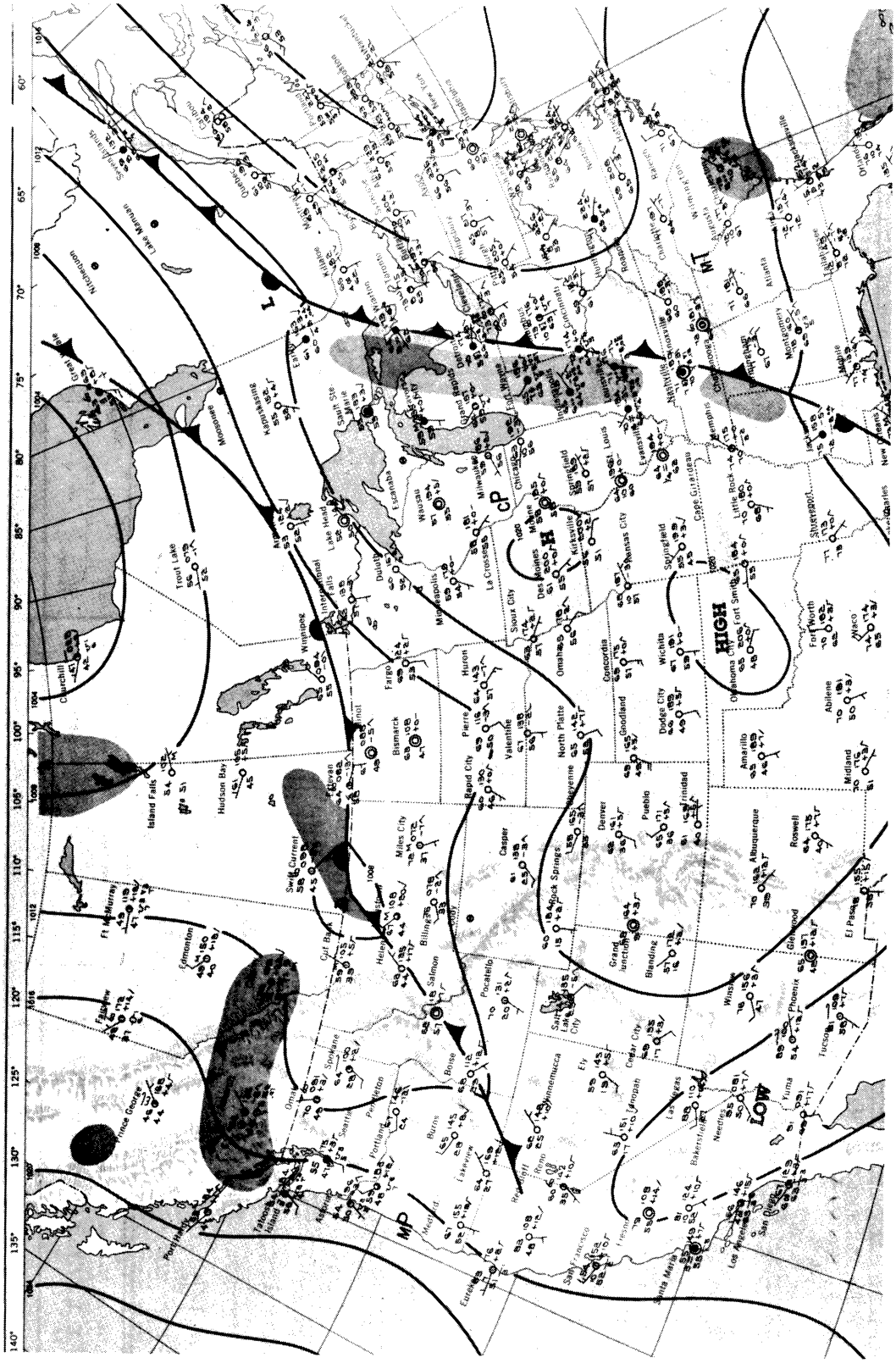

August 26, 1962

Fig. C.15 (Continued)

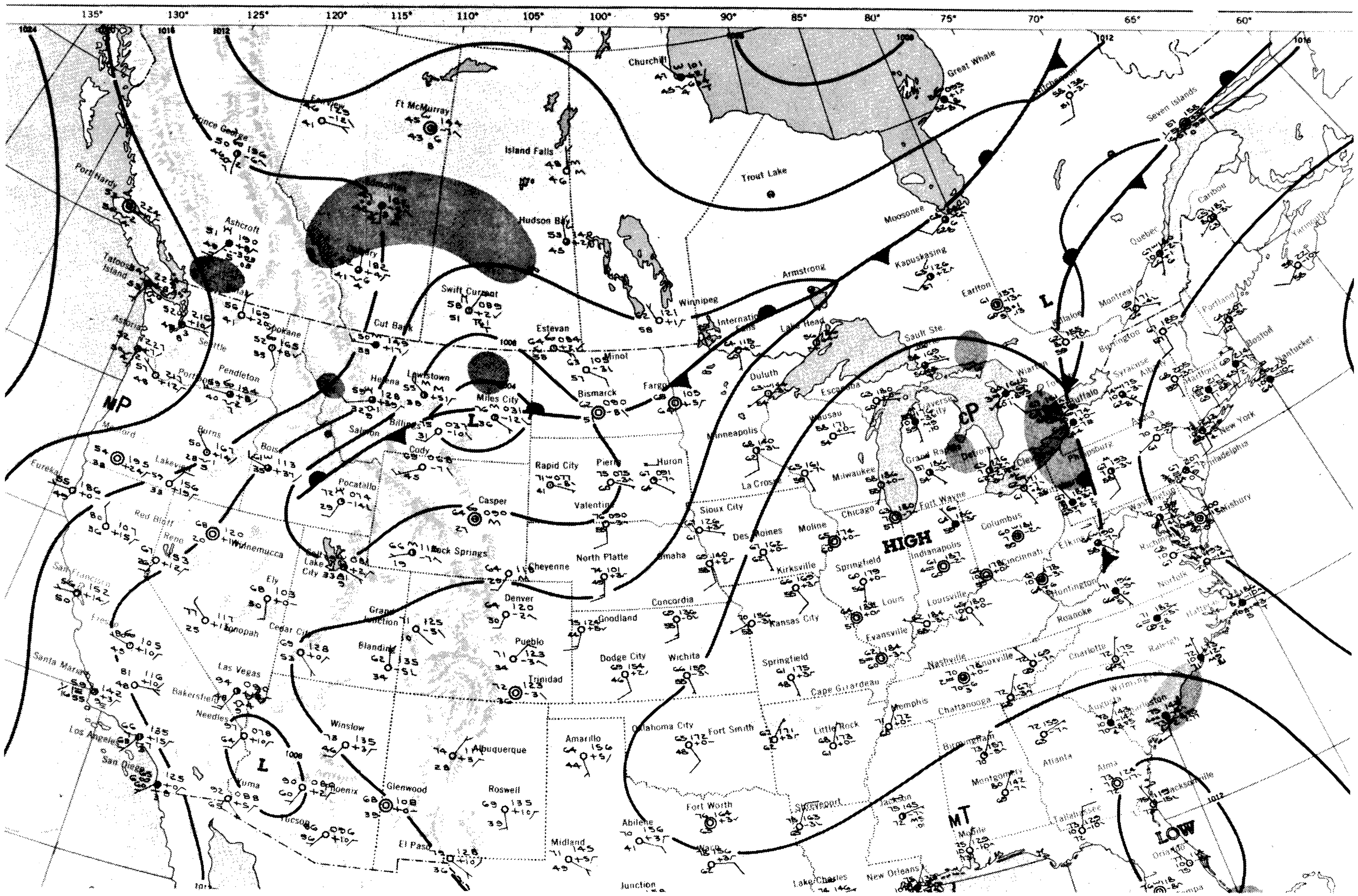

August 27, 1962

Fig. C.15 (Continued)

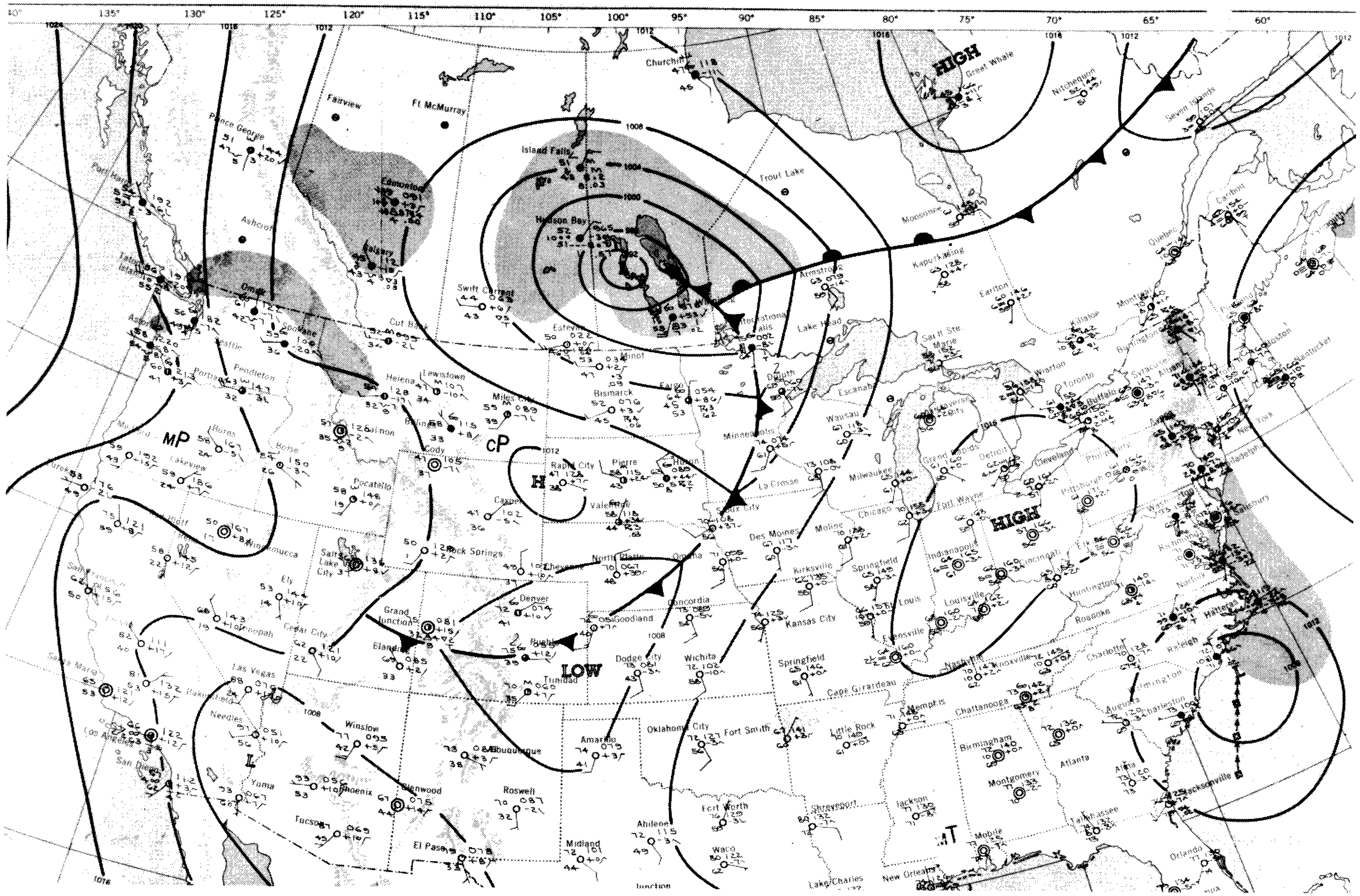

August 28, 1962

Fig. C.15 (Continued)

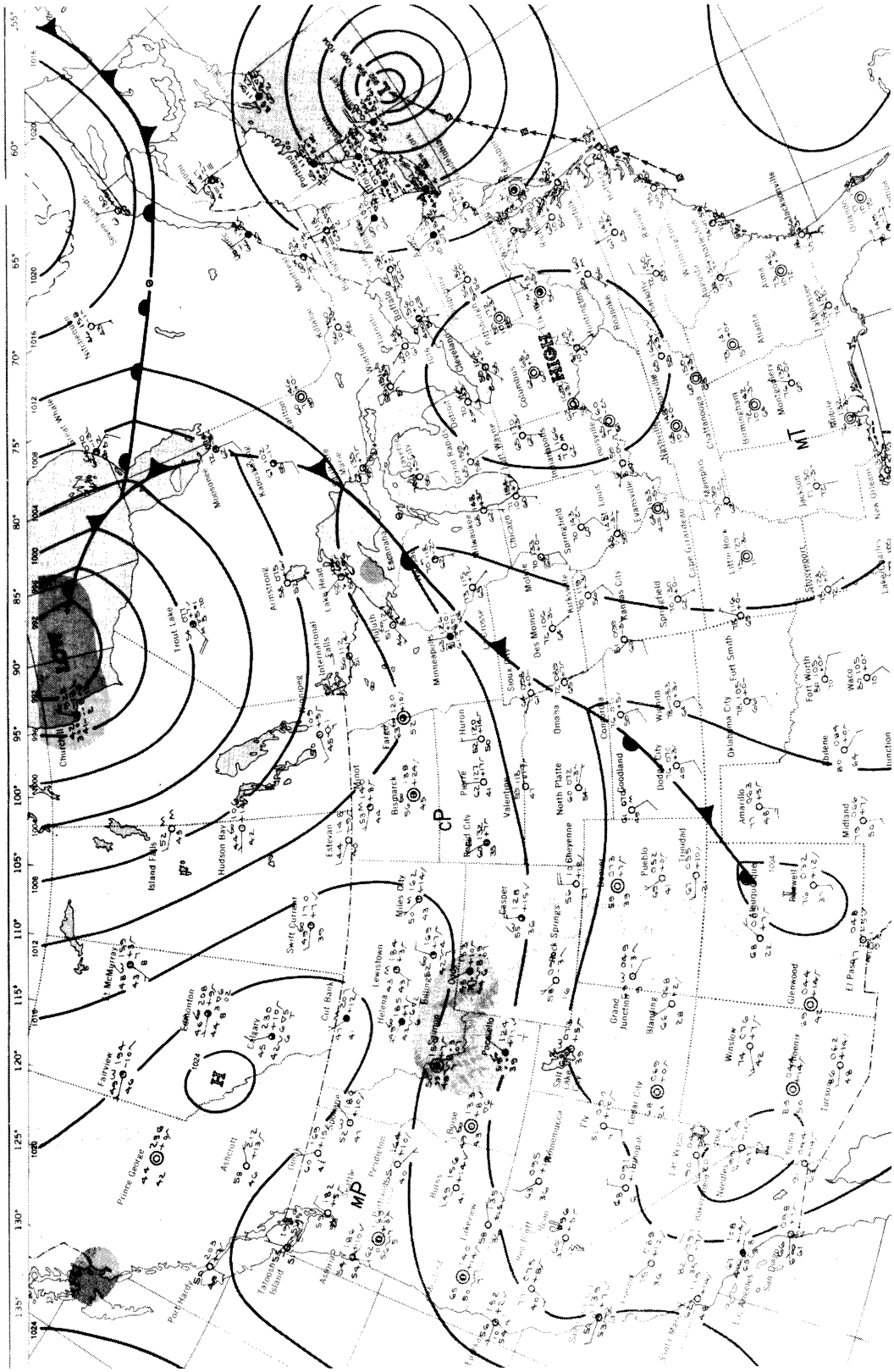

August 29, 1962

Fig. C.15 (Continued)

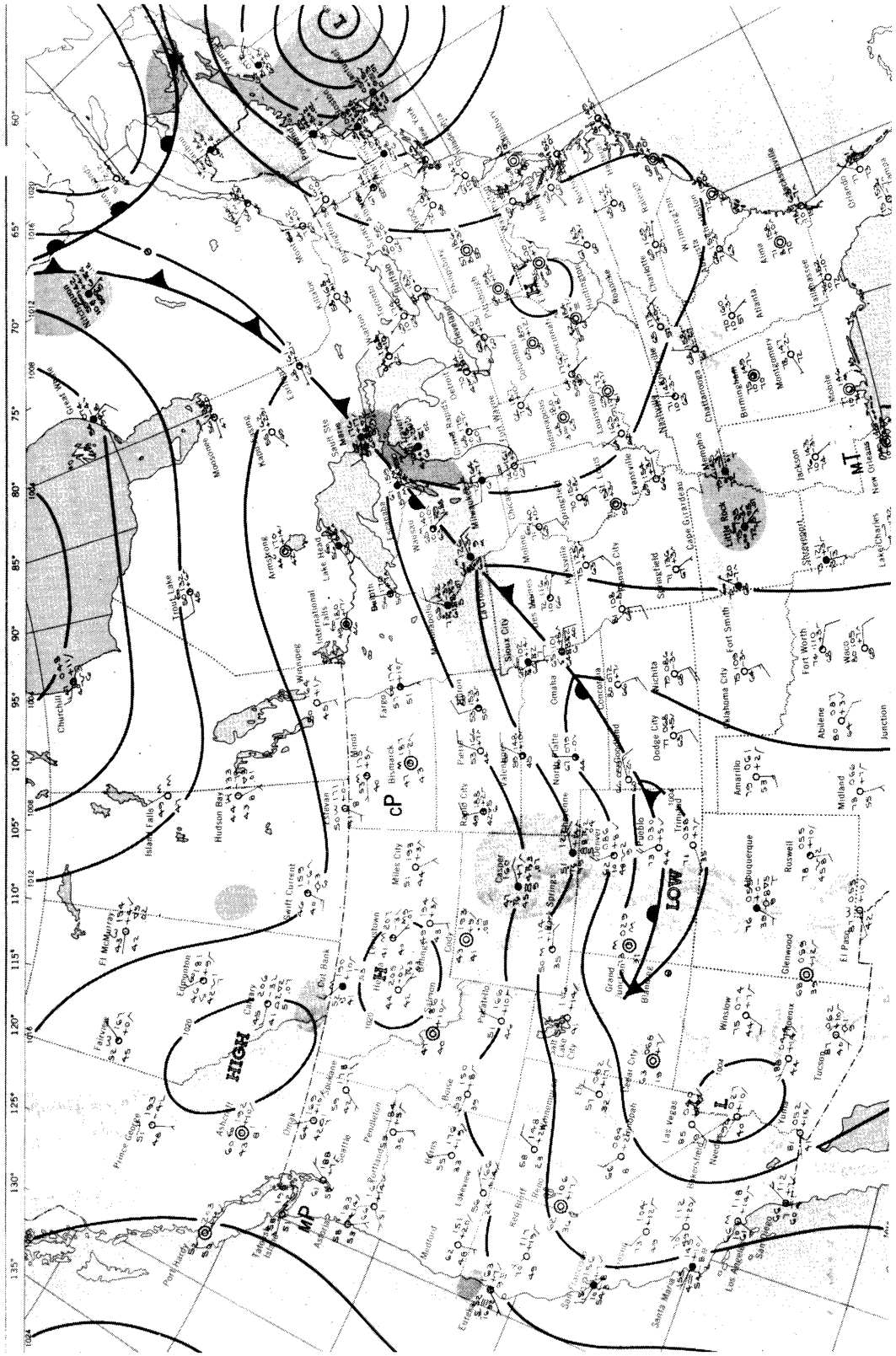

August 30, 1962

Fig. C.15 (Continued)

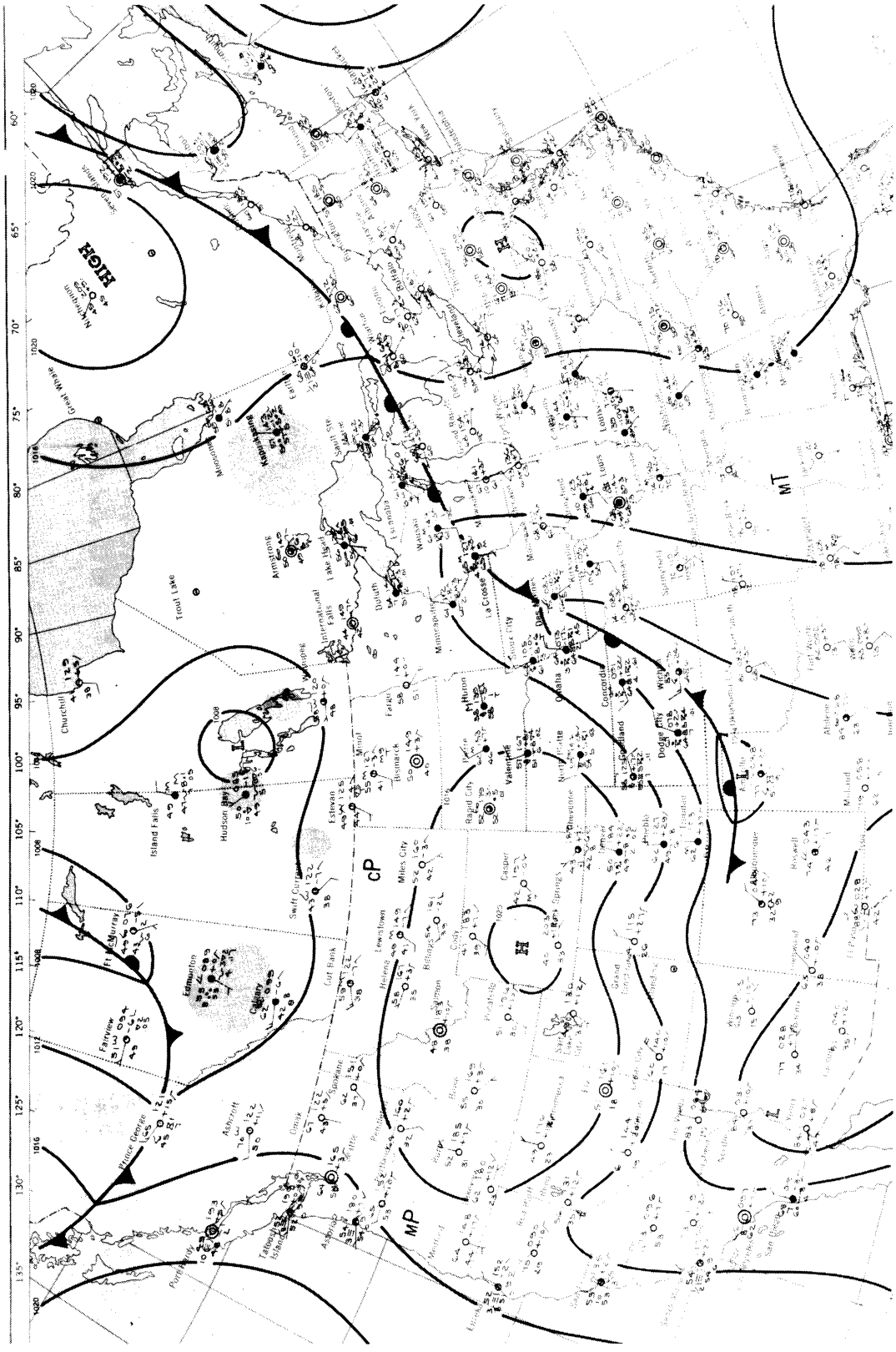

Fig. C.15 (Concluded)

urements. Weather elements such as dew, fog, precipitation, visible sun and cloud were recorded at irregular intervals when a major change occurred in one of the elements. In addition the time at which ragweed floret dehiscence started was recorded.

The pollen sampling equipment was started on the hour (at 0500 or 0600) and samples taken every hour during the morning and every second hour during the afternoon. In case of rain, samples were planned at 15 min intervals.*

C.5.2 Aircraft Observations

A vertical profile of temperature, humidity and pollen concentration was observed at 2 hr intervals during the morning and at 4 hr intervals during the afternoon and evening.

Before each flight the water feed to the wet thermocouple was adjusted to give a slow drip, fresh batteries were installed when needed (every second or third run), the drums were installed and tested and the recorder and pumps were tested. During the runs of August 25 sampling was conducted both on ascent and descent. Later, due to the very slow rate of ascent of the aircraft, sampling was conducted only on descent. During each run pollen samples were taken at 8000, 4000, 2000, 1000, 500, 250, 125 and 60 ft above Willow Run Airport. The aircraft flew either due north or south along a route centered over the

*This latter was a cooperative arrangement with Mr. Gatz who was sampling the washout of pollen and other materials by rain.

ground based tower. At the end of each leg of the flight the aircraft descended to the next lower level and returned along the same route. The sampler drums were rotated by a switching arrangement within the aircraft to produce one sample at each level and one sample between levels. To save the batteries the pump was switched off during a portion of the descent during some of the runs. When this procedure was followed the pump was always turned on for a minute prior to the beginning of the next sample in order to clear the nozzle of pollen. Sample by sample records of the vacuum gage reading, gas meter readings, time, altitude and drum position were made. Frequent time and height checks were entered on the Bristol recorder chart. In addition the standard temperature thermometer was read at the beginning and ending of each flight.

C.5.3 Data Abstraction and Processing

C.5.3.1 Pollen Samples

The rotobars and drums from the tower and aircraft samplers respecitively were observed under a microscope at 100x magnification by an experienced staff. The rotobar counts were converted to concentration by assuming equivalence between the tower and aircraft measurements at 60 ft.

C.5.3.2 Aircraft Temperature Observations

Temperature data from the aircraft were abstracted to the nearest .1° Celsius and averaged over the duration of flight at a given level.

It was desirable to eliminate advective temporal trends from the temperature data because, as indicated in Sect. C.1, no allowance can be made for such changes within the framework of the theory proposed here. The procedure used was as follows: The temperature at a given level over the 5 day period in question was approximated by a third order polynomial of the form

$$T = a_0 + a_1 t + a_2 t^2 + a_3 t^3 \qquad (C.3)$$

where T is the temperature, t is the time and the a's are coefficients. At each observation time the value T on the curve representing the least squares fit of Eq. (C.3) to the temperature data at 4000 ft (see Fig. C.16) was substracted from the observed temperatures at all observation levels.

Observations of temperature profiles were made at 2 hr intervals in the morning and at 4 hr intervals in the afternoons. Each profile was observed over a period of from 1/2 to 1 hr and therefore interpolation was necessary if profiles were to be constructed for any particular time. The selection of a good interpolation scheme is critically important if temperature data are to be successfully employed for computing the eddy conductivity by the method of Eq. (C.2).

The interpolation method finally devised preserved the temperature values at the observation points, yielded reasonable values between observation points and was free from personal bias. An outline of the method follows:

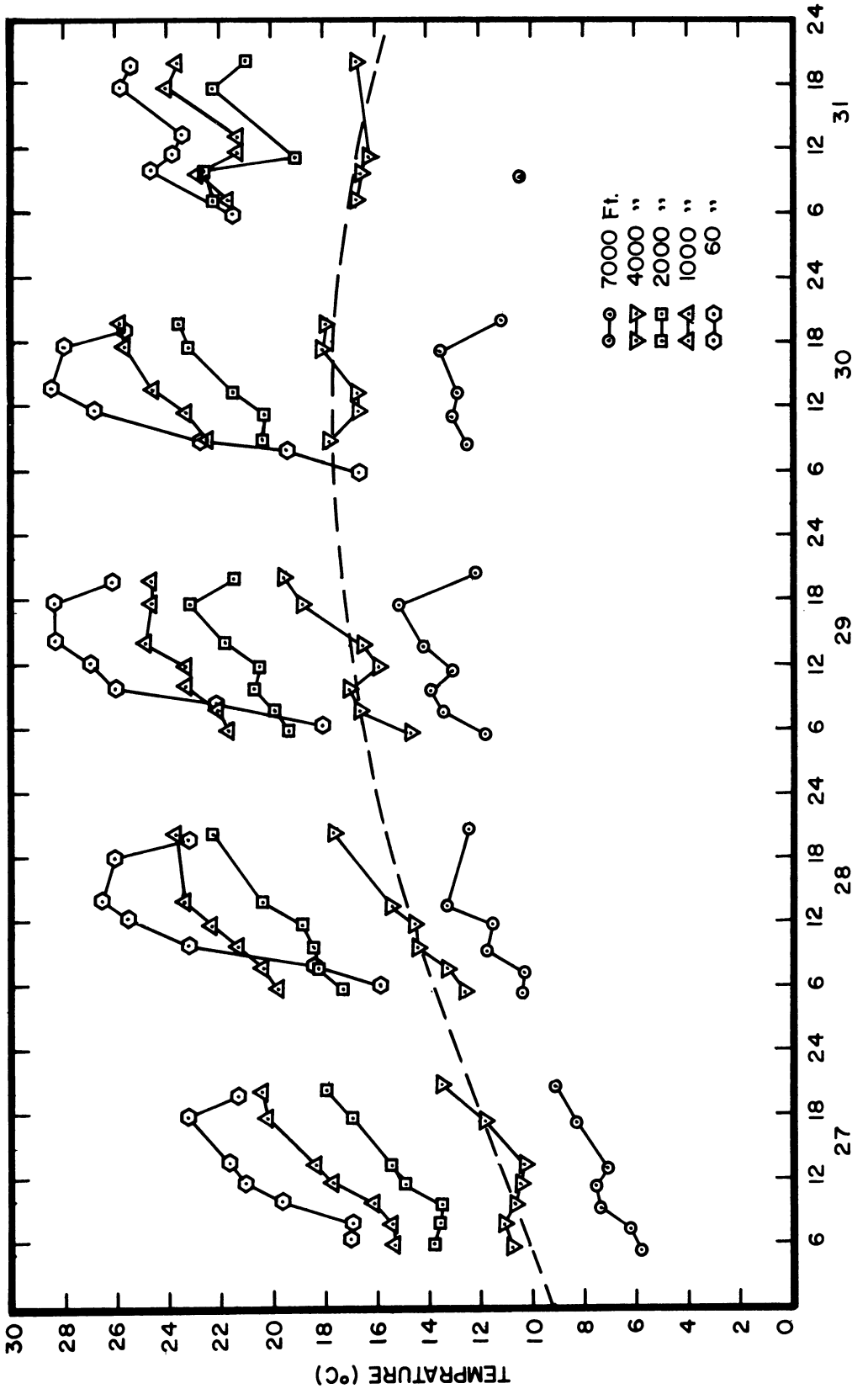

Fig. C.16. The aircraft temperature observations of August 27-31, 1962. The dashed line represents the least squares fit of a third order polynomial to the 4000 ft aircraft temperature observations.

1. An interpolation using second order Lagrangians divided differences was carried out for each day at each level between overlapping groups of three observations. This provided two estimates of the interpolation at each interior point except between the two points at the ends of the series.

2. Between the two end points a second estimate was achieved by linear interpolation.

3. At each time for which a profile was required the two estimates were averaged.

Similar systems using higher order interpolation were also tested, the highest order possible being six because only seven observations were obtained each day. In the case of a sixth order running interpolation each computed temperature was the average of six values.

The interpolation scheme above was tested on the temperature data measured at 60 ft on the meteorological tower. Seven temperatures were taken from the record at time intervals equal to those of the aircraft observations. All orders of interpolation from second to sixth were attempted and the results compared with the actual temperature observations at intermediate times. Second order running interpolation provided the best fit to the observed data and a more conservative estimate of the interpolated temperature than did higher order interpolation. A comparison of the interpolated and observed temperatures for the data of August 27, 1962 is shown in Fig. C.17.

The aircraft observations were spaced logarithmically with increasing height and therefore before proceeding with the solution to Eq. (C.2) it was desirable to investigate the kind of interpolation which would most reasonably represent the vertical temperature profile. It was

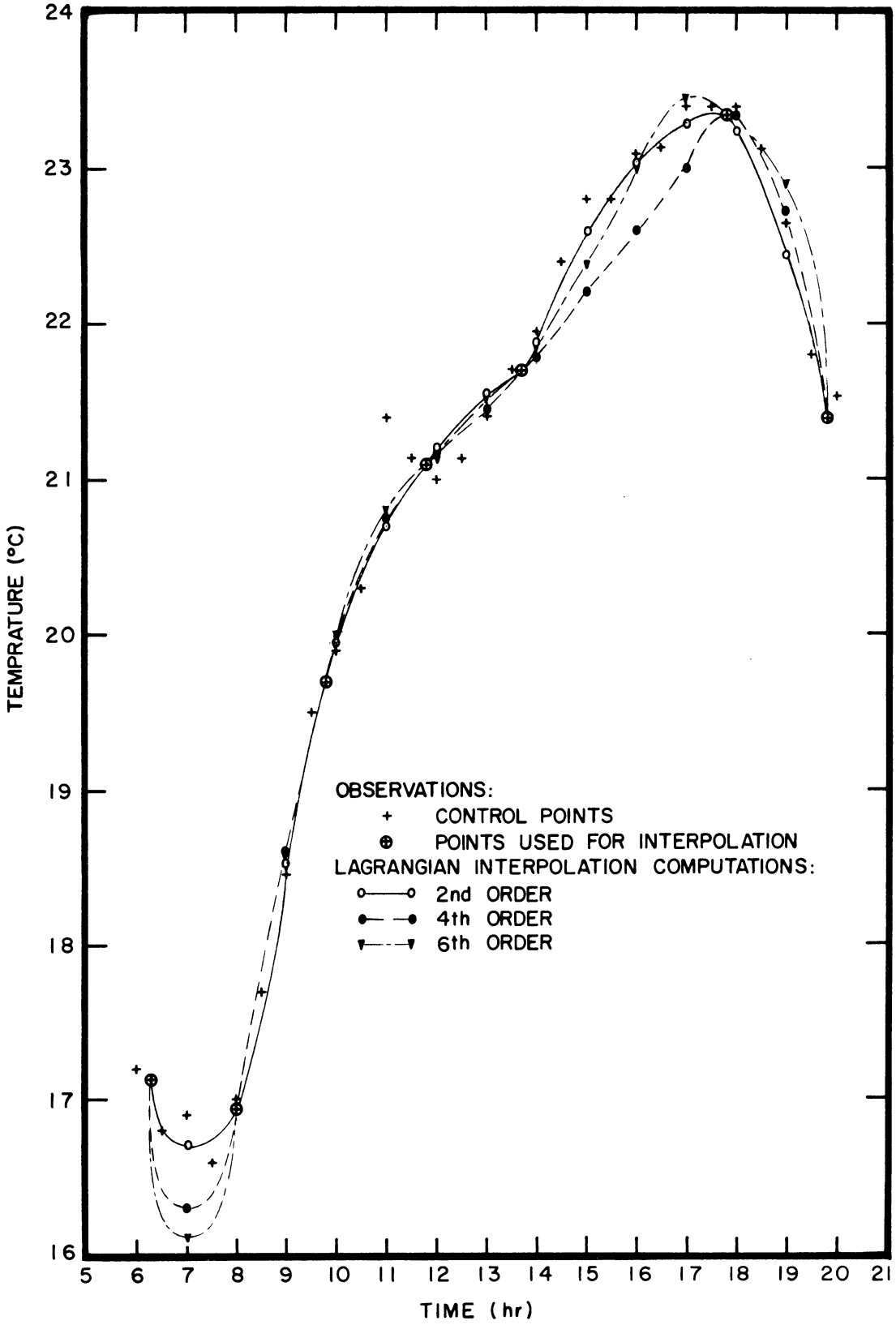

Fig. C.17. A comparison between temperatures obtained from a running second, fourth, and sixth order Lagrangian interpolation and observed temperature data at 60 ft. August 27, 1962.

found that running second order Lagrangian interpolation was most satisfactory; higher order interpolation was prone to produce extreme excursions in regions where data were sparse. Second and third order running Lagrangian interpolation are compared in Fig. C.18 for the aircraft temperature profile of 1700 EST August 27, 1962.

A program was written which would interpolate in time and then in height to produce a rectangular array of equally spaced observations. These observations, automatically punched on cards, were later used to compute heat fluxes and temperature gradients which in turn were used to find the eddy conductivity.

C.5.3.3 Tower Temperature Observations

The temperature record from the Brown recorder was abstracted to the nearest .1°F. The temperature profile data were required in the computation of the scale height, Richardson's number, the diffusivity, etc., all containing the derivative of temperature with respect to height. Because short period observations contain a great deal of high and medium frequency noise, and because derivatives are especially sensitive to such variability it was necessary to smooth the raw temperature data. The smoothing proceeded in two stages: first, half hour average temperatures were found and second, the profiles were graphed on either semi-log or log-log paper and a smooth curve fitted to the points. Temperatures read from the smooth curves were used in the computations mentioned above.

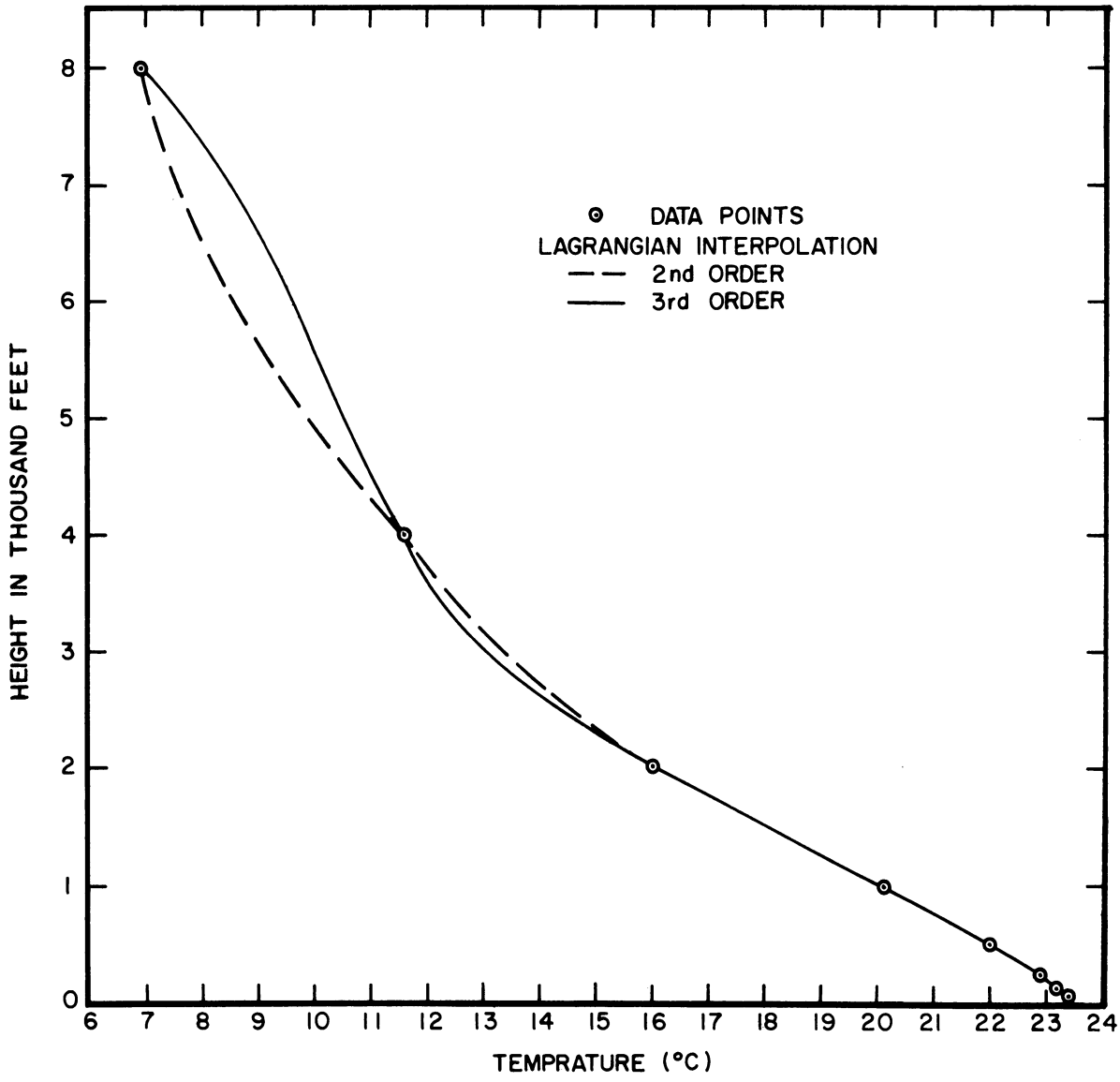

Fig. C.18. Third and second order running Lagrangian interpolation on the temperature data of 1700 EST. August 27, 1962.

C.5.3.4 Wind Observations

Half hour averages of the wind speeds were recorded. Once again a refined smoothing procedure was needed in order to compute derivatives. The wind data were graphed on semi-log or log-log paper and smooth curves drawn through the points. The wind values from the smooth curves were used in the computations of scale height, Richardson's number, etc.

C.6 RESULTS

C.6.1 Observations

The observations are contained in tables at the end of this appendix as follows:

Table C-1* Aircraft Pollen Observations

Table C-2 Weather Observations

Table C-3 Aircraft Wet and Dry Thermocouple Observations

Table C-4 Tower Pollen Observations

Table C-5 Tower Wet and Dry Thermocouple Observations

Table C-6 Tower Wind Observations

C.6.2 The Computation of Eddy Diffusivity Near the Ground

C.6.2.1 Introductory Remarks

Of the many methods mentioned in Chapt. 6, for the computation of the eddy diffusivity near the ground, the data taken in 1962 permit

*Tables not included in the Appendix will be found in Volume III.

the use of only those techniques utilizing profiles of wind and temperature. Most of these techniques require the prior computation of the Richardson number Ri and therefore the next few paragraphs will be devoted to a discussion of observations of this parameter.

C.6.2.2 Computations of the Richardson Number

The Richardson number is usually written in the form

$$R_i = \frac{g}{\theta} \frac{\partial \theta}{\partial Z} \Big/ \left(\frac{\partial U}{\partial Z}\right)^2 \qquad (C.4)$$

where θ is the potential temperature. The methods of Sect. C.5.3.3 and C.5.3.4 were utilized to determine smoothed values of the potential temperature and wind speed profiles. The Richardson numbers, computed from that data using Eq. (C.4) are given in Table C-7.

The value of Ri observed at 2.5, 5.5, 8.5, 11.5, and 14.5 m for the four days August 27 - 31, 1962 are shown in Fig. C.19. The period of observation was one of light winds and strong insolation and therefore the computed Richardson numbers do not conform to the values usually published, these usually being observed during relatively strong wind conditions.

Near the ground Ri may be seen to follow a pattern reported frequently in the literature: soon after sunrise it decreases rapidly from its nocturnal positive values to small negative values which it more or less retains during the day, increasing to positive values again in the late afternoon.

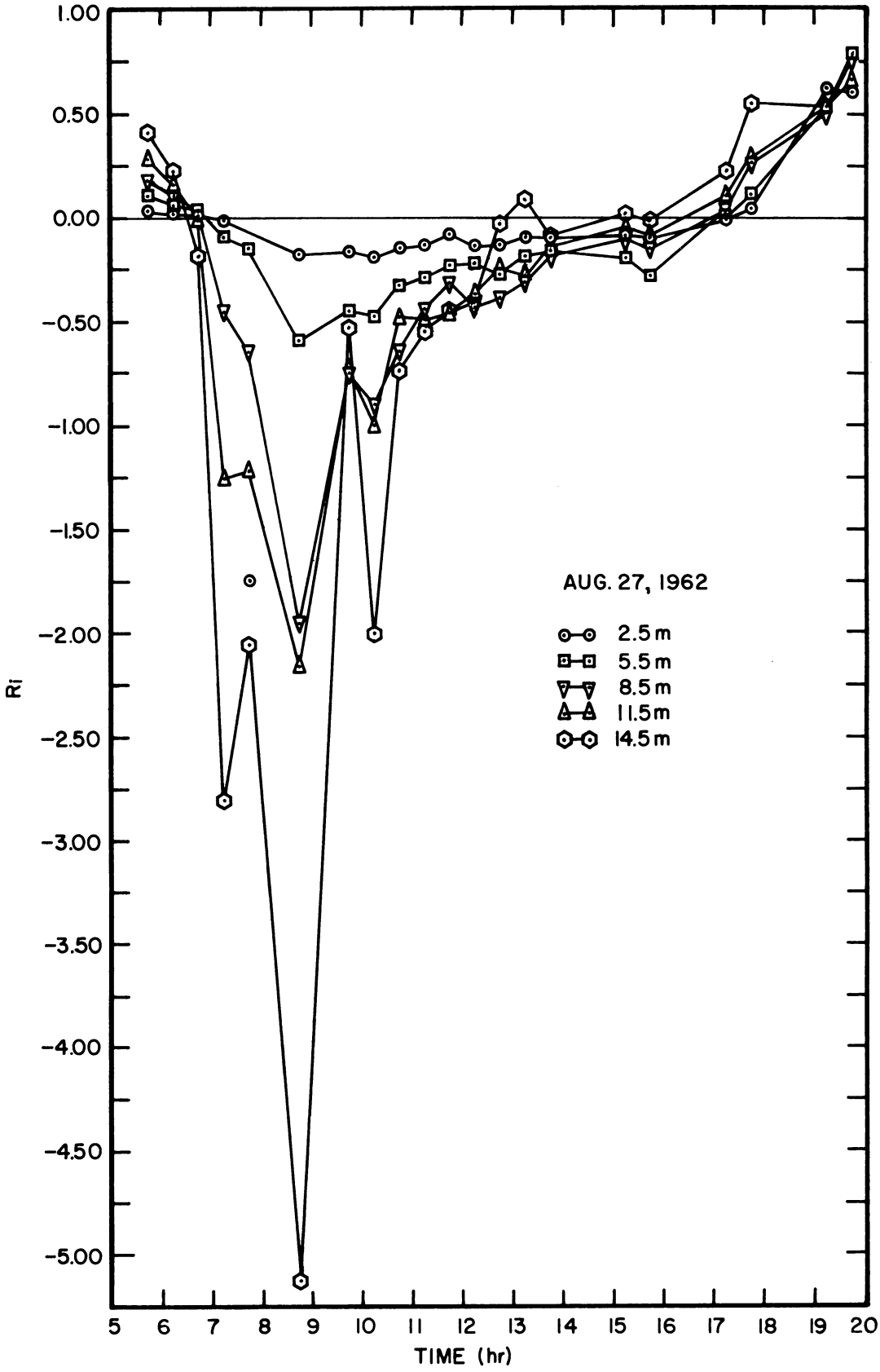

Fig. C.19. The Richardson's number. In-season experiment 1962.

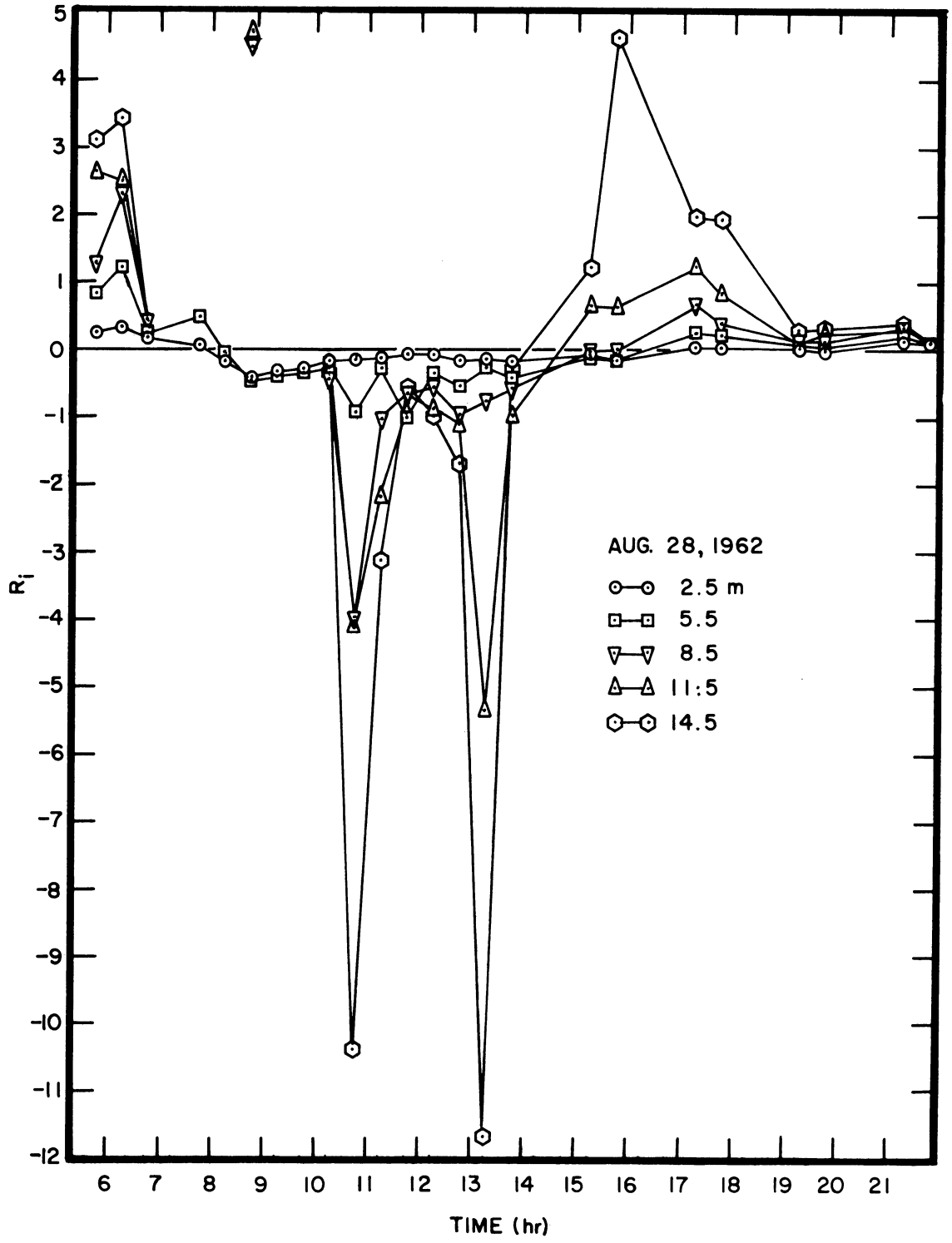

Fig. C.19 (Continued)

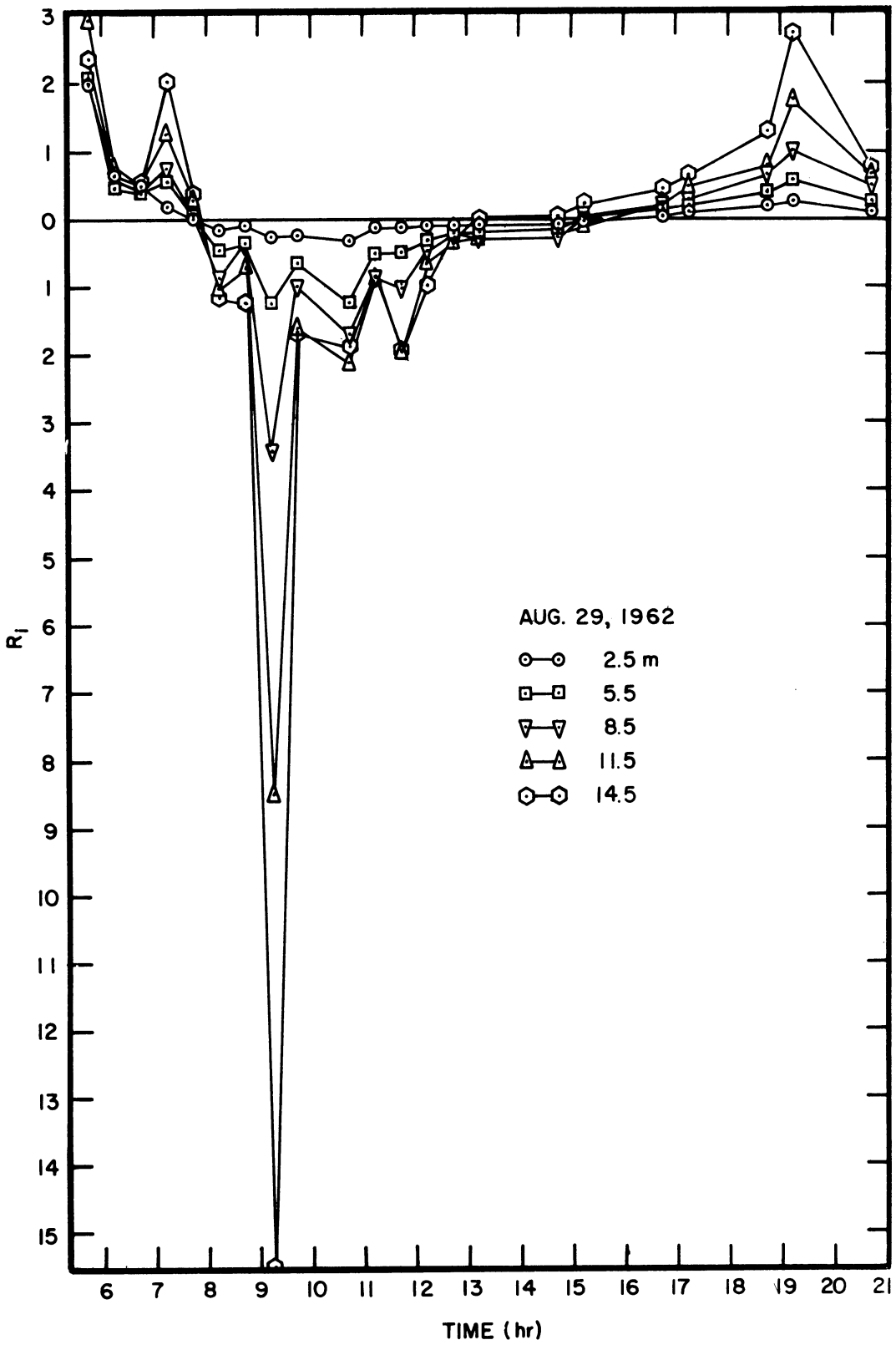

Fig. C.19 (Continued)

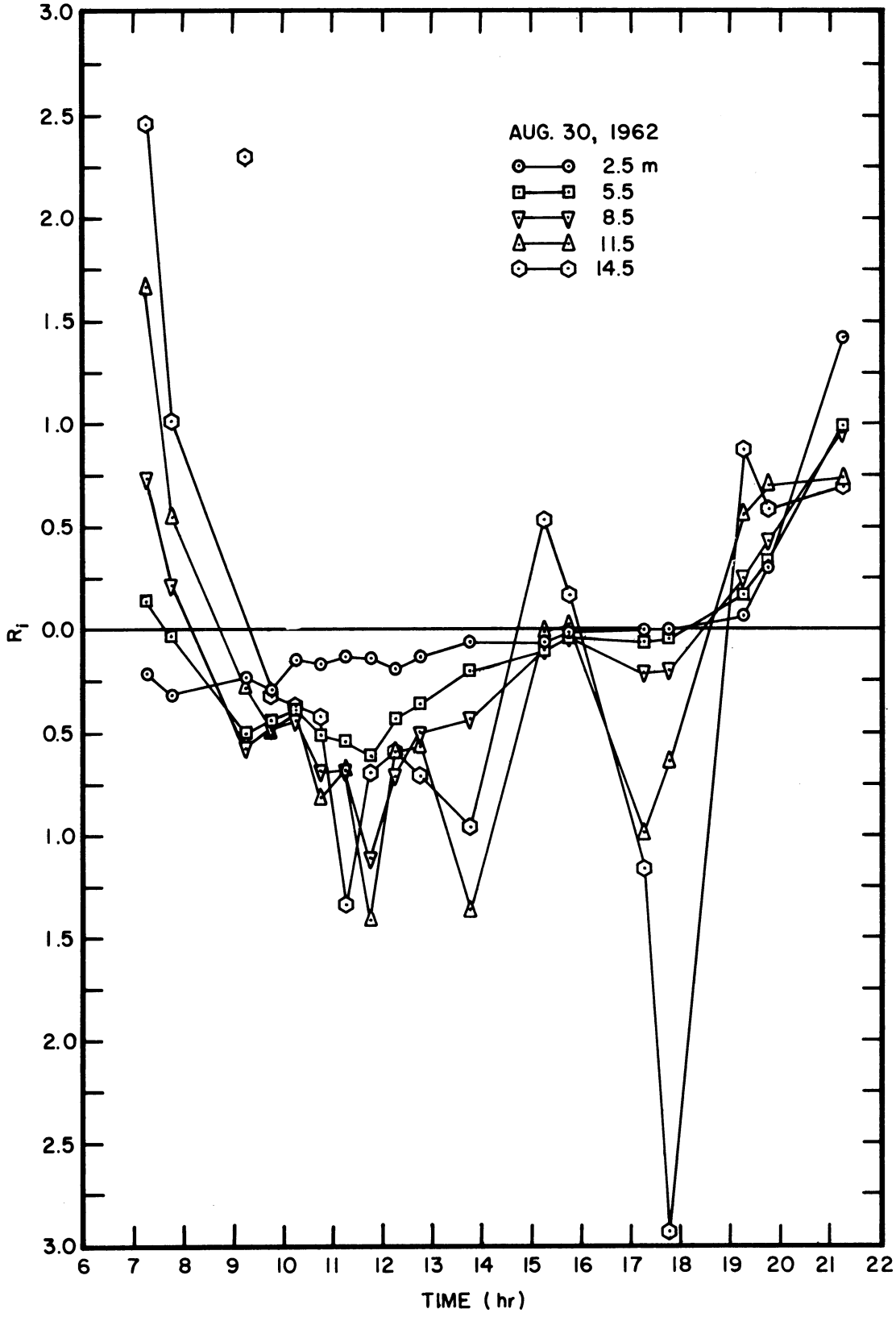

Fig. C.19 (Concluded)

Well above the ground a different pattern emerges: Ri decreases very rapidly after sunrise to a negative peak well below the threshold required for natural convection, i.e. Ri < -1, and immediately thereafter increases at first rapidly and then more slowly, finally reaching a zero or slightly positive value shortly after noon. Still later and well before sunset Ri becomes increasingly positive, achieving values in excess of the so-called critical Richardson number, i.e. +0.3.

The unusual nature of the results leads one to suspect the observations upon which they were based; however, confirmatory evidence is given by Priestley (1959, p. 51) who reports several sets of similar observations. As far as the present observations are concerned the author has complete confidence in the temperature data, but less confidence in the wind data (see sources of error below). In spite of the inadequacies of the wind observations it is felt that the overall trends and magnitudes of the Ri curves are correct. If the curves are accepted they show that the natural convection regime extends briefly down to within about 5 m of the ground during typical calm sunny summer weather, and that weak inversions are not uncommon at 15 m during mid-afternoon.

The rapid increase in Ri after the morning minimum must be associated with the commencement of natural convection. Support for this conclusion is provided by the detailed variations of the temperature record shown in Fig. C.20. For example the temperature at 12 m on August 29 is observed to rise smoothly and rapidly from the nighttime

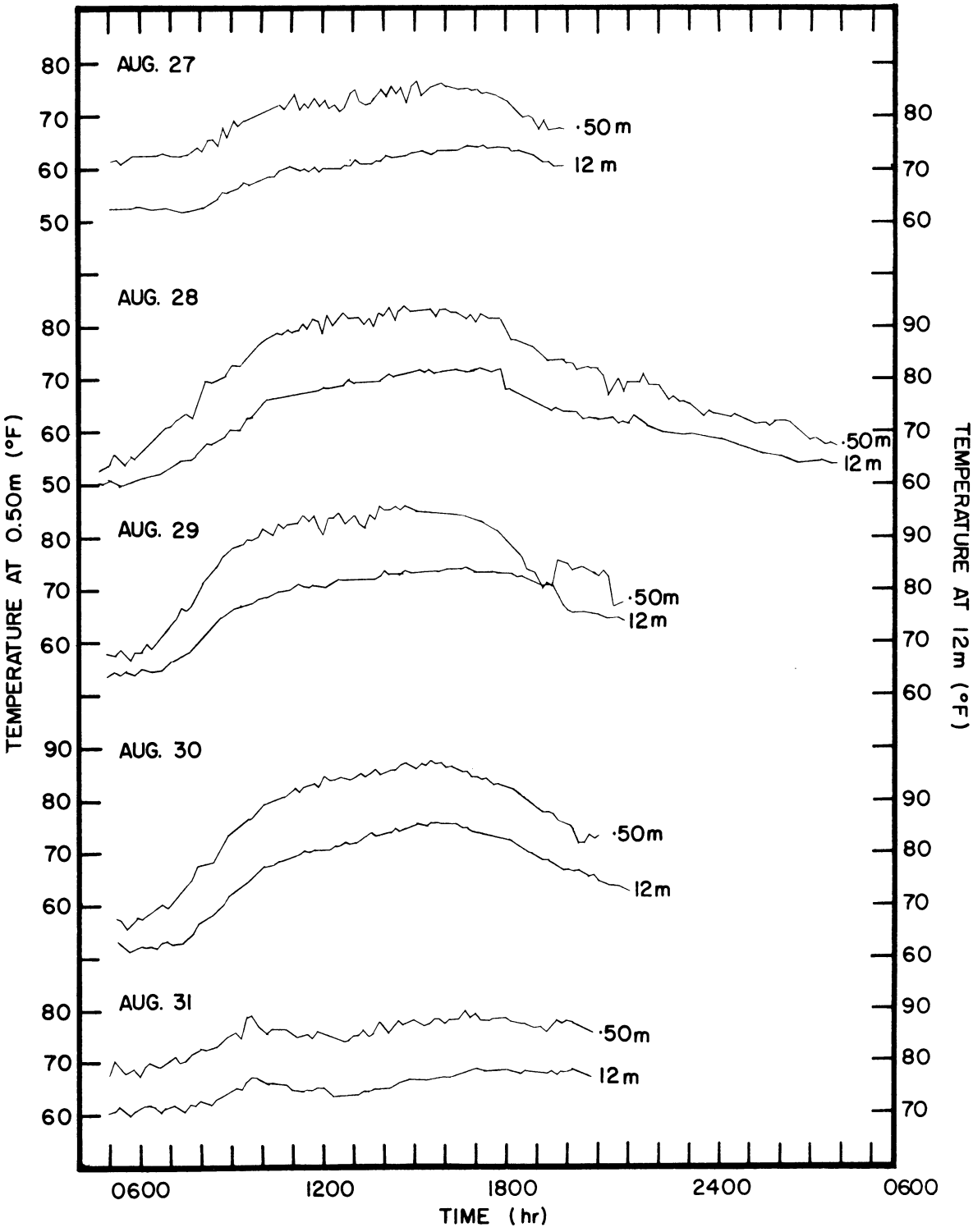

Fig. C.20. The temperature at 0.5 and 12 m measured at 10 min. intervals. In-season experiment 1962.

minimum reaching about midmorning a point at which the slope decreases abruptly and the trace becomes unsteady. It is logical to assume that the cessation of rapidly rising temperature is coincident with the commencement of natural convection. The same pattern is observed, although less distinctly on the other clear days.

The information contained in the temperature and Ri traces suggest the following sequence of events: in the early morning, rapidly increasing temperatures at the ground and damping of convective activity by the nocturnal inversion further aloft combine to cause a steep temperature gradient near the ground and consequently a high negative Richardson number. When the magnitude of the negative Richardson number exceeds 0.03 free convection begins on a small scale within the confines of the inversion but large scale mixing does not occur. Finally the buoyancy of the air near the ground becomes so great and convective elements sufficiently large that the inversion is penetrated and large scale natural convection begins. During this period mixing is sufficiently vigorous to reduce the temperature gradient and thus the Richardson number near the ground. Meanwhile, the air which has been removed from the vicinity of the ground by convection is replaced by subsidence, the rate of descent in the subsiding air reaching a maximum at about the scale height where convective velocities are a maximum. Positive Richardson numbers occur near the scale height in the subsiding remains of the nocturnal inversion.

The most important conclusion which can be drawn from the curves of Fig. C.19 is that the turbulence at a given level is not solely dependent upon conditions at that level. Thus, for example, considering only the 5.5 m Ri curve of August 27 and using any of the equations for the diffusivity which involve the Richardson number (see Sect. 6.3.4.3) one must conclude that the diffusivity reaches a maximum at about 0845 and steadily decreases thereafter. In fact this distribution is patently false since it is well known that on a clear day the turbulence and therefore the diffusivity increases with increasing convective activity, normally reaching a plateau shortly before noon and remaining somewhat constant until late afternoon.

The fact that the value of the gradient Richardson number, Ri or for that matter the flux Richardson number, Rf, cannot be used independently to predict the level of turbulence, when $Ri < -1.0$ goes far toward explaining the wide scatter observed by most authors when they graph the level of turbulence against the Richardson number (see for example Lumley and Panofsky, 1964, p. 112). Without proof it is suggested here that at least three parameters are necessary to specify the level of turbulence during natural convection:

1. The scale height;
2. The depth of the adiabatic layer; and
3. The difference in temperature between the surface air and the adiabatic layer.

C.6.2.3 The Eddy Diffusivity*

The graphs of Fig. C.19, showing the Richardson number as a function of time, can be used as a guide in selecting the proper formulation for the eddy diffusivity. The models selected and their effective ranges are as follows:

$0.01 < Ri$	Rossby-Montgomery formula
$-0.03 \leq Ri \leq 0.01$	Monin-Obukhov formula
$-1.00 \leq Ri < -0.03$	Prandtl formula
$Ri < -1.00$	Prandtl formula

where the Rossby-Montgomery formula is

$$K = ku_*z(1 + 10Ri)^{-1/2} \tag{C.5}$$

the Monin-Obukhov formula is

$$K = ku_*z\left(1 - \frac{0.6z}{L}\right) \tag{C.6}$$

and the Prandtl formula is

$$K = 0.9z^2\left(\frac{g}{T}\left|\frac{\partial\theta}{\partial z}\right|\right)^{1/2} \tag{C.7}$$

The diurnal variation of the eddy diffusivity, as given in Table C-7, follows a pattern which might have been predicted on the basis of meteorological insight (see Fig. C.21). The rate of increase of diffusivity in the early morning depends on the presence of fog or cloud and strength of the inversion, but, generally, it rises to a plateau,

*The term eddy diffusivity is used interchangeable with eddy viscosity and eddy conductivity.

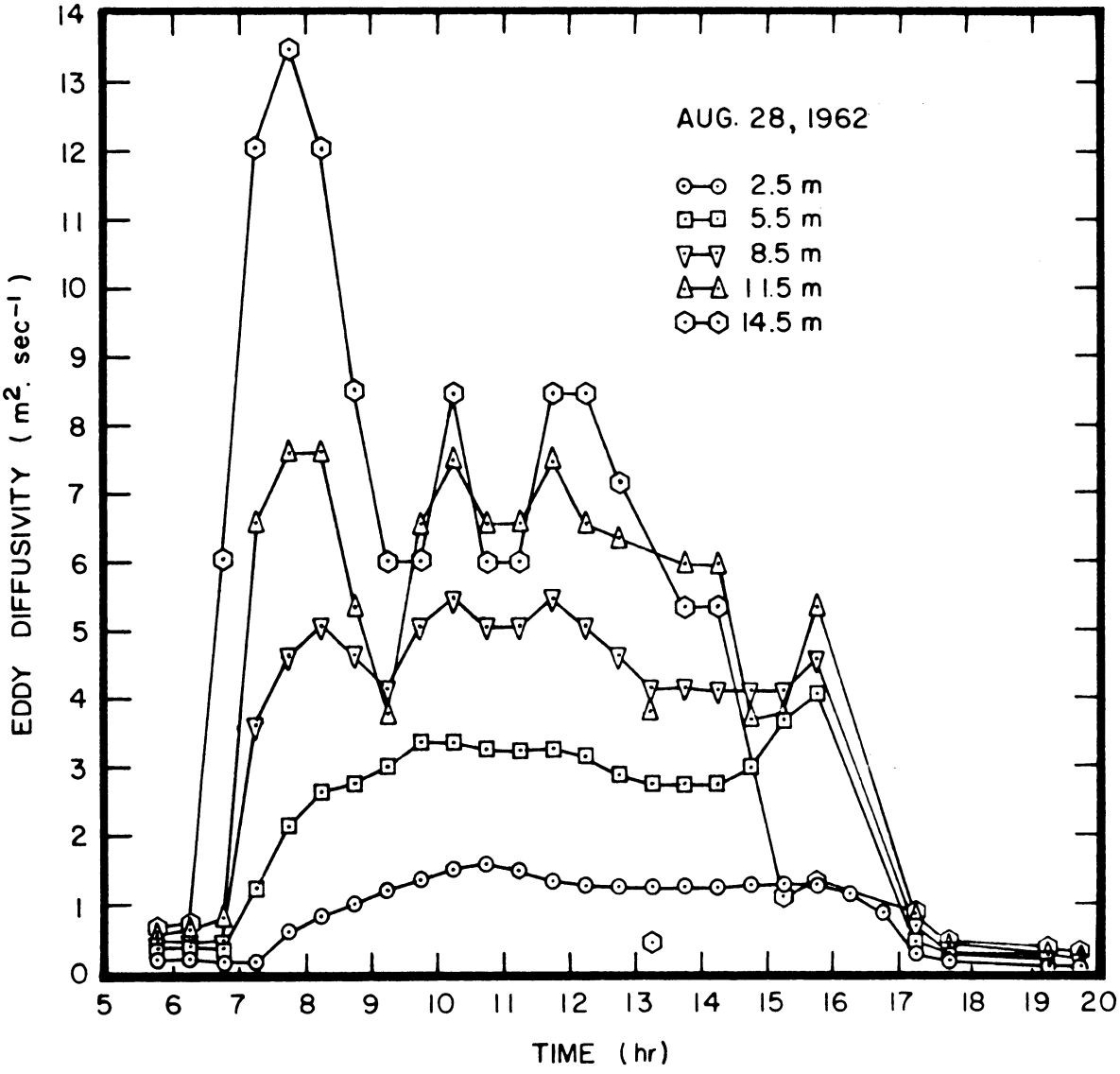

Fig. C.21. The diurnal variation of the eddy diffusivity near the ground. In-season experiment 1962.

remains fairly steady during the day and then declines during the latter half of the afternoon. The abnormally high values for the 11.5 and 14.5 m curves at 0800 shown in Fig. C.20 are artificial and a consequence of using Eq. (C.7) during a period for which it is inappropriate (see Sect. 6.3.4.3).

The curves demonstrate a roughly linear increase of diffusivity with height at least to 11.5 m in agreement with the relationship $K_z \alpha z^{4/3}$ given by Priestley (1959, p. 41). The value obtained for K_z at one meter is about 0.5 m^2 sec^{-1}, a large value, but not unexpected during free convection conditions.

C.6.3 The Computation of Eddy Diffusivity Aloft

C.6.3.1 Introductory Remarks

An attempt made to measure the vertical component of the eddy diffusivity aloft by the method of Eq. (C.2) failed; but, it is considered worthwhile to report the reasons for the failure because similar attempts may be made in the future.

C.6.3.2 Eddy Diffusivity From the Pollen Profiles

The pollen profiles recorded in Table C-1 are reproduced in Fig. C.22. A glance at the figures is enough to show that, if sampling error is assumed small, advective influences are sufficiently large and random to prevent the use of such data in the computation of eddy diffusivity.

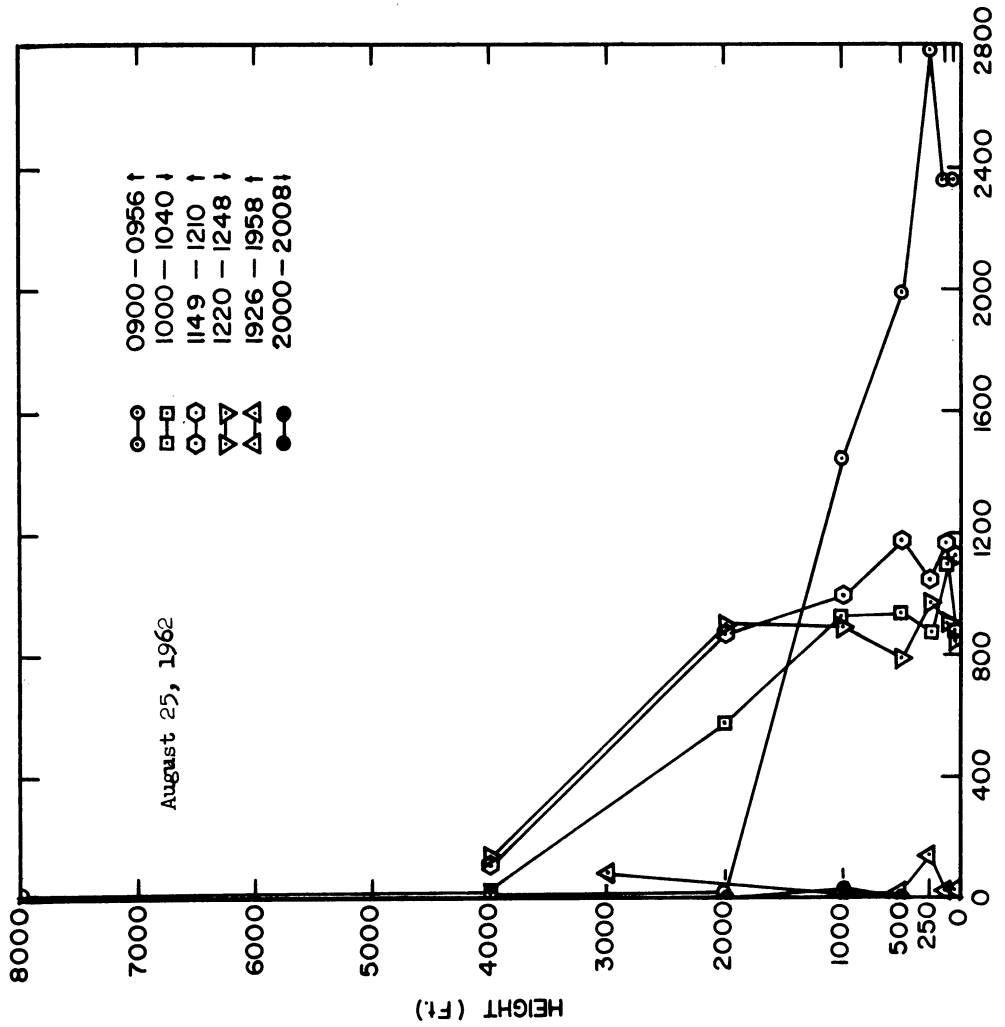

Fig. C.22. Measured ragweed pollen concentration profiles over a 3 mile flight path near Willow Run Airport.

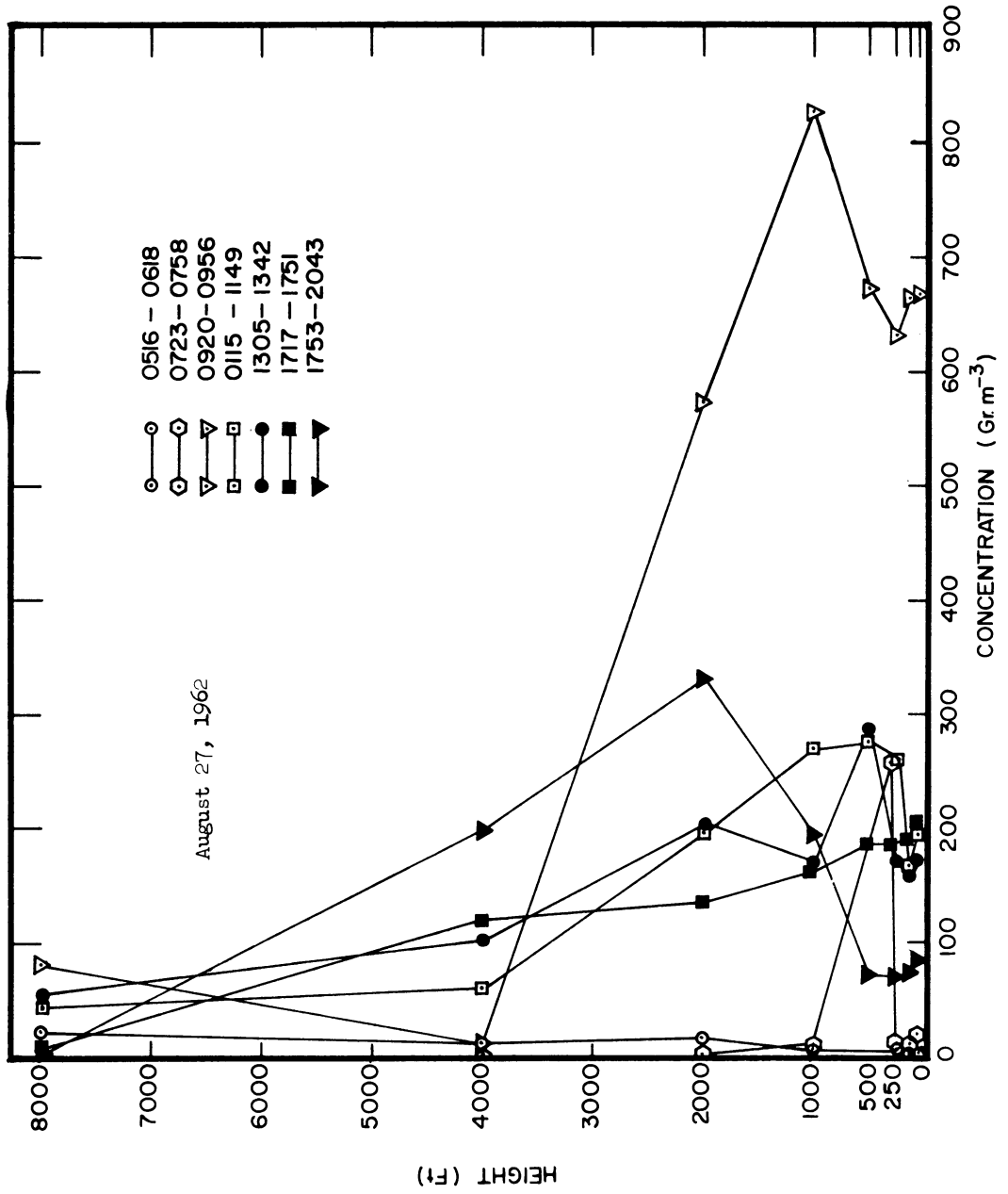

Fig. C.22 (Continued)

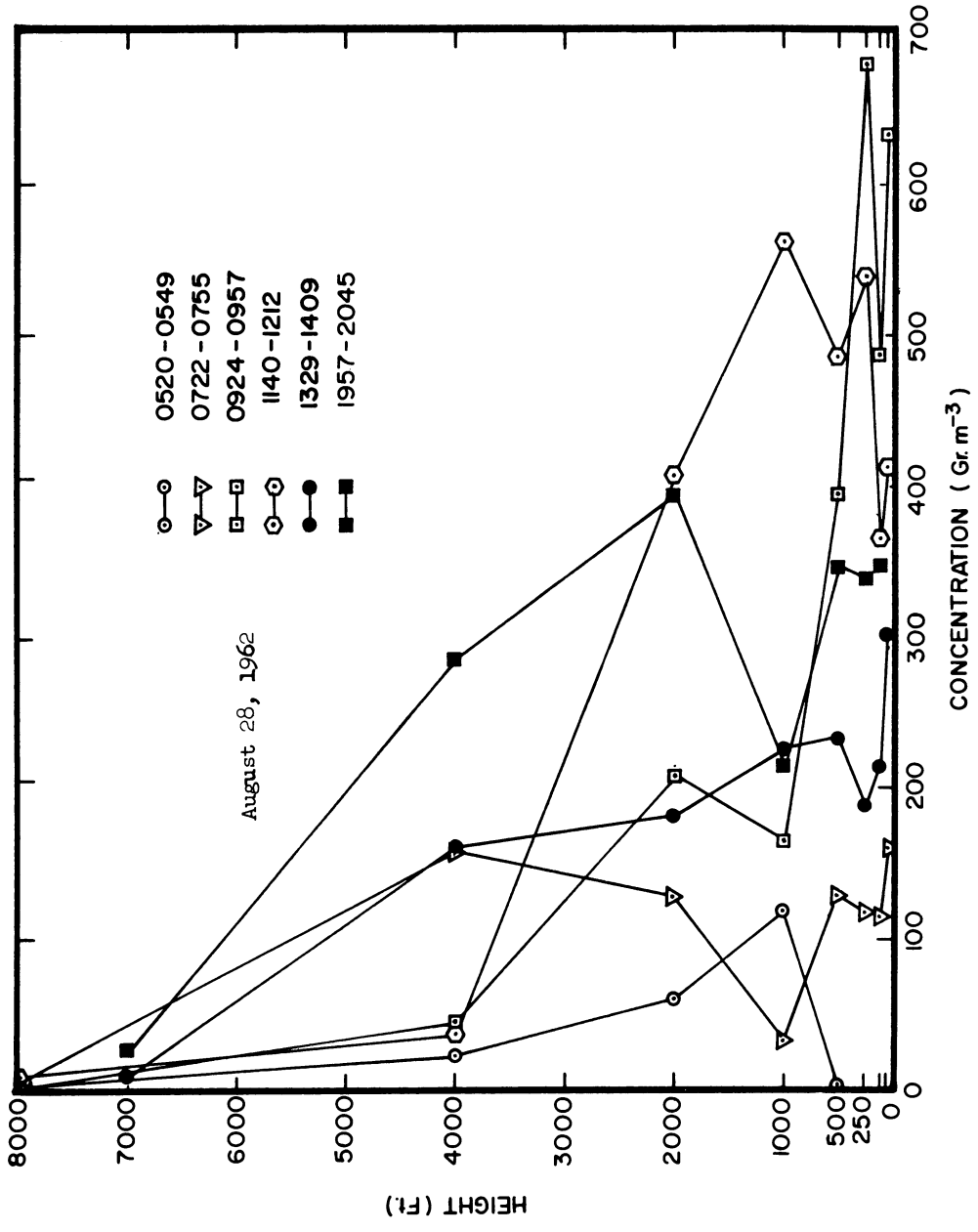

Fig. C.22 (Continued)

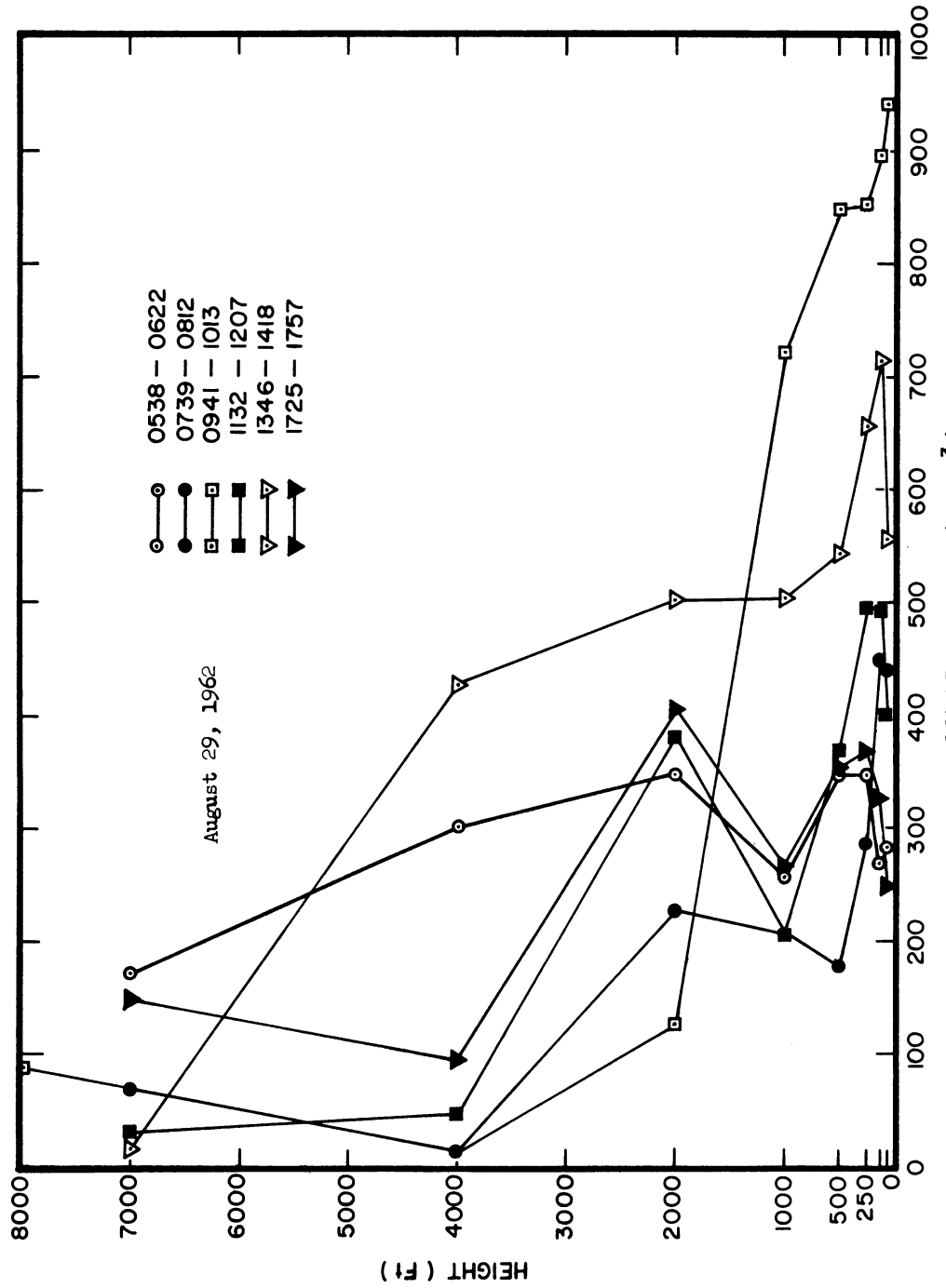

Fig. C.22 (Continued)

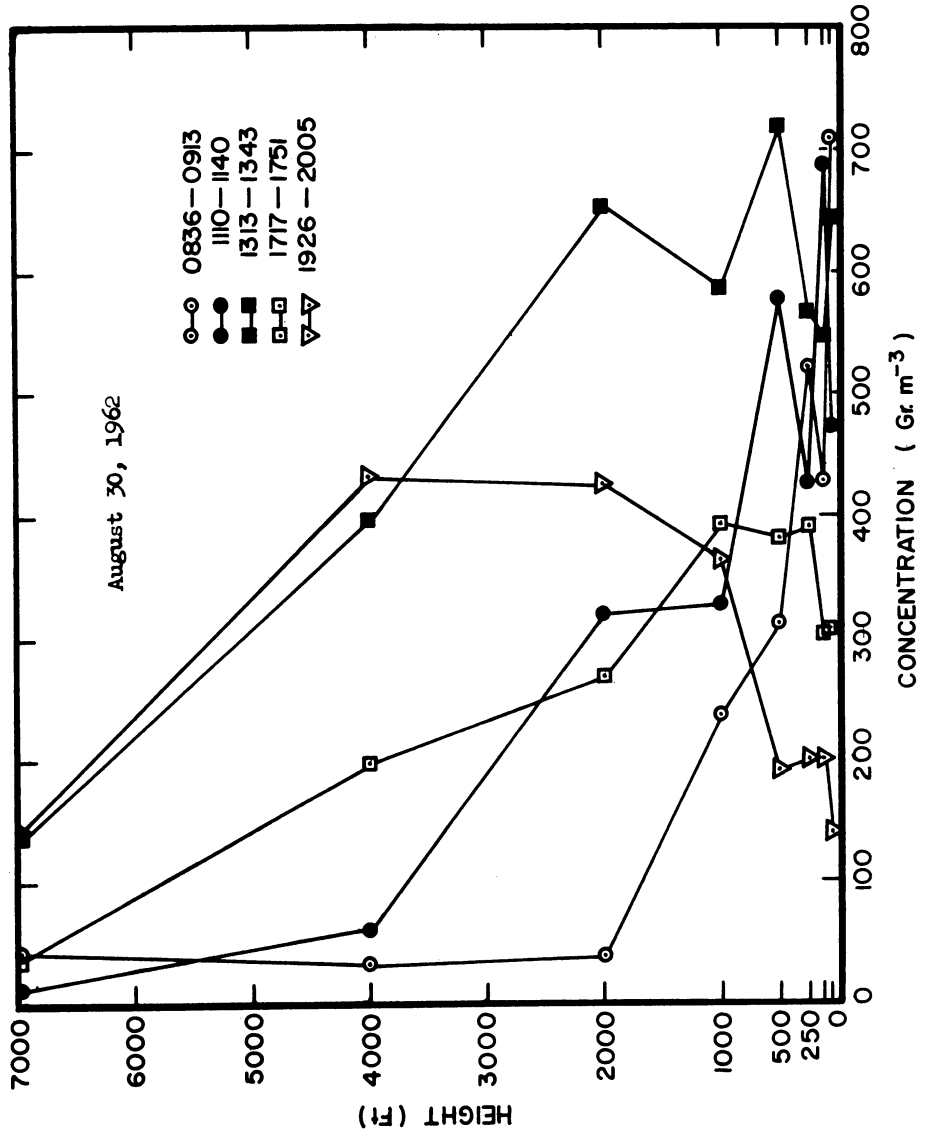

Fig. C.22 (Continued)

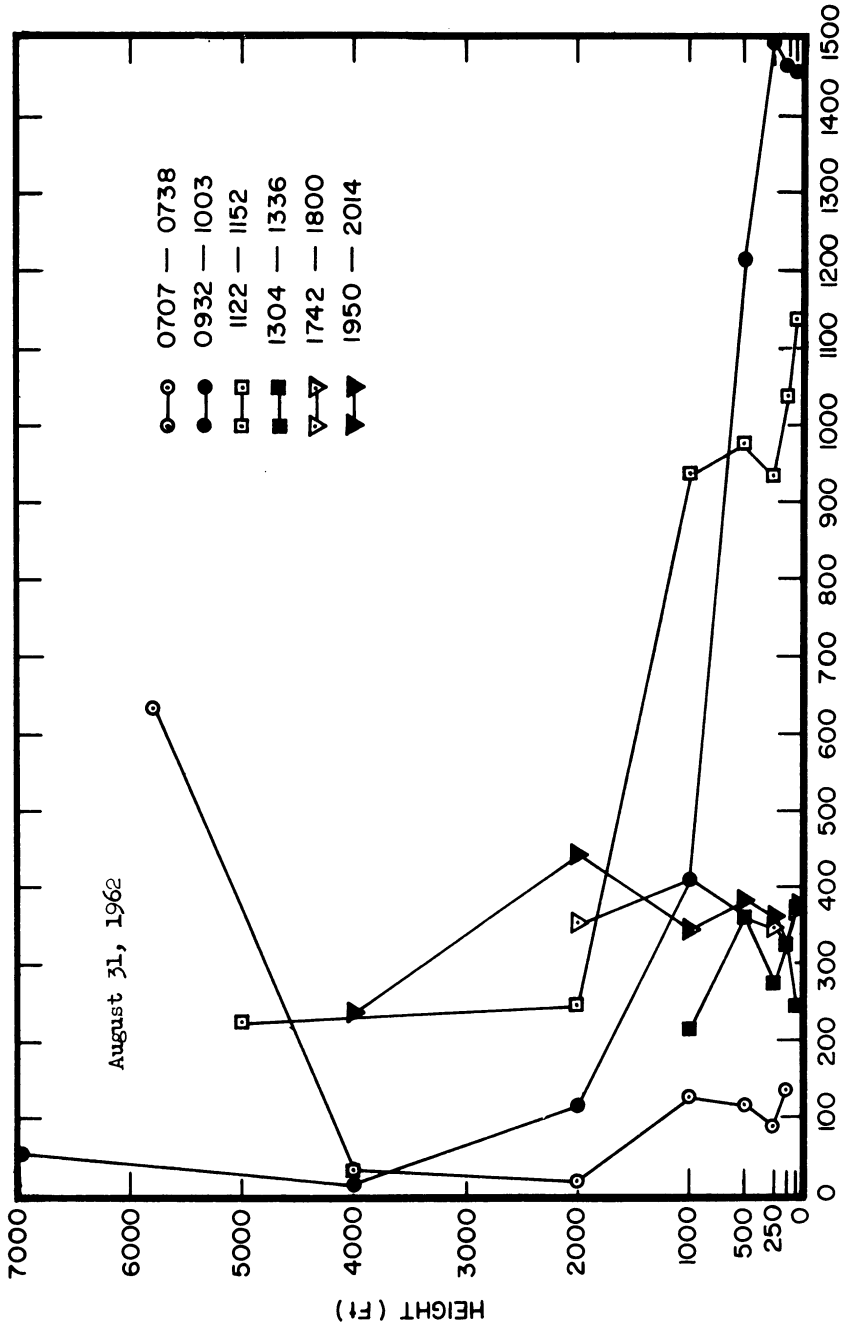

Fig. C.22 (Concluded)

C.6.3.3 Eddy Diffusivity from Temperature and Moisture Profiles

The temperature data with the trend removed (see Sect. C.5.3.2) were interpolated in time and height to form a matrix with values computed at 1 hr and 100 ft intervals for each of the four days August 27 - 30.

To compute the heat content of the air per unit mass the temperatures were first converted to potential temperature by the equation

$$\theta = T_z \left(\frac{P_s}{P_z} \right)^{R/C_p} \qquad (C.8)$$

where T is measured in degrees Kelvin, P_s is a standard pressure, R is the universal gas constant and C_p is the specific heat of dry air at constant pressure.

Because the aircraft altimeter reading is calibrated according to the I.C.A.N.* standard atmosphere

$$\frac{P_o}{P_z} = \left(1 - \frac{0.0065}{288.16} z \right)^{-5.256} \qquad (C.9)$$

where z is height in meters above sea level and p is mean sea level pressure.

Substitution for P_z in Eq. (C.8) and conversion of the height unit to feet above ground yields the equation

*The I.C.A.N. atmosphere was used rather than the I.C.A.O. atmosphere because it was convenient. The maximum height difference in the troposphere occurring between the two is 0.4 m

$$\theta = T\left\{\left(\frac{29.53}{P_o}\right)\left[1 - 6.879 \times 10^{-6}(714 + h)\right]^{5.256}\right\}^{0.2857} \qquad (C.10)$$

where P_o is the altimeter setting in inches of mercury and h the height of the aircraft in feet as read on the altimeter.

Now the heat content of a given volume of air is

$$H = \rho C_p \theta \qquad (C.11)$$

and the density ρ can be computed fromthe hydrostatic equation, the perfect gas law and the I.C.A.N. standard atmosphere as

$$\rho = \rho_o\left[1 - 6.879 \times 10^{-6}(714 + h)\right]^{4.256} \qquad (C.12)$$

Finally the diffusivity may presumably be computed from Eq. (C.1), which in the case of heat flux takes the form

$$K_{z_2} = \frac{\dfrac{\partial}{\partial t}\displaystyle\int_{z_1}^{z_2} H\,dz + \left(HK\,\frac{\partial \ell n\theta}{\partial z}\right)_{z_1}}{\left(H\,\frac{\partial \ell n\theta}{\partial z}\right)_{z_2}} \qquad (C.13)$$

If the upper level of integration is selected at the height where the temperature gradient becomes zero Eq. (C.13) reduces to the form

$$K_{z_1} = \frac{-\displaystyle\int_{z_1}^{z_2} H\,dz}{\left(H\,\frac{\partial \ell n\theta}{\partial z}\right)} \qquad (C.14)$$

Unfortunately, the errors in the aircraft temperature measurement (see sources of error below) and the errors produced by interpolation over a large height interval combined to make the use of Eq. (C.14) impractical.

Using the data available one can compute K more satisfactorily from Eq. (C.13). The terms on the right hand side are computed as follows:

1. The total heat per unit area between the levels z_1 and z_2, i.e. the integral on the right of Eq. (C.13) is found at times $t-\Delta t$ and $t+\Delta t$ and the derivative approximated using the central difference formula.

2. The second term on the right of Eq. (C.13) is evaluated from the 14.5 m data observed on the meteorological tower.

3. The denominator can be evaluated from the aircraft temperature profile data.

An error has been found in the computation of the diffusivity by this method so that the results are not reported. A quick check of the values however shows that they are likely to be satisfactory in the height range from 100 to 2000 ft but erroneous above that height.

C.6.4 The Pollen Profiles

C.6.4.1 Introduction

The pollen profiles, although inadequate for the computation of the eddy diffusivity, as noted earlier, can serve several useful functions: first, the total pollen in the air at any given time together with the estimated surface deposition can be used to estimate the rate of pollen emission at the ground; second, the shape of the profile can be used to infer, crudely, the distribution of eddy diffusivity in the convective layer; third, the observed profiles can be used as an initial condition for the steady three-dimensional diffusion equation; and

fourth, the profiles permit reasonable estimates to be made of the range of distances over which pollen can be expected to travel.

C.6.4.2 The Rate of Emission Inferred from Pollen Profiles

Let us suppose that the distribution function of the rate of pollen emission is normal with mean M and standard deviation S. Let us suppose further that the rate of deposition at the ground is equal to the product of the average concentration at ground level and the pollen settling velocity. Then the total pollen in the air at any time t will be

$$\int_{z=0}^{z=\infty} \chi(z)\,dz = \frac{A}{\sqrt{2\pi}S}\int_{t=-\infty}^{t=t} \exp\left(-\frac{1}{2}\left(\frac{t-M}{S}\right)^2\right)dt = \int_{t=-\infty}^{t=t} q\chi_o(t)\,dt \qquad (C.15)$$

From the observed pollen profiles one can compute terms 1 and 3 and estimate the values of M and S; hence A, the total daily emission per unit area, can be computed.

To perform the actual computations the aircraft pollen concentrations are adjusted so that 60 ft aircraft and tower measurements are in agreement. The assumption is then made that the 60 ft tower concentration is equal to the average concentration at ground level. The results of the computations are given in Table C-8 for the dates August 27 - 30. Crude estimates of M.S.A and E_{max}, the peak emission rate, for the four days are given in Table C-9.

TABLE C-8

THE COMPUTATION OF POLLEN SOURCE STRENGTH—IN-SEASON EXPERIMENT 1962

August 27

Time	Accumulated Deposition (gr m-2)	Integrated Pollen (gr m^{-2})	Total Input (gr m^{-2})
0723	0	0	0
0920	29,158	2,031,821	2,060,979
1115	99,339	833,948	933,287
1305	114,317	1,316,970	1,431,287
1717	148,488	725,270	873,758
2043	161,514	1,195,908	1,357,422
	August 28		
0520	0	0	0
0722	6,351	543,525	549,876
0924	41,232	694,025	735,257
1140	95,864	1,278,573	1,374,437
1329	125,988	767,751	893,739
1957	199,036	1,512,471	1,711,507
	August 29		
0739	0	0	0
0941	60,251	776,365	828,616
1132	91,212	375,143	466,355
1346	136,475	1,839,629	1,976,104
1942	199,489	211,255	410,744
	August 30		
0836	0	0	0
1110	302,477	603,535	906,012
1313	315,954	2,410,712	2,762,666
1717	436,948	819,817	1,256,765
1926	452,235	1,659,743	2,111,978

TABLE C-9

POLLEN EMISSION STATISTICS

Date	M	S (hr)	A ($gr\ m^{-2}$)	E_{max} ($gr\ m^{-2}\ sec^{-1}$)
August 27	0900	0.5	1.4×10^{6}	3.1×10^{2}
August 28	0820	1.5	1.4×10^{6}	1.0×10^{2}
August 29	1040	1.5	2.0×10^{6}	1.5×10^{2}
August 30	1030	1.25	2.5×10^{6}	2.2×10^{2}

C.6.4.3 Homogeneity of the Source

The last column of Table C-8 shows that the total pollen in a vertical column from the ground to the top of the convective layer varies markedly from one observation period to the next. Because the changes are downward as well as upward, and because they continue after pollen emission has ceased they are likely a result of inhomogeneities in source strength. It should be emphasized that these inhomogeneities must be larger than the three mile path length of the sampling flight and therefore occur over areas of 5 to 10 mi^2 or more. Apparently, the source strengths over areas of this size vary by factors of two to four.

C.6.4.4 Conclusions Regarding the Diffusivity Profile

There is no question but that observed pollen profiles as shown in Fig. 22 appear similar to theoretical profiles computed from Eq. (7.1) and illustrated in Fig. 7.4. Unfortunately, time has not allowed the

author to solve Eq. (7.1) under a variety of diffusivity distributions and thereby find a distribution which satisfactorily reproduces the observed profiles.

C.6.4.5 The Range of Ragweed Pollen Travel

In the absence of turbulence the distance a ragweed pollen grain will travel is determined by its settling speed, i.e. 50 m hr^{-1}, its height and the wind speed. A grain located at 1500 m will, for example, settle to the ground in 30 hr and if carried by a 20 km hr^{-1} wind will travel a distance of 600 km or about 360 miles.

During the daylight hours in normal sunny August weather in southern Michigan ragweed pollen is carried by atmospheric turbulence to heights of 1500 m and more as shown in Fig. 22.1. At night when the turbulence has died out the pollen will settle about 600 m or about one half to one third of the total depth of daylight mixing, suggesting that a fraction of each day's pollen emission accumulates within a given airmass.

The type of accumulation postulated above is evident in Fig. 22.1, although not as consistent and progressive as might be supposed. The weather sequence during the period of observation, August 25 - 31 is illustrated in Fig. 15.1. On August 25 a slowly moving cold front was approaching the observation site from the west. Ahead of the warm front the weather was cloudy with occasional very light rain. Because of the cloud the air was relatively stable and the ragweed pollen was confined

to a 600 m layer near the ground. The shallowness of the mixing depth resulted in extraordinarily high pollen concentrations as shown in Fig. 22.1. At 1730 a squall line passed the observing site accompanied by moderate to heavy rain. The cold front passed without accompanying weather the following morning. After the passage of the squall line the air was practically free of ragweed pollen.

August 26 was a cloudy day with rain showers. No pollen observations were made, but it might be assumed that the concentration was low and that pollen was not carried above 600 m.

August 27 was a sunny day with scattered to broken cumulus clouds. The air was relatively free of ragweed pollen in the early morning. Later, the cycle of emission and mixing followed the pattern predicted by the solutions of the unsteady one-dimensional diffusion equation (see Chapt. 7) as shown in Fig. C.22. An anomalous increase in concentration observed during the 1753-2043 observation period may be attributed to pollen advection from a region of stronger emission.

August 28 was a sunny day with a few scattered cumulus clouds. The early morning pre-emission pollen profiles exemplified by the 0520 and 0722 sampling periods of Fig. C.22 showed concentrations at some levels in excess of 100 gr m^{-3}. Subsequent profiles show changes similar to those observed on August 27. It is interesting to note that the 1957-2045 profile shows an anomalous increase in concentration similar to that observed on the 27th.

August 29 was a sunny day with a few scattered cumulus clouds. The pre-emission profiles show concentrations in excess of 300 gr m^{-3} at some levels, supporting the argument for an accumulation of pollen in the airmass. The profile changes for the remainder of the day again follow the pattern established during the preceding days excepting the 1132-1207 run which appears to have abnormally low concentrations.

The earliest observation period of August 30 was delayed by the presence of fog on the airport runways until 0836 at which time pollen was alreayd being emitted. The day was clear and the profile changes followed the typical pattern established on August 27 and 28. It will be noted that the 1926-2005 run of Fig. C.22 once again shows the anomalous evening increase observed on the two days mentioned above.

On August 31 a cold front was approaching from the west. The sky was overcast, diffusion was relatively poor and pollen concentrations were high, albeit only one half as large as the values observed on August 25. The residual pollen in the air prior to emission was only 100 gr m^{-3}, a lower value than had been observed on previous days. The reason for the decrease is unknown, but may be attributed to a slight change in wind direction.

A crude estimate of the range of ragweed pollen travel may be inferred from the pollen profiles given in Fig. C.22. If ragweed pollen is well mixed to 1500 m during the day, if mixing ceases at night and if the loss of pollen at the ground is equal to the product of the ground level concentration and the pollen settling speed, then the

number of pollen grains per square meter N present in the atmosphere after a time interval Δt will be equal to

$$\frac{N(\Delta t)}{N(o)} = e^{-v_g \Delta t/H} \tag{C.16}$$

during the day and

$$\frac{N(2\Delta t)}{N(\Delta t)} = 1 - \frac{v_g \Delta t}{H} \tag{C.17}$$

at night. If $v_g = 0.014$ m sec^{-1}, $\Delta t = 12 \times 3600$ sec and $H = 1500$ m, then $v_g \Delta t/H = 0.4$ and the total pollen in the air at the end of the day will be

$$\frac{N(z\Delta t)}{N(o)} = e^{-v_g \Delta t/H} \cdot \left(1 - \frac{v_g \Delta t}{H}\right) \approx 0.4 \tag{C.18}$$

and the concentration will follow the approximate law

$$\chi(t) = \chi(o) e^{-0.6t} \tag{C.19}$$

where t is in days. On the basis of Eq. (C.19) the fractional pollen concentration in air over a land surface free of pollen sources would be as shown in Table C-10.

TABLE C-10

FRACTIONAL POLLEN CONCENTRATION
OVER A SOURCE FREE AREA AS A FUNCTION OF TIME

Time (days)	$\chi(t)/\chi(o)$
0	1.00
1	0.55
2	0.30
3	0.17
4	0.09
5	0.05

The computations performed above are extremely sensitive to variations in H. If, for example, H is reduced to 600 m or less all the pollen will be deposited in a single night.

C.7 SOURCES OF ERROR

The remarks here will be brief since the error associated with most of the instrumentations has been thoroughly discussed in the previous two appendices.

C.7.1 Ground Based Equipment

C.7.1.1 Rotobar Samplers

In addition to errors discussed previously, the direct observations of the bars under reflected light added greatly to the difficulty of identifying the pollen. Several factors contributing to this difficulty were associated with the unevenness of the background including minute ridges in the milled edges of the bar, uneven application of the rubber cement due to excessive spraying and uneven application of the black background. Without extra care being taken in counting, the errors could have been excessive. With great care and frequent checking the additional error produced by these factors is estimated to have been kept to about 10%.

C.7.1.2 Anemometers

Tested on a horizontal bar in the open air both Thornthwaite and Beckman and Whitley anemometers appear to meet the specifications

claimed by the manufacturers. Used together, however, the two sets of anemometers do not seem to produce similar wind profiles, the graph of wind speed versus height showing a distinct change in slope at the juncture of the two.

A number of techniques were used in an attempt to align the two sets of observations. First, those periods having neutral lapse conditions were selected and the winds graphed on semi-log paper. The upper level wind observations were then aligned with those from the lower wind observations using constant multipliers, constant rotation and a number of other methods. No method proved uniformly satisfactory, and therefore it was finally decided to abandon all efforts to adjust the profiles.

No explanation for the unusual profile measurements has been given although there is a possibility that differential response of the anemometers to the spectrum of wind speeds may have been a contributing factor as noted by MacCready (1965).

There is no absolute evidence that the wind profiles are in error (on semi-log paper they do exhibit the correct curvatures for stable, unstable and neutral lapse conditions) and therefore it is difficult to assess the magnitude of the error. Other workers using the same combination of anemometers and having had similar problems (Elder, 1965) have estimated the maximum error at 10%.

C.7.1.3 Wet and Dry Thermocouples

The error in these measurements is probably no greater than the chart reading accuracy, namely about 1/10° Celsius.

C.7.2 Aircraft Equipment

C.7.2.1 Drum Samplers

Observations of the drum samples showed that the pollen and other debris was all located within narrow bands, with little scattering. This is taken to be a sign that the pollen entering the sampler was retained with 100% efficiency.

The flow into the entrance duct was approximately one half the isokinetic rate and according to the discussion earlier should result in an efficiency of 120%.

The flow meters attached to each sampler were carefully checked and are expected to introduce no error. The same vacuum gage was used for both meters. The measured volumes were corrected for the deficiency in pressure at the gas meters.

Difficulty was encountered in counting the pollen on the drum just as on the rotobars. The maximum counting error is unlikely to exceed 10%.

If the experimental accuracy is as great as indicated above, the difference in the counts on two drums located in identical exposures on the two wings of an aircraft is difficult to explain (see Table C-1). Aside from the possibility that the differences are due to random

fluctuations in air concentration no explanation can be given because adequate tests of the samplers have never been completed.

C.7.2.2 Wet Thermocouple

The steady drip method of wetting the thermocouple wick did not prove satisfactory, particularly after the instrument was mounted on the wing strut. No reliability is attached to the observations and no use is made of the data.

C.7.2.3 Dry Thermocouple

Considerable difficulty was encountered in the operations of the Bristol recorder. Two particularly serious sources of error occurred, one due to a lack of adequate grounding and the second to the development of contact potentials in the potentiometer switch box. These errors showed up in the trace as noise and drift respectively. The scientist who operated the equipment estimates that under normal operation the average error in degrees Celsius is 0.2 to 0.4 with occasional excursions to as much as 1.0 as noted in Table C-3.

BIBLIOGRAPHY

Bard, M.L., 1963: Examination of a wind profile proposed by Swinbank. J. appl. Meteor., 2, 6, 747.

Batchelor, G.K., 1947: Kolmogoroff's theory of locally isotropic turbulence. Proc. Cambr. phil. Soc., 33, 533.

Batchelor, G.K., 1949: Diffusion in a field of homogeneous turbulence, I. Eulerian analysis. Australian J. sci. Res., 2, 437.

Batchelor, G.K., 1950: The application of the similarity theory of turbulence to atmospheric diffusion. Quart. J.R. meteor. Soc., 76, 133.

Baynton, H.W., 1963: The penetration and diffusion of a fine aerosol in a tropical rain forest. Doctoral dissertation, University of Michigan, Ann Arbor.

Benninghoff, W.S., 1964: Personal communication, University of Michigan, Ann Arbor.

Blackadar, A.K., 1962: The vertical distribution of wind and turbulent exchange in a neutral atmosphere. J. geophys. Res., 67, 8, 3095.

Blackley, C.H., 1873: Experimental Researches on the Causes and Nature of Catarrhus Aestivus. Balliere, Tindall and Cox, London (Reprinted: Dawson, London, 1959).

Bosanquet, C.H., and J.L. Pearson, 1936: The spread of smoke and gases from chimneys. Trans. Faraday Soc., 32, 1249.

Brock, F.V., 1962: Analog computing techniques applied to atmospheric diffusion: continuous line source. J. appl. Meteor., 1, 4, 444.

Brock, F.W., and E.W. Hewson, 1963: Analog computing techniques applied to atmospheric diffusion: continuous point source. J. appl. Meteor., 2, 1, 129.

Brun, R.J., and H.W. Mergler, 1953: Impingement of water droplets on a cylinder in an incompressible flow field and evaluation of rotating multcylinder method for measurement of droplet-size distribution, volume-median droplet size, and liquid water content in clouds. Tech. Note 2904, N.A.C.A., Washington, D.C.

Brunt, D., 1939: Physical and Dynamical Meteorology. Cambridge University Press.

Buajitti, K., and A.K. Blackadar, 1957: Theoretical studies of diurnal wind-structure variations in the planetary boundary layer. Quart. J.R. meteor. Soc., 83, 358, 486.

Bunker, A.F., 1960: Heat and water-vapor fluxes in air flowing southward over the western North Atlantic ocean. J. Meteor., 1960.

Bunker, A.F., 1952: Measurements of the vertical water vapor transport and distribution within unstable atmospheric ground layers and the turbulent mass exchange coefficient. Pap. phys. Ocean. Meteor., Mass. Inst. Tech. and Woods Hole ocean. Instn., 12, 3, 42pp.

Businger, J.A., 1958: Similarity and dissimilarity between turbulent transfer of heat and momentum near the Earth's surface. In "Studies on the Structure of Turbulence," University of Wisconsin, Dept. of Meteor.

Byers, H.R., J.R. Sievers, and B.J. Tufts, 1955: Distribution in the atmosphere of certain particles capable of serving as condensation nuclei. In "Artificial Stimulation of Rain," Proc. of 1st Conf. Phys. of Cloud and Pcpn. Particles. Pergamon, New York.

Byers, H.R., 1937: Synoptic and Aeronautical Meteorology. New York, McGraw-Hill.

Calder, K.L., 1949: Eddy diffusion and evaporation in flow over aerodynamically smooth and rough surfaces: a treatment based on laboratory laws of turbulent flow with special reference to conditions in the lower atmosphere. Quart. J. mech. and appl. Math., II, 153.

Calder, K.L., 1952: Some Recent British Work on the Problem of Diffusion in the Lower Atmosphere Air Pollution. Proc. U.S. Tech. Conf. Air Poll., New York, McGraw-Hill.

Carré, B.A., 1961: The determination of the optimum accelerating factor for successive over-relaxation. Computer J., 4, 73.

Carslaw, H.S., J.C. Jaeger, 1959: Conduction of Heat in Solids. London, Oxford University Press.

Chamberlain, A.C., 1956: Aspects of travel and deposition of aerosol and vapour clouds. Atomic Energy Res. Est. Harwell, Berks.

Crank, J., 1956: The Mathematics of Diffusion, London, Oxford University Press.

Csanady, G.T., 1963: Turbulent diffusion of heavy particles in the atmosphere. J. atm. Sci., 20, 3, 201.

Davis, R.D., 1950: Three dimensional turbulence and evaporation in the lower atmosphere I and II. Quart. J. mech. and appl. Math., 3, 1, 51.

Deacon, E.L., 1949: Vertical diffusion in the lowest layers of the atmosphere. Quart. J.R. meteor. Soc., 75, 89.

Deacon, E.L., 1957: Wind profiles and the shearing stress-an anomaly resolved. Quart. J.R. meteor. Soc., 83, 358, 537.

DeMarrais, G.A., 1959: Wind speed profiles at Brookhaven Laboratory. J. Meteor., 16, 2, 181.

Dingle, A.N., 1959: Personal communication, University of Michigan, Ann Arbor.

Elder, F.C., and E. Ryznar, 1965: Personal communication, University of Michigan, Ann Arbor.

Elliott, W.P., 1964: The height variation of vertical heat flux near the ground. Quart. J.R. meteor. Soc., 90, 385, 260.

Ellison, T.H., 1957: Turbulent transport of heat and momentum from an infinite rough plane. J. Fluid Mechanics, 5, 456.

Ericksson E., 1959: The yearly circulation of chloride and sulphur in nature; meteor., geochemical and pedological implications part I. Tellus, 11, 4, 375.

Ericksson E., 1960: The yearly circulation of chloride and sulphur in nature; meteor., geochemical and pedological implications part II. Tellus, 12, 1, 63.

Fons, W.L., 1940: Influence of forest cover on wind velocity. Jour. Forestry, 38, 6, 481.

Fourier, J.B., 1822: Theorie Analytique de la Chaleur. Oeuvres d'Fourier.

Fox, L., 1962: Numerical Solution of Ordinary and Partial Differential Equations. Oxford, Pergamon.

Frost, R., 1946: Turbulence and diffusion in the lower atmosphere. Proc. R. Soc. A., 186, 20.

Frost, R., 1947: The Velocity Profile in the Lowest 400 ft. Meteor. Mag., 76, 14.

Fuks, N.A., 1964: The Mechanics of Aerosols. Oxford. Pergamon.

Geiger, R., 1925: Unters. u.d. Bestandsklima, Forstw. C., 47, 629-644, 848-854.

Geiger, R., 1926: Unters. u.d. Bestandsklima, Forstw. C., 48, 337-349, 495-505, 523, 532, 749, 758.

Geiger, R., 1959: The Climate Near the Ground. Harvard University Press, 302-308, 336-338.

Geiger, R., and H. Amann, 1931: Forstmet. Mess. in e. Eichenbestand Forstw. C., 53, 237-250, 341, 351, 705-714, 809-819.

Geiger, R., and H. Amann, 1932: Forstmet. Mess. in e. Eichenbestand Forstw. C., 54, 371-383.

Gerhardt, J.R., W.S. Mitcham, and A.W. Straiton, 1962: A 1400 ft. meteorological tower with automatic readout. Proc. Inst. Radio Engrs. 50, 2263.

Gifford, F.A., and D.H. Pack, 1959: Statistical properties of a fluctuating plume dispersion model, atmospheric diffusion and air pollution, edited by F.N. Frenkiel and P.A. Sheppard, Adv. in Geophys. Academic Press, 6, 117.

Gill, G.C., 1965: Personal communication, University of Michigan, Ann Arbor.

Goldberg, L., and E.A. Mueller, 1953: The vertical distribution of nitrousoxide and methane in the earth's atmosphere. J. Optical Soc. Am. 43, 1033.

Goldstein, S., 1951: On diffusion by discontinuous movements and on the telegraph equation. Quart. J. mech. and appl. Math. IV, 129.

Goldstein, S., 1952: Modern Developments in Fluid Dynamics. Oxford, Clarendon Press.

Green, H.L., and W.R. Lane, 1957: Particulate Clouds: Dusts, Smokes and Mists, Princeton, New Jersey. D. Van Nostrand.

Gregory, P.H., 1961: The Microbiology of the Atmosphere. London, Leonard Hill.

Gumbel, E.J., J.A. Greenwood, and D. Durand, 1953: The circular normal distribution: theory and tables. Amer. stat. assoc. Jour., 48, 131.

Hahn, M., 1909: Die Bestimmung und meteorologische Verwertung der Keimzahl in den höheren Luftschichten. Nach vom Luftballon aus angestellten Beobachtungen. Zbl. Bakt., Abt. I, 51, 97.

Halstead, M.H., 1943: A stability-term in the wind-gradient equation. Trans. A.G.U., 24, 204.

Harrington, J.B., M.A. Gill, and B.R. Warr, 1959: High efficiency pollen samplers for use in clinical allergy. J. Allergy, 30, 4, 357.

Harrington, J.B., and K. Metzger, 1963: Ragweed pollen density. Amer. J. Botany, 50, 5, 532.

Harrison, P.R., 1965: Personal communication, University of Michigan, Ann Arbor.

Hay, J.S., and F. Pasquill, 1957: Diffusion from a fixed source at a height of a few hundred feet in the atmosphere. J. Fluid Mechanics, 2, 290.

Hay, J.S., and F. Pasquill, 1959: Diffusion from a continuous source in relation to the spectrum and scale of turbulence. In atmospheric diffusion and air pollution edited by F.N. Frenkiel and P.A. Sheppard, Adv. in Geophys., Academic Press, 6, 345.

Hildebrand, F.B., 1956: Introduction to Numerical Analysis, New York, McGraw-Hill.

Holzman, B., 1943: The influence of stability on evaporation. Annals New York Acad. Sci., 44, 13.

Hubert, K., 1932: Beobachtungen uber die Verbreitung des Gelbrostes bei kunstlichen Feldinfektronen. Fortschr. Landw., 7, 195.

Jacobi, W., and K. Andre, 1963: The vertical distribution of radon 222, randon 220, and their decay products in the atm. J. geophys. Res., 68, 3799.

Jacobs, S.J., 1965: Personal communication, University of Michigan, Ann Arbor.

Johnson, O., 1959: An examination of the vertical wind profile in the lowest layers of the atmosphere. J. Meteor., 16, 2, 144.

Junge, C.E., 1963: Air Chemistry and Radioactivity. London, Academic Press.

Kampé de Fériet, M.J., 1939: Les fonctions aleatoires stationnaires et la theorie statistique de la turbulence homogene. Annals Soc. sci. Brux., 59, 145.

Krug-Pielsticker, U., 1949: Messungen der Sonnenstrahlung bei Flugzeuganfstiegen bis 9 km Hoche, Ber. dtsch. Wetterd. US Zone Nr 8.

Kung, E., 1961: Derivation of roughness parameters from wind profile data above tall vegetation. In Studies of the three-dimensional structure of the planetary boundary layer. University of Wisconsin, Dept. of Meteor. Annual Report.

Laikhtman, D.L., 1944: Profiles of wind and interchange in the layer of atmosphere near the ground. Bull Acad. Sci. USSR., Geogr. and Geophys. Sec. 8, 1, 1.

Lettau, H.H., 1961: Studies of the three dimensional structure of the planetary boundary layer. University of Wisconsin, Dept. of Meteor. Annual Report.

Liljequist, G.H., 1955: Norweigian-British-Swedish Antarctic Expedition, 1949-52, Scientific Results Vol. II Part 1-C, Energy Exchange of an Antarctic Snow Field-Wind Structure in the Low Layer--Norweigian Polar Institue Oslo.

Liu, V.C., 1956: Turbulent dispersion of dynamic particles. J. Meteor. 13, 4, 399.

Lodge, J.P., 1955: A study of sea-salt particles over Puerto-Rico. J. Meteor., 12, 5, 493.

Lumley, J.L., and H.A. Panofsky, 1964: The Structure of Atmospheric Turbulence. New York, Interscience.

MacCready, P.B., 1953a: Atmospheric turbulence measurements and analysis. J. Meteor., 10, 325.

MacCready, P.B., 1953b: Structure of atmospheric turbulence. J. Meteor., 10, 434.

MacCready, P.B., 1965: Mean wind measurements in turbulence. J. appl. Meteor. (submitted 1964).

MacCready, P.B., and H.R. Jex, 1964: Response characteristics and meteorological utilization of propellor and vane wind sensors. J. appl. Meteor., 3, 2, 182.

MacKay, K.L., 1965: Some consequences of the exponential wind profile. Masters Thesis, University of Michigan, Ann Arbor.

McVehil, G.E., 1964: Wind and temperature profiles near the ground in stable stratification. Quart. J.R. meteor. Soc., 90, 384, 136.

Mickelsen, W.R., 1955: An experimental comparison of the Lagrangian and Eulerian correlation coefficients in homogeneous isotropic turbulence, N.A.C.A.. Washington, Tech. Note No. 3570.

Monin, A.S., 1955: The equation of turbulent diffusion. Dokl. Akad. Nauk., 105, 256.

Monin, A.S., 1959: Smoke propagation in the surface layer of the atmosphere, atmospheric diffusion and air pollution, edited by F.N. Frenkiel and P.A. Sheppard, Adv. in Geophys., Academic Press, 6, 331.

Monin, A.S., and A.M. Obukhov, 1954: Basic regularity in turbulent mixing in the surface layer of the atmosphere. U.S.S.R. Acad. Sci. Works of geophys. Inst., No. 24.

Morton, B.R., G.I. Taylor and J.S. Turner, 1956: Turbulent gravitational convection from maintained and instantaneous sources. Proc. R. Soc. A, 234, 1.

Munn, R.F., 1961: The vertical diffusion in the atmosphere from a continuous point source. Doctoral dissertation, University of Michigan, Ann Arbor.

National Phys. Lab., 1961: Modern Computing Methods, London. H.M.S.O.

Ogura, Y., 1957: The influence of finite observation intervals on the measurement of turbulent diffusion parameters. J. Meteor., 14, 2, 176.

Ogura, Y., 1952a: The theory of turbulent diffusion in the atmosphere (II). J. meteor. Soc. Japan, 30, 23.

Ogura, Y., 1952b: The theory of turbulent diffusion in the atmosphere (III). J. meteor. Soc. Japan, 30, 386.

Ogura, Y., 1959: Diffusion from a continuous source in relation to a finite observation interval, Atmospheric Diffusion and Air Pollution, edited by F.N. Frenkiel and P.A. Sheppard, Adv. in Geophys., Academic Press, 6, 149.

Owen, P.R., 1960: Dust deposition from a turbulent airstream, Aero-Dynamic Capture of Particles, Ed. E.G. Richardson. Pergamon, New York.

Paeschke, W., 1937: Experimentelle Untersuchungen zum Rauhigkeits-und Stabilitäts-Problem in der bodennaken Luftschicht, Beitr. Phys. d. fr. Atm., 24, 163.

Panofsky, H.A., A.K. Blackadar, and G.E. McVehil 1960: The diabatic wind profile. Quart. J.R. meteor. Soc., 86, 369, 390.

Panofsky, A.A., 1961: An alternative derivation of the diabatic wind profile. Quart. J.R. meteor. Soc., 87, 371, 109.

Pasquill F., 1962: Atmospheric Diffusion. London, D. Van Nostrand.

Pasquill F., 1963: The determination of eddy diffusivity from measurements of turbulent energy. Quart. J.R. meteor. Soc., 89, 379, 95.

Pasteur, L., 1861: Mémoire sur les corpuscles organisés qui existent dans l'atmosphère. Examin de la doctrine des générations spontanées. Annual Sci. Nat. (Zool.) 4^{e} sér., 16, 5.

Penndorf, R., 1954: The vertical distribution of Mie particles in the troposphere. Geophys. Res. Papers No. 25 Geophys. Res. Dir. A.F.C.R.L.

Perepelkina, A.V., 1957: Some results of the investigation of turbulent fluctuations of temperature and the vertical component of the wind velocity. J. acad. Sci. USSR, Geophys. Ser., 6, 765. (Trans. by A. Nurklik-Toronto).

Peturson B., 1931: Epidemiology of cereal rusts. Dom. Canada Dept. Agric., Div. Bot. Rept. Dom. Botanist, 1930, 44.

Philip, J.R., 1959: The theory of local advection (I). J. Meteor., 16, 5, 535.

Poppendiek, H.F., 1949: Investigation of velocity and temperature profiles in air layers within trees and brush. University of California, Dept. of Engineering.

Portman, D.J., F.C. Elder, E. Ryznar, and V.E. Noble, 1962: Some optical properties of turbulence in stratified flow near the ground. J. geophys. Res., 67, 8, 3223.

Prandtl, L., 1932: Meteorologische Anwendung der Strömungslehre. Beitr. Atmosphäre, 19, 188.

Priestley, C.H.B., 1959: Turbulent Transfer in the Lower Atmosphere. Chicago, University of Chicago Press.

Priestley, C.H.B., 1953: Buoyant motion in a turbulent environment. Australian J. Phys., 6, 279.

Priestley, C.H.B., 1954a: Convection from a large horizontal surface. Australian J. Phys., 7, 176.

Priestley, C.H.B., 1954b: Vertical heat transfer from impressed temperature fluctuations. Australian J. Phys., 7, 202.

Priestley, C.H.B., 1957: The evolution of energy gain by the atmosphere through contact with the ground or ocean. University of Chicago, Sci. Dept. No. 2, Chicago, University of Chicago Press.

Priestley, C.H.B., 1960: A determinant hypothesis for the superadiabatic wind and temperature profiles. Quart. J.R. meteor. Soc., 86, 232.

Ramdas, L.A., 1946: The micro-climates of plant communities. The Indian Ecologist, 1, 1, 1.

Rempe, H., 1937: Untersuchungen über die Verbreitung des Blütenstaubes durch die Luftstromungen. Planta, 27, 93.

Richardson, L.F., 1926: Atmospheric diffusion shown on a distance-neighbor graph. Proc. R. Soc. A., 110, 709.

Richtmyer, R.D., 1957: Difference Methods for Initial-Value Problems. New York, Interscience.

Rider, N.E., 1954: Eddy diffusion of momentum, water vapor, and heat near the ground. Phil. Trans. R. Soc. A., 246, 481.

Rider, N.E., and G.D. Robinson, 1951: A study of the transfer of heat and water vapor above the surface of short grass. Quart. J.R. meteor. Soc., 77, 333, 375.

Roberts, O.F.T., 1923: The theoretical scattering of smoke in a turbulent atmosphere. Proc. R. Soc. (London) A., 104, 640.

Rossby, C.G., 1932: A generalization of the theory of the mixing length with application to atmospheric and oceanic turbulence. Mass. Inst. Tech., Papers in Phys. Ocean. and Meteor., 1, 4.

Rossby, C.G., 1935: The layer of frictional influence in wind and ocean currents. Mass Inst. Tech., Papers in Phys. Ocean and Meteor., 3, 3.

Rounds, W. Jr., 1955: Solutions of the 2-dimensional diffusion equations. Trans. Amer. geophy. Union, 36, 3, 395.

Sheldon, J.M., and E.W. Hewson, 1959: Atmospheric Pollution by Aeroallergens. Progress Report No. 3, University of Michigan, Report No. 2421-3-P.

Sheldon, J.M., and E.W. Hewson, 1960: Atmospheric Pollution by Aeroallergens. Progress Report No. 4, University of Michigan Report No. 03440-1-P.

Sheldon, J.M., and E.W. Hewson, 1962: Atmospheric Pollution by Aeroallergens. Progress Report No. 5, University of Michigan Report No. 04772-1-P.

Sheppard, P.A., 1958: Transfer across the earth's surface and through the air above. Quart. J.R. meteor. Soc., 84, 361, 205.

Simmons, L.F.G., and C. Salter, 1938: An experimental determination of the spectrum of turbulence. Proc. R. Soc. A., 165, 920, 73.

Smith, F.B., 1957a: The diffusion of smoke from a continuous elevated point-source into a turbulent atmosphere. J. Fluid Mech. 2, 49.

Smith, F.B., 1957b: Convection-diffusion processes below a stable layer. Meteor. Research Committee (London) M.R.P., 1048.

Smith, F.B., 1957c: Convection-diffusion process below a stable layer-Pf. 2. Meteor. Research Committee. (London) M.R.P., 1073.

Smith, F.B., 1959: The turbulent spread of a falling cluster. Adv. Geophys., 6, 193.

Smith, F.B., 1962: The problem of deposition in atmospheric diffusion of particulate matter. J. atm. Sci., 19, 5, 429.

Stakman, E.C., A.W. Henry, G.C. Curran, and W.N. Christopher, 1923: Spores in the upper air. J. Agric. Res., 24, 599.

Stocker, O., 1923: Klimamess. auf kleinstem Raum in Wiesen-Wald- u. Heidepflanzen, Ber. D. Bot. G., 41, 145-150.

Stohrer, A.W., 1964: Personal communication, University of Michigan, Ann Arbor.

Stoller, J., and E.R. Lemon, 1963: In The energy budget at the earth's surface, (II), Production Res. Rpt. No. 72, U.S.D.A.

Sulton, W.G.L, 1943: On the equation of diffusion in a turbulent medium. Proc. R. Soc. A., 182.

Sutton, O.G., 1934: Wind structure and evaporation in a turbulent atmosphere. Proc. R. Soc. A., 146, 701.

Sutton, O.G., 1953: Micrometeorology: A Study of Physical Processes in the Lowest Layers of the Earth's Atmosphere. New York, McGraw-Hill.

Swinbank, W.C., 1964: The exponential wind profile. Quart. J.R. meteor. Soc., 90, 384, 119.

Tan, H.S. and S.C. Ling, 1963: A study of atmospheric turbulence and canopy flow. In The energy budget at the earth's surface (II), Production Res. Rpt. No. 72, U.S.D.A.

Taylor, G.I., 1915: Eddy motion in the atmosphere. Phil. Trans. R. Soc. A., 115, 1.

Taylor, G.I., 1921: Diffusion by continuous movements. Proc. London Math. Soc. ser., 2, 20, 196.

Taylor, G.I., 1935: Statistical theory of turbulence (I). Proc. R. Soc. A., 151, 421.

Taylor, G.I., 1938: The spectrum of turbulence. Proc. R. Soc. A., 164, 476.

Thomas, D.C., and A.A. Townsend, 1957: Turbulent convection over a heated horizontal surface. J. Fluid Mechanics, 2, 473.

Thuillier, R.H., and U.O. Lappe, 1964: Wind and temperature profile characteristics from observations on a 1400 ft. tower. J. appl. Meteor., 3, 3, 299.

Turner, JS., 1963: The motion of buoyant elements in turbulent surroundings. J. Fluid Mechanics, 16, 1, 1.

Varga, R.S., 1962: Matrix Iterative Analysis. New Jersey, Prentice-Hall.

Wandel, C.F., and O. Kofoed-Hansen, 1962: On the Eulerian-Lagrangian transform in the statistical theory of turbulence. J. geophys. Res., 67, 8, 3089.

Warner, J., 1963: Observations relating to theoretical models of a thermal. J. atm. Sci., 20, 6, 546.

Watson, H.H., 1954: Errors due to anisokinetic sampling of aerosols. Amer. Ind. Hyg. Ass. Quart., 15, 1, 21.

Webb, E.K., 1958: Vanishing potential temperature gradients in strong convection. Quart. J.R. meteor. Soc., 84, 118.

Webster, C.A.G., 1964: An experimental study of turbulence in a density-stratified shear flow. J. Fluid Mechanics, 19, 2, 221.

Wigand, A., 1919: The vertical distribution of condensation nuclei in the free atmosphere. Ann. Physik, IV, 59.

Wiin-Nielsen A.C., 1965, Personal communication, University of Michigan, Ann Arbor.

Woelfle, M., 1939: Windverkaltnisse in Walde, Forstw. C., 61, 65.

Woodcock, A.H., 1953: Salt nuclei in marine air as a function of altitude and wind force. J Meteor., 10, 5, 362.

Yamamoto, G., and A. Shimanuki, 1964: The determination of lateral diffusivity in diabatic conditions near the ground from diffusion experiments. J. atm. Sci., 21, 2, 187.

Yamamoto, G., and A. Shimanuki, 1960: Numerical solution of the equation of atmospheric turbulent diffusion. Sci. Rep. Tohoku University, Ser. 5, 12, 24.

Yang, C.H., 1959: In Air Pollution by Aeroallergens, Progress Report No. 3, University of Michigan Report No. 2421-3-P, edition by J.M. Sheldon and E.W. Hewson, University of Michigan, Ann Arbor.

Yudine, M.I., 1959: Physical consideration on heavy-particle diffusion. Adv. in Geophys., Vol. 6, 185.

Yih, C.S., 1952: On a differential equation of atmospheric diffusion. Trans. A.G.U., 33, 1, 8.